Technische Universität München
Fakultät für Medizin

Improvement of Chimeric Antigen Receptor-Specific T Cells for Adoptive T Cell Transfer

Sarah Claudia Dötsch

Vollständiger Abdruck der von der Fakultät für Medizin der Technischen Universität München zur Erlangung einer

Doktorin der Naturwissenschaften (Dr.rer.nat.)

genehmigten Dissertation.

Vorsitz: Prof. Dr. Ulrike Protzer

Prüfer*innen der Dissertation:

1. Prof. Dr. Dirk H. Busch
2. Prof. Dr. Gabriele Multhoff
3. Prof. Dr. Dr. Michael von Bergwelt-Baildon

Die Dissertation wurde am 28.06.2022 bei der Technischen Universität München eingereicht und durch die Fakultät für Medizin am 18.04.2023 angenommen.

The way of progress is neither swift nor easy.
Marie Curie

Table of contents

Summary

Adoptive T cell transfer of high-affinity chimeric antigen receptor (CAR)- T cells targeting CD19 has shown impressive clinical success in the treatment of some B cell malignancies. However, the development of potentially life-threatening side effects still hinders broader clinical application. Additionally, continuous and strong activation results in non-persisting and exhausted CAR-T cells, which represents one of the main reasons for tumor relapses in patients treated with CAR-T cell products. Modifications of the CAR molecule have shown to improve efficacy and persistence, but barely the toxicity profile of the respective CAR-T cells. Recently, it was suggested that the generation of low-affinity anti-CD19 CARs might represent a strategy to maintain clinical efficacy while improving safety. However, more systematic investigations on the influence of receptor binding affinities on the functionality and safety of CAR-T cells, as well as on how to optimally exploit them for adoptive T cell therapy, are still missing.

Therefore, in this thesis work, we compared two anti-CD19 CARs with a 40-fold difference in their antigen-binding strengths. Additionally, based on an *in silico* prediction, we generated 32 new CAR mutants with even lower affinities down to the range of T cell receptors (TCRs) by single amino acid exchanges in the extracellular binding domain of the low-affinity CAR. Binding strengths were determined by an in-house developed k_{off}-rate assay based on the dissociation rates of monomeric CAR:CD19 interactions. CAR-T cells were functionally characterized by canonical *in vitro* assays and *in vivo* xenograft models, whereas the safety profile was assessed in a novel humanized mouse model. In addition, we investigated the *in vivo* functionality and persistence of low and high-affinity CAR-T cell mixtures, mimicking natural immune responses with T cells expressing TCRs with different binding strengths and functionalities.

Using a conventional retroviral engineering platform, we observed that the *in vitro* functionality remained remarkably similar among a broad range of affinities. Only extremely weak binders showed reduced cytokine production and cytotoxicity. In contrast, significant differences in the anti-tumor efficacy were already observed between CAR-T cells expressing either high or low-

affinity CARs *in vivo,* and functionality was almost lost with extremely low CAR affinities. In line, lowering CAR/antigen binding correlated clearly with milder toxicities as determined in a humanized Cytokine Release Syndrome (CRS) mouse model. Although high-affinity CAR-T cells showed the best *in vivo* performance at similar cell doses, they also produced the most substantial side effects, which could be mitigated by using lower T cell doses. On the contrary, increasing doses of low-affinity CAR-T cells did not associate with exacerbated CRS. Impressively, mixing high doses of low-affinity CAR-T cells with low numbers of high-affinity CAR-T cells, which alone showed only mild CRS toxicities but limited tumor killing, demonstrated significantly improved *in vivo* functionality.

In summary, our data confirm that affinity reduction of CAR-target binding can be used to reduce the extent of CRS but can also negatively affect tumor clearance. Interestingly, transferring mixed populations of T cells engineered with high and low-affinity CARs might compensate for this limitation and offer an unprecedented clinically relevant option to reduce the risk of CRS and other toxicities during CAR-T cell treatment while still preserving therapeutic efficacy.

1 Introduction

1.1. Developments in adoptive cell therapy

For decades, cancer therapy has relied mainly on surgery, radiotherapy, and small-molecule drugs as anticancer agents. In the 1950s, hematopoietic stem cell transplantation (HSCT) paved the way for a new generation of cancer treatment[1], namely adoptive cell therapy (ACT). ACT, which uses the protective capacity of immune cells to fight different human diseases, has constantly evolved over the last 30 years. While the adoptive transfer of unedited T cells in the form of donor lymphocyte infusion (DLI)[2], virus-specific T cells[3,4] or tumor-infiltrating lymphocytes (TILs)[5] has clearly shown the therapeutic value of antigen recognition through T cells already decades ago, improvements based on T cell engineering have made cellular immunotherapies an indispensable tool in the treatment of several tumor malignancies. In particular, the adoptive transfer of T cells equipped with chimeric antigen receptors (CAR) has demonstrated great success rates and durable cancer regression of previously incurable patients[6–10]. The latest Food and Drug Administration (FDA) approval and the European Medicines Agency (EMA) approval of the first CAR-T cell therapies have set another milestone in medicine[11,12]. Currently, nearly 120 clinical trials investigate different engineered CAR-T cell products, emphasizing the importance and expectations for this rapidly evolving treatment option (clinicaltrials.gov website – 05/25/2022).

1.1.1 Transfer of genetically unmodified lymphocytes

The first and still widely used form of adoptive immunotherapy is HSCT[1]. Initially, this form of transplant was used to substitute the patient's hematopoietic system after intensive chemoradiotherapy during cancer treatment[1]. Unexpectedly, the transfer of the donor cells also eradicated the recipient's malignant cells, demonstrating that donor lymphocytes can transfer functional immunity by mediating strong anti-leukemic responses, described as graft versus leukemia (GvL) or graft versus tumor (GvT) effect[13,14].In order to exploit the full potential of tumor eradication, donor lymphocyte infusions (DLI) were performed to help patients with

relapsed chronic myelogenous leukemia[2]. This study, and also subsequent ones, reported complete cytogenetic remission, thereby strengthening the potential of adoptive cell transfer[14,15]. Unfortunately, patients who benefited from this new form of cancer treatment also suffered from graft versus host disease (GvHD)[14,15], which is a severe and even life-threatening tissue pathology mediated by donor lymphocytes attacking healthy cells of the recipient[16]. As T cell-depleted transplants could reduce GvHD but with a higher risk of tumor relapse, alloreactive T cells were identified as responsible players for GvT and GvHD[17]. Nevertheless, especially for patients with a high risk of tumor relapses, potentially developing mild and moderate forms of GvHD are tolerated to achieve long-term remission. Another complication of HSCT is that patients have a temporal window in which they are highly immunosuppressed and thus more vulnerable to severe virus infections and reactivations, as the transplanted stem cells need a particular time to restore a functional immune system[18].

An elegant way to guarantee immediate protection against latent reactivating viruses during this recovery time was the direct transfer of virus-specific T cells to immunosuppressed patients after HSCT. The first antigen-specific T cell products targeted Cytomegalovirus (CMV)[3] and Epstein-Barr virus (EBV)[4]. As both have a high prevalence in the population[19], seropositive donors have been used as a valuable source for isolating virus-specific T cells for adoptive cell transfer. Using such more defined cell products in terms of target specificity circumvented unspecific side effects like GvHD and thereby provided another critical step towards a safer therapy. Additionally, clinical studies have proven that virus-specific T cells can persist and enable a protective immune response against CMV[3,20] and EBV[21], laying the foundation for developing ACTs for treating malignant diseases.

Already in 1863, Rudolf Virchow observed that tumor-infiltrating lymphocytes (TILs) are predictive markers for improved clinical outcome[22], which was also reported in later studies[23,24]. However, it needed over 100 years until Steven Rosenberg, the pioneer of TIL therapy, showed astonishing response rates in multiple myeloma patients by exploiting isolated tumor antigen-specific T cells[25]. He and his team successfully isolated tumor-specific T cells from melanoma resections, *ex vivo* expanded, and reinfused them into the patient. Recent clinical trials have

shown objective response rates of over 50 % in metastatic melanoma patients without substantial adverse side effects caused by the T cell infusion product[6,26].

This strong protective response demonstrates again the high potency and efficacy of naturally occurring antigen-specific T cells. However, besides its promising and outstanding clinical success, TIL therapy has several downsides[27,28]. While virus-specific T cells are easy to identify, autologous T cells specific for tumor antigens are much more challenging to isolate. Indeed, TILs are generated from resected tumor tissues that are often of limited accessibility[29]; thus, clinical benefits have mainly been achieved in metastatic melanoma patients. Additionally, the number of genuinely tumor-specific T cells in patients' tumor tissue or peripheral blood is often low, and T cells are of weak functionality[30]. Tumors can shape the patient's TCR repertoire by continuous TCR triggering and immunosuppressive signals within the tumor microenvironment, leading to T cell dysfunction[32]. In addition, isolated T cells are often heterogeneous with unknown TCR specificities and functionality, and in only 50 % of the cases, a sufficient therapeutic cell dose can be expanded by *ex vivo* manufacturing.

1.1.2 Genetically re-directed T cells for adoptive immunotherapy

Introducing antigen-specific transgenic receptors directed against tumor cells into autologous (patient-derived) or allogenic (donor-derived) lymphocytes is an elegant way to overcome the limitations of adoptive cell transfer of tumor-reactive T cells. Required specificity of the T cells can be achieved by genetic engineering of transgenic T cell receptors (TCRs)[33] or chimeric antigen receptors (CARs)[34,35] targeting any chosen tumor-associated antigen (TAAs), thus avoiding limitations of the repertoire, immune tolerance, or uncertain endogenous responses. To provide the patient with the engineered cell product, T cells are collected by leukapheresis, *ex vivo* manipulated to deliver the specific receptor, expanded, and re-infused into the patient for tumor eradication[36].

While transgenic TCRs are mostly derived from natural repertoires of tumor- or pathogen-reactive T cells of either patients or healthy donors, CARs are synthetic receptors that usually comprise a single-chain variable fragment (scFv) of a tumor-specific antibody fused with

signaling molecules derived from a TCR. One of the significant advantages of synthetic CARs over TCRs is their ability to target any antigen of choice in an MHC-independent manner[37]. While transgenic TCRs only enable engineered T cells to target specific cognate peptides in a Major Histocompatibility Complex (MHC)-restricted context, CAR-T cells can also attack and eliminate target cells that have downregulated their HLA expression as an escape and immune evasion mechanism[38].

So far, clinically approved cell products have been generated by viral gene transfer of the transgenic receptor, which has to deal with safety and functionality concerns due to random genome integration and continuous receptor expression under a constitutively active promoter[39]. To better mimic the physiological expression of endogenous TCRs, which should enhance the success of long-term functionality, the recently described genome editing technology CRISPR/Cas9[40] could be an efficient tool for transgenic TCR or CAR engineering[41–43]. We and others applied this technique to disrupt the endogenous TCR to replace it with a new transgenic TCR[44] or CAR[42]. Introducing the engineered receptors into the endogenous TCR locus allows physiological expression of the receptor under the control of the endogenous promoter. Additionally, TCR mispairing can lead to diminished expression of the correctly paired newly integrated TCR, and the creation of potentially self-reactive TCRs is circumvented[44]. However, the long-term functionality of cell products manufactured using this advanced engineering method needs further investigation in clinical settings[45]. Overall, ACT has revolutionized cancer immunotherapy as it is now relatively broadly applicable and, for the first time, enables the generation of pre-clinically well-characterized T cell products with highly defined functionality.

1.1.3 Clinical experience with genetically engineered T cells

The enormous increase of clinical trials in the field of adoptive cell therapy with transgenic receptor-engineered T cells demonstrates the clinical expectations for more effective therapies coming from this new approach. While TCR-transgenic T cells have been mainly tested in melanoma[46,47] and sarcoma patients[48], most clinical trials with CAR-modified T cells are

conducted in patients with B cell malignancies[7,49]. So far, studies with TCR-engineered T cells showed only limited clinical benefits[46] and need further improvements to gain clinical success. In contrast, the application of CAR-engineered T cells targeting B cell malignancies represents a significant clinical breakthrough of adoptive cell therapy. Still, only few cell products targeting either CD19 or BCMA are approved as second-line treatments by the FDA and EMA. Therefore, the primary goal is to develop improved T cell products to efficiently treat a broader range of tumors with high efficacy and safety.

Clinical studies with TCR-transgenic T cells

In 2006, Morgan and his colleagues performed the overall first clinical study with autologous TCR-engineered T cells[46]. MART-1 specific TCR-transgenic T cells were adoptively transferred into patients suffering from metastatic melanoma. Interestingly, few patients responded to the treatment, providing a first proof-of-concept for the *in vivo* functionality of TCR-engineered T cells. However, overall response rates were relatively low and only temporary, as reported in following studies treating different types of cancer[46,50]. The use of affinity-enhanced TCRs showed some improved benefits but at the unacceptable price of severe and partially even fatal toxicities due to shared antigens with healthy tissues and loss of antigen specificity[47,51,52]. Indeed, missing selectivity of high-avidity MART-1 specific TCR transgenic T cells resulted in severe toxicities due to the disruption of Melan-1-expressing melanocytes in half of the patients[47], and the use of affinity-enhanced TCRs targeting MAGE-A3 revealed unpredictable severe side effects due to unspecific cross-reactivity and cardiotoxicity[52].

To circumvent severe off-target effects, an increasing number of clinical trials with TCR-transgenic T cells moved to target cancer antigens, which are only expressed on tumor and healthy germline tissues. The cancer antigen NY-ESO-1 (New York-esophageal squamous cell carcinoma) represents the most promising candidate, as it is mainly expressed in various cancers but not on healthy tissues except for testicular cells. In a small clinical study, at least 5 out of 17 melanoma patients and 4 out of 6 synovial sarcoma patients showed clinical

responses without developing toxicities after the treatment with NY-ESO-1-specific TCR-transgenic T cells[50].

Identifying suitable tumor targets plays an essential role in improving TCR therapies. Even though the number of pre-clinically evaluated TCR targets is constantly increasing, only a limited number of cancer antigens have been clinically targeted so far, e.g., the melanoma-related antigens MART-1[48], MAGE-A3[52], and the colorectal cancer antigen CEA[53]. Other promising targets are WT-1[54], tumor suppressor gene p53[55], and HA1-specific leukemia antigen56, but also tumor neoantigens have become a new research hotspot to provide high-quality targets for TCR therapy.

In summary, most studies provide evidence for a high clinical potential of adoptively transferred TCR-engineered T cells. However, the overall therapeutic success is still relatively low and, in most cases, only temporary, especially for the treatment of solid tumors. Therefore, finding more suitable targets and corresponding highly functional TCRs are essential to developing successful TCR-transgenic T cell therapy.

Clinical studies with CAR-engineered T cells

The clinical application of CAR-T cells revolutionized the treatment of patients with hematological malignancies[56]. Remarkable outcomes for relapsed and refractory B cell malignancies treated with CD19-directed CAR-engineered lymphocytes have moved the research of cell-based immunotherapy forward.

Initial clinical studies in the 1990s using first-generation CARs comprising only the CD3ζ activation domain for the treatment of neuroblastoma[57] and ovarian cancer[58] have been somewhat disappointing as the transferred T cells failed to mediate antitumor responses due to a lack of long-term persistence. Over the following decades, optimized second-generation CARs with an additional costimulatory domain upstream of CD3ζ, especially CD28 and 4-1BB, resulted in enormously improved antitumor efficacies and longevity of CAR-T cells[59,60]. First clinical trials using CD19-specific second-generation CAR-T cells in 2010 and 2011 pioneered by the groups of Steven Rosenberg[8] and Carl June[7,61] reported significant tumor regression

and partial remission together with B cell aplasia in lymphoma and leukemia patients. These promising results were also observed in other clinical trials, e.g., at the Fred Hutchinson Cancer Research Center, and further improved by optimized cell dosages and T cell populations[62,63]. Since then, many clinical CAR-T cell studies in patients with chemo-refractory and relapsed diseases have been conducted. In August 2017, Tisagenlecleucel (Kymriah™), an anti-CD19 CAR-T cell product, received FDA approval, followed by EMA approval one year later. Together with an extremely high response rate and overall survival rate of 81 % and 76 %[11,64], respectively, of patients with relapsed and refractory B cell acute lymphoblastic leukemia (B-ALL), it set the milestone as the first ever approved genetically modified cell product. As of March 2022, six different CAR-T cell products are approved as second-line treatments of hard-to-treat blood and bone marrow cancers, with four directed against CD19 and two CAR-T cell products targeting the B cell maturation antigen (BCMA). An overview of the different CAR-T cell products approved by the FDA and EMA until March 2022 is listed in Tab.1.

Besides ALL[11,65], anti-CD19 CAR-T cells were also approved to treat further relapsed and refractory diseases, including diffuse large B-cell lymphoma (DLBCL)[66–68] and different types of Non-Hodgkin lymphoma, e.g., transformed follicular lymphoma[68] and mantle cell lymphoma (MCL)[69,70]. In addition, CAR-T cell products targeting BCMA have received FDA approval for treating multiple myeloma (MM)[71,72]. Just recently, impressive long-term remission and persistence of CD19-targeting CAR-T cells for one decade were reported in two patients with chronic lymphocytic leukemia (CLL), which again strengthens the high potential of CAR-T cell therapy[73]. On the contrary, although initial overall response rates of CAR-T cell treatments are up to 90 % for patients with relapsed ALL and greater than 60 % for patients with relapsed NHL, intermediate follow-ups indicate a drastic decline in the durability of remission rates. For example, the progression-free five-year survival rates of patients with diffuse B-cell lymphoma or follicular lymphoma massively decrease to only 31 % and 43 %, respectively, due to tumor relapses[74]. In line, several studies highlight the antigen-escape of tumor cells and an intrinsic failure of the CAR-T cells as emerging obstacles to the curative potential of CAR-T cells. Consequently, the development of new CAR-T cell therapies targeting alternative antigens and

other co-engineering strategies, e.g., to simultaneously target several antigens, are urgently needed to guarantee the long-term functionality of CAR-T cells.

Tab. 1 Overview of FDA and EMA-approved CAR-T cell products.
ORR = overall response rate, CR = complete remission, OS = overall survival, PFS = progression free survival

	KYMRIAH®		YESCARTA®	TECARTUS®		BREYANZI®	ABECMA™	CARVYKTI™
Generic name	Tisagenlecleucel[64,66]		Axicabtagene Ciloleucel[12,68]	Brexucabtagene Autoleucel[65,70]		Lisocabtagene Maraleucel[67]	Idecabtagene Vicleucel[71,75]	Ciltacabtagene Autoleucel[72]
Company	Novartis		Kite/Gilead	Kite/Gilead		BMS	BMS	Janssen
Target epitope	CD19		CD19	CD19		CD19	BCMA	BCMA
FDA approved indications	R/R B-ALL	R/R DLBCL	R/R DLBCL	R/R MCL	R/R B-ALL	R/R DLBCL	R/R MM	R/R MM
FDA approval	2017	2018	2017	2020	2021	2021	2021	2022
EMA approval	2018	2018	2018	2020	n/a	pending	conditional authorization	n/a
Underlying clinical study	ELIANA	JULIET	ZUMA-1	ZUMA-2	ZUMA-3	TRANSCEND	KarMMa	CARTITUDE-1
Number of patients	75	93	101	68	55	269	128	97
ORR	81%	52%	82%	93%	84%	73%	73%	97%
CR	59%	40%	40%	67%	71%	53%	33%	67%
12-month OS	76%	49%	52 %	61%	71%	58%	78%	89%
PFS	50 % (12 months)	65 % (12 months)	n/a	83 % (12 months)	58 % (6 months)	44 % (12 months)	n/a	77 % (12 months)

Besides BCMA and CD19, additional novel TAAs are under investigation to broaden the spectrum of available CAR-T cells also toward solid tumors. The most prominent ones are HER2[76], EGFRvIII[77], ROR1[78], MUC16[79], and NKG2D[80] for treating metastatic colorectal cancer, recurrent glioblastoma, lung cancer, multiple myeloma, or triple-negative breast cancer. In contrast to the use in blood-born cancers, CAR-T cells need to migrate to the tumor

site and bypass complex immune suppression mechanisms of the tumor microenvironment in solid malignancies[81]. Unfortunately, the clinical efficacy has been limited so far. In clinical trials with mesothelin-specific CAR-T cells, transferred cells were detected in the tumor but caused only small lesions and tumor shrinkage[82,83]. Another study with sarcoma patients treated with HER2-specific CAR-T cells reported detectable CAR-T cells over six weeks, but again no considerable tumor killing[84]. Even though HER2 was one of the most promising targets due to its overexpression in many different types of cancer, another case study reported strong side effects with HER2-specific CAR-T cells due to the recognition of low HER2 expression levels on lung epithelial cells[85]. Altogether, these results indicate that overexpressed TAAs on solid tumors can serve as targets for CAR-T cells. However, enormous improvements are necessary to overcome the main limitations of poor antitumor activity and safety in solid tumors. Advanced clinical studies try to prevent exhaustion and dysfunction of the infused T cells by combining CAR-T cells with checkpoint inhibitors (e.g., anti-CTLA-4 or anti-PD-1 antibodies)[86], while *in vivo* persistence might be improved by the use of immune-stimulatory cytokines(e.g., IL-12, IL-15, IL-7)[87]. Furthermore, multi-antigen targeted CAR-T cells are currently tested for their ability to overcome antigen-escape relapses after single antigen-directed CAR-T cell treatment[88], while T cell co-engineering strategies are established to improve long-term functionality and survival of CAR-T cells by delaying effector T cell differentiation and exhaustion[42]. Recently, new CAR structures more similar to endogenous TCRs, called HLA-independent T cell receptors (HITs), have been proposed to target cell surface antigens of low abundance and thus make CAR-T cells more sensitive[89].

Taken together, these findings highlight the enormous power and therapeutic value of genetically engineered T cells for treating several tumors with poor prognosis but also clearly underline the importance of further necessary improvements to guarantee therapeutic efficacy and safety.

1.2 Risks and side effects of CAR-T cell therapy

Although impressive outcomes in B cell malignancies have been achieved with CAR-T cell therapy, most of the observed clinical benefits also come at some costs. In up to one-third of the patients, the transfer of CAR-T cells is directly associated with severe, potentially even life-threatening toxicities, due to the induction of a potent immune response[90]. The development of acute toxicities is still difficult to predict and thereby complicates a broader application of the adoptive transfer of engineered T cells. Although clinical studies differ in their CAR-T cell products, patient's characteristics and disease burden, observed toxicities are strikingly similar. The most frequently observed CAR-T cell-related side effects are cytokine release syndrome (CRS), immune effector cell-associated neurotoxicity syndrome (ICAN), also often referred to as neurotoxicity, and on-target/off-tumor effects[90,91]. Even though significant toxicities are reversible in most cases, they must be promptly recognized and managed via early medical interventions[92].

1.2.1 Cytokine release syndrome

The earliest occurring and most common CAR-T cell-related adverse event with a potentially fatal outcome is cytokine release syndrome (CRS)[90]. It typically begins within the first week after CAR-T cell administration and is mainly characterized by strong CAR-T cell activation and expansion together with an enormous release of inflammatory cytokines in the peripheral blood due to a strong induction of the host immune system[93].

Directly after infusion, CAR-T cells start trafficking to the tumor site and become activated by CAR-mediated recognition of the antigen-expressing target cells. Afterward, depending on the activation strength, T cells start to massively proliferate while secreting high amounts of cytokines, which triggers a cascade of reactions leading to CRS. Especially the release of INF-γ and TNF-α recruits and activates immune and non-immune bystander cells within the tumor environment. Also, these cells release pro-inflammatory cytokines, and large amounts of IL-6 produced by macrophages and endothelial cells subsequently activate T cells and other immune cells, initiating a storm of inflammatory cytokines which overwhelms the counter-

regulatory homeostatic mechanism. The interactions between CAR-T cells and myeloid cells at the tumor site have been reported to be mainly responsible for increased levels of pathological cytokines[94]. While activated T cells produce chemokines and cytokines, including IL-2, IL-2Ra, IFN-γ, IL-6, IL-1R, and GMCSF, macrophages are the primary producers of IL-6 and IL-1[95].

On the clinical site, the first symptoms of CRS are usually mild fever and constitutional symptoms like malaise and arthralgia. However, they can rapidly progress to severe forms of CRS represented by systemic inflammatory responses with widespread life-threatening organ toxicities, ranging from cardiovascular disorders with endothelial injuries in multiple tissues with hypotension, hypoxia, and respiratory compromise to multi-organ failure[96]. Most common interventions to treat CAR-T cell-related CRS involve corticosteroids and the monoclonal antibody anti-IL-6 tocilizumab[97]. Even though the application of corticosteroids was proven to be effective in managing CRS, these anti-inflammatory drugs are also immunosuppressive for the therapeutic CAR-T cells and thereby can limit the efficacy of CAR-T cell therapy[98]. On the contrary, as CRS is associated with increased levels of IL-6, the IL-6 receptor antagonist tocilizumab has shown impressive and immediate efficacies in resolving CRS-related symptoms in most patients[99] without compromising the clinical efficacy of the transferred CAR-T cells[11]. Current investigations are ongoing to define the optimal timing of the administration. Recent animal models have also shown an important role for IL-1 signaling in the development of CRS[94,95]. Therefore, the administration of anakinra, a recombinant IL-1 receptor antagonist, has been suggested as a third-line treatment for refractory CRS. Its application has shown remarkable efficacy in managing CRS in humanized mouse models[95]. However, in a clinical study with only a few patients, anakinra revealed only poor outcomes when used to treat CRS[100]. Therefore, more clinical studies are necessary to clarify its efficacy in CAR-T cell therapies.

Different factors can influence the development of CRS, including tumor burden, CAR-T cell dosage, and the use of lymphodepletion chemotherapy[101–103]. Additionally, standard clinical rates of severe inflammation and elevated levels of specific inflammatory cytokines like IFN-γ,

IL-2R, and IL-6 can indicate the patient's risk potential[93,104], although they are not sufficient to predict CRS severity. Therefore, fine-tuning CAR-T cell activation to balance cytokine secretion is a relevant option for manufacturing CAR-T cells with powerful anti-tumor efficacy without an exceeding release of cytokines.

1.2.2 Neurological side effects

Neurological toxicities represent the second main CAR-related acute side effect[90], with incidences ranging from 2 % to 64 %. They generally occur early after CAR-T cell infusion once the symptoms of CRS have subsided, but in a few cases, they have also been described to coincide with CRS or weeks later[70]. Consequently, CRS is considered an initiating event or cofactor of neurotoxicity. In a meta-analysis of 1,860 patients to determine the safety of CAR-T cell products, severe CRS was reported to occur in a range between 19 % to 55 % depending on the type of tumor, type of CAR-T cell product, and type of grading system. In contrast, 2,079 patients were included in the ICANS evaluation, and overall between 10 % to 31 % developed severe ICANS[105].

Neurological adverse events are numerous and typically manifest as toxic encephalopathy. The first clinical signs include aphasias, visual and auditory hallucinations, and impaired fine motor skills, which can further evolve into neurological complications like seizures and rapid-onset cerebral edema. As patients developing cerebral edema are often unresponsive to medical interventions, CAR-T cell therapy has caused several fatal events[101].

Although an increasing number of studies has tried to understand the underlying mechanisms, the pathophysiology of neurotoxicity remains unclear and is still differentially discussed. Numerous clinical trials have shown that the presence of tumor cells in the central nervous system is not required for the development of ICANS[90], while increased levels of various pro-inflammatory cytokines and elevated numbers of T cells in the cerebrospinal fluid (CSF) are associated with the risk of neurological side effects[106]. Interestingly, increased levels of both endogenous immune cells, engineered CAR-T cells, and peripherally activated monocytes

were detected in the CSF of patients with severe ICANS, indicating a general loss of integrity of the blood-brain barrier (BBB)[107].

Like CRS, neurotoxicity is reversible in most patients with no permanent neurological deficits if promptly treated after the onset[96]. As the mechanisms behind neurotoxicity are less well understood, it is mainly managed with corticosteroids, which dampens CAR-T cell function[92]. In contrast to the treatment of CRS, the administration of tocilizumab has not improved neurological toxicities, probably due to its disability to penetrate the BBB and reduction of the transient increase in IL-6 levels in the central nervous system after its administration[92]. In contrast, IL-1R blockade with anakinra improved clinical signs of inflammation and reduced cytokine levels of refractory CRS and ICANS, as it can cross the BBB[95,100,108]. However, it is still difficult to ascribe the reduction of neurotoxicity only to anakinra, as patients were treated with a mix of corticosteroids. Therefore, future clinical trials are necessary to better evaluate the function of current interventions for the management of CAR-T cell-related side effects, especially regarding neurological toxicities.

1.2.3 Hematological toxicities

Another major clinical challenge of adoptive CAR-T cell therapy is the hematotoxicity of the transferred CAR-T cell product[109–112]. While protracted cytopenia of grade 3 or higher was reported in 20 - 40 % of patients[113], cytopenia beyond 90 days occurs in 33 % of patients[114]. Although early clinical trials have been investigating the directly occurring CAR-T cell-related adverse events Cytokine-Release-Syndrome and Neurotoxicity, the understanding and knowledge about CAR-T cell-associated cytopenia is still limited. However, in recent years, the interest in hematological toxicities is constantly rising, as more and more long-term follow-ups of CAR-T cell-treated patients with relapsed and refractory hematological malignancies, also report prolonged and recurrent cytopenia. Especially as it can result in further complications like increased infectious complications, diminished response to vaccines, and hemorrhage[115–117], it has emerged as another very important adverse event of CAR-T cell therapy.

In general, hematologic toxicity (neutropenia, anemia, thrombocytopenia) can be bi- or triphasic, self-limited, or late appearing[112,118], and its recovery can take weeks to months.

The first phase of early cytopenias occurs within 3 – 4 weeks after CAR-T cell transfer, which has been shown to be related to the myelosuppressive effect of lymphodepletion regimens like chemo- or radiotherapy[70,71,118–120].

However, prolonged and recurrent cytopenias (> 90 days post–CAR T-cell therapy) have other implicating factors than the myelotoxic effect of the pretreatment conditioning alone. It has been reported that CRS, high tumor burden, and elevated inflammatory markers may induce severe cytopenias and impact hematopoietic recovery[111,121]. Besides bacterial, fungal, or viral infections that occur due to the immunosuppressive setting, which represent the most common reasons for non-relapse mortality after CAR-T cell therapy, can lead to post–CAR T-cell therapy cytopenias[122]. Additionally, clonal hematopoiesis or the development of myelodysplastic syndrome can be potential reasons for developing cytopenias after CAR T-cell transfer[123].

Overall, cytopenias are universally observed in patients with various hematologic malignancies[71] and are more severe in heavily pretreated patients or after the use of alkylating agents[123]. Besides, hematotoxicities have been associated with all types of CAR constructs. However, whether there is a correlation between the expansion and persistence of the CAR-T cell product[110] and the different costimulatory domains[124] is still under debate.

Although several management strategies to minimize hematologic side effects have been proposed, including hematopoietic stem cell transfusions[125], prophylactic antivirals, antimicrobials and antifungals, granulocyte colony-stimulating factors (G-CSF)[126], and post–CAR T-cell therapy immunization, only limited to no data are available which demonstrate a clear benefit of these treatment options.

Therefore, late cytopenia still poses a clinical challenge in diagnosis and risk management, and defining a potential mitigation strategy remains elusive[118].

Rejeski[112] and colleagues tried identifying predictive biomarkers in a multicenter, retrospective analysis of over 250 patients with relapsed refractory large B cell lymphoma receiving CD19

CAR-T cells. Based on this screen, they developed a CAR-HEMATOX model, which identified predictive biomarkers of hematotoxicity and which could be used as a risk-stratification tool for patients.

However, additional prospective studies investigating the pathophysiology of late-stage cytopenias will be required to investigate different factors of cytopenia incidence further to overcome this late-occurring toxicity after CAR-T cell transfer.

1.2.4 On-target/off-tumor toxicities

On-target/off-tumor toxicities describe side effects due to the recognition of target molecules by CAR-T cells on healthy tissues other than the targeted malignant cells[91]. It commonly occurs with all types of CAR-T cells, as most CAR-specific antigens are only over- and not exclusively expressed on tumor cells and thereby shared with healthy tissues. The severity of CAR-T cell-related on-target/off-tumor side effects depend on the dispensability of the targeted tissue. Therefore, on-target/off-tumor side effects are less severe in hematological malignancies, where B cell aplasia represents a predicted and modest on-target effect for patients treated with CD19-specific CAR-T cells[127], as CD19 is restricted to lymphocytes of the B-cell lineage[128]. Indeed, consequences of B cell aplasia, like hypogammaglobulinemia, can be effectively managed by administering well-tolerated immunoglobulins without enormous restrictions for the patients[103]. Additionally, long-term B cell aplasia can be used as a marker for successful engraftment and persistence of CAR-T cells. Hence, early loss of B cell aplasia after CD19 CAR-T cell therapy is associated with an increased risk of tumor relapse[129]. However, it has been described that CD19 is also expressed in brain mural cells, which could be one reason for off-tumor neurotoxicity in CD19-directed therapies[130].

In contrast, treating solid tumors with CAR-T cells specific for HER2[85] or CAIX[131] had severe and fatal outcomes. CAR-T cells targeting HER2 in a patient with metastatic colorectal cancer also recognized HER2 low expressing lung epithelial cells leading to respiratory distress followed by pulmonary edema[85]. In another clinical study enrolling patients with renal cell carcinoma, CAIX redirected CAR-T cells to eradicate epithelial cells in liver bile ducts, which

were unknown to express CAIX[131]. In summary, on-target/off-tumor toxicities represent only a limited problem for the adoptive transfer of CD19-targeting CAR-T cells. However, it will be necessary to rigidly monitor patients treated with CAR-T cells targeting novel antigens in case of any unpredicted on-target/off-tumor toxicities.

1.2.4 Tumor relapses after CAR-T cell therapy

Despite the favorable clinical response rates of relapsed and refractory cancer patients after CD19-CAR T cell transfer, many patients still relapse. While it was reported that the treatment of pediatric patients with refractory and relapsed ALL treated with anti-CD19 CAR-T cells showed an overall response rate of 90%, the relapse-free survival after six months dropped down to 66.4 %, indicating a high relapse rate already briefly after the infusion of the CAR-T cell product[132]. The result was also confirmed for other cancer types with similarly increasing relapse rates, especially in the longer follow-up. While the five-year progression-free survival of patients with follicular lymphoma was 43 %, only 31 % of patients with DLBCL were still progression-free at five years[74]. Two types of relapses were mainly recognized: CD19 positive and CD19 negative relapses. While $CD19^+$ relapses can occur due to poor T cell function and persistence, $CD19^-$ relapses in most cases result from evasion of specific antigen-negative tumor cell variants. The frequency of CD19 epitope loss was estimated between 10 % to 20 % of pediatric B-ALL patients treated with CD19 targeting CAR-T cells[103]. Therefore, the use of multi-antigen targeting CAR-T cells is currently under investigation in order to avoid this mechanism of tumor escape.

1.2.5 Engineered safety tools for adoptive T cell therapy

CD19-targeting CAR-T therapy for treating malignant diseases with currently poor outcomes is still the most widely used clinical application of adoptive T cell transfer. Therefore, most clinical research is done in this area, and results are mainly reported for this type of therapy. Nevertheless, adverse events and toxicities have been observed in multiple clinical studies for different CAR-T cell specificities, highlighting the importance of improving CAR-T cell products'

safety to broaden their applicability. While the described approaches try to mitigate the symptoms of developing side effects, other approaches try to engineer therapeutic CAR-T cells in a way that directly tackles the underlying cause.

One efficient safety strategy to specifically kill the transferred T cells in case of the development of adverse effects is so-called “OFF-switches”. The additional incorporation of these genes enables the elimination of over-activated CAR-T cells by administration of external molecules. Until 2022, two suicide genes have been tested clinically. Incorporating the herpes simplex virus thymidine kinase (HSV-TK) represents the first investigated safety switch[133,134], which eliminates dividing cells by administering ganciclovir. However, slow response rates and immunogenicity[135] make the HSV-TK only a suboptimal approach for safer CAR-T cell therapy. The second clinically tested safety switch is iCasp9, representing a safe, effective and non-immunogenic apoptosis system[136]. In case of adverse events, the essential chemical inducer for dimerization can be easily applied intravenously, activating the newly incorporated caspase and leading to cell apoptosis. After many promising preclinical studies in treating B cell lymphoid malignancies, results of first clinical studies are awaited with great excitement.

Another strategy to eliminate toxic CAR-T cells is using clinically approved mAbs to target co-expressed, truncated versions of cell-surface proteins. The administration of monoclonal antibodies can initiate antibody-dependent cellular cytotoxicity (ADCC) or complement-dependent cytotoxicity[137], which results in permanent ablation of the co-engineered CAR-T cells. The two mainly tested proteins so far are truncated versions of CD20 (recognized by rituximab)[138] and the human epidermal growth factor receptor (EGFRt) (recognized by Cetuximab)[139]. Even though several phase I clinical trials have been initiated so far, it is still too early to predict whether this type of safety strategy will be conventionally applied in adoptive cell therapy.

Although “OFF-switches” enable fast elimination of CAR-T cells whenever toxicities occur in patients, they also permanently eliminate the transferred cells, thereby hindering long-term antitumor efficacy. Therefore, reversible mechanisms to turn CAR-T cells on and off without eradicating the transferred cells have been developed. One recent approach is called “ON-

switches"[140], in which an inducible system is connected to the expression of the CAR transgene. By administration of dimerizing small molecules, the surface expression of the CAR is initiated, and the CAR-T cell is activated. In the event of severe adverse reactions, the administration of the small molecule can be immediately discontinued, and the expression of the CAR on the T cell will return to baseline[140]. Instead of eliminating over-reacting CAR-T cells, this switch can precisely control cells in terms of timing and dosage and thus improves their safety. However, it can take several days to slow down the CAR-T cells, which can be critical for fast-developing side effects[141].

Also, the tyrosine kinase inhibitor dasatinib has been shown to reversibly inhibit the proliferation and cytokine production of CAR-T cells in preclinical studies[142]. It mediates the inhibition of the phosphorylation of the lymphocyte-specific tyrosine kinase and thereby blocks T cell signal transduction. Although dasatinib outperformed corticosteroids in preclinical models, it is not clear whether the use as an emergency tool would be beneficial for the patients, as dasatinib was less efficient at inhibiting already activated CAR-T cells.

In addition, several strategies to prevent antigen escape and off-target effects by multi-targeting antigens have also been tested so far[88]. While dual CAR-T cells combine different CARs recognizing different TAAs in a single CAR-T cell, tandem and trivalent CAR-T cells target distinct TAAs by linking two or more different CARs in a tandem structure. Another approach combines conventional activating constructs with inhibitory CARs[143]. Most recently, specific logic-gate operations to decrease off-tumor effects have been developed[144]. Here, OR-, AND-, and NOT-gate transmission patterns are used to ensure sufficient and specific signaling of the activated CAR-T cell. Currently, additional diverse logic-gate strategies are developed to combine them with multi-antigen targeting CAR-T cells.

Overall, the mentioned strategies represent a first try to optimize the safety of CAR-T cell therapy. However, their success is still quite uncertain as most engineering approaches need either too long to be fully activated or constant activation by additional drugs. Logic-gate operations might help to improve the specificity, but overall no approach can solve the problem of the development of acute CAR-T cell-related toxicities such as CRS and ICANS. Therefore,

the most promising solution is to fine-tune the binding strength of the CAR itself in order to decrease potential severe side effects. Here, the overall efficacy of the CAR-T cells can still be maintained, but a reduced activation potential can, in return, lower the release of inflammatory cytokines. In the end, finding an optimal binding affinity of the CAR-T cell to its target will slow down the cascade of the cytokine storm, which represents the main reason for acute CAR-T cell-related toxicities and thereby enables the generation of efficient and exceptionally safe next-generation CAR-T cells.

1.3 Structure and function of the CAR complex

1.3.1 The structure of chimeric antigen receptors

CARs are synthetic recombinant receptor constructs organized on a gene set coding for five different components. As they combine parts of a naturally occurring TCR for activation with parts of an antibody for target recognition, they were initially called T-bodies by Eshhar and collegues[37]. However, since then, the term for these artificial constructs has been Chimeric Antigen Receptor.

The extracellular antigen binding domain of CAR receptors usually consists of a mAb-derived single-chain variable fragment (scFv), which facilitates specific recognition and binding of target TAAs on the tumor cells. An scFv consists of the immunoglobulin light and heavy chain variable regions (V_L, V_H) connected by a peptide linker sequence. Both variable domains comprise three hypervariable parts termed complementarity determining regions (CDR), surrounded by highly conserved framework regions. Individual scFvs are either derived from murine or humanized antibodies or synthesized and screened via phage display libraries.

Similar to the natural TCR/CD3 complex, CARs are also equipped with an intracellular activating domain which enables signal transduction and T cell activation after antigen recognition[37]. In addition to the intracellular CD3ζ domain, the CAR sequence is further extended with co-stimulatory signaling domains. The additional integration of either CD28[124] or 4-1BB[60] was shown to enable target-specific killing and expansion of the corresponding T cell after tumor antigen recognition. It was also observed that the choice of the particular co-stimulatory domain influences the cytokine secretion profile and proliferation capacity of the corresponding CAR-T cell[145,146].

A hinge and a transmembrane domain covalently link the extracellular binding and intracellular signaling domains of the CAR molecule. While the hinge region enables spatial arrangement and flexibility of the extracellular binding domain of the CAR[147], the transmembrane domain, as the name states, functions as an anchor of the CAR into the cell membrane. So far, no optimal spacer or hinge length could be determined, as it seems highly dependent on the target epitope and its location. Modifying this region can significantly impact the receptor stability and

substrate binding strength, as CARs targeting different targets showed the best functionalities with different hinge lengths[148].

Due to its unique structure, incorporating the CAR facilitates tumor targeting of the corresponding T cell in an HLA-independent manner[37], which improves otherwise poor T cell responses due to the downregulation of tumor-associated pMHC complexes. In contrast to natural TCRs, CARs do not need to be matched to the patient's immune type, and a single CAR construct can be used to target all patients.

1.3.2 Evolution and next-generation CARs

The approach to combining an antibody-derived extracellular domain connected by a hinge and transmembrane domain to a cytoplasmic CD3ζ signaling domain to enable the killing of tumor cells was first pioneered in the 1980s by Gross and colleagues[37]. Since then, the CAR design has evolved through different generations via a largely empiric process to improve its signaling output.

First-generation CARs did not have costimulatory elements incorporated, which later proved to be necessary for complete T cell activation[124]. Although these CAR-T cells could generate a cytotoxic response in murine models[149], the clinical outcome was more than disappointing[131,150]. As the CD3ζ domain alone was insufficient to sustain T cell functionality in primary T cells, the endodomain of the CAR was further extended with either one or two costimulatory domains in subsequent second and third-generation CARs[151,152]. As known from endogenous TCRs, one activation signal is not enough to sufficiently activate T cells, and therefore the additional fusion of either CD28[145] or 4-1BB[60] to their intracellular domain improved CAR-T cell persistence and cytotoxicity. A clinical trial using CAR-T cells incorporating CD28 demonstrated that second-generation CAR-T cells expanded and persisted better than autologous T cells transduced with a CAR lacking a costimulatory domain[124]. Also, a pre-clinical study using CARs containing the 4-1BB co-stimulatory domain revealed superior efficacy and improved persistence in a primary human ALL xenograft model[60].

However, it was observed that the choice of the particular co-stimulatory domain influences the cytokine secretion profile and proliferation capacity of the corresponding CAR-T cell[153]. As known from endogenous T cell behavior, CD28 is particularly important in the early activation of naïve T cells, while 4-1BB is associated as fundamental for memory formation and persistence[154]. So far, all clinically approved CAR-T cell products belong to the group of second-generation CARs, and their backbone encompasses either CD28 or 4-1BB as a costimulatory domain together with their corresponding advantages and disadvantages.

In third-generation CARs, multiple costimulatory domains are placed in tandem. Pre-clinical *in vitro* studies exhibited superior proliferation and cytotoxicity compared to second-generation CARs transduced with a CD28 co-stimulatory domain[155]. However, limited data have been published on the clinical experience using these constructs so far[156].

The latest generation of CARs (fourth generation) so far includes armored CARs and TRUCKs (T cells redirected for universal cytokine-mediated killing)[157,158], which were engineered to provide local cytokine secretion (such as IL-4, IL-2, Il-7, IL-15, and IL-21) to attract more immune cells and to enhance the infiltration, persistence and antitumor activity of the associated CAR-T cells. Although these new generation CARs already showed improved functionality in pre-clinical animal models, long-term side effects and functionality need further investigation in clinical settings.

1.4 Impact of receptor affinity on T cell function and safety

1.4.1 Definitions of receptor binding strength

The functionality of a T cell is mainly determined by its receptor-antigen interactions, which can be defined by the terms ‘affinity’, ‘TCR avidity’, ‘structural avidity’, and ‘functional avidity’. With this, the extent of TCR-mediated signal transduction (hours) and the duration of the TCR/pMHC binding half-lives (seconds) are critical parameters for activating the associated T cell[159].

The TCR/pMHC affinity represents the binding strength of a single receptor (e.g., the TCR) to its cognate antigen (e.g., the pMHC complex) and is reciprocally related to the binding kinetics of the receptor. The affinity can be described by the dissociation constant (K_D), which is precisely calculated by the relation of the association (k_{on}-rate) and dissociation (k_{off}-rate) of the pMHC-molecule and the corresponding TCR[160]. These parameters are typically measured by surface plasmon resonance (SPR) spectroscopy, where TCR and pMHC molecules are recombinantly expressed to determine their monomeric interactions. In addition, the half-life ($t_{1/2}$) of the TCR/pMHC interaction describes the rate at which the TCR dissociates from the pMHC complex and is related to the dissociation constant by the equation $t_{1/2} = \ln 2/k_{off}$[161]. In contrast, the TCR avidity describes the overall strength of multiple interactions between the T cell and its target cell[162]. Analyzing the TCR avidity of a cell is more challenging, as it is influenced by different parameters, in particular the affinity of each TCR and their structural arrangement in combination with the number of receptors (TCR expression level) and co-receptors (CD4 and CD8) on the cell surface. Since the affinity of a TCR does not fully represent the actual TCR binding strength *in vivo*, as co-receptors always support the TCR binding, our group has established a flow cytometry-based method to determine the structural avidity of a TCR[163–165] in the cellular context. Here, the monomeric TCR/pMHC dissociation rates (k_{off}-rate) of living T cells, including the CD8 co-receptor, are analyzed. Finally, the functional avidity of a TCR is defined as the overall sensitivity and functional response of the T cell to the pMHC antigen density and its ability to respond to a given concentration of cognate peptide antigen[166]. It comprises the relative affinity and structural avidity of the TCR, as well as

the subsequent efficiency of the downstream signal transduction. In summary, the binding strength of a TCR, as the fingerprint of a T cell, directly influences activation, expansion, and differentiation[167,168], while other parameters, e.g., phenotype and TCR density, contribute to the overall functionality[163].

1.4.2 Influence of transgenic receptor binding strength on T cell functionality

TCRs of mature T cells are of relatively low affinity (1-100 µM) for their cognate pMHC ligands, with fast k_{off}-rates[169]. Consistent with the low-affinity and generally quick dissociation rate of most TCR/pMHC interactions, T cells display extraordinary sensitivity and specificity for even very low antigen levels. T cells work along a serial triggering model to reach sufficiently high activation levels despite short interaction times, suggesting that multiple TCRs on the cell surface must be sequentially bound by a single pMHC[170].

As increased affinities within the natural range of TCRs have been demonstrated to directly correlate with accelerated T cell functionality against viruses[163] and tumors[171], high TCR affinities are considered to result in stronger T cell responses[172]. On the contrary, low binding strengths and too fast dissociation rates of the pMHC molecule and the TCR negatively influence the T cell functionality, as they prevent productive TCR triggering. Therefore, mutational screens of the CDR regions of the TCR have been used to generate even improved supraphysiological TCRs[173] with significantly higher avidity than their natural counterparts. Interestingly, increasing the TCR affinity beyond 10 µM or even into the range of nanomolarity did not further improve the *in vitro* and *in vivo* function of the corresponding T cell[169,174]. It even seems that high-affinity TCRs follow a bell-shaped behavior, suggesting that increasing receptor affinities beyond a certain threshold could not improve but even reduces T cell functionality[175,176]. A main reason for this phenomenon might be that enhanced binding strengths exceed the optimal interaction time and force the T cell into prolonged contact times with its cognate antigen[177], decreasing the efficiency of TCR serial engagement.

Furthermore, supraphysiological interactions have been shown to lead to cross-reactivity of T cells with self-derived peptides[173]. Indeed, missing selectivity of high avidity TCR-transgenic T

cells has been noticed to induce severe side effects in patients in several clinical studies[47,52]. Conversely, T cells with lower affinities within the physiological TCR affinity range displayed better selectivity as they were only activated by tumor cells overexpressing the target antigen and not by healthy cells.

In contrast to TCRs which possess affinities in the µM range, conventionally used scFvs of CARs are preferable selected from high-affinity mAbs in the range of medium to low nM, as they were shown to induce strong activation of the regarding T cell[178]. Indeed, all currently FDA-approved CD19 targeting CAR-T cell products rely on the high-affinity anti-CD19 antibody clone FMC63[179], which has an affinity several magnitudes higher than TCR/pMHC interactions[177]. Comparable to super-high-affinity TCRs, few studies have also investigated whether an increase in affinity affects CAR-mediated T cell functionality. While affinity-enhanced CAR-T cells targeting HER-2 revealed improved *in vitro* T cell activation with an increased affinity of the CAR[60], also ROR1-specific CAR-T cells showed superior functionality represented by higher cytokine release and more significant proliferation of the stimulated T cells[168]. However, as observed with TCR-transgenic T cells, increased affinity beyond a particular affinity ceiling (in this case, 10^{-8} M) did not improve T cell function but even impaired CAR-T cell functionality[60]. CAR-T cells targeting CD20 with excessively high affinity above the mentioned threshold were susceptible to activation-induced cell death (AICD) upon engagement to their target[162]. In line with the results of TCR studies, non-specific target recognition was observed with increased binding strength of the CAR. The use of high-affinity HER2-specific CAR-T cells in a clinical setting resulted in decreased selectivity for the tumor target[181] and thus lead to the development of associated on-target/off-tumor toxicities of the patients. Also few preclinical studies support the concept that low-affinity CAR-T cells can avoid potential off-tumor toxicities, as they are more selective in killing tumor cells with high antigen load, instead of healthy cells expressing only low amounts of antigen[178].

Overall, the influence of receptor affinities on the functionality of transgenic TCR and CAR-T cells are comparable. For both engineered T cell products, an increase in affinity can enhance the functionality, however, only until a certain threshold. Affinities above this ceiling result in

strongly reduced T cell function and increased toxicities. Therefore, careful selection of optimal transgenic receptors is necessary to guarantee a highly functional and safe adoptive (CAR-) T cell therapy.

1.4.3 Adaptation of artificial CAR-T cell therapy to optimal natural T cell responses

Basic interactions of TCRs and their cognate antigens have been intensively investigated, and the findings of optimal TCR avidity can be easily implemented into the concept of adoptive T cell therapy. However, the correlation between CAR binding strengths and optimal CAR-T cell functionality seems more complex, and little is known so far. So far, all approved high-affinity CAR-T cells have been quite promising in treating B cell malignancies. However, significant downsides such as loss of long-term functionality and the development of severe acute side effects need to be tackled to provide clinically efficient and safe T cell products. While an increase of TCR avidity in the physiological range results in better functionality of the corresponding T cell, it has only been shown that an upper-affinity ceiling for CARs exists and not whether reduced CAR affinities in the range of TCRs could have major advantages for the overall CAR-T cell functionality, but also safety.

As already described, the binding and interaction of a receptor to its specific target is pivotal in regulating the activity and specificity of the T cell by starting a cascade of intracellular signals leading to cytokine production, proliferation, and cytotoxicity. This relationship becomes especially interesting as, despite their much lower affinity than CARs, naturally occurring T cells possess strong long-term functionality with a high safety profile. It has also been shown that lower-affinity TCRs can have superior sensitivity and efficacy compared to high-affinity CARs targeting the same antigen[182]. Endogenous TCRs have evolved with fast dissociation rates, which enable serial triggering and high sensitivity towards the cognate pMHC molecule. High-affinity CARs, however, have enormously prolonged dissociation rates, leading to a reduction of their antigen sensitivity. Since CAR affinities are over several magnitudes higher than TCR affinities, it is pretty intriguing to investigate whether lowering the CAR affinity could reveal an optimal affinity window of CARs with a good balance of functionality and safety.

One first clinical study reported that anti-CD19 CAR-T cells expressing a low-affinity scFv, called CAT, obtained good tumor-killing efficacy without inducing severe CRS in pediatric patients with ALL[25,183]. Additionally, compared to already published studies using Tisagenlecleucel, an approved high-affinity anti-CD19 CAR-T cell product (clone: FMC63), they observed enhanced expansion and prolonged persistence of their low-affinity CAR-T cells. However, as the patients treated with the low-affinity CAR-T cell product had only low tumor burdens (high tumor burden is a major risk factor for developing CAR-associated side effects), conclusions regarding improved clinical toxicity profiles can not be deducted yet.

Therefore, the question remains how and if lower affinities could improve CAR-T cell therapy. One major fear is that, although low-affinity CAR-T cells are less susceptible to over-activation and lost selectivity, complete tumor eradication may not be guaranteed. Indeed, it has already been claimed that while low-affinity Herceptin-based CAR-T cells revealed a better safety profile in sarcoma patients than high-affinity CAR-T cells, only modest clinical results were achieved. This difference in the functional affinity windows of CARs and TCRs could be due to several factors. Most importantly, although TCRs possess relatively low affinities in the µM range, it is compensated by different aspects, e.g., co-receptor help, serial triggering, and high sensitivity. In contrast, the scFv, integrated into the CAR structure, is out of context from its natural property. Therefore, it is not clear yet, whether additional binding help by other receptors is happening.

Despite major differences between TCRs and CARs, the receptor affinity is likely to represent a major parameter in tuning engineered T cell products for an optimal balance between safety and efficacy. The gap between TCR and CAR affinity currently explored in clinical trials opens a big range in which CAR affinities could be reduced to find an optimal window where lower affinity with fewer toxicities co-incidences with good functionality. Therefore, it is crucial to understand the underlying mechanisms of the effects of reduced CAR affinity on the functionality and toxicity of the corresponding CAR-T cell.

In addition to an optimal affinity range comparable to naturally occurring TCRs, other strategies could be applied to mimic an optimal natural immune response with CAR-T cells. The human

immune system has evolved into a powerful defense mechanism to eliminate a huge variety of pathogens over a long time. Natural T cell responses comprise a heterogeneous repertoire of TCRs with a broad range of affinities and avidities for a given antigen. This diversity of different TCR affinities is essential, as each has its unique role during the development of the immune response[184]. Lower-avidity TCRs are particularly important during the early phase of an acute immune response, while high avidity T cells start to dominate over time due to stronger proliferation and clonal expansion[168]. Especially upon antigen re-exposure (recall responses), high avidity T cells become the dominating subfraction of antigen-specific T cell populations. Nevertheless, low avidity T cells seem less susceptible to exhaustion during chronic antigen exposure and, therefore, can show improved maintenance of T cell responses in chronic disease settings. In contrast, chronic exposure of higher affinity T cells to antigens can lead to impaired T cell responses due to over-activation and activation-induced cell death[185]. In addition to the activation and survival profile, different TCR avidities also enable the generation of a broad spectrum of different phenotypes, resulting in a diverse and successful weapon against invaders and re-occurring infections and relapsing tumors[186].

Consequently, mimicking these basic mechanisms of the human immune system to adoptive T cell therapy by generating more diverse (“polyclonal”) CAR-T cell products with distinctly mixed affinities could represent an attractive solution for an improved safety and functionality profile of CAR-T cell therapies.

2 Aim of this PhD thesis

CAR-T cell therapy has been a significant breakthrough in the treatment of relapsed and refractory B cell malignancies. However, the development of severe acute toxicities such as CRS and ICANS, as well as an increasing number of tumor relapses due to non-functional exhausted CAR-T cells, reflect the high need to improve this promising clinical immunotherapy further.

The goal of this thesis was to investigate the role of receptor affinity on CAR-T cell functionality and safety and to exploit the newly generated knowledge to develop more optimal CAR-T cell products with improved long-term efficacy and persistence, as well as lower toxicity for clinical application.

To achieve this, we selected four known CAR scFv clones targeting human CD19 and characterized their affinities by conventional surface plasmon resonance and their *in vitro* functionalities. Furthermore, starting from the CAR clone with the lowest binding strength towards CD19, we generated a CAR library of additional 32 point mutants by single amino acid exchanges covering affinities down to the TCR range. CAR mutant affinities were measured by an in-house developed flow-based k_{off}-rate assay utilizing CAR:CD19 half-lives.

In a second step, we explored the effects of CAR affinity on the functionality of engineered T cells in both *in vitro* and *in vivo* models. Specifically, we evaluated *in vitro* antigen specificity, sensitivity, and cytotoxic capacity by co-culture with CD19-expressing tumor cell lines. Moreover, antigen recognition and potential tumor killing of five selected representative CAR-T cells with different affinities were confirmed in immunocompromised xenograft tumor models. The influence of affinity and a potential dose dependency on the development of CAR-T cell-mediated toxicities was tested in a newly established clinically relevant advanced humanized CRS xenograft mouse model.

Finally, we examined whether mimicking features of polyclonality of natural T cell response by combining high and low-affinity CAR-T cells could improve the overall *in vivo* functionality of the transferred CAR-T cell product.

In summary, with this thesis work, we aimed to determine an optimal CAR affinity window to generate clinically highly functional and safe CAR-T cell products and to study how CAR affinity could be used as a relevant prediction tool for the success of CAR-T cell therapy.

3 Material and Methods

3.1 Material

3.1.1 Antibodies

Epitope	Fluorophore	Dilution	Supplier
α CD19	PE	1:100	BioLegend
α CD19	eF450	1:200	eBioscience
α CD20	PE	1:200	eBioscience
α CD20	eF450	1:200	eBioscience
α CD20	APC-eF780	1:50	Life Technologies
α CD223 (Lag-3)	PC7	1:50	BioLegend
α CD3	PC7	1:100	Beckman Coulter
α CD3	APC	1:200	Life Technologies
α CD366 (TIM-3)	PB	1:50	BioLegend
α CD4	Pacific Orange	1:25	Life Technologies
α CD45	ECD	1:50	Beckman Coulter
α CD45	Pacific Blue	1:50	Exbio
α CD45	PerCP	1:50	Thermofisher
α CD45	Pacific Orange	1:25	Life Technologies
α CD45RA	APC	1:50	BD Pharmingen
α CD62L	PE	1:400	BioLegend
α CD8	APC	1:400	Biolegend
α CD8	APC-eF780	1:100	eBioscience
α CD8	FITC	1:100	Beckman Coulter
α CD8	PE	1:100	eBioscience
α CD8	PE-Cyanine7	1:200	eBioscience
α CD8	eFlour 450	1:50	eBioscience
α EGFR	eFlour 450	1:200	BioLegend
α EGFR	APC	1:2000	BioLegend
α EGFR	PE	1:2000	BioLegend
α HLA-DR	PO	1:50	Exbio
α IFN-γ	PE	1:20	Beckman Coulter
α IL-2	APC	1:20	BD Pharmingen
α PD-1	APC	1:100	Life Technologies
Streptavidin	eFlour 450	1:50	Life Technologies
Streptavidin	FITC	1:50	BD Pharmingen
Streptavidin	PE	1:50	Invitrogen
Streptavidin	APC	1:50	eBioscience
α TNF-α	PE-Cyanine7	1:300	eBioscience

3.1.2 Cell lines and bacteria

Cell line	Manufacturer
Human Embryonic Kidney 293T (HEK 293T)	ATCC, Teddington, UK
Jurkat, acute T cell leukemia	ATCC, Teddington, UK
K562, chronic myeloid leukemia	ATCC, Teddington, UK
Nalm6, acute lymphoblastic leukemia (ALL)	ATCC, Teddington, UK
Nur77-tdTomato - transgenic Jurkat	Juno Therapeutics, Munich, Germany
Raji, Burkitt's lymphoma	ATCC, Teddington, UK
RD114, human rhabdomyosarcoma cell line	ATCC Teddington, UK

Bacteria	Manufacturer
E. coli JM83	IBA, Göttingen, Germany
E. coli Stbl3	Thermo Fisher Scientific, Waltham, USA
E. coli NEB5 alpha	New England Biolabs, Frankfurt, Germany

3.1.3 Chemicals and reagents

Reagent	Supplier
123count eBeads™ Counting Beads	Thermo Fisher Scientific, Waltham, USA
1 kb GeneRuler	Thermo Fisher Scientific, Waltham, USA
ß-Mercaptoethanol	Sigma-Aldrich, Taufkirchen, Germany
Acrylamide/Bis 30%	Biorad, München, Germany
Adenosine triphosphate (ATP)	Roth, Karlsruhe, Germany
Agarose	PAA Laboratories, Pasching, Austria
Ammonium chloride (NH_4Cl)	Sigma-Aldrich, Taufkirchen, Germany
Ammonium peroxidsulfate (APS)	Sigma-Aldrich, Taufkirchen, Germany
Ampicillin	Sigma-Aldrich, Taufkirchen, Germany
Anhydrotetracycline (AHT)	IBA, Göttingen, Germany
Anti-APC MicroBeads	Miltenyi Biotech, Bergisch-Gladbach, Germany
Azido-L-Tyrosine	Watanabe Chemical, Osaka, Japan
Biocoll Ficoll solution	Biochrom, Berlin, Germany
Bovine serum albumin (BSA)	Sigma-Aldrich, Taufkirchen, Germany
Bromophenol blue	Roth, Karlsruhe, Germany
Calcium chloride ($CaCl_2$)	Merck, Darmstadt, Germany
Carbenicillin	Sigma-Aldrich, Taufkirchen, Germany
Cell Proliferation Dye eF450™ 450	Thermo Fisher Scientific, Waltham, USA
Chloramphenicol	Roth, Karlsruhe, Germany
cOmplete Mini Protease Inhibitor tablets	Roche Diagnostics, Mannheim, Germany
Coomassie Blue	SERVA, Heidelberg, Germany
D-Biotin	Sigma-Aldrich, Taufkirchen, Germany
DBCO-PEG4-Atto-488	Jena Biosciences, Jena, Germany
Desthiobiotin	Sigma-Aldrich, Taufkirchen, Germany
Dimethylsulfoxide (DMSO)	Sigma-Aldrich, Taufkirchen, Germany
Dithiothreitol (DTT)	Agilent, Waldbronn, Germany

Reagent (continued)	Supplier
DMEM	PAA Laboratories, Pasching, Austria
dNTP	Roche, Mannheim, Germany
Ethylenediaminetetraacetic acid (EDTA)	Sigma-Aldrich, Taufkirchen, Germany
Ethanol	Klinikum rechts der Isar, Munich, Germany
Ethidium-monoacid-bromide (EMA)	Molecular Probes, Leiden, The Netherlands
Expamer™ Reagent	Juno Therapeutics, Munich, Germany
Fetal calf serum (FCS)	Biochrom, Berlin, Germany
Formaldehyde (HCOH), 37%	Merck KgaA, Darmstadt, Germany
Gentamycin	GibcoBRL, Karlsruhe, Germany
Glycerin	Sigma-Aldrich, Taufkirchen, Germany
Golgi-Plug	BD Biosciences, Heidelberg, Germany
Heparin-Natrium-25000	Ratiopharm, Ulm, Germany
Hydrochloride (HCl)	Roth, Karlsruhe, Germany
HEPES	GibcoBRL, Karlsruhe, Germany
Interleukin-2, human	PeproTech, Hamburg, Germany
Interleukin-7, human	PeproTech, Hamburg, Germany
Interleukin-15, human	PeproTech, Hamburg, Germany
Ionomycin	Sigma-Aldrich, Taufkirchen, Germany
Isopropanol	Roth, Karlsruhe, Germany
Kanamycin	Sigma-Aldrich, Taufkirchen, Germany
L-Glutamine	GibcoBRL, Karlsruhe, Germany
Magnesium sulfate ($MgSO_4$)	Sigma-Aldrich, Taufkirchen, Germany
Magnesium chloride ($MgCl_2$)	Sigma-Aldrich, Taufkirchen, Germany
N-Morpholino-ethanesulfonic acid (MES)	Sigma-Aldrich, Taufkirchen, Germany
Methanol	Roth, Karlsruhe, Germany
PageRuler Protein Ladder	Fermentas, St. Leon-Rot, Germany
Paraformaldehyde (PFA)	Sigma-Aldrich, Taufkirchen, Germany
Penicillin	Roth, Karlsruhe, Germany
Phorbol-myristate-acetate (PMA)	Sigma-Aldrich, Taufkirchen, Germany
Phosphate buffered saline (PBS)	Biochrom, Berlin, Germany
Poly-L-Lysine	Sigma-Aldrich, Taufkirchen, Germany
Potassium phosphate (K_2PO_4)	Sigma-Aldrich, Taufkirchen, Germany
Propidium iodide (PI)	Life Technologies, Carlsbad, CA, USA
Protamine sulfate	Sigma-Aldrich, Taufkirchen, Germany
RetroNectin	Takara, Saint-Germain-en-Laye, France
Rotisafe GelStain	Roth, Karlsruhe, Germany
RPMI 1640	PAA Laboratories, Pasching, Austria
Sodium acetate ($C_2H_3NaO_2$)	Merck KGaA, Darmstadt, Germany
Sodium carbonate (Na_2CO_3)	Merck KGaA, Darmstadt, Germany
Sodium chloride (NaCl)	Roth, Karlsruhe, Germany
Sodium EDTA (Na_2-EDTA)	Sigma-Aldrich, Taufkirchen, Germany
Sodium hydroxide (NaOH)	Roth, Karlsruhe, Germany
Sucrose	Sigma-Aldrich, Taufkirchen, Germany
Tetramethylethylenediamine (TEMED)	Life Technologies, Paisley, United Kingdom

Reagent (continued)	Supplier
Tris-hydrochloride (Tris-HCl)	Roth, Karlsruhe, Germany
Triton X-100	Biorad, Munich, Germany
Trypan Blue	Sigma-Aldrich, Taufkirchen, Germany
Tween-20	Sigma-Aldrich, Taufkirchen, Germany
β-Mercaptoethanol	Sigma-Aldrich, Taufkirchen, Germany
XenoLight™ D-Luciferin Potassium Salt	Perkin Elmer Inc., Waltham, USA
Yeast extract, micro-granulated	Roth, Karlsruhe, Germany

3.1.4 Consumables

Consumables	Supplier
0.22 µm sterile filter	Millipore, Eschborn, Germany
0.45 µm sterile filter	Millipore, Eschborn, Germany
1.0 ml Eppendorf tube	Eppendorf Munich Germany
1.5 ml Eppendorf tube	Eppendorf Munich Germany
2.0 ml Eppendorf tube	Eppendorf Munich Germany
2.0 ml Cryo vial	Alpha Laboratories, Eastleigh, UK
10 kDa AmiconR Ultra-4, 15 centrifugal filters	Millipore, Eschborn, Germany
15 ml Falcon tube	Cell Star Greiner bio-one, Heidelberg, Germany
50 ml Falcon tube	Cell Star Greiner bio-one, Heidelberg, Germany
5 ml Polystyrol round-bottom tube	Corning, Durham, USA
70 µm Nylon Cell Strainer	BD Falcon Heidelberg, Germany
96-well E-plate®	ACEA Biosciences, San Diego, USA
96-well V-bottom plate	Josef Peske, Aindlfing-Arnhofen, Germany
Costar 24-well tissue untreated well plate	Corning, Durham, USA
Costar tissue culture treated well plates	Corning, Durham, USA
Electroporation cuvette	Sigma-Aldrich Aldrich Hamburg, Germany
Injection needle (20 G)	Braun, Melsungen, Germany
Leucosep centrifuge tubes	Greiner bio-one, Heidelberg, Germany
LS columns	Miltenyi Biotech, Bergisch-Gladbach, Germany
PCR tube	Eppendorf Munich, Germany
Petri dish	BD Falcon Heidelberg, Germany
Pipette filter tips (1 µl, 20 µl, 200 µl, 1000 µl)	STARLAB, Hamburg, Germany
Plastic cuvettes	Peske, Karlsruhe, Germany
Safety-Multifly 21G	Sarstedt, Nümbrecht, Germany
Serological pipettes (5 ml, 10 ml, 25 ml)	Greiner bio-one, Heidelberg, Germany
Strep-Tactin® Superflow ®high capacity column	IBA, Göttingen, Germany
Syringe (1 ml, 3 ml, 5 ml, 50 ml)	Braun, Melsungen, Germany
T25 cell culture flask	Th. Geyer, Renningen, Germany
T75 cell culture flask	Th. Geyer, Renningen, Germany
Zeba™ Spin Desalting Columns	Thermo Fisher Scientific, Waltham, USA

3.1.5 Enzymes

Enzyme	Supplier
BamHI	Thermo Fisher Scientific, Waltham, USA
Benzonase	Sigma-Aldrich, Taufkirchen, Germany
DNAse	Sigma-Aldrich, Taufkirchen, Germany
Esp3I	Thermo Fisher Scientific, Waltham, USA
EcoRI	Thermo Fisher Scientific, Waltham, USA
Herculase II	Stratagene, London, UK
HindIII	Thermo Fisher Scientific, Waltham, USA
NotI	Thermo Fisher Scientific, Waltham, USA
Phosphatase	Thermo Fisher Scientific, Waltham, USA
T4 DNA ligase	Fermentas, St. Leon-Rot, Germany
Taq Polymerase	Thermo Fisher Scientific, Waltham, USA
Trypsin	SAFE Biosciences, Hampshire, UK
Tubulin-tyrosine ligase (TTL)	in-house

3.1.6 Equipment

Equipment	Model	Supplier
Balance	ACS/ ACJ 320-4M	Kern & Sohn, Balingen, Germany
	EG 2200-2NM	Kern & Sohn, Balingen, Germany
Centrifuges	Biofuge fresco	Heraeus, Hanau, Germany
	Biofuge statos	Heraeus, Hanau, Germany
L8-70M Ultracentrifuge	Beckman, Krefeld, Germany	
	Multifuge 3 S-R	Beckman, Krefeld, Germany
	Sorvall RC6+	Thermo Fisher Scientific, Ulm, Germany
Cell Sorter	MoFlo XDP Cell Sorter	Beckman Coulter, Fullerton, USA
	MoFlo Legacy Cell Sorter	Beckman Coulter, Fullerton, USA
	FACSAria cell sorter	BD bioscience, Heidelberg, Germany
Electroporator	Gene Pulser	Biorad, Munich, Germany
Electrophoresis Chamber	Perfect Blue™ Gel System	Peqlab, Erlangen, Germany
Flow cytometer	Cytoflex	Beckman Coulter, Fullerton, USA
	Cytfolex S	Beckman Coulter, Fullerton, USA
FPLC	Äktapurifier™ 10	GE Healthcare, Chalfon St. Giles, UK
Freezing container	Mr. Frosty	Thermo Fisher Scientific, Paisley, USA
Gel Imaging System	Molecular Imager®	BioRad, München, Germany
	Amershan Imager 600	GE Healthcare, Chalfont, UK
Eagle Eye		BioRad, Munich, Germany
Heating block	Thermomixer compact	Eppendorf, Hamburg, Germany
Ice machine	ZBE 30-10	Ziegra, Isernhagen, Germany
Imaging system	IVIS® Lumina X5	PerkinElmer Inc., Waltham, USA
Incubator	HERAcell 240	Heraeus, Hanau, Germany
Laminar flow hood	HERAsafe	Heraeus, Hanau, Germany

Equipment (continued)	Model	Supplier
Magnetic separator	Magnetic cell separator	Miltenyi Biotech, Bergisch-Gladbach, Germany
Microscope	Axiovert S100	Carl Zeiss, Jena, Germany
Nanodrop device	ND-1000	Kisker, Steinfurt, Germany
Neubauer Chamber	Neubauer Improved	Schubert, München, Germany
PCR cycler	T3000 Thermocycler	Biometra, Göttingen, Germany
pH-meter	MultiCal pH 526	WTW, Weilheim, Germany
RTCA xCelligence	xCelligence RTCA W380	ACEA Bioscience, San Diego, USA
Spectrophotometer	NanoDrop ND-1000	Thermo Scientific, Ulm, Germany
Ultrasonic device	UW 2070	Bandelin, Berlin, Germany
Water bath	Type 1002	GFL, Burgwedel, Germany

3.1.7 Gels

Gel	Composition
1.2 % Agarose gel	0.6 g Agarose 50 ml TAE buffer, boil 5 µl Rotisafe
10 % SDS PAGE Running gel	3.3 ml Acrylamide 2.5 ml 1.5 M Tris-HCl, pH 8.8 100 µl 10 % (w/v) SDS 4 ml H_2O 10 µl TEMED 100 µl 10 % APS
10 % SDS PAGE Stacking gel	0.66 ml Acrylamide 0.3 ml 2 M Tris-HCl, pH 6.8 200 µl 10 % (w/v) SDS 3.9 ml H_2O 5 µl TEMED 25 µl 10 % APS

3.1.8 Kits

Kit	Supplier
CD34 MicroBead Kit, human	Miltenyi Biotech, Bergisch-Gladbach, Germany
Cytofix/Cytoperm™	BD Biosciences, Heidelberg, Germany
LEGENDplex™ HU Th1/Th2 Panel (8-plex)	Biolegend, San Diego, USA
Pierce BCA Protein Assay	Thermo Fisher Scientific, Waltham, USA
PureLink Hi Pure Plasmid Filter Maxiprep Kit	Thermo Fisher Scientific, Waltham, USA
Q5 Site-Directed Mutagenesis Kit	NEB, Massachusetts, USA
SV Miniprep DNA Purification System	Promega, Mannheim, Germany
Wizard SV Gel and PCR Clean-Up System	Promega, Mannheim, Germany

3.1.9 Media and buffers

Media	Composition
Complete RPMI (cRPMI)	10% (v/v) FCS 0.02% (w/v) L-Glutamine 0.12% (w/v) HEPES 0.1% (v/v) Gentamycin 1.0 % (v/v) Penicillin/Streptomycin 0.1% (v/v) ß-Mercaptoethanol
Complete DMEM (cDMEM)	10% (v/v) FCS 0.02% (w/v) L-Glutamine 0.12% (w/v) HEPES 0.1% (v/v) Gentamycin 1.0 % (v/v) Penicillin/Streptomycin 0.1% (v/v) ß-Mercaptoethanol
Complete freezing medium (CFM)	90% FCS 10% DMSO
Lysogeny broth medium (LB_0)	10 g/l Bacto-Tryptone 5 g/l yeast extract 10 g/l NaCl pH 7,0

Buffers	Composition
Ammonium chloride-Tris (ACT)	0.17 M NH_4Cl 0.3 M Tris-HCl, pH 7.5
Developer solution (Na_2CO_3) 0.05 % (v/v) CH_2O (37 %)	0.2 % (v/v) $Na_2S_2O_3$
FACS buffer	1x PBS 0.5 % (w/v) BSA, pH 7.45
FPLC buffer	20 mM Tris-HCl, pH 8.0 50 mM NaCl
High density medium (HD)	0.04 % (w/v) yeast extract 42 mM Na_2HPO_4 51 mM KH_2PO_4 10 mM NaOH 24 % (w/v) $MgSO_4*7H_2O$ 0.7 % (v/v) Glycerin
5x MES/K buffer	100 mM MES 500 mM KCl 50 mM $MgCl_2$ 1 mM EDTA

Buffers (continued)	Composition
Periplasmic lysis buffer (P)	100 mM Tris/HCl, pH 8.0 500 mM sucrose 1 mM EDTA
Protein purification wash buffer (W)	100 mM Tris/HCl, pH 8.0 150 mM NaCl 1 mM EDTA
Protein purification elution buffer (E)	100 mM Tris/HCl 150 mM NaCl 1 mM EDTA 2.5 mM Desthiobiotin, pH 8.0
Running gel (4%)	1.5 M Tris (pH 8.8) 30 % Acrylamide 10 % SDS
0.5 % TEMED	
	10 % APS
Sample buffer (Laemmli)	10 % (w/v) SDS 10 mM DTT 20 % (v/v) glycerol 0.2 M Tris-HCl, pH 6.8 0.05 % (w/v) Bromophenol blue
Stacking gel (4%)	0.5 M Tris (pH 8.8) 30 % Acrylamide 10 % SDS 0.5 % TEMED 10 % APS
50x TAE buffer	2 M Tris-HCl 2 M CH_3COOH 50 mM EDTA, pH 8.0
Transfection buffer	100 ml H_2O 0.27 M NaCl 9.9 mM KCl 3.5 mM Na_2HPO_4 4.2 mM HEPES
TTL reaction buffer	20 mM MES 100 mM KCl 10 mM $MgCl_2$ 2.5 mM ATP
	5 mM reduced glutathione
Running buffer	10 % EZ-Running buffer stock solution 90 % (v/v) bi-distilled H2O

3.1.10 Mice

Mouse strain	Provider
NSG-SGM3	bred in house, Busch lab

3.1.11 Plasmids

Epitope	Clone	Vector	Molecular details
α-human CD19 JCAR017	FMC63	pMP72	3xSTII hinge + EGFRt (+/- Ametrine) kindly provided by Juno Therapeutics – a BMS company
		pASG	FLEXamer
α -human CD19 JCAR021	n/a	pMP72	3xSTII hinge + EGFRt kindly provided by Juno Therapeutics – a BMS company
		pASG	FLEXamer
α-human CD19 JCAR021 mutants (scFv point mutants of JCAR021)	n/a	pMP72 pASG	3xSTII hinge + EGFRt FLEXamer
α-human CD19 4G7	4G7	pMP72 pASG	3xSTII hinge + EGFRt FLEXamer
α-human CD19 CAT	CAT	pMP72 pASG	3xSTII hinge + EGFRt FLEXamer

3.1.12 Sequencing Primer

Primer	Sequence
SD30 (pMP72_fwd)	AGTTAAGTAATAGTCCCTCTCTCC
SD31 (pMP72_rev)	CCCAGTTTAGTAGTTGGACTTAG
SD34 (JCAR017_fwd)	CGGCTGACCATCATCAAGGACAAC
SD35 (JCAR021_fwd1)	CAGCCTGATCATCTCTGGAC
SD36 (JCAR021_fwd2)	CAAGCCCAGACGGAAGAATC

3.1.13 Software

Software	Supplier
Affinity Designer v1.10.4	Serif, Nottingham, UK
BioRender	BioRender, Toronto, Canada
CytExpert Acquisition and Analysis Software v2.4	Beckman Coulter, Brea, USA
FlowJo v10.8.1	Treestar, Ashland, USA
Graph Pad Prism v9.0	Graph Pad Software, La Jolla, USA
ImageJ	Wayne Rasband, NIH, USA
LEGENDplex™ Data Analysis Software	BioLegend, San Diego, USA
Living Image® Software	PerkinElmer, Waltham, USA
Microsoft Office	Microsoft, Redmond, USA

Software (continued)	Supplier
RTCA xCelligence v2.0	ACEA Bioscience, San Diego, USA
SnapGene v6.0	GSL Biotech LLC, San Diego, USA
Unicorn	GE Healthcare, Chicago, USA

3.1.14 Vectors

Vector	Molecular details
pASG-IBAwt2	periplasmic expression vector N-terminal Twin-StrepTag®
pMP72	retroviral expression vector selection marker: Ampicillin

3.2 Molecular biology techniques

3.2.1 CAR DNA template design for retroviral transduction

DNA templates of different anti-human CD19 targeting CAR clones (JCAR017, JCAR021, CAT, 4G7) for retroviral transduction were designed *in silico* and synthesized by GeneArt (Thermo Fisher Scientific) or Twist Bioscience. All CAR constructs had the same structure, except different scFvs recognizing the human CD19 protein. Extracellular scFvs were generated by fusing the variable regions of the heavy (V_H) and light (V_L) variable chains of different CD19-specific antibody clones with a short $(G_4S)_3$ linker.

scFv sequences of JCAR017 (clone: FMC63) and JCAR021 were kindly provided by Juno Therapeutics – a Bristol Myers Squibb company. scFv sequences of the clones CAT and 4G7 were obtained from their publicly available patents (WO 2016/139487A1; WO 2014/184143A1, respectively).

CAR constructs for retroviral transduction had the following general structure: the signal peptide of GM-CSF receptor subunit α, which enabled the transport and integration of the receptor into the membrane at the 5'-end of the DNA gene, was followed by one of the different CD19-specific scFvs. The extracellular binding domain was linked to a spacer domain comprising a triple repetitive sequence of Strep-tag II (STII)[187,188] and parts of the IgG4-Fc molecule, followed by a transmembrane region originated from the CD28 chain. The following intracellular signaling domains, CD3-zeta and 4-1BB, were separated by a viral T2A peptide from a truncated version of EGFR (EGFRt) used as a transduction marker[139,189]. For *in vivo* mixing experiments of JCAR017 and JCAR021, the sequence of the fluorescent protein Ametrine was included on the C'-terminus of JCAR017 and connected by a T2A element.

All constructs were cloned into pMP72 vectors (containing the EF1 promoter and a Kozak consensus sequence 5'-GCCGCCACC-3' upstream of the integration site for the gene of interest. Gene expression was driven by the 5' LTR sequence.

3.2.2 CAR DNA template design for periplasmic protein production

DNA templates of different anti-human CD19 targeting CAR clones (JCAR017, JCAR021, CAT, 4G7) for periplasmic scFv protein production were designed *in silico* and synthesized by GeneArt (Thermo Fisher Scientific) or Twist Bioscience. CAR scFv sequences used for retroviral transduction were linked to a Twin-Strep-tag® and a Tub-tag sequence building scFv FLEXamers[190]. The expression cassette of the FLEXamer scFv genes is under transcriptional control of a tetracycline promoter/operator. The Omp sequence (start codon) at the beginning of the genes enabled the start of transcription and release of the proteins into the periplasm. All scFv FLEXamer constructs were introduced into the acceptor vector pASG-IBAwt2 (IBA), which is adapted for the periplasmic expression of soluble proteins.

3.2.3 General cloning procedure of vector constructs

To introduce the different CAR DNA strings for retroviral transduction and periplasmic protein production into their corresponding vectors, the respective plasmids were digested with restriction enzymes. Therefore, 256 ng of the ordered gene strings and 1 µg of the two vectors (pMP72, pASG-IBAwt2) were incubated with 0.5 µl restriction enzymes in NEBuffer™ for 30 min at 37 °C. CAR gene strings for retroviral transduction and the pMP72 plasmid were digested with NotI and EcoRI, while CAR FLEXamers and pASG-IBA-WT2 were digested with Esp3I, according to the manufacturer's protocol.

Digested plasmids were supplemented with 6x Loading Dye and separated on a 2 % agarose gel by electrophoresis at 130 V for 90 min. Bands were visualized by UV light (band sizes: pASG-IBA-WT: 4 kB, scFv-FLEXamer: 1kb, pMP72: 3 kB, CAR-transduction: 2.7 kb) and removed from the gel. DNA was purified with the help of the 'Wizard SV Gel and PCR Clean-up System kit according to the manufacturer's protocol. CAR inserts and vector backbones were ligated at a ratio of 4:1 with 1 µl T4 DNA ligase in 20 µl ligase buffer at RT for 1 h.

3.2.4 Amplification of vector DNA

One Shot™ Stbl3™ *E. coli* (NEB) were transformed with vector DNA by heat shock at 42 °C for 40 s. Transformed bacteria were plated on pre-warmed LB_{amp} plates and incubated overnight at 37 °C. One colony was inoculated in 4 ml of LB_{amp} pre-culture and incubated at 37 °C and 180 rpm for at least 7 h. For large-scale DNA production, half of the pre-culture was added to 400 ml LB_{Amp} medium and shaken overnight at 37 °C and 180 rpm. The plasmid DNA was isolated using the PureLink™ HiPure Maxiprep kit according to the manufacturer's protocol. DNA sequences were validated by Sanger sequencing (Eurofins Genomics) and analyzed with SnapGene v5.0. The purity of the purified DNA was determined by spectrophotometric analysis, concentration was adjusted to 1 µg/µl, and DNA was stored at -20 °C.

3.2.5 Alanine Scanning of JCAR021

In order to generate a CAR library of JCAR021 point mutants with lower binding strength, alanine scanning was performed within the framework regions of the light and heavy chain of JCAR021. All aromatic amino acids (phenylalanine, tryptophan, tyrosine) in the framework region were substituted with alanine by site-directed mutagenesis. Complementary-determining regions (CDRs) were kept in their original forms to preserve the native binding specificity of JCAR021. 16 different JCAR021 alanine substitution mutants were generated and cloned via Q5 site-directed mutagenesis PCR into the constructs of the JCAR021 FLEXamer and JCAR021 for retroviral transduction.

3.2.6 *In silico* modeling of JCAR021 substitution mutants with lower binding strength

The three-dimensional structure of the extracellular JCAR021 scFv binding domain was modeled *in silico* with the ABodyBuilder by SAbPred[191] and applied to the webserver mCSM-AB[192] for the prediction of mutational affinity changes.

Gibbs free energy changes ($\Delta\Delta G$) of the binding of JCAR021 to the extracellular domain (ecd) of the CD19 protein were calculated for all possible single amino acid exchanges within the

JCAR021 scFv. Finally, 32 JCAR021 substitution mutations were selected of the 231 calculated ones: 19 point mutations located in the framework regions and 14 point mutations in the CDRs were chosen for further testing. Single mutations within the framework region were selected based on the substitutions with predictions for the biggest Gibbs free energy change. To preserve the specificity of the CAR, amino acid changes in the CDRs were only considered if the exchanged amino acids had similar biochemical properties (groups: hydrophobic, polar, acidic, and nonpolar). Again amino acid substitutions with the biggest Gibbs free energy changes were chosen as potential candidates from the remaining predictions.

3.2.7 Q5-mutagenesis PCR

JCAR021 mutants for retroviral transduction and periplasmic protein production were generated by Q5 site-directed mutagenesis PCR (NEB) of JCAR021 cloned in the pMP72 and pASG-IBAwt2 vector, respectively. 5'-phosphorylated back-to-back primers containing the site of mutagenesis were designed with the NEBase Changer™ following the recommended guidelines. The PCR reaction was performed with the reagent mix according to the manufacturer's instructions (NEB) and the following PCR program:

Step	***Temperature in °C***	***Time in s***	***Cycles***
Initial denaturation	98	30	
Denaturation	98	10	34
Annealing	67 ± 5	30	
Elongation	72	450	
Final elongation	72	120	
Pause	4	∞	

After the PCR run, the template DNA was digested, and products of the mutagenesis PCR were phosphorylated and ligated with the KLD enzyme mix (NEB) for 30 min at RT.

Transformation of NEB 5-alpha competent *E. coli* (NEB) with the newly generated plasmids by heat-shock and the following large-scale DNA production were performed as already described

in chapter 3.2.4. Point mutations of newly generated JCAR021 mutants were validated by Sanger sequencing (Eurofins Genomics) and analyzed with SnapGene. The purity of the purified plasmid DNA was determined using spectrophotometric analysis, concentrations were adjusted to 1 µg/µl, and plasmids were stored at -20 °C.

3.3 Cell culture techniques

3.3.1 General techniques

Cell lines were cultivated in cRPMI (Raji, Nur77-Jurkat, Nalm6 cell lines) or cDMEM (RD114, HEK293T) at 37 °C, 5 % CO_2, and 95 % humidity. Adherent cell lines were trypsinized and split 1:10 every 3 - 4 days, depending on their confluency. Suspension cell lines were controlled for medium usage and cluster formation and split accordingly 2 – 3 times per week.

Cells were counted using a Neubauer counting chamber, and live/dead discrimination was performed using a 0.1 % trypan blue/PBS solution.

Cell lines and isolated human hematopoietic stem cells were stored in freezing medium (10 % DMSO/90 % FCS) for cryopreservation at a maximum concentration of $10x10^6$ cells/ml.

For thawing of frozen cells, cryotubes were immersed in a 37 °C water bath for 30 s. Contained cells were quickly diluted and washed in 10 ml cRPMI or cDMEM. According to the experimental requirements, cells were seeded at $1x10^6$ cells/ml in T25 cell culture flasks.

3.3.2 Isolation of peripheral blood mononuclear cells and *in vitro* cultivation of T cell

Blood was obtained from whole blood or buffy coats of healthy donors. Written informed consent was obtained from the donors, and usage of the blood samples was approved according to national law by the local Institutional Review Board (Ethikkommission der Medizinischen Fakultät der Technischen Universität München). Peripheral blood mononuclear cells (PBMCs) were isolated via density gradient centrifugation using Ficoll solution (density 1.077 g/ml) according to standard protocols. In brief, buffy coats were diluted 1:4 and whole blood 1:1 with sterile PBS.

15 ml Ficoll were overlaid with 35 ml blood/PBS mixture and centrifuged at 1,000 g and RT for 20 min. The white layer of mononuclear cells called PBMCs was transferred to a fresh falcon and washed twice with 50 ml sterile PBS. For retroviral transduction, human T cells were activated with 3.2 µl/ml CD3/CD28 Expamers[193] and 360 IU/ml interleukin-2 (IL-2) and seeded at a density of $1x10^6$ cells/ml in cRPMI. For *in vitro* cell culture, bulk T cells were generally cultured at a density of $1x10^6$/ml in cRPMI supplemented with 50 IU/ml IL-2 and passaged every 2 – 3 days, depending on their cell density. For rapid expansion, T cells were cultured at a density between 0.25 – $0.5x10^6$/ml in cRPMI supplemented with 200 IU/ml IL-2, 0.5 ng/ml IL-7 and 0.5 ng/ml IL-15. Half medium exchange and cell number adjustment was performed every second day.

3.3.3 RD114 transfection for retroviral vector production

For the production of retroviral CAR particles, the virus-producing murine GP101 RD114 packaging cell line, containing the onco-retroviral genes for group antigens (gag), reverse transcriptase (pol), and the envelope protein (env), were transfected with the different CAR constructs via $CaCl_2$-precipitation. One day before the transfection, $1x10^6$ RD114 were plated in 3 ml cDMEM in one well of a 6-well plate. After 18 - 20 h or at 80 % confluency of the cells, 18 µg of target DNA were mixed with 15 µl freshly prepared $CaCl_2$ solution and ddH_2O to 150 µl. The $CaCl_2$-DNA mixture was pipetted to 150 µl transfection buffer under constant vortexing. After 20 min incubation, the DNA-$CaCl_2$-transfection solution was added dropwise to the cells. Six hours later, the medium was gently exchanged with fresh cDMEM, and RD114 cells were further incubated for two more days at 37 °C. The supernatant containing the retroviral particles was collected, filtered through a 0.45 µm filter, and either used directly for retroviral transduction or stored at 4 °C for up to one month.

3.3.4 Retroviral transduction

One day before the retroviral transduction of primary T cells or cell lines, non-treated 24-well plates were coated with 250 µl RetroNectin (1:100) and incubated in the fridge overnight. 500

– 700 µl filtered retroviral supernatant, depending on the required MOI, were transferred onto the washed RetroNectin-coated wells, and plates were spun down for 90 min at 2,000 and 32°C.

For the transduction of human cell lines, cells were seeded at a density of $1x10^5$ cells/ml one day before the transduction. The next day, $1x10^5$ cells were added to 200 µl medium on top of the spinoculated virus and centrifuged again for 30 min at 800 g and 32 °C.Primary T cells were retrovirally transduced two days after their activation with CD3/CD28 Expamer. Cell concentrations were adjusted to $2.5x10^6$ cells/ml in cRPMI (containing 200 U IL-2), and 200 µl cell suspension was added to the spinoculated virus. Plates were centrifuged again at 800 g and 32 °C for 30 min and incubated at 37 °C for 48 h before the validation of their transduction efficacy via flow cytometry.

3.3.5 MicroBead-based cell selection of CAR-T cells

For some *in vivo* experiments, T cells were sorted for successful CAR transduction (reflected by EGFRt-expression on the cell surface) before their injection into tumor-bearing mice. Anti-APC MicroBeads (Miltenyi Biotec) were used to purify CAR-T cells from bulk populations according to the manufacturer's instructions. Briefly, up to $1x10^7$ bulk T cells were stained in 100 µl staining solution containing primary APC-conjugated anti-EGFR antibody at 4 °C for 20 min in the dark. After two rounds of washing, stained cells were incubated in 80 µl FACS buffer and 20 µl anti-APC MicroBeads in the refrigerator for 15 min. Washed cells were applied onto an equilibrated magnetic MACS column in a magnetic field and washed three times with the required amount of FACS buffer. The size of the MACS column was dependent on the total and labeled number of cells. For elution of the trapped cells, the column was removed from the separator, placed in a new collection tube, and magnetically labeled cells were flushed out by pushing the plunger into the column. The purity of isolated cells was analyzed by flow cytometry, and counted cells were cultivated at a density of $1x10^6$ cells/ml in cRPMI with supplements as described before.

3.3.6 Purification of hematopoietic stem cells from human umbilical cord blood

Immunocompromised NSG-SGM3 mice were humanized with umbilical cord blood-derived (UCB) human hematopoietic stem cells (hHSCs). Written informed consent was obtained from the donors, and usage of the blood samples was approved according to national law by the local Institutional Review Board (Ethikkommission der Medizinischen Fakultät der Technischen Universität München).

Lymphocytes were isolated via density gradient centrifugation using Ficoll solution (density 1.077 g/ml) according to standard protocols. Briefly, UCB was diluted 1:1 with sterile PBS, and the 40 ml blood/PBS mixture was overlaid on 10 ml Ficoll. The density gradient was centrifuged at 800 g for 20 min at RT without using the brake, and the white layer of PBMCs was transferred into a fresh falcon. After two rounds of washing with 10 ml ice-cold FACS buffer, the cell pellet of 20 ml initial UCB was resuspended in 300 µl ice-cold FACS buffer. Higher blood volumes were diluted accordingly.Human hematopoietic stem cells were purified with the human CD34 MicroBead Kit (Miltenyi Biotech) according to the manufacturer's handbook. Brief, for magnetic labeling, 100 µl FcR Blocking Reagent and 100 µl CD34 MicroBeads were mixed with 300 µl cell suspension and incubated for 30 min in the refrigerator. Afterward, cells were washed twice with 10 ml FACS buffer, and the cell pellet was resuspended in 500 µl FACS buffer. In the meantime, MACS LS Columns were equilibrated in the MACS Separator for magnetic separation. Stained cells were applied onto the columns, washed three times with 3 ml ice-cold FACS buffer, and finally eluted by firmly pushing the plunger into the column outside the magnetic field. Isolated cells were analyzed by flow cytometry and directly frozen in 200 µl freezing medium (10 % DMSO/90 % FCS) in a freezing container at - 80 °C. After 48 h, frozen cells were transferred into liquid nitrogen for storage until the humanization of the mice.

3.4 Production of fluorophore-labeled scFv-FLEXamers

3.4.1 Production of electrocompetent *E. coli* JM83

For the production of electrocompetent *E. coli* JM83*,* bacteria were pre-cultured in 5 ml LB_0 medium overnight at 37 °C under constant agitation. The next day, 1 l LB_0 was inoculated with 5 ml pre-culture and incubated (37 °C, 150 rpm) until an optimal density at 600 nm (OD_{600}) of 0.5 was reached. The cells were left on ice for 10 min and centrifuged at 4,000 g and 4 °C for 15 min. The supernatant was discarded, and the cell pellet was resuspended in 5 ml ice-cold 1 mM HEPES buffer. After resuspension, another 350 ml ice-cold 1mM HEPES was added. The washing process was repeated twice.After the last washing step, the cell pellet was resuspended in 5 ml ice-cold 10 % glycerin and centrifuged again (4,000 g, 4 °C, 15 min). Finally, the pellet was resuspended in 2 ml ice-cold 10 % glycerin, aliquoted in 20 µl stocks, shock-frozen in liquid nitrogen, and stored at -80 °C.

3.4.2 Recombinant protein expression of soluble scFvs

Sequence validated pASG-IBAwt2 plasmids containing Twin-Strep-tagged, and Tub-tagged CAR scFvs (scFv-FLEXamers) were transformed into electrocompetent *E. coli* JM83. Therefore, 20 µl bacteria were diluted 1:10 with sterile ddH_2O and mixed with 100 ng target DNA. The mixture was electroporated twice in a 1 mm Gene Pulser electroporation cuvette (1.8 kV, Pulse Controller & Gene Pulser (Biorad)). Electroporated bacteria were immediately supplemented with 800 µl pre-warmed LB_0 medium and incubated at 37 °C for 1 h to develop their antibiotic resistance. Bacteria were further diluted with LB_0 medium (1:4). 250 µl bacteria solution was plated on pre-warmed LB_{amp} plates and incubated overnight at 37 °C. For the periplasmic expression of recombinant scFvs, one CFU was pre-cultured in 3 ml LB_{amp} liquid culture and grown at 37 °C and under 200 rpm agitation. After at least 7 h of shaking, 1 l high-density medium was inoculated with the pre-culture, and bacteria were grown at 22 °C under 180 rpm agitation overnight. After reaching an OD_{600} of 3.0, periplasmic expression of the scFv FLEXamer was induced by adding anhydrotetracycline (AHT - $1:10^5$) to activate the tet-promoter of the pASG-IBAwt2 vector.After at least 3 h of protein expression or as soon as

OD_{600} values stagnate, bacteria were centrifuged (5,000 rpm, 4°C, 12 min), and the pellets were stored at -80 °C for further protein purification.

3.4.3 Strep-tag-based protein purification

For extracting the scFv FLEXamer proteins from the bacterial periplasm, frozen pellets were thawed on ice, resuspended in 10 ml buffer P, and incubated at 4 °C for 30 min. In order to remove cell debris from the expressed proteins, lysed bacteria were pelleted by centrifugation (15,000 rpm, 4°C, 15 min).

Afterward, the supernatant was incubated with Benzonase (125 U) on a tube roller for 1 h at 4 °C to enzymatically digest contaminating nucleic acids, and the scFv containing protein solution was filtered through a sterile 0.2 µm filter.Meanwhile, Strep-Tactin superflow columns (IBA) were equilibrated four times with 1 ml buffer W. The Strep-tag containing scFv protein solutions were applied on the columns, washed five times with 1 ml buffer W, and eluted from the column by adding six times 0.5 ml buffer E (containing 5 mM D-Desthiobiotin). Eluates 2 to 6 were pooled and ran over Zeba Spin desalting columns to perform buffer exchange into FPLC buffer according to the manufacturer's instructions. Protein concentrations were measured via spectrophotometry at 280 nm, and purity was determined via SDS-PAGE. Purified scFv protein aliquots were shock-frozen in liquid nitrogen and stored at -80 °C.

3.4.4 TTL mediated functionalization of scFv FLEXamers

Purified soluble scFv FLEXamers were conjugated with the fluorophore Atto-488 by TTL-mediated functionalization of their Tub-tags as previously described[190]. In general, the TTL catalyzes the ligation of 3-acid tyrosine to the C-terminus of the Tub-tag during the first step, which enables the reaction of the activated tag with DBCO-Atto-488 via click chemistry in the second step. The following described functionalization steps were optimized for CAR scFvs.

After the TTL-inhibiting FPLC storage buffer of the CAR scFvs was exchanged with the MES/K reaction buffer via Zeba Spin desalting columns, the ligation of 3-acid tyrosine to the scFv FLEXamers was performed. Therefore 20 µM scFv FLEXamers, 5 µM TTL, and 1 mM 3-acid

tyrosine were incubated in 100 µl TTL-reaction buffer at 25 °C for 3 h. Subsequently, excessive azido-tyrosine was removed combined with FPLC storage buffer exchange by size exclusion chromatography using 7 kDa MWCO desalting spin columns. The resulting purified azido-FLEXamers were directly functionalized via click chemistry. 20 µM azido-FLEXamers were incubated with 200 µM DBCO-PEG4-Atto-488 at 16 °C for 15 h, followed by buffer exchange to FPLC storage buffer.Functionalization efficacy and concentration were determined by SDS-PAGE. Functionalized proteins were shock-frozen in liquid nitrogen and stored as aliquots at -80 °C for further usage.

3.4.5 SDS-PAGE and coomassie staining

Purity and successful functionalization of the periplasmic expressed scFv FLEXamers was assessed by sodium dodecyl sulfate-polyacrylamide gel electrophoresis (SDS-PAGE). Protein samples were thawed on ice, supplemented with 5x Laemmli loading dye, and denatured at 95 °C for 5 min. Subsequently, samples were loaded onto a 12.5 % SDS-PAGE gel and separated by electrophoresis (80 V, 10 min followed by 130 V, 90 min). The gel was stained with Coomassie Blue staining solution for 1 - 2 h at RT before being destained in destaining solution for up to 5 h. Repeated cycles of destaining were performed until the protein bands were visible. The final protein gel was covered in transparent foil and scanned for further analysis. For semi-quantitative protein concentration measurements of low protein concentrations, different BSA standards (0.1 µg – 50 µg) were freshly prepared in 5x Laemmli loading dye, denatured as described before, and loaded next to the scFv protein samples on the SDS-PAGE gel. Each gel was analyzed via ImageJ. Determining protein concentrations was confirmed by spectrophotometry analysis.

3.5 Flow cytometry

3.5.1 Surface staining

For antibody surface stainings, up to $5x10^6$ cells were transferred together with 5 µl 123count eBeads™ counting beads into 96-well V-bottom plates and spun down. Cells were washed once with 200 µl FACS buffer and incubated with 50 µl antibody master mix containing all required fluorophore-conjugated antibodies at recommended dilutions for 20 min on ice in the dark. Each fluorophore used in the respective experiment was also displayed as a single color. For live/dead discrimination, propidium iodide (PI – 1:100) was added during the last 3 min of incubation. Cells were washed twice and filtered with 200 µl FACS buffer prior to acquisition on a Cytoflex (S) flow cytometer. Data analysis was performed with the FlowJo software (Treestar, Ashland, USA).

3.5.2 CD45 multiplexing for high-throughput k_{off}-rates

In order to process and analyze multiple samples in parallel during one round of k_{off}-rate measurements, samples were color-coded with CD45 mAbs carrying different fluorophores during the antibody surface staining. Combinations of 4 different CD45 mAbs (conjugated with Pacific Blue, Pacific Orange, PerCP, ECD) allowed simultaneous measurement of 16 different samples. Different color codes of CD45 mAbs were applied after 25 min of scFv StrepTamer incubation, simultaneously with the surface antibody master staining for 20 min on ice. After the addition of PI (1:100) for 3 min and two rounds of washing with ice-cold FACS buffer, cells of different samples were pooled and filtered through a nylon mesh for further analysis.

3.5.3 Fluorescent-activated cell sorting of CAR-T cells

For some *in vitro* experiments, CAR transduced PBMCs were purified by fluorescent-activated cell sorting (FACS) before the further investigation of their *in vitro* functionality. Therefore, cells were washed once with ice-cold FACS, and up to $5x10^6$ cells were stained in 50 µl antibody master mix, and the required volumes of antibodies were calculated according to their recommended dilutions. Cells were stained in the antibody mix for 20 min in the dark at 4 °C

and washed at least twice with 10 ml ice-cold FACS buffer. Cell aggregates were removed by passing cells through a sterile 30 µm filter. The whole procedure was performed on ice in the dark and under sterile conditions. PI (1:100) was added immediately before acquisition on the cell sorter. CAR-T cells were sorted on a MoFlo Astrios cell sorter at RT to obtain living $EGFRt^+$ lymphocytes and collected in 15 ml falcons containing 2 ml FCS. The falcons were prepared beforehand and coated with the FCS using a rolling device. After the fluorescent-activated cell sorting, cells were centrifuged and cultivated at a concentration of $1x10^6$ cells/ml cRPMI supplemented with 200 IU/ml IL-2, 0.5 µl/ml IL-7, and IL-15.

3.6 Affinity determination by flow cytometry-based k_{off}-rate measurement

To determine the CAR/CD19 dissociation rate (k_{off}-rate) of the different generated CD19-CAR constructs, a flow-cytometry-based k_{off}-rate assay, following the idea for TCR avidity measurements[164,165,194], was performed.

In brief, 0.2 µg Atto-488-conjugated scFv molecules were multimerized with 1 µl Strep-Tactin (ST) APC in 50 µl FACS buffer for 30 min on ice in the dark. In the meantime, at least $40x10^6$ PBMCs were freshly isolated from 60 ml of whole human blood, as described before. After one washing step, up to $5x10^6$ PBMCs were incubated with 50 µl scFv-StrepTamer for 45 min on ice in the dark. During the last 20 min, cells were additionally stained with combinations of CD45 antibodies conjugated with different fluorophores for multiplexing and CD20 antibodies for discrimination of target B cells.

PI staining for life/dead discrimination was performed for 3 min at the end of the staining. Cells were washed twice with FACS-buffer and filtered through a nylon mesh for further analysis.

For the k_{off}-rate measurement, scFv StrepTamer-stained cells were mixed and split into six samples. Each sample was filled up to 2.1 ml with FACS-buffer to ensure sufficient volume for the whole k_{off}-rate measurement. Around $7x10^6$ cells were analyzed by flow cytometry at a flow rate of 130 µl/min for 30 min under constant cooling using a Peltier cooling device set at 4 °C or 20 °C on a Cytoflex S flow cytometer. After 40 s of acquisition, 2.1 ml freshly made 2 mM D-Biotin solution was injected into the ongoing measurement. Sample left-over was stored in

the dark for two more hours at RT or 4 °C, accordingly. Final acquisitions of the remaining samples allowed the determination of baseline mean fluorescent intensities (MFIs) of APC and Atto-488. Measured background levels were important for CAR scFvs with a strong binding strength to CD19, for which the baseline was not reached within 30 minutes of acquisition. All measurements were performed in technical triplicates, and JCAR021 was analyzed in each run as an internal control.Dissociation kinetics were analyzed using FlowJo (Treestar, Ashland, USA). Cells were gated on the population of interest (living $CD20^+$ lymphocytes), and samples were differentiated by their respective CD45 color code. Mean fluorescence intensities (MFIs) of scFv-Atto-488 and the Strep-Tactin-APC backbone were exported into GraphPad Prism (GraphPad Software, La Jolla, USA). Curve fitting and calculation of dissociation kinetics were performed using a non-linear regression function. The starting value of the curve was set directly at the beginning of the dissociation of Strep-Tactin APC. Baseline values of FITC (scFv-Atto-488) which were not reached during the acquisition at 4 °C, were adapted by hand using measured baseline values during the 20 °C measurements.

3.7 *In vitro* functional assays

3.7.1 Determination of cell numbers

To determine frequencies and total numbers of the 33 different CAR-T cell products in a comparable and repeatable way, transduced primary T cells and Nur-77 Jurkat cells were stained for their Strep-tag and EGFRt expression and acquired together with 123count eBeads™ counting beads on a flow cytometer before the respective *in vitro* assay. 5 µl reference beads were added to the cells during their surface staining, which enabled the exact calculation of cell numbers and frequencies of the bulk CAR-T cell populations. Transduction efficacies were determined via gating on living $EGFRt^+$ lymphocytes, as not all JCAR021 mutants expressed their CAR, including the Strep-tag sequence on their surface. Cell counts within the positive gate and acquired bead counts were exported, and total cell numbers were calculated using Microsoft Excel (Microsoft, Redmond, USA).

3.7.2 Reporter cell assay for antigen-specific activation

The Nur77 Jurkat activation assay was performed to determine the ability of different CAR-T cells to be specifically activated by $CD19^+$ Raji target cells. The Nur77-tdTomato Jurkat reporter cell line was a kind gift from Juno Therapeutics - a Bristol Myers Squibb company. Jurkat cells had been transduced with a Nur77-tdTomato reporter transgene which is immediately upregulated upon stimulation of the corresponding cell. Due to the parallel expression of the fluorescent protein tandem dimer Tomato (tdTomato), CAR signaling activation can be detected by flow cytometry.

Nur77-tdTomato Jurkats were transduced with the 33 different CAR constructs as previously described and cultivated without stimulation for two weeks to reduce Nur77-tdTomato background signaling due to the transduction process. $CD19^+$ Raji-GFP target cells were adjusted to $0.5x10^6$ cells/ml in cRPMI. 100 µl target cells were distributed into a 96-well U-bottom plate.

The frequency and cell number of $EGFRt^+$ CAR transduced Nur77 Jurkat effector cells were determined via flow cytometry as described before. The required cell number was resuspended at a concentration of $2.5x10^6$ $EGFRt^+$ cells/ml in cRPMI.

100 µl cRPMI medium containing $5x10^4$ $EGFRt^+$ Nur77 Jurkats were co-incubated with the already plated Raji-GFP target cells at 37 °C for 24 h. Nur77-tdTomato background signaling was determined in samples containing only CAR-transduced Nur77 Jurkat cells without the addition of Raji-GFP cells. Phorbol-mystriate-acetate (PMA - 25 ng/ml) and ionomycin (1 µg/ml) were used as positive controls. After 24 h, co-cultures were harvested and stained for EGFRt and Strep-tag expression. Raji target cells were distinguished from Nur77 Jurkat cells by expression of GFP. Reporter gene activation was analyzed by measuring the frequency of tdTomato of $EGFRt^+$ GFP^- lymphocytes. Experiments were performed in technical duplicates and biological triplicates.

3.7.3 Intracellular cytokine staining

In order to assess specific cytokine production of different genetically modified human CAR-T cells after stimulation, T cells were co-incubated with $CD19^+$ Raji-GFP target cells, and intracellularly produced cytokines were measured via flow cytometry.

$CD19^+$ Raji-GFP target cells were adjusted to $1x10^6$ cells/ml in cRPMI. Two different E:T ratios (1:1, 1:0.25) were investigated. Therefore, a serial dilution of the target cells was performed, and 50 µl with $5x10^4$ (1:1 ratio) or $12{,}5x10^3$ (1:0.25 ratio) target cells were transferred into a 96-well U-bottom plate.

Effector CAR-T cells were rested for two days prior to the co-culture. Therefore, T cells were cultured in cRPMI without additional interleukins to ensure the intrinsic production of IL-2 during the assay. Frequencies and cell numbers of $EGFRt^+$ CAR-T cells were determined via flow cytometry as described before.

Required cell numbers were resuspended in cRPMI at a concentration of $0.5x10^6$ $EGFRt^+$ cells/ml in cRPMI. 100 µl containing $5x10^4$ cells were added to the Raji target cells and incubated for 4.5 h at 37 °C. CAR-T cells without additional $CD19^+$ Raji-GFP cells were used to determine the basal cytokine release of the different CAR-T cells. PMA (25 ng/ml) and ionomycin (1µg/ml) were used as positive controls. After 30 min, cytokine secretion was stopped by adding 50 µl Brefeldin A (‘Golgi Plug’) at 1 µg/ml.Co-incubated cells were harvested, washed with FACS buffer, and incubated with ethidium monazide bromide (EMA - $1:10^3$) for 15 min on ice exposed to bright light for live/dead discrimination. Surface staining (CD8, EGFRt, Strep-tag) was performed as described before at 4 °C in the dark for 20 min. After two additional washing steps with FACS buffer, cells were fixed and permeabilized with Cytofix/Cytoperm™ at 4 °C for 20 min, as recommended by the manufacturer’s instructions. Following two washing steps with PermWash™ buffer, the intracellular staining of IFN-γ, TNF-α and IL-2 was performed on ice in the dark for 20 min. Cells were washed twice with PermWash™ buffer and filtered into 200 µl FACS buffer for analysis on a flow cytometer. Raji target cells were distinguished from CAR-T cells by their intrinsic expression of GFP. Experiments were performed in technical triplicates and biological triplicates.

3.7.4 xCelligence® killing assay

The cytotoxic capacity of different CAR-T cells was investigated using the impedance-based xCelligence® assay, which allows real-time monitoring of cytotoxic kinetics. $CD19^+$ and $CD19^-$ HEK293T cells were a kind gift from the Riddell lab at the Fred Hutchinson Cancer Research Center in Seattle Riddell.

Initially, the wells of a 96-well E-Plate ™ were filled with 50 µl cDMEM, and the plate was equilibrated in the xCelligence RTCA MP Real-Time Cell Analyzer for 30 min at 37 °C to determine the baseline of the impedance signal.

In the meantime, $CD19^+$ and $CD19^-$ adherent HEK293T cells, latter used as a negative control, were prepared and adjusted to a concentration of $1.5x10^5$ cells/ml cDMEM. After the equilibration time, 100 µl of target cells were pipetted onto the E-plate and incubated under regular cell culture conditions for 24 h, while the growth was monitored every 15 min.

Frequencies and numbers of $EGFRt^+$ CAR transduced T cells were determined by flow cytometry as described before. Two different E:T ratios (1:1, 4:1) were investigated. Therefore, a serial dilution of the target cells was performed. 100 µl cDMEM was aspirated from the 96-well E-Plates™, and 100 µl with $1.5x10^5$ (1:1 ratio) or $7.5x10^5$ (4:1 ratio) target cells were added to the wells. 2 % Triton-X solution was used as a positive control of complete killing, while cRPMI medium without effector CAR-T cells served as a negative control. Effector and target cells were co-incubated for 48 - 72 h, and target cell growth was monitored every 15 min. Cytotoxic kinetics were analyzed using the software RTCA xCelligence®. Cell indices were normalized to the last measurement before the effector cells had been introduced. Samples were measured in technical triplicates and biological duplicates.

3.7.5 Flow cytometry-based cytotoxic CAR-T cell assay

Cytotoxic *in vitro* effector function of different CAR-T cells was determined in a co-culturing approach of CAR transduced T cells with $CD19^+$ Raji-GFP target cells, in which the reduction of GPF^+ target cells after 24 h and 48 h served as a readout.

$CD19^+$ Raji-GFP leukemia cells were resuspended in 50 µl containing $2x10^5$ target cells and were plated in a 96-well U-bottom plate. Frequencies and cell numbers of $EGFRt^+$ CAR transduced T cells were determined as described before. Serial dilution of CAR-T cells was performed, and 150 µl with either $8x10^4$ or $2x10^4$ $EGFRt^+$ CAR-T cells were added to the target cells (E:T = 4:1 and 1:1, respectively). Untransduced mock T cells derived from the same donor and only Raji-GFP cells were used as negative controls. After 24 h or 48 h of co-culture, cells were transferred to a 96-well V-bottom plate containing 123count eBeads™, washed with ice-cold FACS buffer, and stained with dye-conjugated anti-EGFRt, Streptavidin, and anti-CD8 antibodies as described before.

Cell composition was analyzed by flow cytometry, and target cells were discriminated by their internal expression of GFP. All samples were measured in triplicates.The percentage (%) of target cell killing was calculated based on the absolute number of target cells in the untdx T-cell condition. That absolute number of the untdx T-cells was set as 100%, and the number of targets in the following T-cell conditions was expressed as a percentage of survival. The elimination index was calculated as follows: 1 – (number of residual target cells in the presence of target antigen-specific CAR-T cells/ number of residual target cells in the presence of mock T cells).

3.8 *In vivo* functional assays

3.8.1 Experimental overview of *in vivo* functionality experiments

For *in vivo* functionality experiments with CAR affinity mutants, 8 weeks old female and male NSG-SGM3 mice, bred in-house, were used. Functional *in vivo* analyses were performed with JCAR017, JCAR021, and three selected JCAR021 mutants (L237W, M35A, V236W). All animals were kept under specific pathogen-free conditions at the institute's mouse facility. All animal experiments were approved by the local authorities.

One-week prior to CAR-T cell injection, $0.5x10^6$ $CD19^+$ GFP^+ Raji-ffluc leukemia cells were prepared in sterile PBS and injected via the tail vein in NSG-SGM3 mice. These tumor cells have been modified to express both the firefly luciferase (ffluc) and GFP, allowing non-invasive serial imaging by bioluminescence (BLI) and flow cytometry. Raji-ffluc tumor cells were kindly provided by the Riddell lab at the Fred Hutchinson Cancer Research Center in Seattle.

After six days, the tumor engraftment was analyzed by bioluminescent imaging (BLI) using the IVIS® *in vivo* Imaging System. Tumor-bearing mice were distributed equally among the six different groups (JCAR017, JCAR021, L237W, M35A, V236W, untdx) with 6-8 mice or 3 mice (repetition experiment) per group. CAR-T cells were injected into tumor-bearing mice via the tail vein as bulk populations, back-calculated to transfer $0.8x10^6$ $CD8^+$ $EGFRt^+$ cells. Untransduced (untdx) mock T cells derived from the same donor were used as negative controls.

IVIS® was performed weekly to monitor the tumor development in the mice. Distribution and expansion of the CAR-T cells were analyzed by weekly blood staining. 28 days post CAR-T cell injection, endpoint analysis was performed. Therefore, blood, bone marrow, and spleens were extracted and prepared for flow cytometry. Results were analyzed with FlowJo (Treestar, Ashland, USA).

For *in vivo* functionality testing of CAR affinity mixes, 8 weeks old female and male NSG-SGM3 mice, bred in-house, were used. JCAR017-Ametrine was mixed with JCAR021 according to the following frequencies 50 %, 25 %, 12.5 %, 6.25%, for a total of $1.6x10^6$ $CD8^+$ $EGFRt^+$. Additionally, $1.6x10^6$ $CD8^+$ $EGFRt^+$ JCAR021 only, $0.8x10^6$ $CD8^+$ $EGFRt^+$ JCAR017 only and

$1.6x10^6$ $CD8^+$ $EGFRt^+$ untransduced (untdx) mock T cells derived from the same donor were used as controls.

One-week prior to CAR-T cell injection, $0.5x10^6$ $CD19^+$ GFP^+ Raji-ffluc leukemia cells were prepared in sterile PBS and injected via the tail vein in NSG-SGM3 mice. After six days, the tumor engraftment was analyzed by bioluminescent imaging (BLI) using the IVIS® *in vivo* Imaging System. Tumor-bearing mice were distributed equally among the eight different groups, with 4 mice per group, and CAR-T cell mixtures were injected in bulk into the tumor-bearing mice via the tail vein.IVIS® was performed weekly to monitor the tumor development in the mice. Distribution and expansion of the CAR-T cells were analyzed by weekly blood staining. 28 days post CAR-T cell injection, endpoint analysis was performed. Therefore, blood, bone marrow, and spleens were extracted and prepared for flow cytometry. Results were analyzed with FlowJo (Treestar, Ashland, USA).

3.8.2 Experimental overview of *in vivo* cytokine release syndrome experiments

NSG-SGM3 mice, bred in-house, were used to investigate the development of CAR-related side effects in a humanized cytokine release syndrome (CRS) mouse model. The whole *in vivo* model was established from scratch at the institute, and the general idea was adapted from Norelli et al. [95]. All animals were kept under specific pathogen-free conditions at the institute's mouse facility. All animal experiments were approved by the local authorities.

4 weeks old female NSG-SGM3 mice were reconstituted with umbilical cord blood-derived human hematopoietic stem cells (hHSCs) as described in section 3.8.3. After 8 weeks of humanization, mice were engrafted with $0.5x10^6$ $CD19^+$ GFP^+ Raji-ffluc leukemia cells via the tail vein. Six days later, tumor engraftment was analyzed by bioluminescent imaging (BLI) using the IVIS® *in vivo* Imaging System. Humanized and tumor-bearing mice were distributed equally among the three different groups (JCAR017, JCAR021, untdx), with 7 - 8 mice per group. Untransduced (untdx) mock T cells derived from the same donor were used as negative controls. $0.8x10^6$ $CD8^+$ $EGFRt^+$ cells were injected in bulk into the tumor-bearing mice via the tail vein. For the titration experiment, $0.8x10^6$ or $0.4x10^6$ $CD8^+$ $EGFRt^+$ cells of JCAR017 and

JCAR021 (4 mice per group) were injected in bulk into the tumor-bearing mice via the tail vein. CAR-T cells were transferred as bulk populations, which were back-calculated to contain $0.8x10^6$ $CD8^+$ $EGFRt^+$ or $0.4x10^6$ $CD8^+$ $EGFRt^+$ cells.IVIS® was performed weekly to monitor the tumor development in the mice. Persistence and expansion of the CAR-T cells were analyzed by weekly blood staining. *In vivo* cytokine concentrations were measured by flow cytometry using the LEGENDplex immunoassay, following the manufacturer's instructions. Mice were monitored for body weight loss and rectal body temperature up to seven times per week, depending on their health score. Mice were sacrificed when manifesting clinical signs of suffering and high tumor burden, but latest 28 days post CAR-T cell injection (for titration experiment: 10 days post CAR-T cell injection). At the endpoint, blood, bone marrow, and spleens were extracted and prepared for flow cytometry. Results were analyzed with FlowJo (Treestar, Ashland, USA).

3.8.3 Humanization of NSG-SGM3 mice

Immunocompromised NSG-SGM3 mice were humanized with umbilical cord blood-derived human hematopoietic stem cells (hHSCs), which were purified for $CD34^+$ expression as described before.

4 weeks old female NSG-SGM3 mice were irradiated with 1 Gy 18 – 24 h prior stem cell injection. Frozen and purified $CD34^+$ hHSCs were rapidly thawed in pre-warmed sterile FCS, centrifuged, and resuspended in 1 ml FCS. 50 µl were stained for CD34 and CD45 expression as described previously and analyzed on a Cytoflex flow cytometer. Purity and total cell counts were determined by using 123count eBeads™. 100 µl containing cell solution containing $0.1x10^6$ hHSCs were infused intravenously into irradiated mice. Humanization level (human $CD45^+$ engraftment) and the pattern of hematopoietic reconstitution (human $CD19^+$ B cells, $CD33^+$ myeloid cells, $CD14^+$ monocytes, $CD3^+$ T cells) were determined 8 weeks after stem cell injection by flow cytometry after bleeding from the tail vein.Humanization levels were defined as: "$hCD45^+$ cell counts / all $CD45^+$ cell counts" measured in peripheral blood and are also referred to as the $hCD45^+$ chimera. According to 'The Jackson Laboratory', a mouse is

humanized with a hCD45$^+$ chimera over 25 %. However, we only used mice with humanization levels above 60 % in our experiments.

3.8.4 Bioluminescent imaging of mice

For *in vivo* imaging of the tumor growth, mice were intraperitoneally injected with a sterile solution of 15 mg/ml D-Luciferin PBS solution before they were anesthetized with isoflurane. 10 - 15 min after D-luciferin injection, mice were imaged with an automatically determined exposure time and a maximum threshold of 60 s. After the imaging, mice were placed back into their cages and monitored until they awakened from their anesthesia and showed agile activities. Luciferase activity and radiance were analyzed using Living Image® Analysis Software (Perkin Elmer).

3.8.5 Monitoring of mice

Depending on the experimental setup, mice were closely monitored every 1-3 days for signs of xenogeneic graft-versus-host disease after humanization or other toxicities during the CRS experiments. Weight loss due to tumor growth or CRS development was recorded twice per week, but if required, up to seven times per week. End points were predetermined by the length of the experiment or if animals showed a high sick score, which was regulated in the associated animal approval.

3.8.6 Spleen and bone marrow preparation

Spleens of sacrificed mice were immediately transferred into 10 ml ice-cold cRPMI medium and homogenized and filtered through a 70 µm cell strainer. The single-cell suspension was centrifuged, and the cell pellet was resuspended in 5 ml ACT. Lysis of erythrocytes was stopped after 5 min with the addition of 10 ml ice-cold cRPMI. Cells were again centrifuged and filtered, and total cell numbers were determined using a Neubauer chamber. A maximum of $10x10^6$ cells was transferred with 10 µl 123count eBeads™ into a 96-well V-bottom plate.

One femur and one tibia were uncovered per mouse for bone marrow extraction and cleaned from remaining soft tissue. Femurs were disconnected from the hip joint, and fibers were removed. Bones were separated and cut on both sides. Bone marrow was extracted by flushing the bones with 2 ml ice-cold cDMEM. Isolated cells were collected in 10 ml ice-cold cDMEM, centrifuged, and incubated with 3 ml ACT for 3 min at RT. Erythrocyte lysis was stopped by the addition of 3 ml ice-cold cDMEM, and cells were resuspended in 200 µl FACS buffer and filtered. A maximum of $10x10^6$ cells was transferred together with 10 µl 123count eBeads™ into a 96-well V-bottom plate.Tissue samples were stained as described before, except that cells were stained in 100 µl antibody master mix. Half of the cells were acquired on a Cytoflex S flow cytometer, and frequencies of transferred and endogenous cell subsets were assessed using the FlowJo software. Absolute cell numbers were calculated based on frequencies and total cell numbers for individual cell subsets.

3.8.7 Analysis of blood and serum

The persistence of adoptively transferred CAR-T cells was investigated by weekly blood staining of the mice. Mice were kept under a heating lamp for several minutes to increase the dilatation of the blood vessels, and the tail vein was punctured with a needle.

Blood droplets were collected and mixed with 50 µl Heparin diluted 1:1 with PBS to prevent coagulation. Blood samples were transferred into 15 ml falcon tubes containing 10 ml ACT. After 10 min, erythrocyte lysis was stopped with 5 ml ice-cold cRPMI. Cells were centrifuged and incubated again with 5 ml ACT for 5 min at RT. Lysis was stopped with 5 ml cRPMI, centrifuged, and cells were transferred together with 10 µl 123count eBeads™ into a 96-well V-bottom plate. The whole sample was acquired on a Cytoflex S flow cytometer, and frequencies of transferred and endogenous cell subsets were assessed. Absolute cell numbers were calculated based on frequencies and total cell numbers for individual cell subsets. Results were analyzed using the FlowJo software.

For the preparation of serum samples, 30 µl of blood were drawn from the mice’s tail veins as described before, but without the addition of Heparin. Coagulated blood was centrifuged for 10

min at $5x10^3$ g at RT, and serum was immediately removed and stored at – 20°C. The staining of cytokines was performed with the LEGENDplex Multi-Analyte Flow Assay Kit according to the manufacturer's recommendations.Briefly, serum samples were thawed, mixed, and centrifuged to remove particulates. 15 µl serum was diluted 2-fold with assay buffer, and 12.5 µl were transferred into a 96-well V-bottom plate. Pre-diluted samples were mixed with 12.5 µl assay buffer and 12.5 µl premixed beads and shaken at 800 rpm and 4 °C overnight in the dark. The next day, plates were washed twice with 200 µl wash buffer. Samples were resuspended in 12.5 µl antibody detection mix and incubated under constant shaking at 800 rpm for 1 h at RT in the dark. 12.5 µl Streptavidin-PE was added, and samples were incubated for another 30 min. After two rounds of washing, beads were resuspended in 150 µl wash buffer. Samples were read on a Cytoflex S flow cytometer and analyzed using the LEGENDplex™ Data Analysis Software. Samples were run in technical duplicates.

3.9 Statistical Analysis

All statistical tests were performed using GraphPad Prism8 (GraphPad Software Inc.). Statistical details are indicated in the respective figure legends. Level of significance were defined as the following: ns $p > 0.05$, *$p \leq 0.05$, **$p \leq 0.01$, ***$p \leq 0.001$, ****$p \leq 0.0001$. Data are presented as mean + standard deviation if not stated otherwise specifically.

4 Results

4.1 Characterization of CD19-specific chimeric antigen receptor clones

The extracellular binding domain of the CAR molecule is usually derived from specific monoclonal antibodies (mAbs) and equips the corresponding CAR-T cell with a high binding strength receptor toward its target. So far, only CD19-targeting CAR-T cell products with an scFv derived from the high-affinity antibody clone FMC63 are clinically approved for $CD19^+$ B cell malignancies. Although few CAR-T cell products with different scFvs targeting CD19 have been engineered and tested for their efficacy in clinical settings, most research has focused on FMC63-derived CARs. Consequently, much knowledge has been generated about optimizing signaling domains and the hinge region, but the impact of receptor affinity on the downstream functionality of the CAR-T cell has not been clearly delineated yet.

4.1.1 Structure and binding kinetics of different anti-CD19 CAR clones

To better understand how receptor affinity affects CAR-T cell efficacy and safety, we selected four clinically relevant scFvs derived from CD19-specific mAb and investigated their binding kinetics and *in vitro* functionality.

Modifications in any structural domain of a CAR molecule can have enormous effects on the functionality of the corresponding CAR-T cell. In order to generate CARs that only differ in their binding domain, all four CAR scFvs were introduced into the same second-generation CAR backbone. As illustrated in Fig. 1A, the intracellular activation and signaling domains CD3zeta and 4-1BB were connected to the extracellular binding domain by a triple Strep-tag (STII) hinge and a CD28 transmembrane domain. As the STII hinge, together with the scFv, is part of the CAR ectodomain, it can be used as a marker of CAR expression on the cell surface, e.g., by antibody staining for flow cytometry. In addition, all CAR sequences incorporated a truncated version of the human epidermal growth factor receptor (EGFRt) at the C-terminus. Due to its connection by a T2A-ribosomal skip element, the CAR and EGFRt proteins are co-expressed equimolarly.

As the intracellular signaling domains of the truncated version were removed, this tag can be used as a transduction or selection marker for engineered cells without unintentional activation of the cell[139].

While the JCAR017 scFv was derived from the clinically used high-affinity FMC63 clone, JCAR021 was derived from an unknown humanized antibody. The 4G7 and CAT scFv sequences are similar to the original publications and patents (WO 2016/139487A1; WO 2014/184143A1, respectively).

So far, several groups have determined the binding kinetics of the different CAR clones, except for JCAR021, by Biacore surface plasmon resonance (SPR) measurements. This optical method quantifies reversible interactions between binding partners by monitoring the association and dissociation of protein ligands to their target. However, the published results are not conclusive so far, as the analyzed values vary by a factor of 10 (Fig. 1B). Possible reasons are incorrect experimental setups and the use of unstable and aggregated recombinant CD19 protein for the measurement. The AG Traxlmayr at the University of Natural Resources and Life Sciences (BOKU) in Vienna has engineered a stable version of the extracellular domain (ecd) of the soluble recombinant CD19 protein, called CD19-SF15[195], which enables standardized Biacore SPR measurements of CD19-binders for the first time. In collaboration with the AG Traxlmayr, we used this newly generated technology to determine the equilibrium constant and on- and off-rates for JCAR017, JCAR021, and the CAT scFv (Fig. 1C). Due to limited capacities, we could not perform SPR for the 4G7 clone, but we assumed that the corresponding CAR exhibits a high affinity in the range of JCAR017, as published before (Fig. 1B).

In preparation for the measurement, we produced purified soluble recombinant CAR scFv proteins containing a Twin-Strep-tag, which enabled the immobilization of the protein on StrepTactin molecules covalently bound on the surface of the Biacore chip. In the next step, soluble stabilized CD19-SF15 was applied over the surface at a constant rate to form complexes with the immobilized CAR scFv. The association and dissociation of the CD19 ligand with and off the immobilized CAR scFv result in changes in the refractive light index,

which is proportional to the mass of the bound material and thus can be converted into response units. While an increase in response units after the injection of the CD19 ligand into the flow represents the association rate, a decrease in the response rate reflects the ligand dissociation from the target (Fig. 1C).

As expected, JCAR017 showed the highest affinity among the three measured CAR/antigen interactions, with a long dissociation time (k_{off} = 5.6x10^{-4} s^{-1}), resulting in a K_D-value in the nanomolar range (2.7x10^{-9} M) (Fig. 1D). In contrast, as already published before, the CAT scFv showed substantially lower binding affinity (K_D = 5.5x10^{-8} M) due to a much faster k_{off}-rate (1.3x10^{-2} s^{-1}). Surprisingly, JCAR021, which was measured for the first time, had an even lower binding affinity (K_D = 1.4x10^{-7} M) to CD19 than the CAT scFv. Again, the differences between the calculated K_D-values were mainly due to a faster k_{off}-rate of JCAR021 (2.1x10^{-2} s^{-1}). All three CAR clones revealed similar k_{on}-rates between 2.0x10^{5} M^{-1}s^{-1} to 2.3x10^{5} M^{-1}s^{-1}, enabling an even more conclusive analysis of the impact of CAR affinity on CAR-T cell functionality.

Besides the affinity, also the location at which different antibody clones bind their target can vary. In order to test whether the CAR clones bind the same epitope, we performed epitope mapping of JCAR017 and JCAR021, as well as JCAR017 and CAT, by SPR in collaboration with the AG Traxlmayr. Either the JCAR021 scFv or CAT scFv were immobilized on a StrepTactin-loaded SPR chip. Afterward, a mixture of CD19 and JCAR017 or CD19 alone was associated for 400 s. An increase in response units was only detected after the administration of CD19 alone, whereas no differences were observed when using the CD19 mix with JCAR017 (Fig. 1E). These results indicate that JCAR021 and JCAR017 bind to the same epitope on the extracellular domain of CD19. Similar results were obtained for the CAT scFv and JCAR017 (data not shown), which have also been shown by other groups[95]. In summary, we generated CAR constructs with the same binding site that only differ in their affinities due to different off-rates. Therefore, they represent a valuable tool for investigating the pure effect of affinity on CAR-T cell functionality.

A

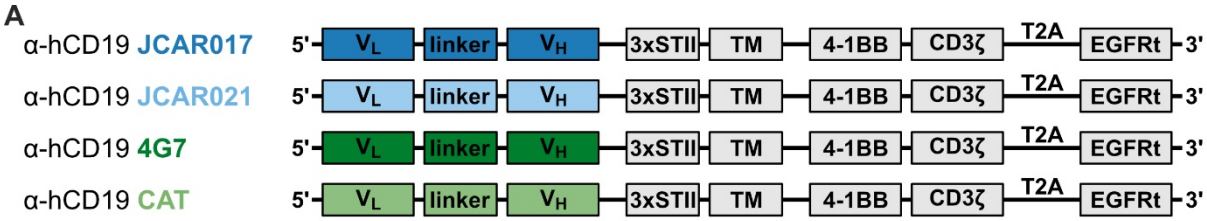

B

CAR clone	k_{on} ($M^{-1}s^{-1}$)	k_{off} (s^{-1})	K_D (nM)	literature
JCAR017/FMC63	$2.0x10^5$	$6.8x10^{-5}$	0.3	Ghorashian et al., Nat. Med., 2019
	$6.2x10^5$	$5.5x10^{-4}$	0.8	Anne Kramer, Dissertation, London, 2017
	n/a	$3.0x10^{-3}$	3.0	Acro Biosystem
JCAR021	n/a	n/a	n/a	
4G7	n/a	n/a	8.4	Markus Kügler, Dissertation, Nürnberg, 2010
	$6.0x10^4$	$1.2x10^{-3}$	20.1	Anne Kramer, Dissertation, London, 2017
CAT	$2.2x10^5$	$3.1x10^{-3}$	14.4	Ghorashian et al., Nat. Med., 2019
	$6.1x10^5$	$7.1x10^{-2}$	116	Anne Kramer, Dissertation, London, 2017

C

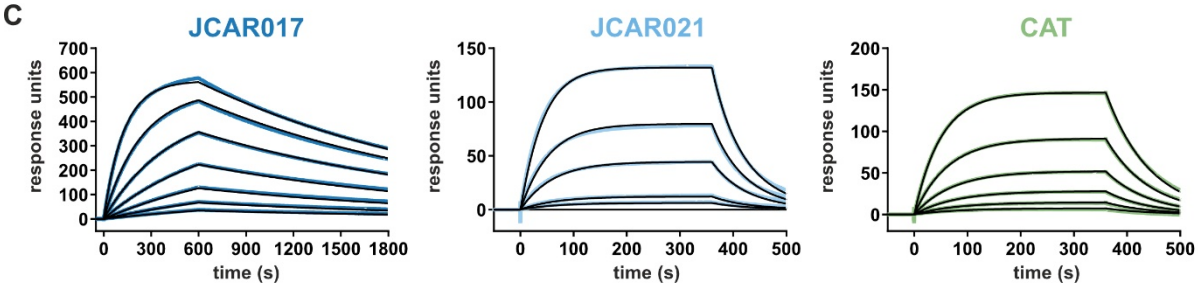

D

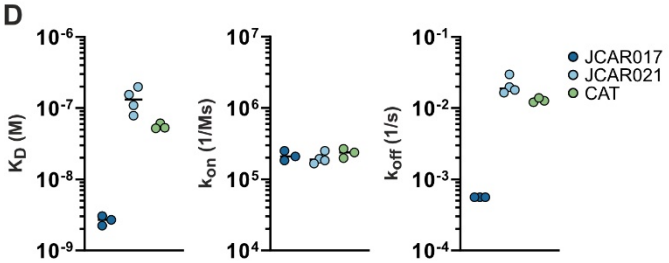

E

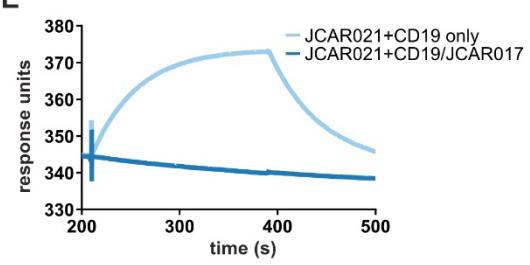

Fig. 1 Structure and binding kinetics of different CD19-targeting CAR clones
(A) Design of different CAR sequences targeting human CD19 for retroviral transduction. **(B)** Published data of binding kinetics of CAR clones. **(C)** Representative surface plasmon resonance sensorgrams of binding kinetics of different concentrations of JCAR017, JCAR021, and CAT scFvs to CD19-SF15. **(D)** Dissociation constant (K_D), association rate (k_{on}) and dissociation rate (k_{off}) of CAR clones (n = 3-4). **(E)** Epitope mapping of JCAR021 and JCAR017 binding towards CD19.

4.1.2 *In vitro* functional testing of different CAR clones

In addition to specific binding properties, also CAR expression levels on the cell surface contribute to the overall functionality of a CAR-T cell. To test whether the different clones are similarly expressed on the cell surface, primary T cells were genetically engineered by retroviral transduction to express one of the four CAR constructs. Three to five days later, CAR-T cells were analyzed by flow cytometry for the expression of the STII in the hinge,

representative for CAR expression, and EGFRt as a marker for successful transduction (Fig. 2A). Untransduced mock T cells from the same donor were used as a negative control. All CAR-T cells showed successful expression of the CAR and EGFRt on the cell surface (Fig. 2A) with donor-dependent transduction efficacies of over 20 %, as indicated by frequencies of EGFRt$^+$ cells (Fig. 2B). While 80-90% of the transduced cells were also STII$^+$ in the JCAR017, JCAR021, and CAT groups, the CAR-EGFRt correlation of the 4G7 clone was slightly decreased (Fig. 2C).

Furthermore, no differences in the median fluorescent intensities (MFI) of STII and EGFRt were observed among the four CAR constructs, except for variabilities among experiments (Fig. 2D-E). Overall, we could conclude that all four CARs can be stably and equally expressed on the cell surface. Therefore, potential functional differences among the CAR-T cell groups are most likely exclusively ascribed to the different CAR binding kinetics.

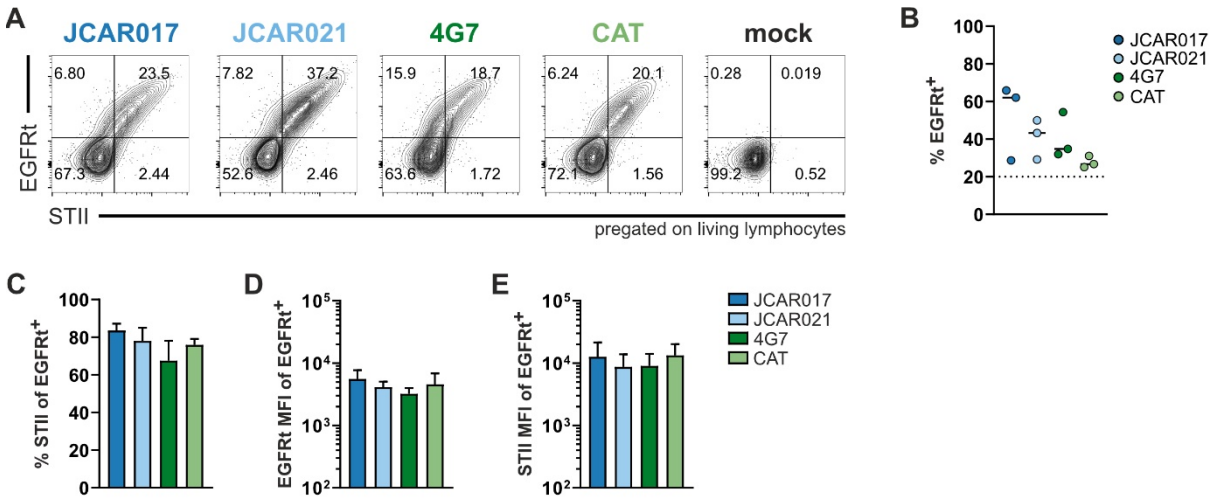

Fig. 2 Expression pattern of CAR constructs on primary T cells after retroviral transduction
(A) Representative flow cytometry plots of retroviral CAR-transduced PBMCs stained for EGFRt and Strep-tag (STII) expression. While EGFRt was stained with a fluorescently labeled primary antibody against the EGFR protein, the Strep-tag in the hinge region was stained with Streptavidin conjugated to a small fluorophore (e.g., FITC or eF450). **(B)** Transduction efficacies of PBMCs are determined by frequencies of EGFRt$^+$ cells at least three days after retroviral transduction. Data are expressed as mean+SD (n = 3). **(C)** Frequencies of STII$^+$ cells of CAR transduced cells expressed as mean+SD (n = 3). **(D)** EGFRt MFI (mean fluorescent intensities) and **(E)** STII MFI of EGFRt$^+$ transduced cells. Data are expressed as mean+SD (n = 3).

Next, we compared our four affinity CAR clones in different *in vitro* assays for their sensitivity, cytokine production, and cytotoxic potential.

Target-specific activation of the CARs was tested with a Nur77-Jurkat reporter assay[196]. This Jurkat cell line is engineered to carry the Nur77-transgene connected via a T2A-element to the DNA cassette of the fluorescent protein tdTomato. Therefore, in the case of cell activation, the transgene is expressed along with tdTomato, and the signal can be easily detected by flow cytometry. The four CARs were introduced into the reporter cell line and co-incubated with CD19$^+$ Raji tumor cells, while background activation was monitored in samples incubated in medium without target cells. After three hours, activation levels of the transduced EGFRt$^+$ Nur77-Jurkats were determined by flow cytometry (Fig. 3A). As expected, CAR transduced Jurkats were specifically activated by CD19$^+$ target cells independent of the CAR construct. Interestingly, we did not detect any differences despite the different CAR affinities (Fig. 3B). We also observed a certain level of background signaling, which was barely detectable in the untransduced mock control (Fig. 3C). Especially viral transduction, but also possible low levels of tonic signaling via the CAR could result in a leakage of the reporter expression. Still, the difference in the percentage of activated cells upon antigen-specific stimulation validates the specificity of the CAR constructs.

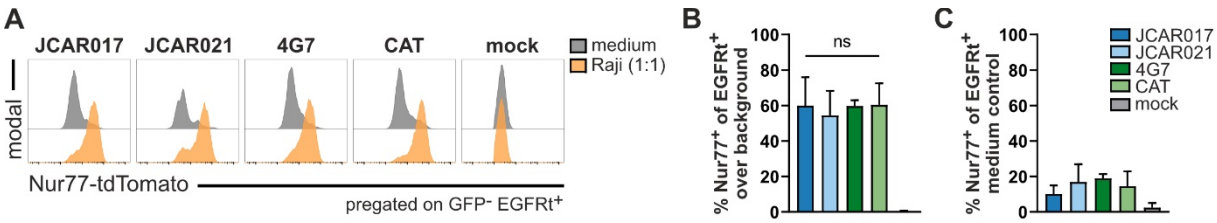

Fig. 3 Nur77-Jurkat activation assay with CD19-targeting CAR clones
(A) Representative flow cytometry histograms of Nur77-tdTomato expression of retrovirally transduced Nur77-Jurkats after either stimulation with CD19$^+$ Raji cells (effector-to-target ratio 1:1) or incubation in medium. **(B)** Specific stimulation of transduced Nur77-Jurkats was calculated by subtracting background frequencies of Nur77$^+$ EGFRt$^+$ cells from Nur77$^+$ frequencies after stimulation with Raji cells. **(C)** Background signaling of transduced Nur77$^+$ Jurkats in the medium control group. Data are expressed as mean+SD of 2-7 biological independent replicates with technical duplicates.

In order to test the influence of affinity on CAR-T cell sensitivity *in vitro*, we performed cytokine release assays to evaluate intracellular cytokine production levels after specific stimulation of the different CAR clones.

Retrovirally transduced and rested CAR-T cells were stimulated with $CD19^+/GFP^+$ Raji tumor cells in two E:T ratios (1:0.25 and 1:1) for five hours. A mixture of PMA and Ionomycin was used as a receptor-independent activation control (positive control), while background levels of cytokine production were measured by incubating CAR-T cells in medium without further stimulation. All CAR-T cells expressing different receptors showed specific production of the effector cytokines IFN-γ, TNF-α, and IL-2 over background levels (Fig. 4). The highest release was detected for TNF-α (60 %), followed by IL-2 (30 %) and INF-γ (20 %). Frequencies of cytokine-producing CAR-T cells decreased when they were co-incubated with fewer target cells. This result illustrates that the tested CAR-T cells can regulate their cytokine release according to the number of tumor cells. Although all CAR-T cells showed specific activation, no affinity-dependent differences in the potential of cytokine production were observed.

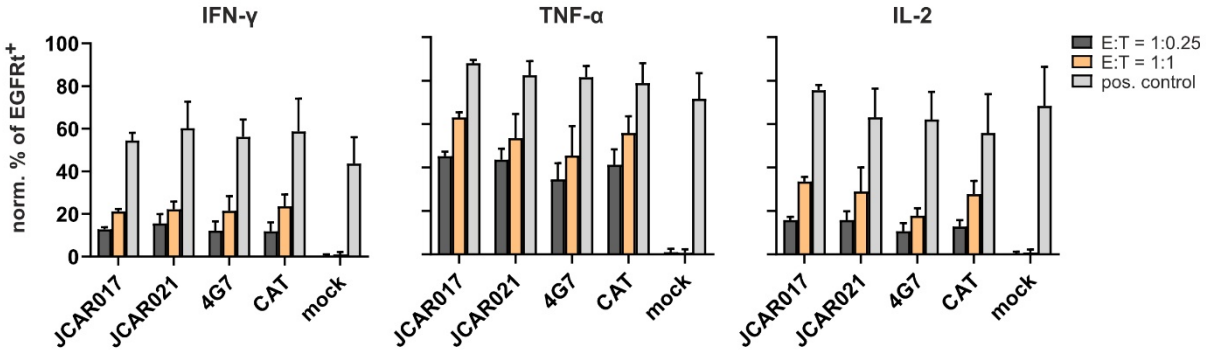

Fig. 4 Intracellular cytokine release of different CAR-T cell clones
Functional *ex vivo* cytokine response of CAR-transduced $EGFRt^+$ cells after 5 h of co-incubation with target cells. The addition of the protein transport inhibitor Brefeldin A after one hour of co-incubation prevented cytokine release from the cells. Analysis of the release of IFN-γ, TNF-α, and IL-2 over background after *ex vivo* stimulation of CAR-T cells with $CD19^+$ Raji cells in E:T ratios of 1:1 and 1:0.25. PMA/Ionomycin stimulation was used as a positive control. Data are expressed as mean+SD of three biologically independent experiments with technical triplicates and normalized to the average release of JCAR017.

Although the first *in vitro* assays demonstrated antigen specificity and sensitivity of the different CAR-T cell products, the results might indicate but not demonstrate their potential to efficiently eradicate tumor cells, a crucial parameter of successful CAR-T cells. Therefore, two different *in vitro* cytotoxic assays were performed to investigate the killing potential of CAR-T cells with different affinities.

In order to monitor the killing kinetics of the different CAR-T cell constructs in real-time, we firstly used the impedance-based technology called xCelligence®. The growth of engineered HEK target cells expressing the extracellular domain of CD19 was followed for one day before sorted $EGFRt^+$ CAR-T cells were applied in E:T ratios of 4:1 and 1:1. Killing kinetics were monitored for 25 hours (Fig. 5A). While untransduced mock T cells did not affect the growth of the target cells, all CAR-T cells eradicated the $CD19^+$ HEK target cells within 10 hours of co-incubation. Killing kinetics overlapped tightly among the different CAR-T cells (Fig. 5A) and were independent of the E:T ratio (Fig. 5B). Besides, no unspecific killing of $CD19^-$ HEK cells was observed in any of the CAR-T cell groups (Fig. 5A-B).

The used immortalized HEK cell line does not endogenously express CD19 on its cell surface. In order to circumvent potentially unwanted effects due to viral overexpression of CD19, a second set of *in vitro* tumor-killing assays was performed. Therefore, CAR-T cells were co-incubated with $CD19^+GFP^+$ Raji tumor cells for 48 hours, which could be distinguished by their intrinsic GFP expression (Fig. 5C). Comparable to the first cytotoxic assay, CAR-T cells of the different groups killed over 95 % of the tumor cells after 48 h of co-incubation independent of their affinity (Fig. 5D). Only low levels of background lysis were detected in the untransduced mock T cell group.

Taken together, the performed *in vitro* killing assays indicate similar antigen sensitivity and cytotoxic potentials of CAR-T cells with either low or high affinities.

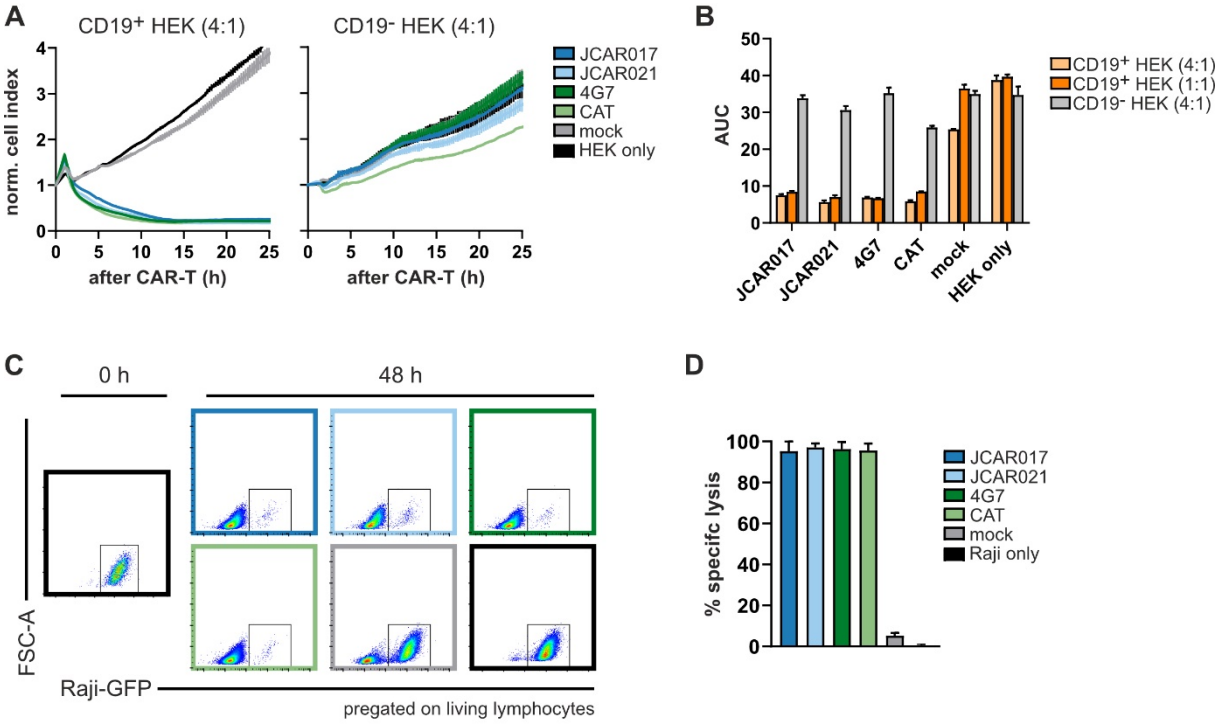

Fig. 5 Analysis of *in vitro* cytotoxicity of different CAR-T cell clones
(A) Representative impedance-based xCelligence killing curves of target HEK cells. $CD19^+$ and $CD19^-$ HEK target cells were co-incubated with CAR-T cells in an effector-to-target ratio (E:T) of 4:1, and growth curves of the target cells were followed for 25 h after CAR-T cell addition. **(B)** Analysis of CAR-T cell killing efficacy by calculating the area under the growth curve (AUC) for E:T ratios of 4:1 and 1:1. Data represent the mean+SD (n = 3). **(C)** Representative flow cytometry plots of remaining $CD19^+GFP^+$ Raji cells after 48 h of co-incubation with CAR-T cells. **(D)** Specific lysis of target cells after 48 h. Absolute remaining numbers of Raji cells were normalized to the mock control sample and depicted as percentages. Data are expressed as the mean of three independent experiments with n = 3.

4.2 Development of a flow cytometry-based k_{off}-rate assay for screening CAR affinities

The four tested CAR clones showed no major affinity-related differences in their *in vitro* functionality. One potential reason could be that the range of the tested CAR affinities still ensures good CAR-T cell functionality. Indeed, although the affinity of CAT and JCAR021 was determined to be over 20 and 50-fold lower than the clinically used JCAR017 clone FMC63, their binding strength is still at least ten times higher compared to avidities measured for endogenously expressed TCRs. To investigate the impact of super-low-affinity on CAR-T cell functionality, we decided to build up a library of CD19-targeting CAR mutants with affinities in the range of more sensitive TCRs. Until today, SPR measurements are considered the gold standard for the affinity measurement of protein-protein interactions. However, this method is labor- and, in particular, time-intensive, as one interaction measurement can take up to one day, and therefore it is not helpful for screening CAR libraries.

Consequently, we established an alternative method for measuring the affinities of CAR-target interactions based on the in-house developed flow cytometry-based TCR-ligand k_{off}-rate assay[164,165,194]. This method determines TCR/pMHC binding kinetics in a rapid flow cytometry-based way and enables the monitoring of monomeric ligand dissociations under natural conditions (e.g., cell surface distribution and expression of the respective receptor). Although the k_{off}-rate assay only measures the dissociation half-live and not the complete K_D-value, it has been shown for TCRs that the k_{off}-rate correlates with the functionality of the corresponding T cell[165]. Indeed, we determined different k_{off}-rates but similar k_{on}-rates for the tested CAR clones and thus are confident to use the dissociation rate as an estimate for CAR affinity.

In brief, pMHC-molecules of interest are fluorescently labeled and multimerized via a Strep-tag on a StrepTactin-backbone. Afterward, target cells expressing the corresponding receptor are stained with the pMHC StrepTamer. Upon administration of D-biotin, the StrepTamer complex is disrupted, leaving monomeric TCR:pMHC interactions on the cell surface. Due to low affinities, pMHC molecules dissociate from the cognate TCR according to their binding strength. Dissociation kinetics can be followed due to the decay of the pMHC fluorescent signal over time by flow cytometry (Fig. 6A).

We investigated two possible options to apply this technology to measure CAR affinities. The first option (Fig. 6B) mimics the existing experimental setup by exchanging the target T cell expressing the TCR of interest with the respective CAR and the recombinantly expressed pMHC molecule with the soluble extracellular domain of CD19. In contrast, the second option turns the system around using target B cells that endogenously express CD19 on the cell surface and recombinantly expressed CAR scFvs as ligands (Fig. 6C). In order to provide reversible StrepTamers for the measurement of the binding kinetics, either CD19-ecd or CAR scFvs are recombinantly expressed as so-called FLEXamers, which contain a Strep-tag and a Tub-tag sequence at their C-terminus. While the first one enables the multimerization on a StrepTactin backbone, the latter is used for the stable conjugation of a fluorescent dye. Both options were tested for their feasibility and reliability.

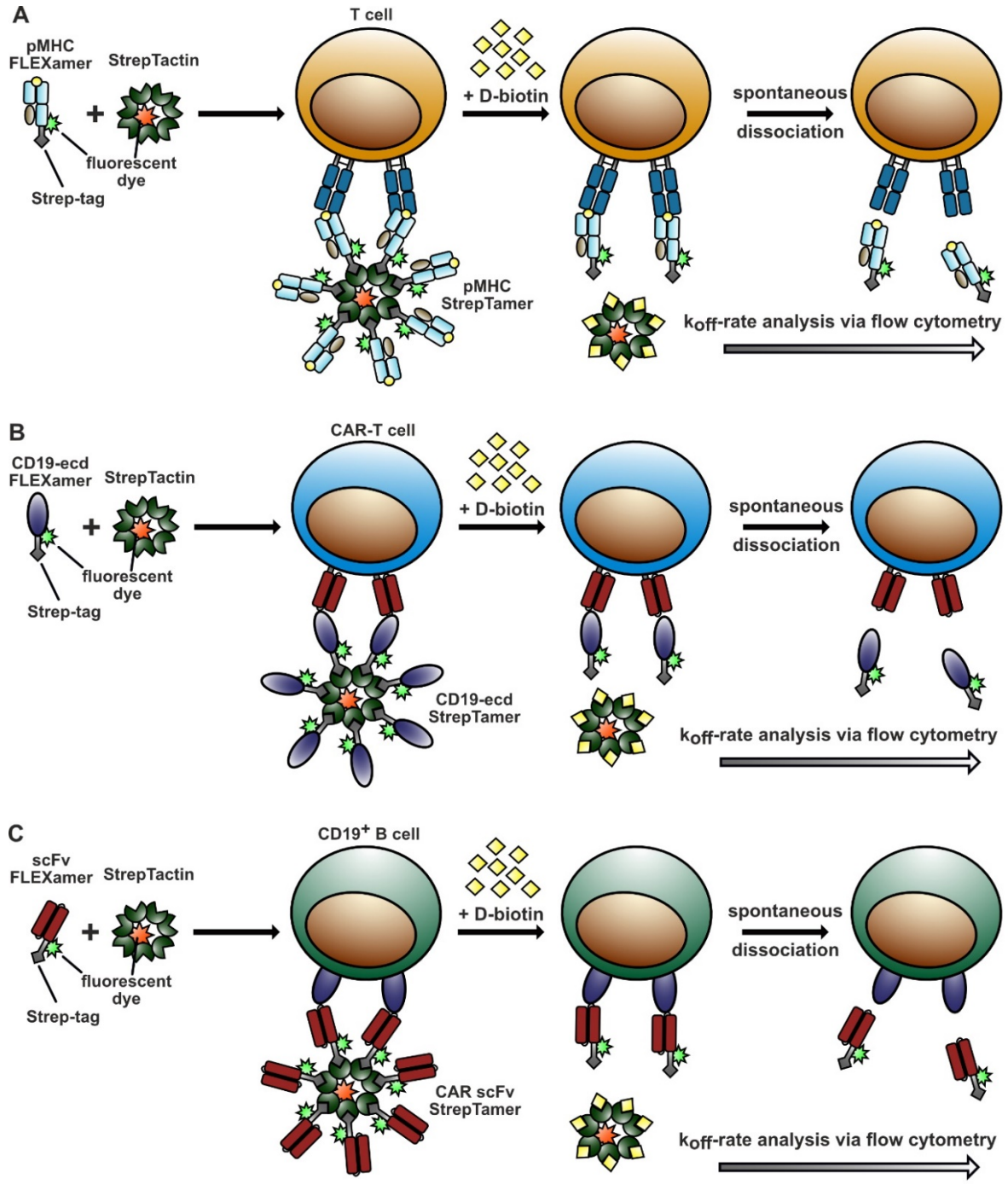

Fig. 6 Experimental setup of flow cytometry-based k_{off}-rate analysis of CD19-specific CARs
(A) T cells expressing the TCR of interest are stained with pMHC-StrepTamers comprising respective recombinantly expressed pMHC molecules with a StrepTag and Atto-488 (called FLEXamers) at their C-terminus and a StrepTactin backbone labeled with another fluorophore. After adding D-biotin, the StrepTactin dissociates from the cell surface, leaving pMHC monomers on the cell surface. The dissociation kinetics of pMHC molecules can be monitored as the decay of Atto488-dependent fluorescence by flow cytometry. **(B)** CAR transduced T cells are stably labeled with a StrepTamer consisting of fluorescently labeled soluble CD19-Atto488 FLEXamers and a StrepTactin backbone conjugated to another fluorophore. The addition of D-biotin disrupts the StrepTamer, and CD19 monomers are left on the T cell surface. The monomeric dissociation (k_{off}-rate) of CD19 can be monitored as the decay of Atto488-dependent fluorescence by flow cytometry. **(C)** The second option is to apply the k_{off}-rate assay to CD19/CAR interactions. $CD19^+$ B cells are stably labeled with a multimer consisting of scFv-Atto488 FLEXamers and StrepTactin backbone conjugated to another fluorophore. The addition of D-biotin disrupts the StrepTamer, and CAR scFv monomers are left on the B cell surface. The monomeric dissociation (k_{off}-rate) of CAR scFvs can be monitored as the decay of Atto488-dependent fluorescence by flow cytometry.

4.2.1 Generation of recombinant CAR scFv FLEXamers

In order to perform flow cytometry-based k_{off}-rate measurements of CAR-antigen interactions, the extracellular domain of either a CAR (scFv) or CD19 had to be produced as a recombinant soluble protein. CD19 belongs to the group of unstable and hard-to-express proteins, as it easily aggregates in solution[195,197]. Therefore, we started with the generation of six different CAR scFvs for the first proof-of-principle experiments.

DNA strings of different CAR scFv FLEXamers were designed *in silico* by connecting a Twin-Strep-tag and a Tub-tag at the C'-terminus of the corresponding scFv DNA sequence, which is similar to the retroviral DNA constructs (Fig. 7A). While the Twin-Strep-tag is used for StrepTactin-based purification and multimerization of the scFv, the Tub-tag is exploited to covalently link a fluorescent dye on the protein. The three-dimensional structure of scFvs is stabilized by disulfide bonds, which can only form correctly in a reducing milieu. Consequently, the DNA strings were cloned into an acceptor vector containing a tetracycline (tet)-promoter and the ompA signal sequence for periplasmic protein production in bacteria. ScFv FLEXamers were expressed in *E.coli* bacteria by inducing the tet-promoter with anhydrotetracycline (AHT), which starts the secretion of the protein into the bacteria periplasm where it can adequately fold. After extraction and affinity purification via the Strep-tag, the purity and size of the recombinant proteins were analyzed by SDS gel electrophoresis (Fig. 7B). A defined band was detected at the expected size of CAR scFvs containing a double-tag (35 kDa) in all samples.

Moreover, purities were also high, as no contaminations or degradation products were observed on the stained SDS gel. In the next step, CAR-FLEXamers were functionalized with a fluorescent dye. The used chemo-enzymatic method is a two-step reaction. First, the tubulin-tyrosine ligase (TTL) enzymatically catalyzes the activation of the C'-terminus of the FLEXamer precursor. In a second step, the activated tag is functionalized with the Dibenzocyclooctin (DBCO) conjugated Atto-488 dye via click-chemistry. The shift assay in Fig. 7C revealed a high efficiency of the Tub-tag mediated conjugation of Atto488 to the six unfunctionalized scFv proteins. Although experimental conditions have been optimized to protect the sensitive scFv

proteins and to guarantee high functionalization efficacies (ref. Material and Methods), some protein loss during the functionalization steps cannot be entirely prevented (e.g., scFv1). However, it was possible to generate sufficient amounts of highly pure scFv-FLEXamers for further experimental testing.

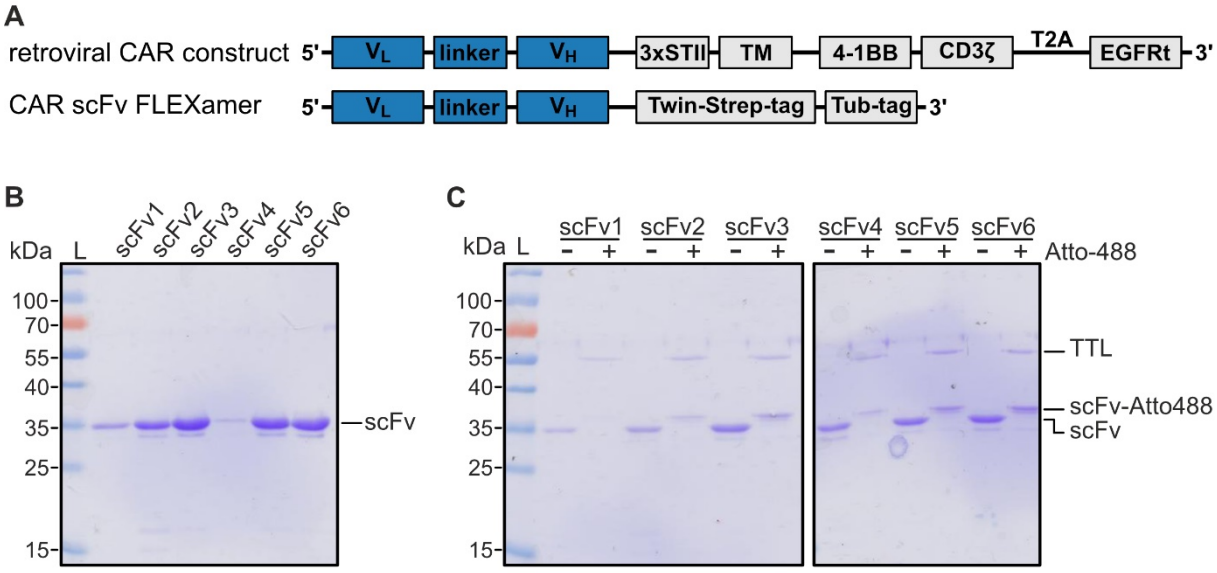

Fig. 7 Generation of CAR scFv FLEXamers
(A) Illustration of the scFv FLEXamer DNA sequence compared to the CAR construct used for retroviral transduction. Extracellular CAR scFvs were linked with a Twin-Strep-tag and a Tub-tag to generate FLEXamers. **(B)** The purity and size of expressed and purified scFv FLEXamers were validated by SDS gel electrophoresis. Proteins were detected via Coomassie staining. **(C)** Shift assay of unfunctionalized scFvs and after functionalization with the Atto488-dye separated by SDS gel electrophoresis. B and C depict exemplary six out of 40 scFv FLEXamers. In general, 300 µl of in average 1.0 µg/µl purified recombinant scFvs and 50 µl of in average 0.4 µg/µ functionalized scFvs were produced.

4.2.3 Flow cytometry-based k_{off}-rate measurement with CAR scFv FLEXamers

After titrating the necessary amount of scFv FLEXamers to successfully generate scFv StrepTamers (data not shown), several parameters of the flow-based k_{off}-rate assay were optimized for the measurement of CAR-antigen interactions (e.g., temperature, volume, duration of measurement). A detailed protocol on how to measure k_{off}-rates of CD19-specific CAR-T cells is described in the Material and Methods section.

All generated CAR scFvs used in this thesis target the B cell lineage protein CD19. Therefore, endogenous B cells of freshly isolated peripheral blood mononuclear cells (PBMCs) from healthy donors were used as target cells. PBMCs were stained *ex vivo* with the scFv StrepTamers and a non-reversible CD20 mAb. Co-staining of the population of interest

enabled continuous tracking of CAR dissociation kinetics from the target cells ($CD20^+$ target population) without previous purification of the B cells.

In order to analyze CD19-CAR dissociation kinetics, fluorescent signals of the CAR scFvs and the StrepTactin-APC backbone were followed over time (Fig. 8A). At the start of the analysis, initial staining intensities of both fluorophores (APC and Atto488) were visible at a constant level. Upon addition of D-biotin, the StrepTactin backbone detached from the cell surface, as reflected by the fast drop of the APC fluorescence signal (Fig. 8A). After an initial de-quenching, Atto488-conjugated scFvs dissociated according to the CAR binding strength.

We observed steep dissociation curves for JCAR021 and CAT scFvs, where the respective monomers detached entirely from the cell surface within minutes after the addition of D-biotin (Fig. 8A-B). On the contrary, JCAR017 and 4G7 revealed slower scFv dissociation curves, and only small amounts of the corresponding scFv monomers were released from the cell surface within 30 minutes. CAR scFv dissociation was quantified and expressed as half-lives, defined by the k_{off}-rate with: $t_{1/2} = \ln 2/k_{off}$. Consequently, low half-lives of a binding interaction correlate with high k_{off}-rates, which entail high K_D-values and thus represent low affinities, given that the association rate remains constant. As predicted, JCAR017 and 4G7 had long half-lives of 2970 s and 1782 s, respectively, and consequently possess strong affinities to CD19 (Fig. 8C). In contrast, calculated half-lives of JCAR021 and CAT were low (167 s and 151 s, respectively), describing them as weak CD19 binders.

Although only half-lives and not absolute K_D-values can be determined with this flow cytometry-based method, relative differences in k_{off}-rates of different CARs can be calculated. Comparing the results of the SPR measurement with the calculated k_{off}-rates measured by flow cytometry, the data confirmed relative differences in the same range (Fig. 8D). While the SPR k_{off}-rate of JCAR021 was 37 times faster than JCAR017, their k_{off}-rate values determined by flow cytometry differed by a factor of 17. Besides, the k_{off}-rates of CAT were 23 and 19 times higher than JCAR017, quantified by the SPR and k_{off}-rate assay, respectively. Additionally, it has been shown that 4G7 is a strong binder of CD19 but slightly weaker than FMC63 (JCAR017) (Fig. 8C, 1B). Also, these findings could be confirmed by our k_{off}-rate assay. Although differences in

relative k_{off}-rates determined by either SPR or flow cytometry were observed, comparing the two methods validated that the flow-based k_{off}-rate measurement can be used as a suitable and reliable tool to detect relative CAR affinity differences.

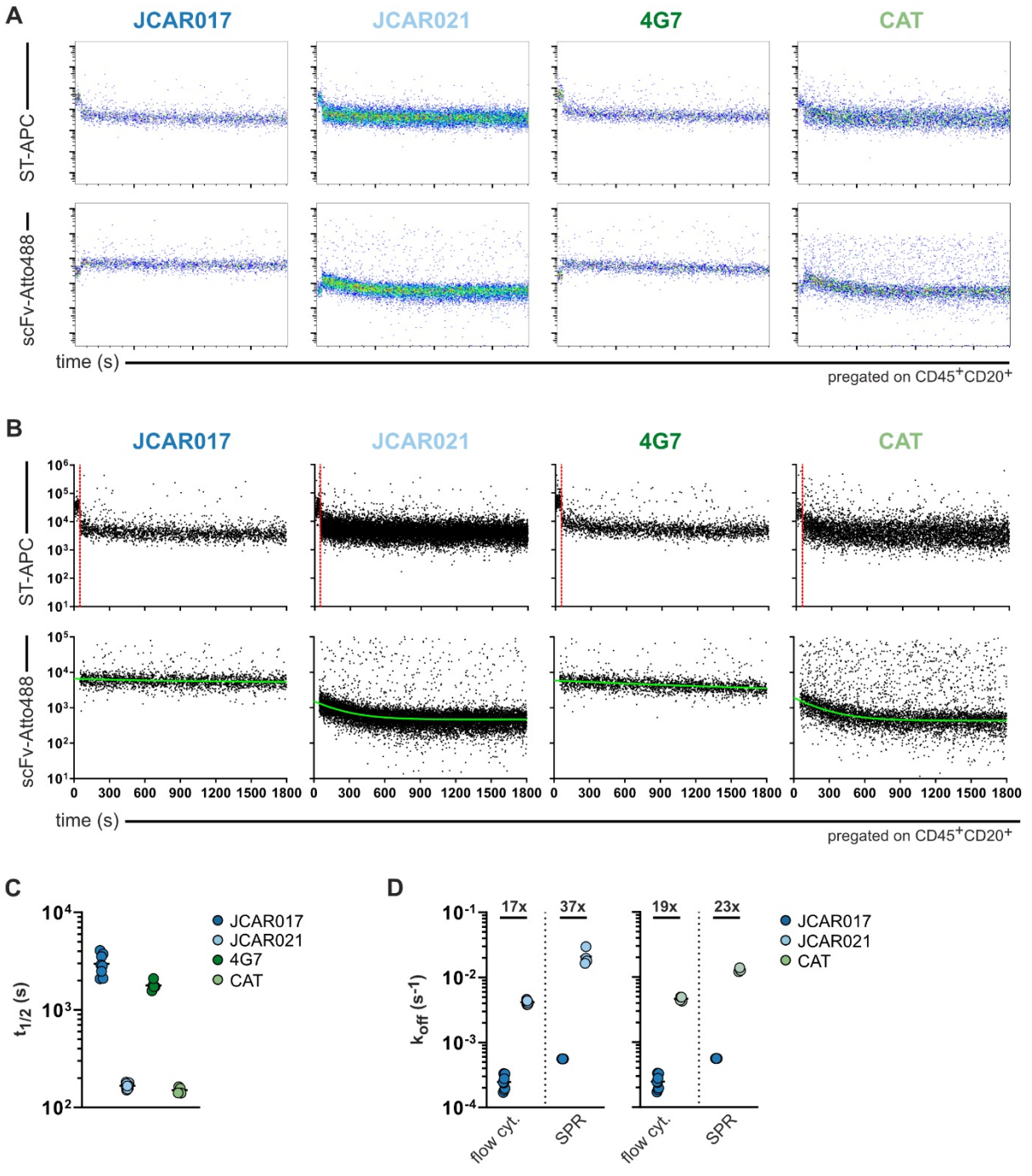

Fig. 8 Flow cytometry-based k_{off}-rate measurement of CAR affinity clones
(A) Representative flow cytometry plots of the dissociation of the StrepTactin-APC backbone or Atto488-conjugated scFv after the addition of D-biotin monitored by flow cytometry for 30 minutes at 20°C. **(B)** Curve fitting of the dissociation kinetics of different CAR affinity clones. Complete dissociation of the StrepTactin backbone (red line) defines the starting point for fitting the scFv-Atto488 dissociation by the exponential decay function (green line). **(C)** Half-lives ($t_{1/2}$) are determined by flow cytometry-based k_{off}-rate measurements. For curve fitting of JCAR017 and 4G7 CARs, a baseline was collected from samples incubated with D-biotin for an additional 4-5 h (n = 3-13). **(D)** Comparison of relative differences of k_{off}-rates analyzed by either flow cytometry (flow cyt.) or SPR measurement (n = 3-13).

Processing and analyzing different CAR scFvs as separate samples are extremely labor- and time-intensive, as one dissociation kinetic is followed for 30 minutes. Including washing and adjustment steps between the samples, data acquisition of 40 different CAR-scFvs on a flow cytometer would at least take 120 hours, including all necessary repetitions. One possibility to perform the assay more efficiently is by analyzing several CAR scFvs simultaneously to reduce the time needed for data acquisition strongly. An idea already proposed for measuring TCR k_{off}-rates utilizes an established color code based on fluorescently labeled CD45 mAbs, which enables multiplexing of several samples for simultaneous processing and acquisition. CD45 also represents an optimal marker for multiplexing different CAR samples. It is expressed on all target B cells but is not part of the B cell complex. Thereby additional staining should not interfere with the scFv StrepTamer binding.

Combining four differently labeled CD45 mAbs allows the generation of 16 unique color codes, which can be mixed before acquisition and thus drastically reduces measurement and analysis time (Fig. 9). Besides, multiplexing of several probes also improves the overall assay quality, as one standardized CAR scFv with an already known half-live can be included in each measurement to serve as an internal control.

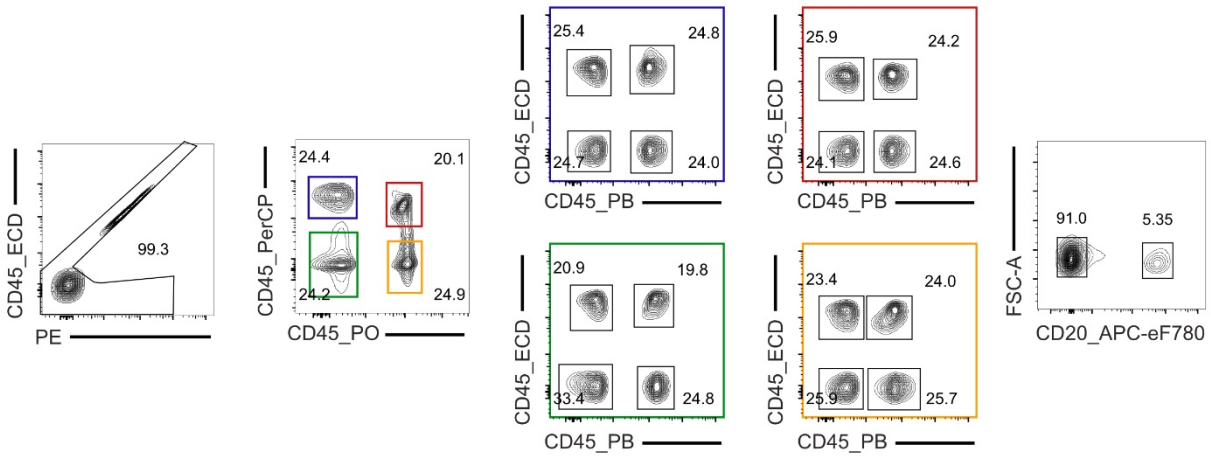

Fig. 9 Multiplexing strategy to improve high-throughput of k_{off}-rate measurements
De-multiplexing of the CD45 color barcode was used to parallel acquire 16 different CAR scFv StrepTamers labeled with four different CD45 monoclonal antibodies by flow cytometry. Mixing several samples before the final acquisition on a flow cytometer saves time and therefore enables a higher throughput of the k_{off}-rate measurement.

4.2.4 Flow-based k_{off}-rates with soluble CD19

Binding strengths between receptors and their antigen can differ whether the receptor is expressed on the cell surface or produced as a recombinant protein. Additionally, binding kinetics measured by SPR spectroscopy only determine the affinity but not avidity. In contrast, our flow cytometry-based k_{off}-rate measurement also considers necessary co-receptor help, thereby allowing the investigation of receptor avidities. So far, it has not been described whether CARs interact with other binding partners on the cell surface, which can influence the binding process and kinetics. To study whether the choice of ligand and receptor influences the measured CAR affinities, we also set up an alternative CAR k_{off}-rate assay where the ligand was produced as a recombinant protein, and the cognate CAR was expressed in primary T cells. Potentially, this alternative provides the opportunity to determine half-lives of a high number of CAR constructs in a fast and easy realizable way, as the same batch of recombinant CD19, instead of multiple individual scFvs, can be used for all experiments.

CD19 was declared a “hard-to-express” protein, as it is unstable and easily aggregates in solution[195]. As the stabilized version CD19-SF15 was not available, we were supported by our collaboration partner, the AG Leonhardt from the Ludwig-Maximilians-University in Munich, to produce the extracellular domain of CD19 (CD19-ecd) as a recombinant protein.

Two different CD19-ecd FLEXamers, containing a Strep-tag and Tub-tag at their C’-terminus, were designed (Fig. 10A). One CD19 version was stabilized with an Fc-tag, enabling the dimerization to build stable Fc-fusions, while the other CD19 version was solely expressed in its monomeric form.

Our CAR constructs contain a Strep-tag in their extracellular hinge region, which has a high binding affinity to StrepTactin. To avoid interference with the StrepTactin backbone of the StrepTamer, we exchanged the Strep-tag hinge with an NMS-linker (WO 2016/042431) and generated new CAR constructs (Fig. 10B).

First, proof-of-principle k_{off}-rate experiments were performed with the high and low-affinity CARs JCAR017 and JCAR021, as these two CARs have been intensely investigated before. Both CAR constructs (Fig. 10B) were retrovirally introduced into PBMCs and stained with a

non-reversible anti-EGFR antibody and a reversible StrepTamer consisting of a StrepTactin backbone with the CD19-ecd FLEXamer as either an Fc-fusion protein or in its monomeric form (Fig. 10A).

Stable fluorescent signals of the StrepTactin-APC backbone were observed among all four conditions during the first 30 seconds of the measurement (Fig. 10C), confirming that both soluble recombinant CD19 versions can bind their target on the cell surface. After the addition of D-biotin, StrepTactin-APC dissociated quickly from the stained CAR-T cells resulting in a de-quenching of Atto488 in all conditions. Comparable with the scFv FLEXamer k_{off}-rate, only flat dissociation curves were detected with JCAR017 CAR-T cells regardless of the CD19 form (Fig. 10C). In contrast, steep dissociation curves were observed with JCAR021 CAR-T cells. However, overall half-lives of CAR-T cells measured with the CD19 Fc-fusion protein (JCAR017: 9530 s; JCAR021: 1510 s) were much longer compared to half-lives of the monomeric form of CD19 (JCAR017: 7190 s; JCAR021: 247 s) (Fig. 10D). Fc-tags represent an elegant option to stabilize recombinant proteins. However, it is not possible to analyze monomeric interactions, as one protein contains two binding sites for its target after fusion via the Fc-tag as it results in stronger protein-protein interactions. As the affinity of the CD19-Fc fusion protein was too high to calculate trustful half-lives, this option was not further pursued. In contrast, the calculated k_{off}-rates of JCAR017 and JCAR021 with the CD19 monomer were comparable to those determined with the scFv FLEXamers. These results confirm again that the flow cytometry-based k_{off}-rate assay represents a valuable tool to test relative affinity differences of CARs.

Together with our collaboration partner, we observed fast degradation of the produced CD19 monomer within 20-24 hours. Although this limitation pushed us to preferentially use the first described flow-cytometry-based k_{off}-rate approach for further CAR testing, these experiments validated the reliability of the flow-cytometry-based k_{off}-rate assay for determining CAR binding strengths, independent of the direction of the assay.

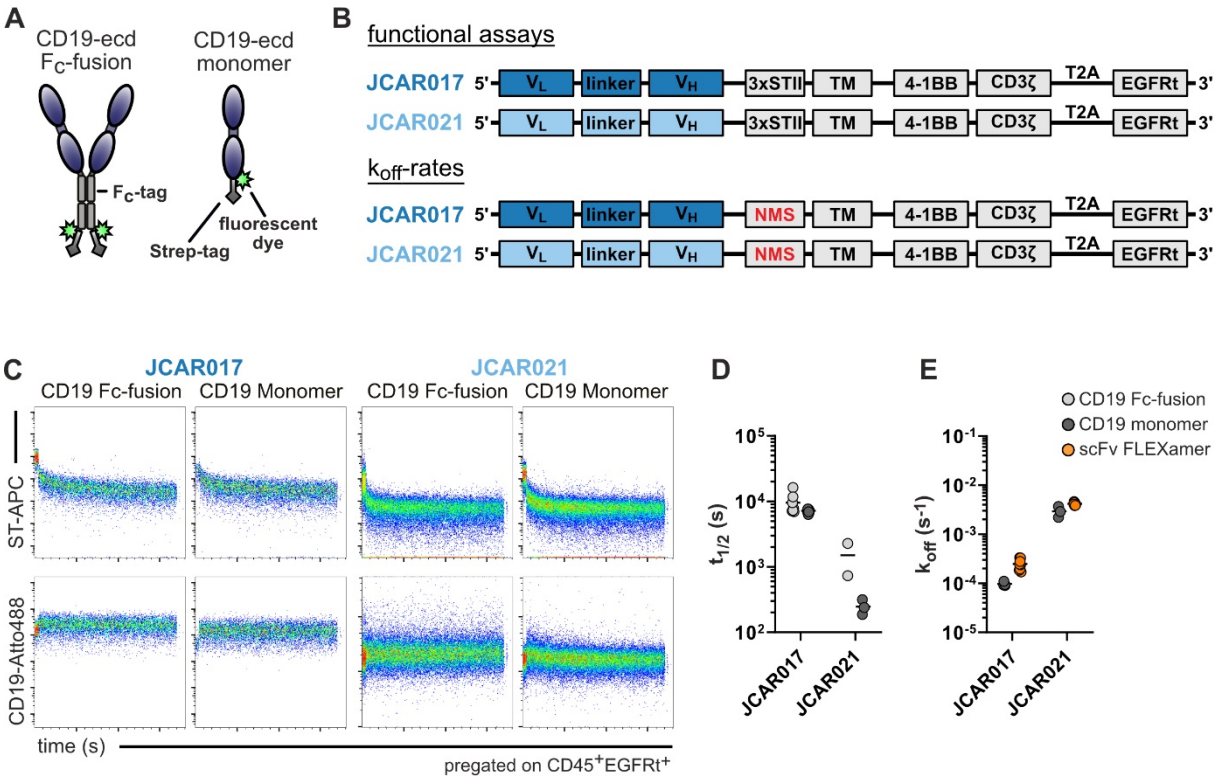

Fig. 10 Flow cytometry-based CAR k_{off}-rate assay with soluble CD19 protein
(A) Illustration of a recombinant CD19 FLEXamers conjugated to a fluorescent dye. The extracellular domain (ecd) of CD19 is stabilized via an Fc-tag or expressed in its monomeric form. **(B)** JCAR017 and JCAR021 CAR sequences were used for either functional assays containing a triple Strep-tag sequence in the hinge or for k_{off}-rates with an NMS linker as hinge domains. **(C)** Representative flow cytometry plots monitoring the dissociation of APC-conjugated StrepTactin backbone and CD19-Atto488 after adding D-biotin. **(D)** Half-lives ($t_{1/2}$) of JCAR017 and JCAR021 were measured either with CD19 Fc-fusion FLEXamers or monomeric CD19 FLEXamers by flow cytometry (n = 2-9). **(E)** Flow cytometry-based k_{off}-rates of JCAR017 and JCAR021 were either calculated for measurements using monomeric CD19 FLEXamers or CAR scFv FLEXamers (n = 3-13).

4.3 Alanine scanning of JCAR021 for the generation of low-affinity CARs

After establishing a relatively fast method for screening CAR affinities, we moved into the generation of a library of CAR mutants, intending to further lower affinities down to the level of TCRs. In order to generate CARs with affinities in the range of TCR avidities, we decided to perform an alanine scanning of the heavy and light chain of JCAR021 - the anti-CD19 CAR clone with the lowest binding strength towards CD19. So far, alanine scanning mutagenesis has been extensively used to map the antigen-binding site of antibodies. With the help of site-directed mutagenesis, each amino acid is individually replaced with an alanine, which enables the identification of amino acids that are essential for antigen binding. For our purpose, we mutated aromatic amino acids within the framework region of the scFv, as these positions are essential for binding kinetics but should not disrupt target specificity[198].

4.3.1 Generation of CAR mutants and characterization of their surface expression

In order to design several JCAR021 affinity mutants, the framework regions of both the heavy and light chains of the JCAR021 scFv were mutated by alanine scanning. Mainly the big aromatic residues phenylalanine (F), tyrosine (Y), and tryptophan (W) were exchanged for alanine (A) to achieve maximum conformational changes.

Twelve different single-point mutants were defined and introduced into the JCAR021 DNA sequence (Fig. 11A). After retroviral transduction of the different constructs into *ex vivo* isolated PBMCs, expression, and transduction profiles were determined by flow cytometry (Fig. 11B), where JCAR017 and JCAR021 CAR-T cells were used as positive controls. The twelve different JCAR021 mutants were divided into three different groups according to the quality of CAR expression (Fig. 11B). The first group of CAR-T cells marked in green showed equally high co-expression of EGFRt and STII, similar to the controls, while the other two groups (orange and red) varied in their staining patterns. Expression of the CAR and EGFRt of CAR-T cells assigned to the orange group was hindered by the amino acid exchange, represented by low frequencies of $EGFRt^+$ and $STII^+$ cells.

In contrast, amino acid exchanges of the four CAR-T cells belonging to the red group impaired only the successful expression of the CAR on the cell surface, as the overall transduction efficacy of EGFRt remained high. Receptor expression levels can highly influence the efficacy of CAR-T cells. In order to correlate functional results solely on receptor affinity, only the six JCAR021 mutants with successful STII and EGFRt co-expression were chosen for further *in vitro* testing.

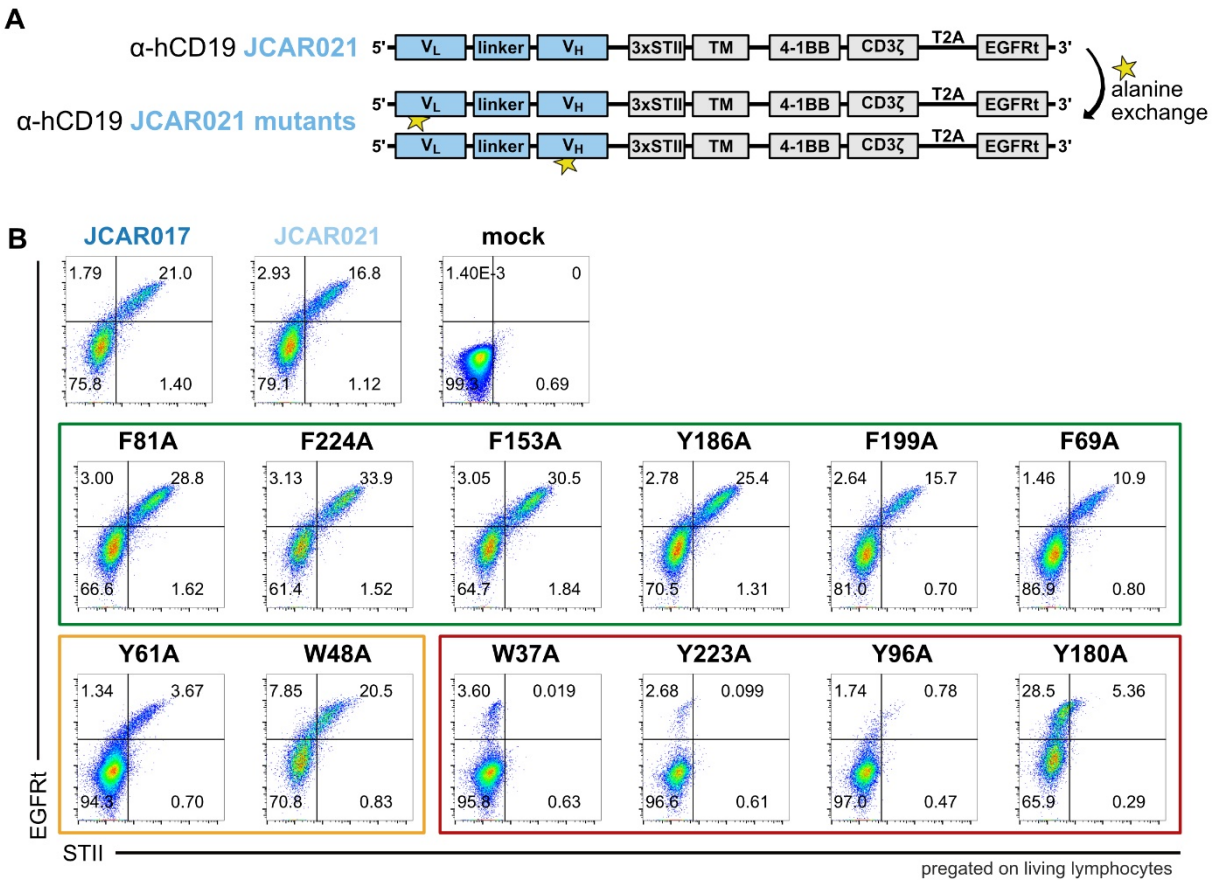

Fig. 11 Alanine scanning approach to generate low-affinity JCAR021 point mutants
(A) Exchange of single aromatic amino acids in the framework region of the heavy and light chain of the extracellular domain of JCAR021 to generate affinity mutants with reduced binding strength but same specificity. **(B)** Co-staining of EGFRt and Strep-tag in CAR-T cells expressing the mutant JCAR021 constructs. CAR-T cells were separated into three groups (green, orange, and red) according to their transduction efficacies and CAR expression.

4.3.2 *In vitro* testing of JCAR021 alanine mutants

In order to determine whether the mutations had an influence on the binding affinity of the engineered CARs, flow-based k_{off}-rate assays were performed. All necessary recombinant scFv FLEXamers were cloned, expressed, purified, and conjugated to Atto488 as described before and tested for their binding strengths to CD19. All mutant scFvs specifically bound $CD20^+$ B cells, as highlighted by the high APC signals (Fig. 12A) before the addition of D-biotin. However, none of the six tested CAR mutants showed decreased affinities compared to the original JCAR021 (Fig. 12B).

Nevertheless, the six mutants with preserved surface expression were tested for their in *vitro* functionality. $CD19^+$ and $CD19^-$ HEK target cells were co-incubated with either JCAR017, JCAR021, or mutant CAR-T cells in different E:T ratios. The killing kinetics of the different mutants were monitored in real-time with the help of the xCelligence system over 25 hours (Fig. 12C). All CAR-T cell constructs efficiently killed $CD19^+$ target cells irrespective of their mutation, while no unspecific killing of $CD19^-$ HEK cells was detected. Also, killing kinetics were similar, independent of the number of used CAR-T cells. $CD19^+$ target cells were eradicated entirely within 5 hours of co-incubation with the different CAR-T cells in a 10:1 and 5:1 ratio, while it lasted 10 hours until all target cells were killed in the 1:1 group. No unspecific killing of either $CD19^+$ or $CD19^-$ HEK cells was observed by the mock control group. As expected, no differences regarding the *in vitro* functionality of the different mutant CAR-T cells were detected. In summary, the alanine scanning approach was not successful in generating JCAR021 mutants with lower binding affinities.

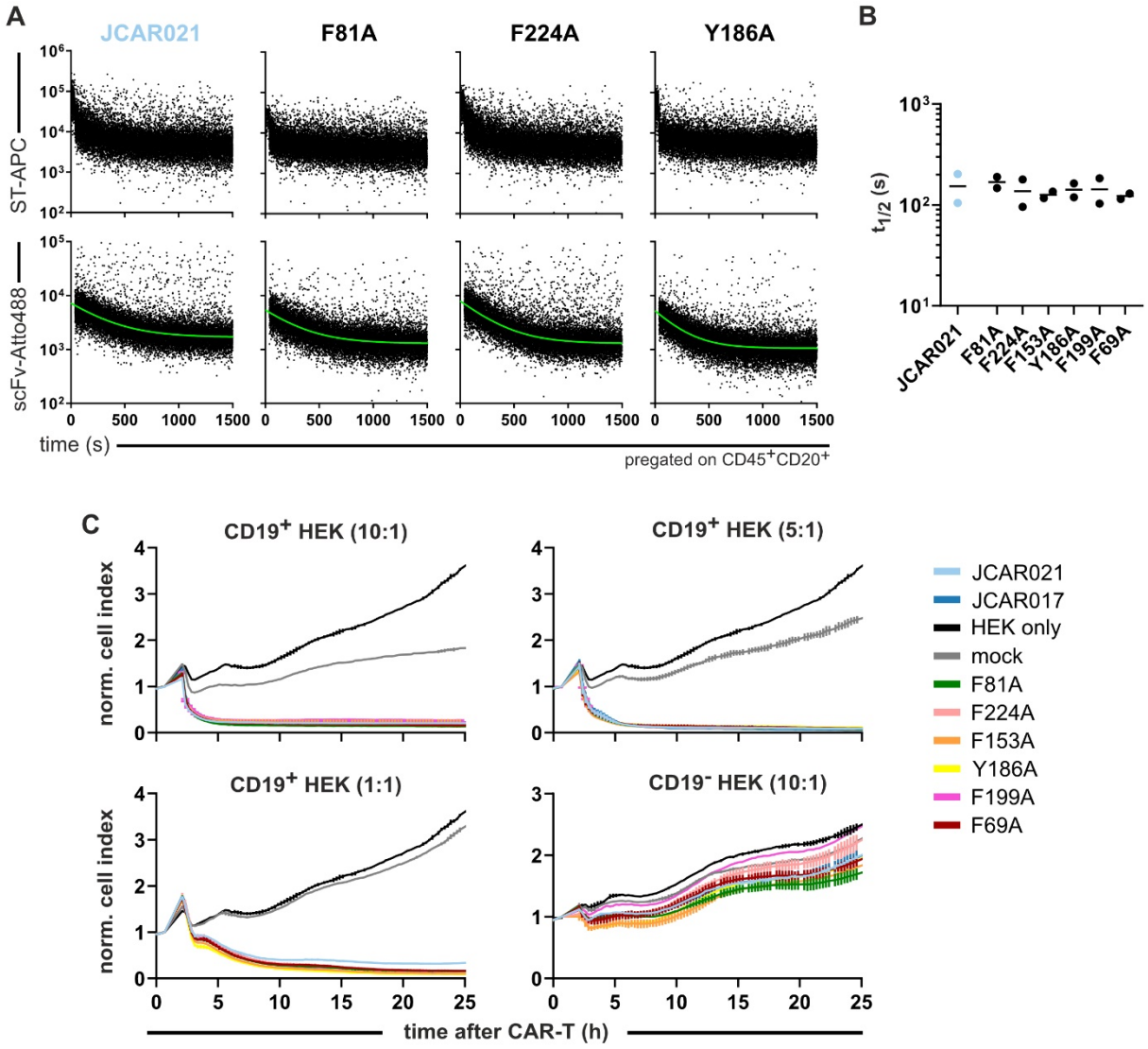

Fig. 12 *In vitro* functional testing and k_{off}-rate measurement of JCAR021 alanine mutants
(A) Representative plots of dissociation kinetics of mutant JCAR021 alanine mutant scFvs measured and analyzed by the flow cytometry-based koff-rate assay. Green lines represent fitted exponential decay curves of the CAR scFv dissociation. **(B)** Half-lives of both JCAR021 and alanine mutants were determined by flow cytometry-based k_{off}-rate measurement (n =2). **(C)** xCelligence killing assay of JCAR017, JCAR021, and six selected mutant CAR-T cells. $CD19^+$ and $CD19^-$ HEK target cells were co-incubated with CAR-T cells in several effector-to-target ratios (10:1, 5:1, 1:1). Killing kinetics were monitored over 25 hours and normalized to the time point before the addition of CAR-T cells (n = 3).

4.4 Generation of an anti-CD19 CAR affinity library

The alanine scanning approach did not help in generating CAR mutants with lower affinity. Therefore, we decided to engineer a broader library of different CD19-targeting CAR-T cells based on an *in silico* screening. The three-dimensional structure of protein-antigen interactions plays an essential role in identifying the domains that are mainly involved in the binding of the two partners and most suitable for mutations. Crystal structures of protein interactions are still

the gold standard for evaluating different binding features. However, nowadays also, an increasing number of machine learning algorithms can predict the influence of structural changes on the overall binding of proteins based on the framework and CDR annotations. Since no crystal structures of the interaction between CD19 and JCAR021 were available, we used a tool called ABodyBuilder SAbPred[191] to model the extracellular domain of JCAR021 *in silico* and applied it to the webserver mCSM-AB[192], which can predict affinity changes due to single amino acid exchanges of antibodies or scFvs. 231 different amino acid exchanges were predicted to result in changes in the Gibbs free energy compared to the original JCAR021-CD19 interaction. 32 new point mutants were selected, of which 19 amino acid exchanges were located in the framework regions and 13 in the CDRs of the JCAR021 scFv (Tab. 2). Only substitutions predicted to achieve the biggest differences in Gibbs free energy were chosen. However, mutations in the CDRs were only considered if the exchanged amino acids carried biochemical properties similar to the original to preserve the CAR's specificity.

Tab. 2 Selected single-point mutations on the structural basis of the scFv of JCAR021

aa substitution	chain	structural position	properties	score
M35A	heavy	framework	nonpolar – nonpolar	-1.3
H36A	heavy	framework	basic - nonpolar	-2.7
H36G	heavy	framework	basic – nonpolar	-2.6
H36P	heavy	framework	basic – nonpolar	-2.7
W48E	heavy	framework	aromatic – acidic	-2.0
S50A	heavy	framework	polar – nonpolar	-2.1
A93W	heavy	framework	nonpolar – aromatic	-2.4
S108C	heavy	CDR	polar – polar	-1.9
F113A	heavy	CDR	aromatic – nonpolar	-3.1
F113L	heavy	CDR	aromatic – nonpolar	-2.7
F113P	heavy	CDR	aromatic – nonpolar	-2.9
W116E	heavy	framework	aromatic –acidic	-3.0
W116P	heavy	framework	aromatic – nonpolar	-1.6
S168C	light	framework	polar – polar	-1.6
S172A	light	framework	polar – nonpolar	-2.1
S172G	light	framework	polar – nonpolar	-2.2
Y174V	light	framework	polar – nonpolar	-3.0
Y174G	light	framework	polar – nonpolar	-3.1
L184D	light	framework	nonpolar – acidic	-3.9
L184E	light	framework	nonpolar – acidic	-3.8
M185A	light	framework	nonpolar – nonpolar	-1.5
K191C	light	framework	basic – polar	-2.3
K191M	light	framework	basic – nonpolar	-2.3
S227K	light	CDR	polar – basic	-2.4
A230M	light	CDR	nonpolar – nonpolar	-2.3
N234C	light	CDR	polar – polar	-1.1
S235C	light	CDR	polar – polar	-2.6
V236F	light	CDR	nonpolar – aromatic	-1.2
V236W	light	CDR	nonpolar – aromatic	-1.3
L237F	light	CDR	nonpolar – aromatic	-1.6
L237M	light	CDR	nonpolar – nonpolar	-1.1
L237W	light	CDR	nonpolar - aromatic	-2.0

4.4.1. Evaluation of binding strengths of JCAR021 affinity mutants

The 32 selected mutations were introduced into the JCAR021 FLEXamer DNA sequence by Q5-mutagenesis. Afterward, mutant scFv-FLEXamers were expressed, purified, and functionalized with Atto488 fluorophores. Freshly isolated human PBMCs were stained *ex vivo* with differently labeled human CD45 mAbs for multiplexing, human CD20 mAb for B cell identification, and the respective CAR scFv StrepTamer. 26 out of 32 scFv StrepTamers showed high fluorescent signals of the StrepTactin-APC backbone before the addition of D-biotin (Fig. 13A), indicating that these CAR scFvs can still recognize cognate CD19 antigen. Besides, clear dissociation curves of the corresponding CAR scFvs were observed, and exponential decay curves were successfully fitted (Fig. 13A). In contrast, half-lives of six mutant scFvs could not be determined. StrepTamers of the mutants H36P, F113P, W116E, and Y174G showed no initial staining and, consequently, no dissociation of their scFv FLEXamers (Fig. 13B), overall suggesting that the introduced amino acid exchanges had significant influences on the protein structure and specificity. StrepTamers of the scFv mutant W116P revealed a weak APC signal, while L184D showed strong APC fluorescent intensity before the addition of D-biotin. However, fitting specific dissociation curves was not feasible in both cases due to high background signals, potentially caused by the degraded scFv protein. Furthermore, protein yields of these six scFvs were low, and several rounds of protein expression were necessary to gain the necessary amount, which further corroborated potential instability due to the mutations. Overall, we classified these six CARs as non-binders.

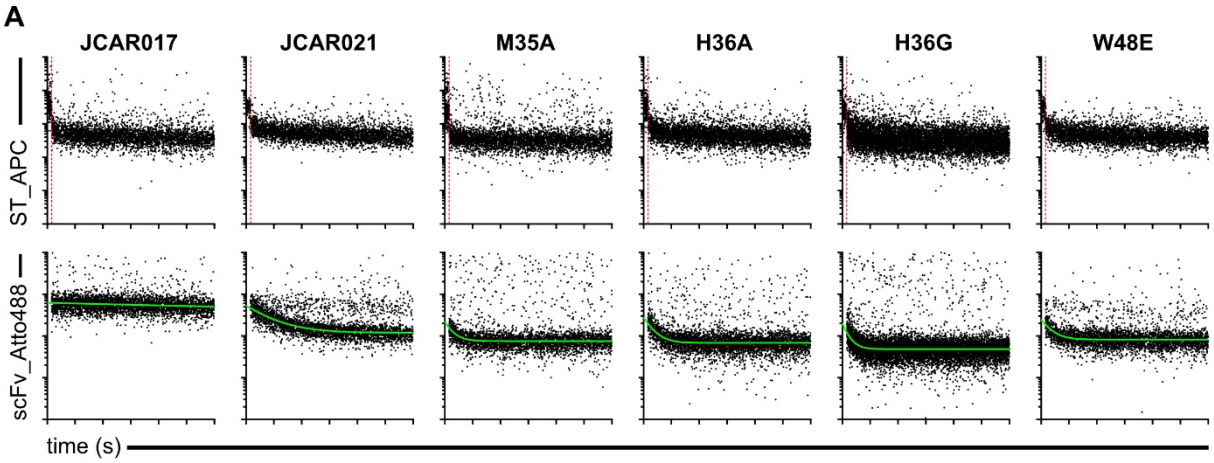

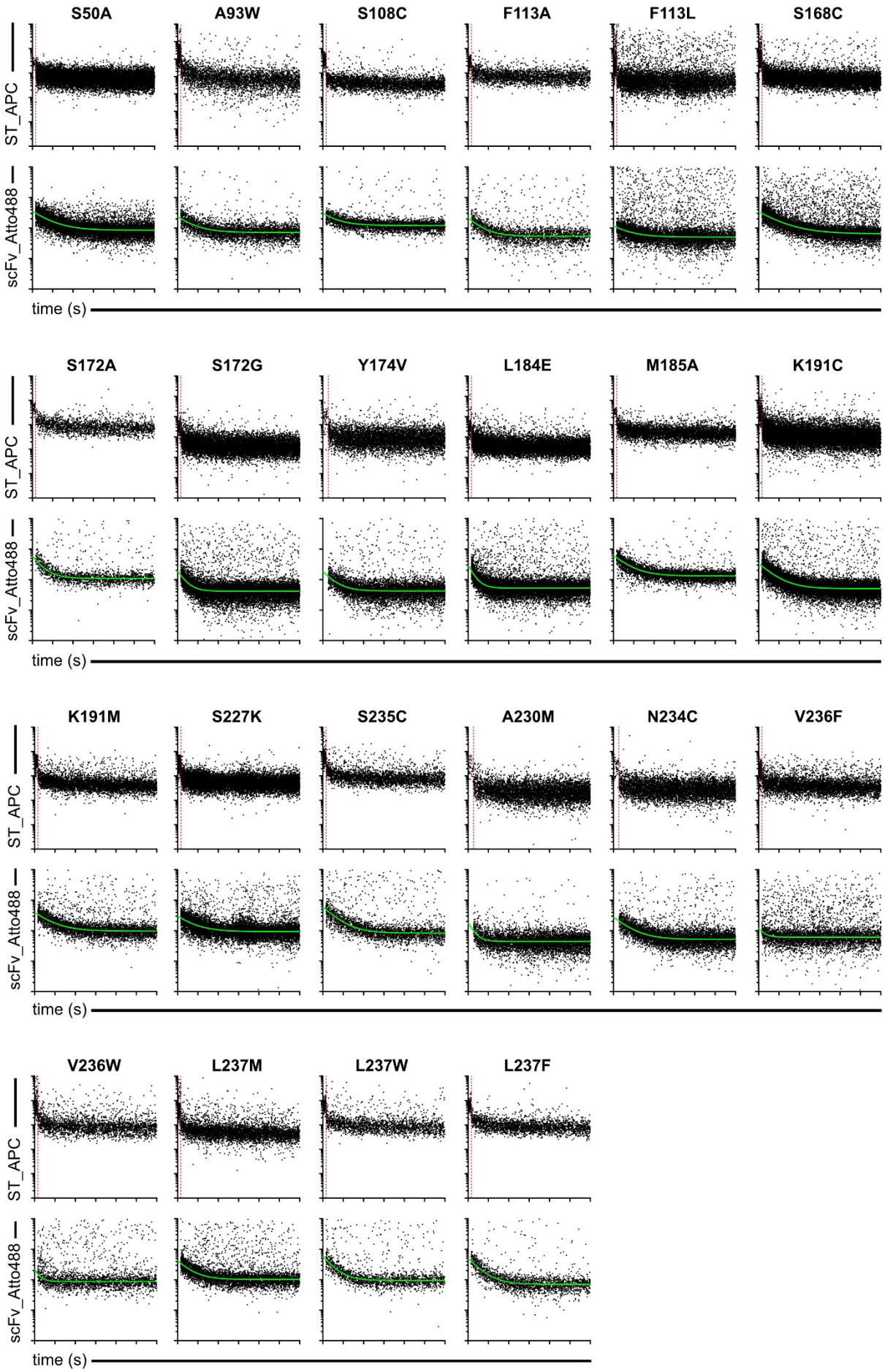
S50A
A93W
S108C
F113A
F113L
S168C
S172A
S172G
Y174V
L184E
M185A
K191C
K191M
S227K
S235C
A230M
N234C
V236F
V236W
L237M
L237W
L237F
ST_APC
scFv_Atto488
time (s)

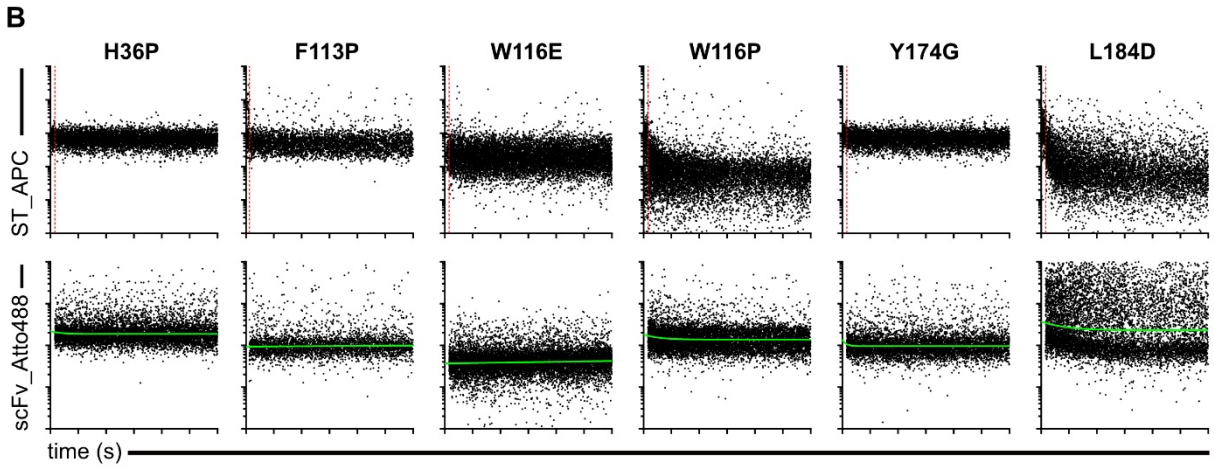

Fig. 13 Flow cytometry-based koff-rate analysis of JCAR021 point mutants
(A+B) CD19$^+$ B cells were stained with mutant JCAR021 scFv StrepTamers. Complete dissociation of the StrepTactin backbone (red line) defines the start of the monomeric scFv-Atto488 dissociation. Results of the fitting of exponential decay curves of the dissociation of scFv-Atto488 are illustrated in green. Binding kinetics of **(A)** 26 JCAR021 point mutants were successfully fitted, while binding kinetics of **(B)** 6 mutants were not analyzable.

Measurable half-lives of the different CAR scFvs ranged from 29.7 s to 196.7 s, with some mutants (e.g., V236F, V236W, H36G) having over five times lower k_{off}-rates compared to the original JCAR021 (Fig. 14A). Therefore, for the first time, we succeeded in generating JCAR021 mutants with preserved specificity but lower affinity than the original CAR construct. In order to examine whether the affinity of the mutants was even as low as naturally occurring TCRs, reference values of CMV-specific TCRs (TCR 1.4, TCR 6.2, TCR 3.4, TCR 10.4) were provided by Thomas Müller, a former PhD student in our working group. Flow cytometry-based k_{off}-rates of TCRs are generally determined at 4 °C since higher temperatures can lead to T cell activation with the internalization of the TCR/ligand complex, which ultimately interferes with the k_{off}-rate measurement. In contrast, the k_{off}-rate approach to measure CAR/CD19 interactions was optimized to be routinely performed at 20 °C; otherwise, dissociations are challenging to be determined due to the long kinetics. In order to compare CAR and TCR half-lives, they must be determined at the same defined temperature. Therefore, CAR k_{off}-rates were also measured at 4 °C, similar to the CMV-specific TCRs (Fig. 14B). In line with the data evaluated at 20 °C, the measurement at 4 °C resulted in a broad range of mutant CAR half-lives ranging from 249.4 s to 1593 s (Fig. 14B). Additionally, half-lives determined at 4 °C and 20 °C strongly correlated with each other (r^2 = 0.978), suggesting that results determined at

both temperatures can be reliably used (Fig. 14C). Notably, half-lives of the CARs with the lowest affinity, V236F, V236W, and H36G, were in the range of CMV-specific TCRs (Fig. 14D). Taken together, we succeeded in the generation of a library of 26 new CD19-targeting CARs with high specificities and affinities extending into the range of pMHC/TCR interactions, which also confirmed the robustness of the *in silico* prediction.

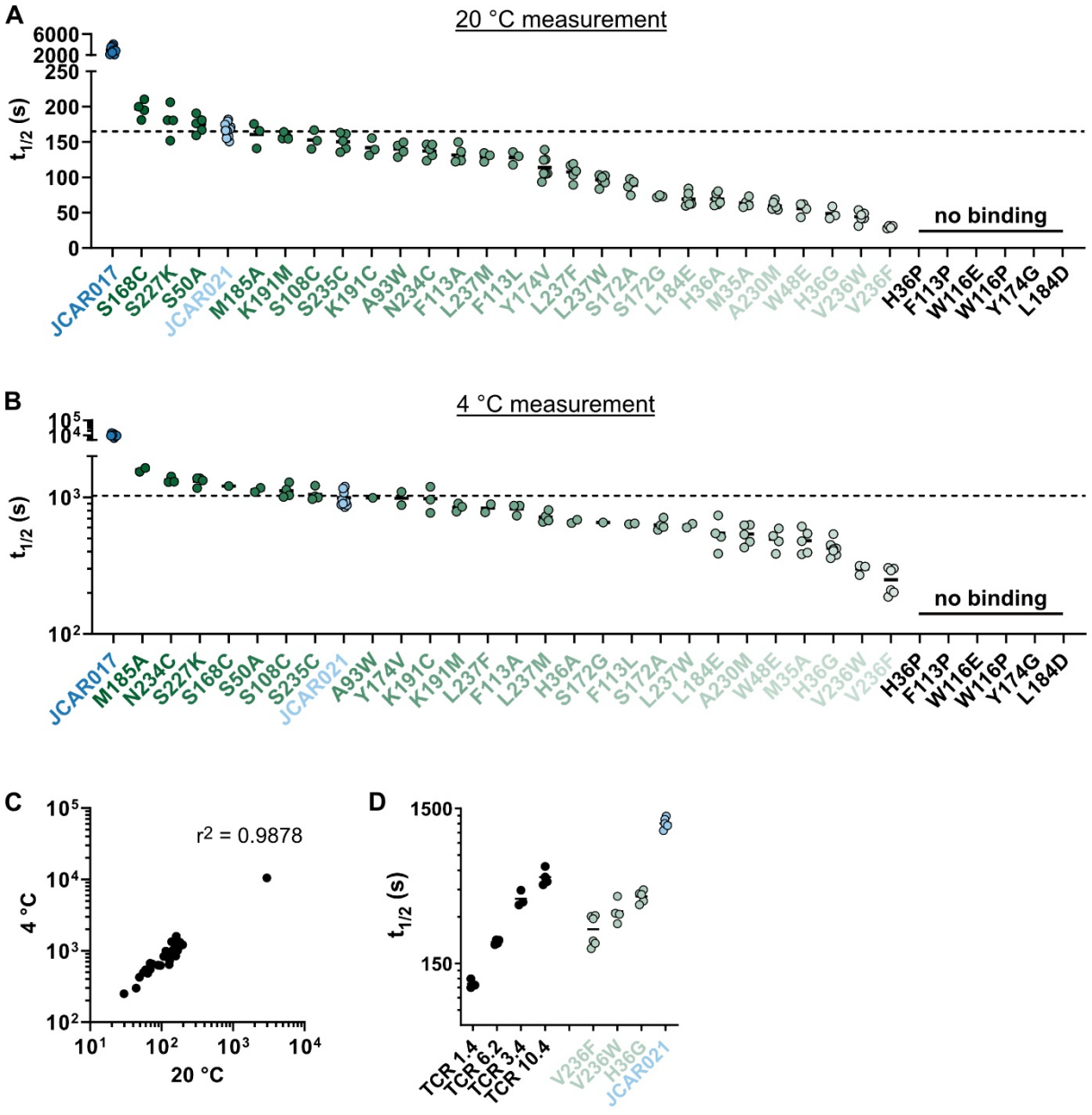

Fig. 14 Anti-CD19 JCAR021 affinity library
(A+B) Half-lives of the binding between CD19 and JCAR017, JCAR021, and mutant JCAR021 scFvs were determined by flow cytometry-based k_{off}-rate assay either at **(A)** 20 °C or **(B)** 4 °C (n = 1-13). CAR scFvs are ordered according to their binding strength. **(C)** Correlation between flow cytometry-based half-lives was determined at 4 °C or 20 °C. **(D)** Half-lives of naïve CMV-specific TCRs (TCR 1.4, 6.2, 3.4, 10.4) received from Thomas Müller (PhD, AG Busch), three different JCAR021 mutants, and JCAR021 determined at 4 °C (n = 3-6).

4.3.2 Influence of point mutations on the receptor expression of low-affinity mutants

The influence of receptor affinity on downstream functionality and safety of the corresponding engineered T cell can only be studied with CARs that are similarly expressed on the cell surface. Therefore, as a first step, we again evaluated the quality of CAR mutant expression. For that, the selected 32 amino acid exchanges were cloned into the JCAR021DNA string, which is used for retroviral transduction by Q5-mutagenesis. Subsequently, freshly isolated PBMCs were transduced with the newly generated CAR constructs and co-stained for EGFRt and Strep-tag expression at least three days after viral genome editing (Fig. 15).

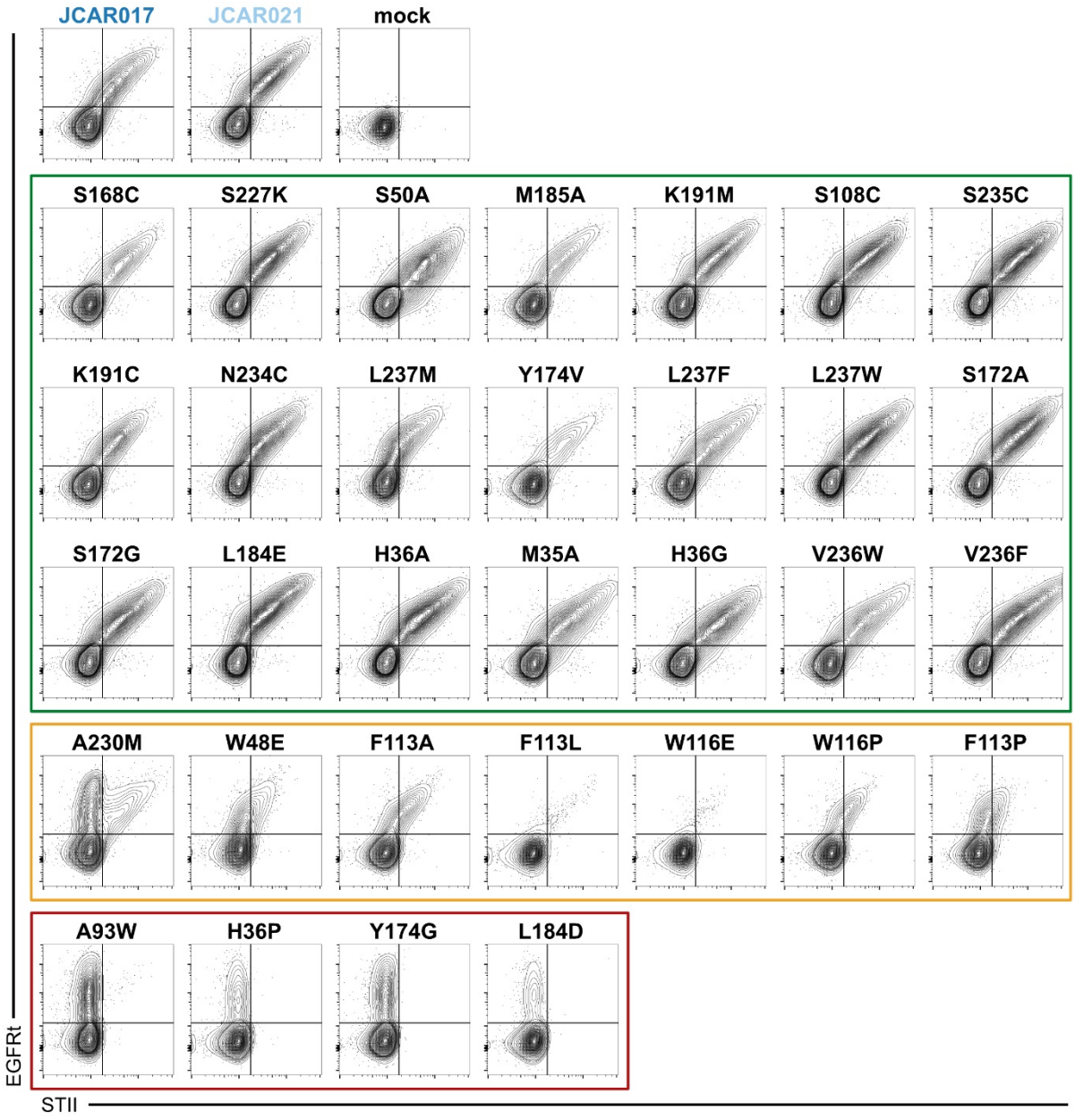

Fig. 15 Co-expression of JCAR021 CAR-T cell mutants after single amino acid exchanges
Representative flow cytometry plots of primary PBMCs retrovirally transduced with mutant CAR constructs and co-stained for EGFRt and Strep-tag (STII) expression three days after retroviral transduction. CAR-T cells were categorized into three groups (green, orange, and red) according to their CAR surface expression.

Comparable to the alanine scanning approach (Fig. 11B), JCAR021 mutants were assigned to three different groups according to their CAR surface expression profile, represented by the frequency of $STII^+$ of transduced ($EGFRt^+$) T cells (Fig. 16B). CAR-T cells belonging to the green group showed a significant correlation between $STII^+$ and $EGFRt^+$ cells and possessed at least 70 % double expression of the two markers. In contrast, CAR-T cells with only weak or no CAR surface expression, despite comparable levels of overall transduced cells, were categorized into the red group. All remaining CAR-T cells, with either transduction rates below 20 % or weak co-expression of the CAR and EGFRt, were allocated to the orange group. 21 of the 32 newly generated mutants were categorized into the green group, while 7 and 4 were assigned to the orange and red groups, respectively (Fig. 15-16). Profound changes of the scFv folding caused by the exchange of single amino acids can result in misfolding, aggregation, and degradation, which ultimately results in missing expression of the CAR on the surface or low transduction efficacies at all.

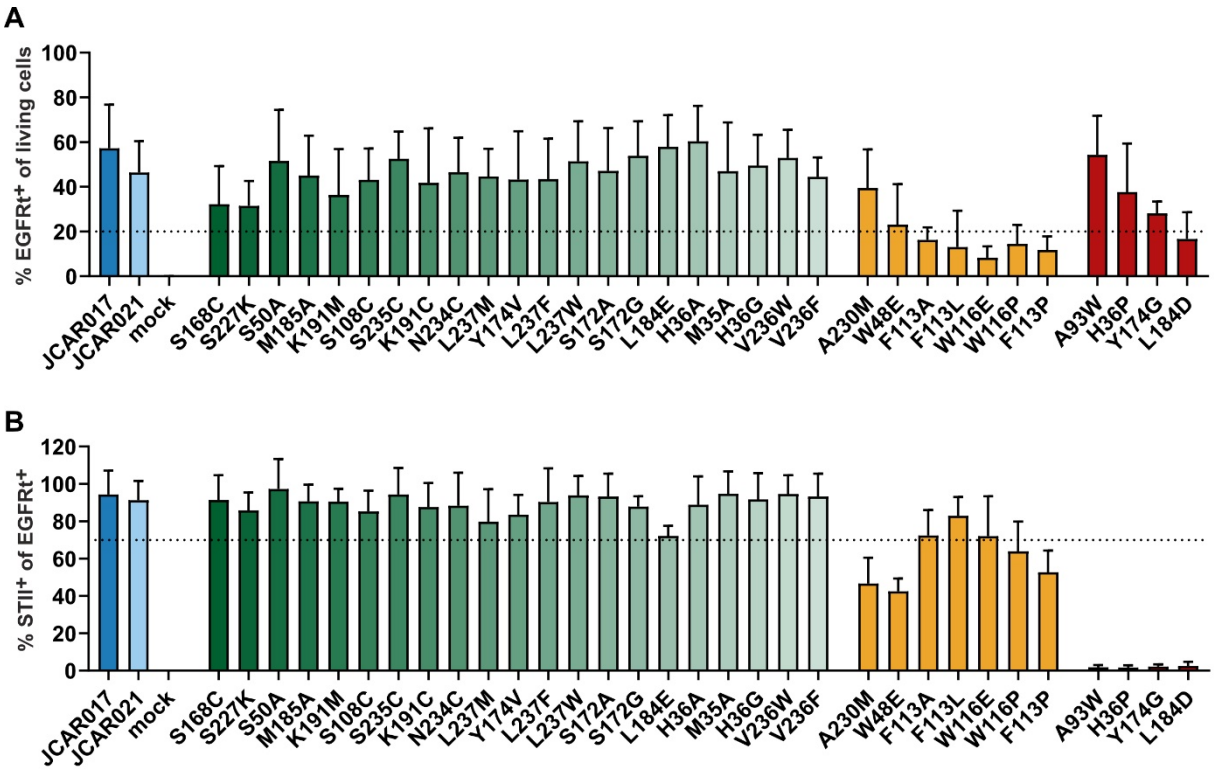

Fig. 16 Transduction and CAR surface expression profiles of JCAR021 mutant CAR-T cells
(A) Frequencies of EGFRt$^+$ transduced T cells are ordered according to their k_{off}-rates and CAR surface expression profile with a 20 % transduction efficacy threshold. Data are expressed as mean+SD (n = 4-5) **(B)** Frequencies of STII$^+$ cells of EGFRt$^+$ transduced T cells. CAR-T cells are ordered according to their k_{off}-rates and CAR surface expression profile. The threshold of positive CAR expression was set at 70 %. Data are expressed as mean+SD (n = 4-5).

The results indicate a potential correlation between the stability of the recombinant CAR scFv FLEXamer, successful StrepTamer staining of B cells, and the corresponding surface expression in living T cells. Indeed, all six CAR scFvs without determinable k_{off}-rates and low yields after expression as recombinant proteins (H36P, F113P, W116E, W116P, Y174G, L184D) were not or only weakly expressed on the cell surface of engineered T cells and thus belonged to the orange or red group (Fig. 17). On the contrary, some CARs that could not be expressed on the T cell surface were successfully used to stain CD20$^+$/CD19$^+$ B cells. In general, the protein stability of a recombinant CAR scFvs could be used as the first prognosis of successfully expressed CARs. However, the final effect of exchanging amino acids within the CAR sequence needs to be tested individually for each position and combination of the mutation.

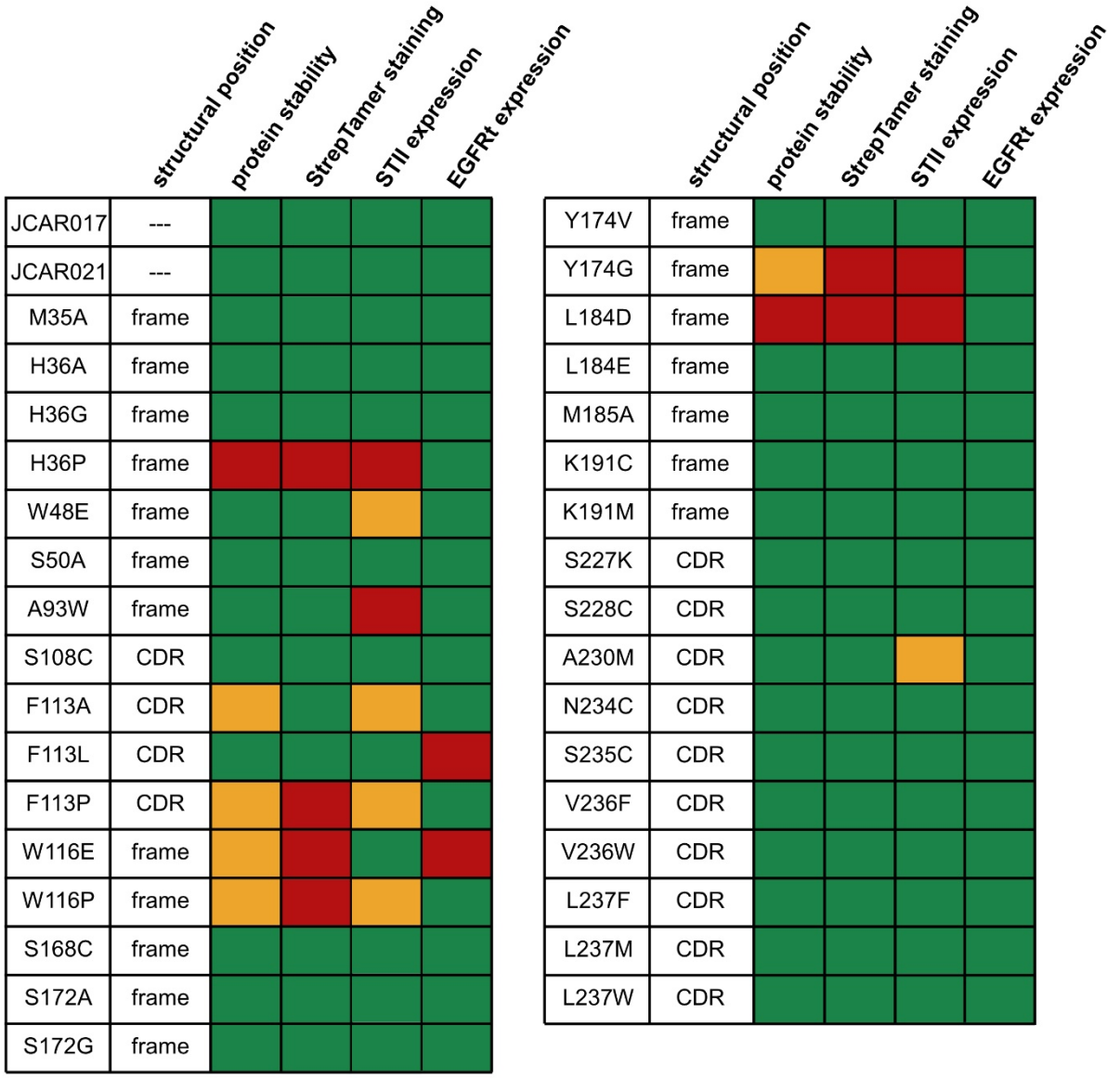

Fig. 17 Summary of properties of JCAR021 mutants
Summary of features of the 32 selected amino acid exchanges of the JCAR021 extracellular domain when introduced into the recombinant protein or the CAR expressed on primary T cells. Colors indicate whether the point mutation can provide the particular property (green), provides it only partially (orange), or does not provide it (red).

4.3.3 *In vitro* characterization of low-affinity anti-CD19 CAR-T cells

The newly generated JCAR021 mutants only differ by one single amino acid but possess a broad spectrum of affinities ranging from low binders comparable to naturally occurring TCRs to strong binders as clinically approved CARs. Importantly, CAR surface expression was maintained for most of the mutants. Therefore, they provide the opportunity to dissect the relative contribution of the CAR binding strength on the corresponding downstream CAR-T cell function and safety. Several *in vitro* functional assays were performed to investigate the

influence of CAR affinity changes. We still included CARs that did not show surface expression (orange + red group) to ensure that this phenotype is not due to impaired staining by conformational changes of the extracellular binding part but rather due to the absence of the receptor.

Nur77-Jurkat activation assay

In order to address the question of whether CAR-T cells can still be specifically activated despite the exchange of selected amino acids, firstly, we performed a rapid screening using the Nur77-Jurkat reporter cell line. Nur77 Jurkat cells were retrovirally transduced with the different mutated CAR constructs and co-incubated with either $CD19^+/GFP^+$ Raji tumor cells or medium as a background control. After 3 hours, $EGFRt^+$ cells were analyzed for their tdTomato expression by flow cytometry (Fig. 18A). After co-incubation with $CD19^+$ target cells, specific signaling was robustly detected among all Jurkat cells expressing either JCAR017, JCAR021, or one of the green mutant CARs. Except for the low-affinity binders V236W and V236F, all green mutants, independent of their affinity, were activated in all five to seven biological replicates. As expected, Jurkat cells transduced with low or not expressed CARs (orange + red groups) were only sporadically activated by the Raji tumor cells except for the clone A93W (Fig. 18B).

In summary, the Nur77-Jurkat screening proves that all CAR-T cells that express their receptors correctly were also specifically activated by their target cells. Consequently, we could confirm that the absence of CAR expression was indicative of a suboptimal receptor expression rather than a lack of detection after antibody staining. However, no conclusions on subtle differences in functionality due to different affinities could be drawn due to the low sensitivity of the test.

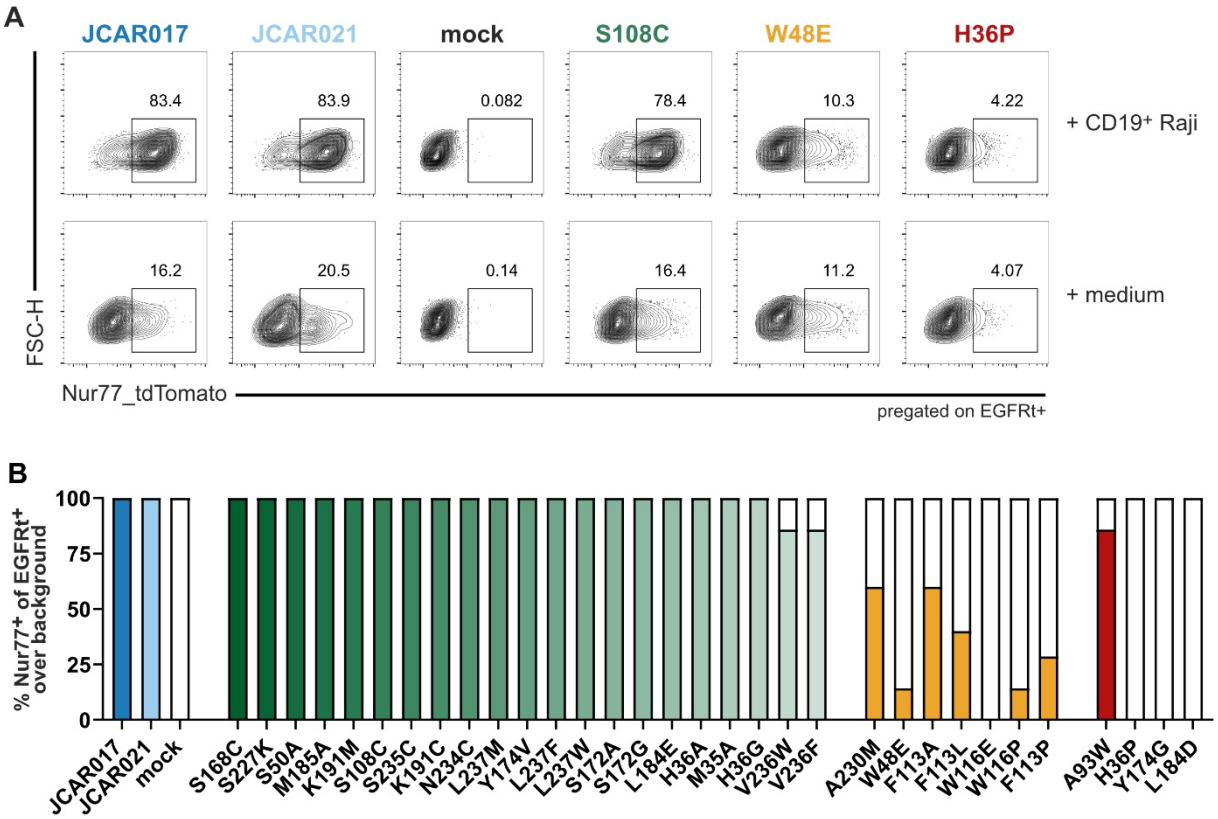

Fig. 18 Nur77 Jurkat activation assay with mutant low-affinity CAR-T cells
(A) Representative flow cytometry plots of the expression of Nur77 transgene conjugated to tdTomato. Depicted are selected CAR transduced Nur77 transgenic Jurkats of each CAR expression group after either specific stimulation with CD19$^+$ Raji cells or incubation in medium for three hours. **(B)** Numbers of experiments in which at least 20 % of EGFRt$^+$ transduced Jurkat cells were activated over the background. Results are calculated as frequencies of all performed experiments. Mutants of the JCAR021 affinity library belonging to the green group are ordered with decreasing affinity. The highest affinity CAR, JCAR017, is shown on the left, while the variant V236F bearing the lowest affinity is located on the far right. Additionally, mutants are grouped into green, orange, and red as determined before (n = 5-7 biological independent replicates with technical duplicates).

Specific cytokine release of low-affinity anti-CD19 CAR-T cells after stimulation

In order to investigate whether lower CAR affinities, in the context of faster k_{off}-rates, would result in a different sensitivity of the corresponding CAR-T cell, we studied the cytokine production of the generated CAR library after specific stimulation with target cells. Resting T cells transduced with and without the different affinity CAR mutants were stimulated with CD19$^+$/GFP$^+$ Raji cells for four hours and analyzed for their specific release of IFN-γ, TNF-α, and IL-2 in an intracellular cytokine release assay. As negative and positive controls, transduced cells were either incubated in medium or activated by PMA/Ionomycin. All EGFRt$^+$ CAR-T cells transduced with mutant CARs of the green group showed specific production of IFN-γ, TNF-α, and IL-2 over background dependent on their E:T-ratio when co-incubated with

CD19-expressing target cells (Fig. 19A). Interestingly, no affinity-dependent differences in the frequencies of IFN-γ and TNF-α producing EGFRt$^+$ CAR-T cells were observed, except for the two low binding mutants V236W and V236F which possessed the fastest k_{off}-rates. Indeed, significantly fewer V236W and V236F CAR-T cells reacted to the CD19$^+$ Raji cells than in the other groups. Besides, levels of IL-2 producing cells after stimulation varied among the different samples, identifying IL-2 expression as an ineligible marker to evaluate CAR-T cell functionality *in vitro*. However, as seen before for the production of IFN-γ and TNF-α, V236W and V236F were by far the two mutants with the lowest frequencies of IL-2 producing CAR-T cells within the green group. As expected, CAR-T cells with insufficient receptor expression showed strongly diminished frequencies of INF-γ, TNF-α, and IL-2 producing cells in comparison to JCAR021 (Fig. 19B). In fact, CAR-T cells transduced with the mutants W116E and F113P of the orange group and H36P, Y174G, and L184D of the red group did not show any cytokine release, while the rest of the mutant EGFRt$^+$ CAR-T cells were marginally above background levels of INF-γ, TNF-α and IL-2 producing cells.

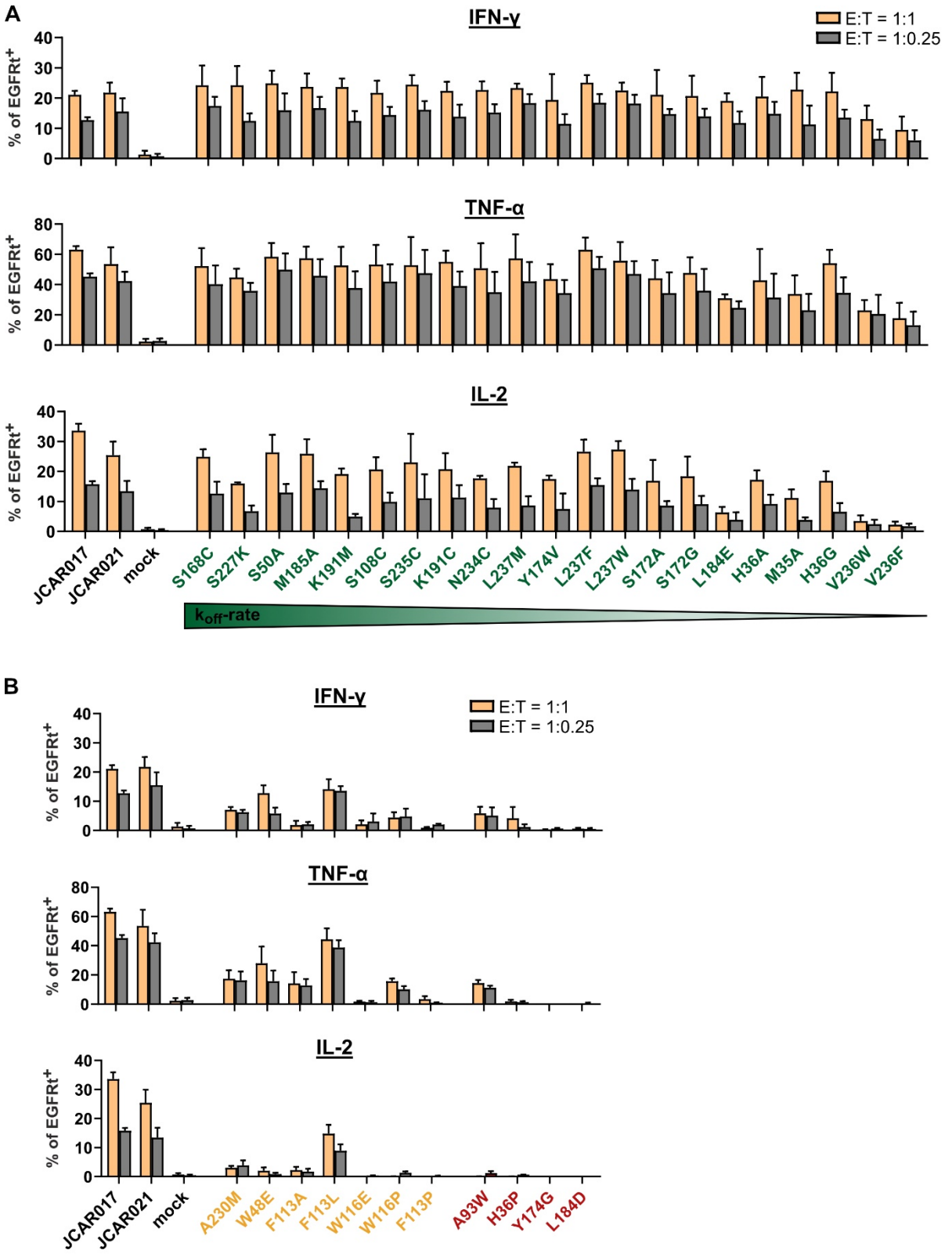

Fig. 19 Intracellular cytokine release of low-affinity CAR-T cells
(A+B) Frequencies of EGFRt$^+$ CAR-T cells releasing either IFN-γ, TNF-α, or IL-2 over background after specific stimulation with CD19$^+$ Raji tumor cells for four hours. Two different effector-to-target ratios were tested (1:1, 1:0.25). **(A)** Cytokine production of CAR-T cells expressing CARs belonging to the green group and **(B)** expressing CAR mutants of the orange and red group. CAR-T cells of the green group are ordered with decreasing affinity. Data are expressed as mean+SD of three biologically independent experiments with technical triplicates.

In vitro killing efficacy of low-affinity CAR-T cell mutants

To further characterize the anti-tumor activity of the 32 CD19-specific CAR mutants, the killing kinetics of the corresponding CAR-T cells were monitored in real-time and analyzed with an xCelligence killing assay. HEK cells engineered to overexpress CD19 and the original $CD19^-$ HEK cell line were used as target cells, while sorted $EGFRt^+$ primary T cells transduced with the different CAR mutants of the library were used as effector cells. Non-transduced mock cells served as negative controls. Cytotoxicity was finally quantified by calculating the area under the growth curve (AUC) of the killing kinetic.

All CAR-T cells with successful CAR surface expression induced CD19-specific killing and no significant differences in the killing kinetics among the CAR constructs were observed (Fig. 20A-C). Indeed, CAR-T cells of the green group, as well as JCAR017 and JCAR021 CAR-T cells, completely eradicated $CD19^+$ target cells within eight hours after the addition of the effector cells applied in a 1:1 or 4:1 ratio (Fig. 20A-B). Additionally, none of the tested CAR-T cells influenced the growth of the $CD19^-$ HEK cells, demonstrating the antigen-specific nature of the observed cytotoxicity (Fig. 20C). Similar results were obtained by applying the CAR-T cells in an effector-to-target ratio of 1:1, albeit ten hours were necessary until the $CD19^+$ target cells were killed (Fig. 20A). Accordingly, no significant differences in the determined AUC values among the CAR-T cells were identified (Fig. 20D-E). It remains to elucidate whether these short-term *in vitro* cytotoxicity assays are not sensitive enough to appreciate minor differences or if the generated lower affinities are still capable of conferring adequate functionality.

Furthermore, no unspecific lysis of $CD19^+$ HEK cells was observed by mock control T cells. In contrast to the results of the green group, CAR-T cells transduced with the orange CAR mutants only controlled the tumor growth but could not efficiently eliminate the target cells. The only two exceptions were clones F113A and F113L, which showed successful killing of $CD19^+$ HEK cells (Fig. 20A-B). Although none of the CAR-T cells of the red group, except the clone A93W, controlled or eradicated the target cells during the monitored 24 hours, a minimal effect was observed compared to mock control T cells. However, this slight difference is insufficient

for any therapeutic application. These findings support that CARs of the red group are not expressed on the cell surface due to the introduced amino acid exchange. For A93W CAR-T cells, the minimal CAR expression seems sufficient to provide at least some killing efficacy.

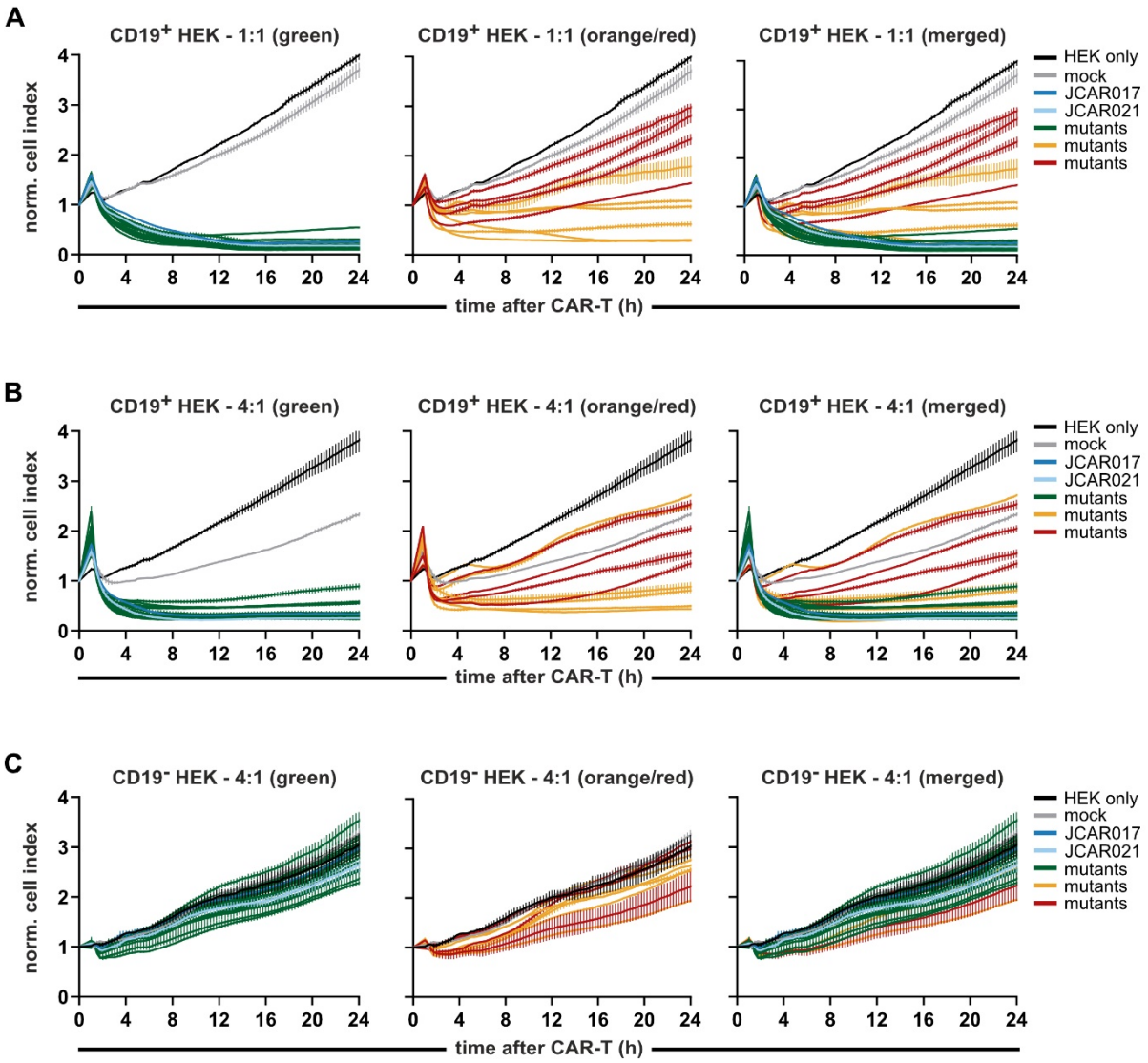

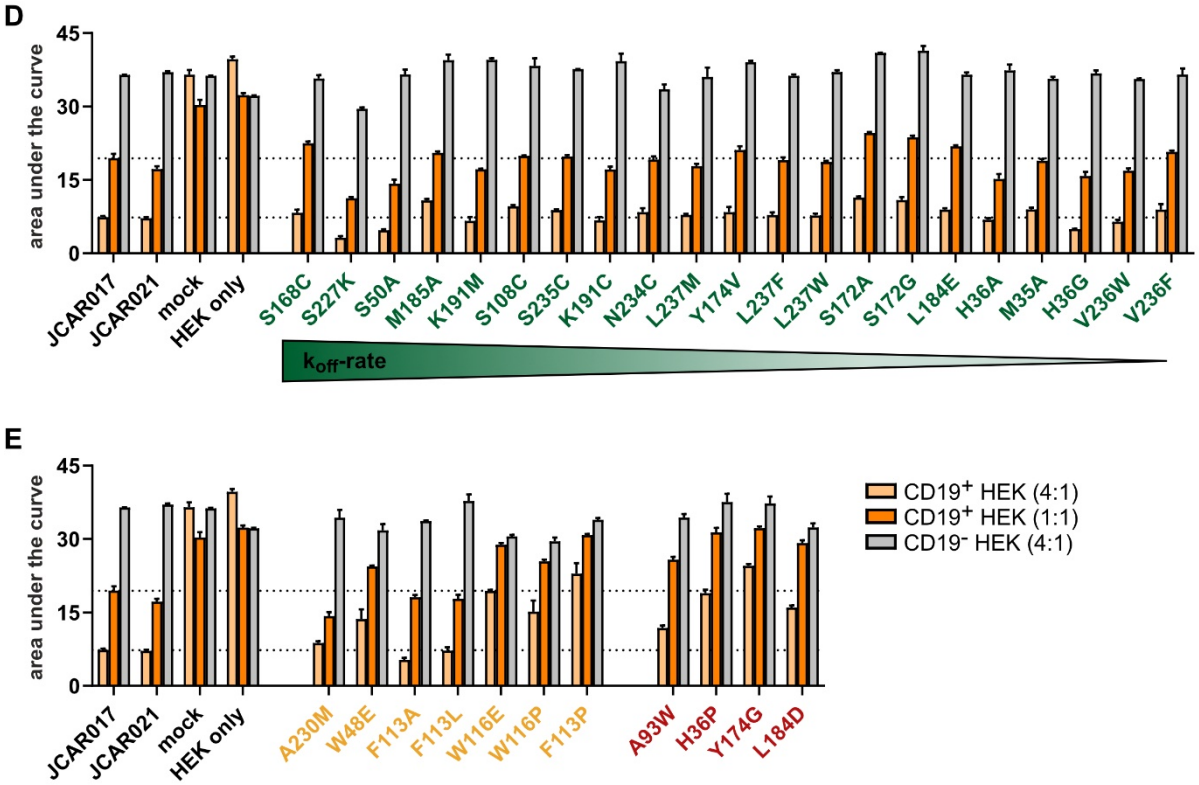

Fig. 20 xCelligence killing assay of low-affinity CAR-T cells
(A-C) Growth curves of **(A)** CD19$^+$ HEK target cells (E:T = 1:1), **(B)** CD19$^+$ HEK target cells (E:T = 4:1) and **(C)** CD19$^-$ HEK target cells (E:T = 4:1) after the addition of sorted EGFRt$^+$ CAR-T cells determined by impedance-based real-time xCelligence assay. CAR-T cells were assigned to the respective CAR expression groups. Untransduced mock T cells from the same donor were used as a negative control. Data are presented as mean+SD. **(D+E)** Calculation of the area under the growth curve (AUC) of CD19$^+$ and CD19$^-$ HEK cells for 24 hours after applying EGFRt$^+$ CAR-T cells. **(D)** The killing potential of CAR-T cells belonging to the green group or **(E)** orange and red group. Data are represented as mean+SD (n = 3) and representative of two biologically independent experiments.

Similar results were obtained in a flow cytometry-based killing assay with naturally CD19-expressing Raji cells. Transduced CAR-T cells were co-incubated in an effector-to-target ratio of 4:1 with CD19$^+$/GFP$^+$ Raji cells. After 48 hours, absolute numbers of remaining target cells were determined by flow cytometry, and specific lysis was calculated relative to the mock control. Raji target cells were distinguished from the effector cells due to their constant GFP expression (Fig. 21A). The killing efficacies of CAR-T cells belonging to the green group were similarly high as JCAR017 and JCAR021 killing efficacies (over 90 % of specific lysis). Interestingly, significant differences were only detected for the mutants V236W and V236F, which possessed the weakest binding strength towards CD19. In contrast to the xCelligence assay, all CAR-T cells of the orange group could efficiently kill the Raji cells, except for the

mutants W116E and W116P, which only moderately lysed the CD19⁺ target cells. Comparable to the xCelligence assay, none of the four red CAR-T cells caused any lysis of the tumor cells.

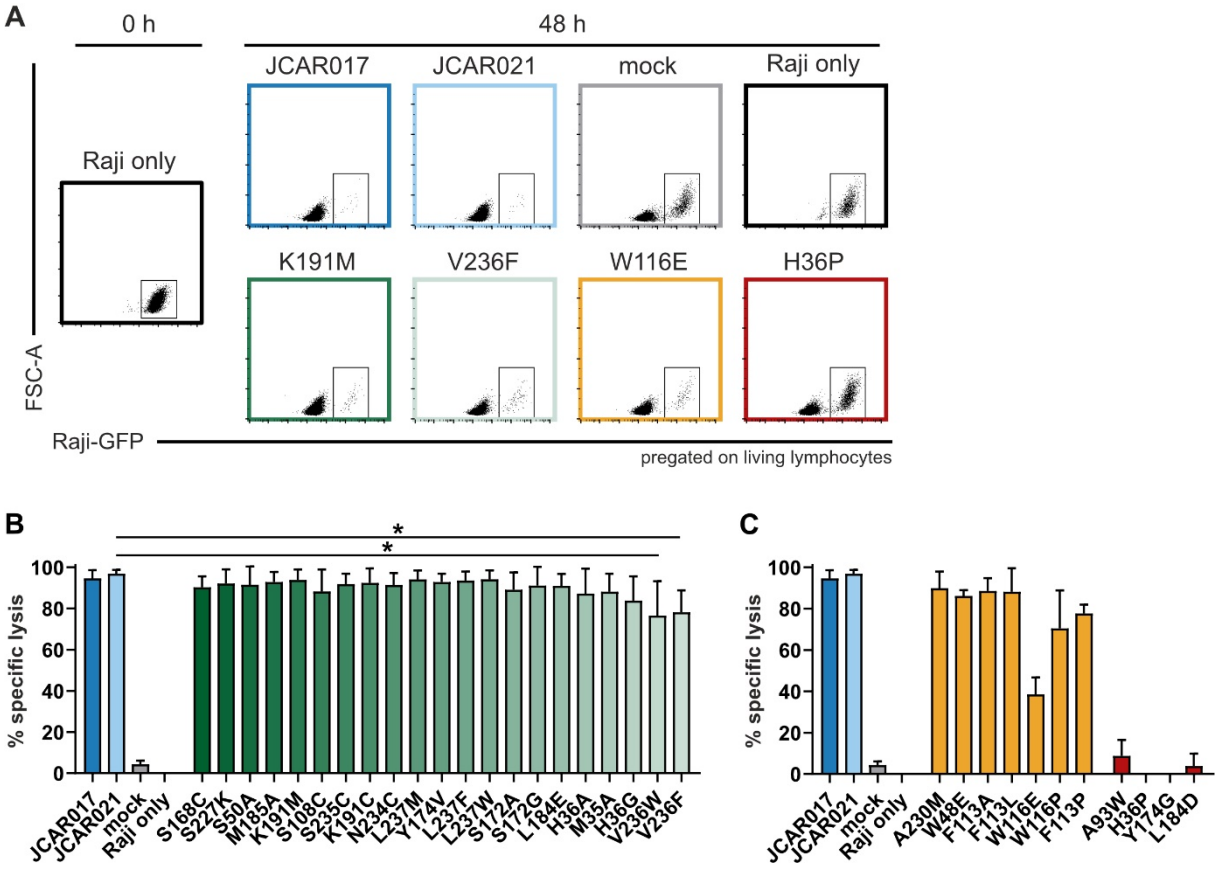

Fig. 21 Flow cytometry-based killing assay of low-affinity CAR-T cell mutants
(A) Representative flow cytometry plots of GFP⁺ Raji tumor cells before and after co-incubation with CAR-T cells for 48 hours in an effector-to-target ratio of 4:1. Colors illustrate to which expression group the different CAR-T cells belong. **(B+C)** Specific lysis of CD19⁺ Raji tumor cells after co-incubation with CAR-T cells belonging to the **(B)** green or **(C)** orange and red group for 48 hours normalized to the mock control group. CAR-T cells of the green group are ordered with decreasing affinity. Data are expressed as mean+SD of three biologically independent experiments with technical triplicates. Statistical testing by one-way ANOVA, *p ≤ 0.05 using JCAR021 as a reference control.

In summary, we generated a library of 32 JCAR021-derived CAR mutants containing single-point mutations in their framework and CDR region, resulting in lower affinities than the original construct, down to affinities even in the range of TCRs. Despite the exchange of amino acids, 21 CAR mutants were easy to transduce into primary human T cells and are successfully expressed on the cell surface. In addition, the findings of the *in vitro* screening demonstrated that all engineered anti-CD19 CAR-T cells with good receptor expression maintained a high functional profile. Intriguingly, we observed a potential threshold of *in vitro* functionality within the group of successfully expressed anti-CD19 CARs at half-lives of around 50 s, suggesting

that *in vitro* functionality of CAR-T cells is highly robust within a broad range of binding strengths but starts to be reduced with receptor affinities in the range of TCRs. Furthermore, the findings of the *in vitro* screening demonstrated that direct staining of the CAR is essential to verify successful receptor surface expression, as co-expressed markers are insufficient for this purpose. Although connected by a T2A element, the use of co-expressed markers, in our case EGFRt, was not sufficient to determine the receptor expression, as some mutations interfered and thus influenced the expression of the CAR but not of the transduction marker.

4.5 *In vivo* functionality of low-affinity CAR-T cells in a sub-optimal Raji tumor model

Findings from the *in vitro* screening of the anti-CD19 CAR affinity library suggested that a relatively broad window of reduced CAR affinities is tolerated in terms of the maintained functionality of the corresponding CAR-T cells. The threshold of the CAR binding strength for sufficient *in vitro* tumor clearance was identified at extremely fast k_{off}-rates for CARs ($t_{1/2}$ = 50 s at 20°C), which were comparable to values determined for highly functional TCRs. All T cells transduced with receptors above this threshold showed similar cytotoxicity and cytokine production after target-specific stimulation. In order to examine whether these results could be confirmed *in vivo*, we investigated the anti-tumor efficacy, expansion, and engraftment potential of CAR-T cells expressing receptors with different k_{off}-rates in an immunocompromised xenograft NSGS tumor model. JCAR017, JCAR021, and three representative JCAR021 mutants belonging to the green group were selected. The three chosen CAR mutants are equally distributed over the JCAR021-derived affinity library and reflect the broad spectrum of accessible CAR binding strengths. While the CAR mutant V236W possesses a k_{off}-rate below the suggested *in vitro* functionality threshold ($t_{1/2}$ = at 43s; 22°C), L237W has an affinity much stronger than the threshold but still weaker than JCAR021 ($t_{1/2}$ = at 64s; 22°C). In order to cover the overall library, the mutant M35A was additionally selected, as its affinity is located at the border of *in vitro* functional and low functional CARs ($t_{1/2}$ = at 96s; 22°C). In addition, untransduced mock T cells derived from the same healthy donor were used to control for potential xenogeneic T cell responses.

4.5.1 Experimental setup of a suboptimal xenograft Raji tumor model

In order to study the anti-tumor efficacy of CAR-T cells with different receptor binding strengths, a xenograft mouse model using $CD19^+/GFP^+$ Raji tumor cells, similar to the *in vitro* assays, was established (Fig. 22A). These tumor cells had been modified to express both the firefly luciferase (ffluc) and GFP, which allowed tracking of tumor growth by non-invasive serial imaging by bioluminescence (BLI) and flow cytometry on blood specimens.

Immunocompromised NSGS mice were inoculated intravenously (i.v.) with $0.5x10^6$ $CD19^+$ Raji tumor cells, followed by another i.v. injection of the respective CAR-T cells one week later. Freshly isolated and activated PBMCs were retrovirally transduced with the different CAR constructs, sorted for $EGFRt^+$ cells, and expanded for three weeks before they were adoptively transferred into the tumor-bearing mice. Successful tumor engraftment before CAR-T cell injection was tested by *in vivo* imaging (IVIS), after which tumor-bearing mice were equally divided into groups of six to eight animals. The survival of the mice was followed for one month, persistence and expansion of CAR-T cells were monitored by weekly blood staining, and tumor growth was followed by *in vivo* imaging. After 28 days, CAR-T cell engraftment was determined by flow cytometry analysis of blood, spleen, and bone marrow. Given the previously reported high *in vivo* efficacy of JCAR017 (FMC63), we decided to test our CARs in a suboptimal tumor setting, established by lowering the injected CAR-T cell dose to $4x10^6$ $EGFRt^+$ CAR-T cells, including $0.8x10^6$ $CD8^+$ $EGFRt^+$ cells per mouse. In this way, we expected to emphasize putative existing differences in CAR functionality.

All five CAR-T cell products showed transduction efficacies between 80-90 %, as indicated by EGFRt and Strep-tag co-staining prior to CAR-T cell infusion (Fig. 22B-C). Also, the MFIs of EGFRt and STII of the $EGFRt^+$ T cells were similar (Fig. 22D), indicating equal expression levels of the CAR on the cell surface. Additionally, all $EGFRt^+$ CAR-T cell products were composed of 18-20 % $CD8^+$ cells (Fig. 22E), expressed similar low levels of the activation marker PD-1 (Fig. 22F), and showed a comparable *ex vivo* phenotype pattern (Fig. 22G). Overall, we could not find major differences in the quality and composition of the generated CAR-T cell products.

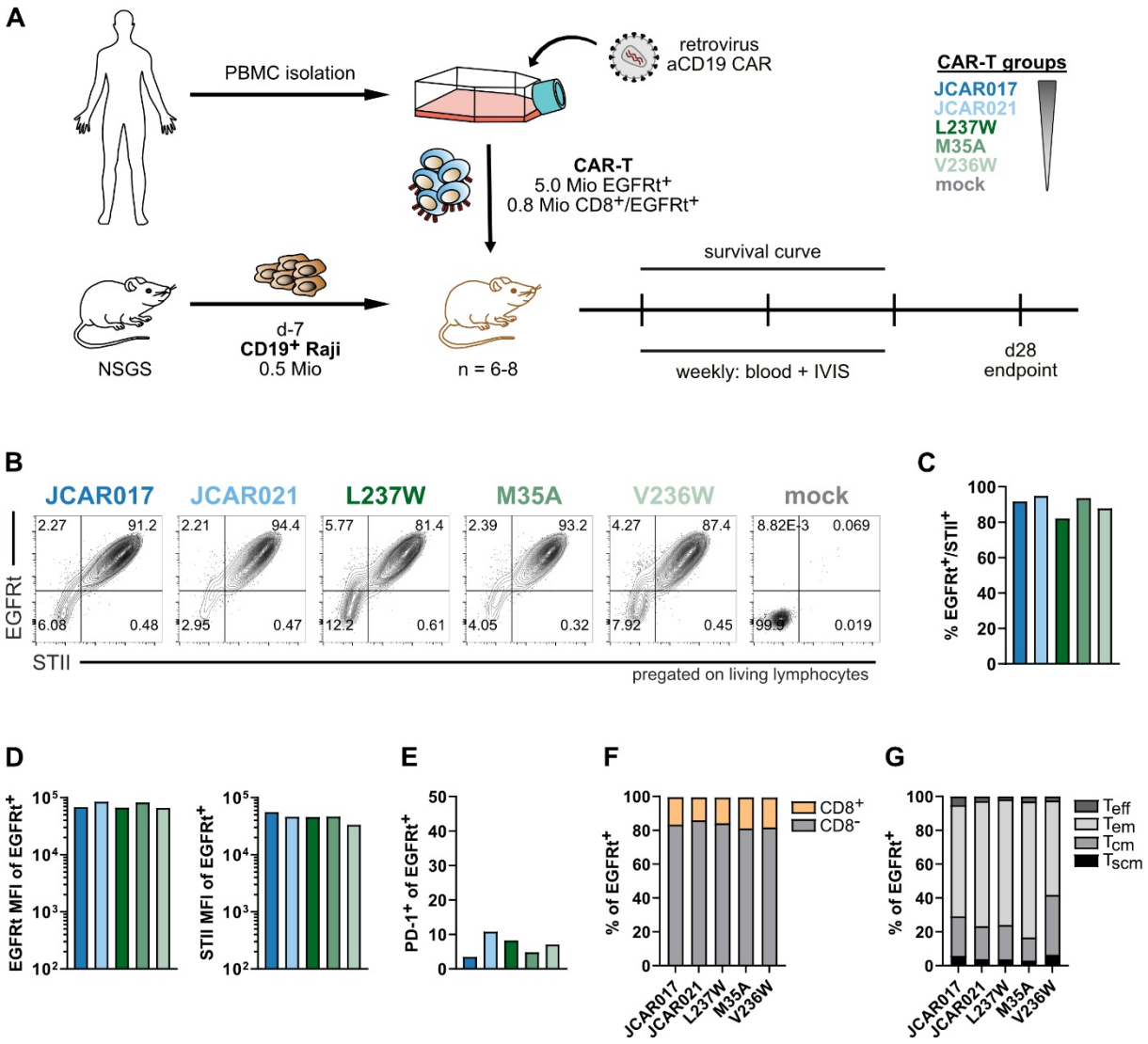

Fig. 22 Experimental set-up of a suboptimal Raji tumor model to test low-affinity CAR-T cells
(A) Schematic overview of the experimental setup of the *in vivo* functional testing of CAR-T cells with different affinity in a suboptimal tumor Raji xenograft tumor model. **(B)** Representative flow cytometry plots of CAR-T cell infusion products. Transduction efficacy and CAR surface expression were determined by co-staining of EGFRt and Strep-tag (STII). **(C)** Transduction efficacies of the different CAR-T cell products are represented by frequencies of EGFRt/STII double-positive cells. **(D)** EGFRt and STII mean fluorescent intensities (MFI) of EGFRt$^+$ CAR transduced T cells. **(E)** Frequencies of PD-1 expressing cells of the transduced T cells composing the injection products. **(F)** Distribution of CD8$^+$ and CD8$^-$ cells within the EGFRt$^+$ transduced CAR-T cell products. **(G)** The phenotypic pattern of the five different CAR-T cell products.

4.5.2 *In vivo* cytotoxicity of low-affinity CAR-T cells

The survival of the tumor-bearing mice was followed for one month after CAR-T cell injection (Fig. 23A). All mice treated with T cells expressing JCAR017 survived, as the tumor growth was successfully controlled by the transferred CAR-T cells. As expected, control mice receiving mock T cells had to be sacrificed due to a high tumor burden between days eleven and twelve post T cell injection. Mice treated with the low-affinity CARs JCAR021, L237W and

M35A showed significantly enhanced survival compared to the mock control group, but surprisingly and in sharp contrast to the *in vitro* data, they did not adequately control tumor growth as compared to high-affinity JCAR017 CAR-T cells. Indeed, some mice had to be sacrificed before the planned endpoint. Finally, super-low-affinity V236W CAR-T cells had almost no effect on the survival of the treated mice. In this group, all mice succumbed between days 11 and 15 post CAR-T cell injection.

Furthermore, the tumor burden of the mice was routinely monitored by *in vivo* imaging (Fig. 23B). One day prior to CAR-T cell injection, similar bioluminescence signals of Raji tumor cells were detected in all mice, mainly localized in the bone marrow and femurs (Fig. 23B). Seven days after CAR-T cell injection, mice receiving mock T cells and CAR-T cells expressing the V236W mutant showed rapidly disseminated tumor infiltration and high levels of bioluminescence (Fig. 23B-D). The four other CAR-T cell groups could delay tumor growth, albeit JCAR017 and JCAR021 CAR-T cells were more effective in inhibiting tumor progression than L237W and M35A expressing CAR-T cells. Although the tumor was continuously growing in all groups due to the relatively low dose of administered therapeutic T cells, a significantly lower tumor burden was found in mice treated with high-affinity JCAR017 CAR-T cells compared to the low-affinity ones on day 14 post CAR-T cell transfer. In general, low-affinity CAR-T cells revealed high *in vivo* cytotoxic potentials, but, in contrast to the *in vitro* experiments, their killing efficacy correlated closely with the affinity of the CAR. Indeed, functional differences were already observed when comparing high-affinity JCAR017 and low-affinity JCAR021 CAR-T cells. Further reducing the CAR affinity diminished the cytotoxic potential of the corresponding CAR-T cells. Interestingly, we also identified a lower CAR affinity threshold, similar to the determined *in vitro* affinity limit, below which CAR-T cells did not improve the survival of the treated mice.

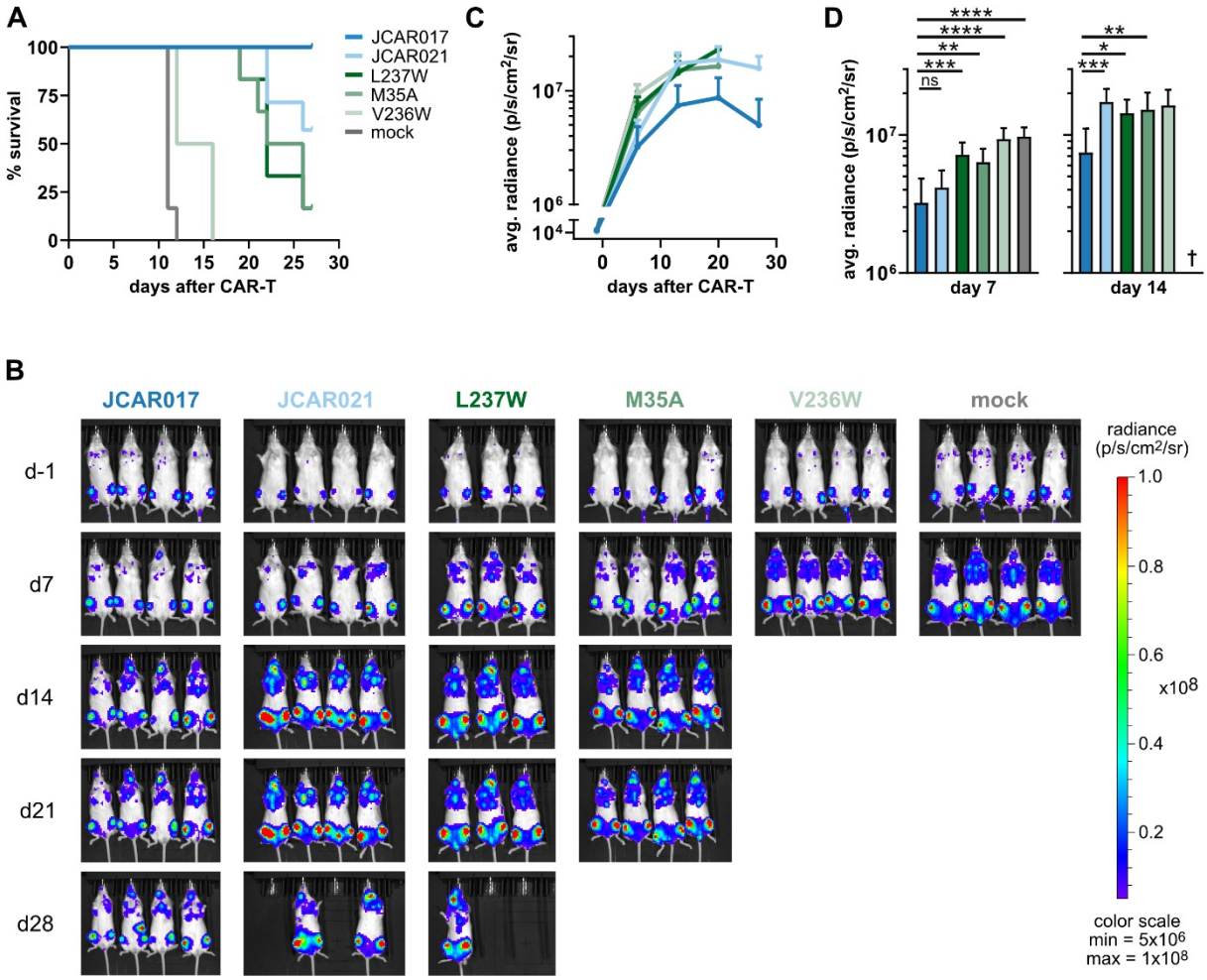

Fig. 23 *In vivo* cytotoxicity of low-affinity CAR-T cells
(A) Kaplan Meier curve of mice treated with low-affinity CAR-T cells in a suboptimal tumor model followed for 28 days after the CAR-T cell transfer. **(B)** Representative bioluminescence images of Raji-bearing mice treated with different CAR-T cell products were followed weekly over one month. Only 3-4 mice are depicted per group. **(C)** The tumor burden of Raji-ffluc tumor cells was quantified and measured as the maximum photon per second per cm^2 per steradian of the whole body of the mouse. Lines represent the mean+SD of average bioluminescence signals (n = 6-8) **(D)** Average radiance of different groups on day 7 and day 14 post CAR-T cell transfer expressed as mean+SD (n = 6-8). Statistical testing by one-way ANOVA, ns $p > 0.05$, *$p \leq 0.05$, **$p \leq 0.01$, ***$p \leq 0.001$, ****$p \leq 0.0001$ using the JCAR017 group as a reference control.

Findings of this first performed suboptimal tumor model were confirmed in a small repetition experiment (n =3-4). One week after the inoculation of $0.5x10^6$ $CD19^+$ Raji tumor cells, $0.8x10^6$ $CD8^+$ $EGFRt^+$ T cells, corresponding to a total number of $2x10^6$ $EGFRt^+$ CAR-T cells, were intravenously injected as bulk populations. CAR-T cells were not sorted prior to the transfer, but transduction efficacies (Fig. 24A-B) and transgenic receptor expression levels (Fig. 24C) were similar among CAR-T cells. Due to a higher but overall similar ratio of $CD8^+$ to $CD8^-$ cells among the groups (Fig. 24D), a lower number of total CAR-T cells was injected compared to the first experiment.

As observed before, all CAR-T cells, except for super-low-affinity V236W CAR-T cells, improved the overall survival of the treated mice in comparison to the mock control group (Fig. 25E). However, the overall survival of the mice and the tumor progression depended on the receptor affinity (Fig. 25F). While all mice treated with JCAR017 CAR-T cells survived the observation period, some of the mice treated with lower affinity CAR-T cells had to be sacrificed at later time points due to the development of a high tumor burden. Again, due to the use of a suboptimal model, none of the constructs completely eradicated the tumor cells (Fig. 25E).

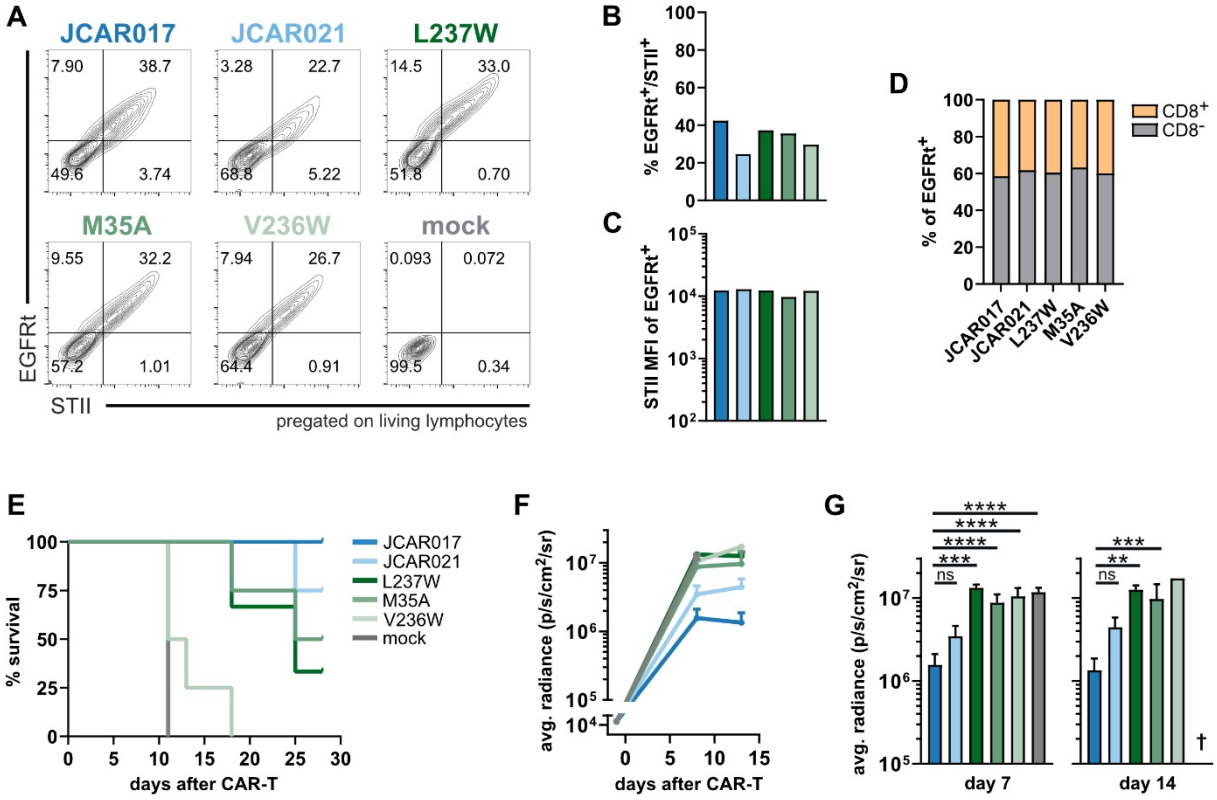

Fig. 24 Repetition of testing low-affinity CAR-T cells in a suboptimal tumor model
(A) Flow cytometry plots illustrating the co-staining of EGFRt and Strep-tag of the different CAR-T cell products prior to the adoptive transfer into mice. **(B)** Transduction efficacies of injection CAR-T cells are represented by frequencies of EGFRt/STII double-positive cells. **(C)** STII mean fluorescent intensities (MFI) of EGFRt$^+$ CAR-T cell products. **(D)** The ratio of CD8$^+$ and CD8$^-$ cells of infused EGFRt$^+$ CAR-T cells. **(E)** Survival curves of mice treated with CAR-T cells expressing CARs with different affinities. Mice were followed for 30 days. **(F)** The tumor burden of Raji-ffluc tumor cells was quantified and measured as the maximum photon per second per cm^2 per steradian of the whole body of the mouse. Lines represent mean+SD of average bioluminescence signals (n = 3-4). **(G)** Average radiance of different CAR-T cell groups on day 7 and day 14 post CAR-T cell infusion (n = 3-4). Data expressed as mean+SD. Statistical testing by one-way ANOVA, ns $p > 0.05$, $^{**}p \leq 0.01$, $^{***}p \leq 0.001$, $^{****}p \leq 0.0001$ using the JCAR017 group as a reference control.

The repetition experiment confirmed that low-affinity CAR-T cells with binding strengths above a certain threshold have the potential to eradicate tumor cells *in vivo*. However, in contrast to the *in vitro* experiments, low-affinity CAR-T cells cannot control high tumor burdens long-term. Consequently, the findings suggest a correlation between CAR-T cell efficacy and receptor affinity, at least in the performed suboptimal tumor model.

4.5.3 Expansion, persistence, and engraftment of low-affinity CAR-T cells

In order to examine why low-affinity CAR-T cells showed reduced *in vivo* cytotoxicity compared to high-affinity JCAR017 CAR-T cells, we investigated the proliferative capacity and activation of the different CAR-T cell groups in the first performed *in vivo* experiment.

Robust expansion of all EGFRt$^+$ CAR-T cell products in the circulation was observed from day 14 after CAR-T cell transfer onwards (Fig. 25A). Seven days after the adoptive transfer of CAR-T cells, only very few EGFRt$^+$ cells were detected in the peripheral blood, with JCAR017 CAR-T cells revealing the highest numbers. One week later, a substantial expansion of all EGFRt$^+$ CAR-T cells was detected, with significantly higher numbers of low-affinity CAR-T cells circulating in the bloodstream than JCAR017 CAR-T cells. This difference was compensated on day 21 post CAR-T cell injection when similarly high CAR-T cell numbers among the different groups were observed. Interestingly, while lower affinities seemed to correlate with the extent of CAR-T cell expansion on day 14, we detected a lower frequency of PD-1 expressing cells in mice treated with CAR-T cells of the groups M35A and V236W, indicating a higher accumulation in the circulation but overall lower activation of low-affinity CAR-T cells (Fig. 25B-C). Although this result appears contradictory, the number of circulating CAR-T cells does not necessarily represent the accumulation of CAR-T cells at the tumor site.

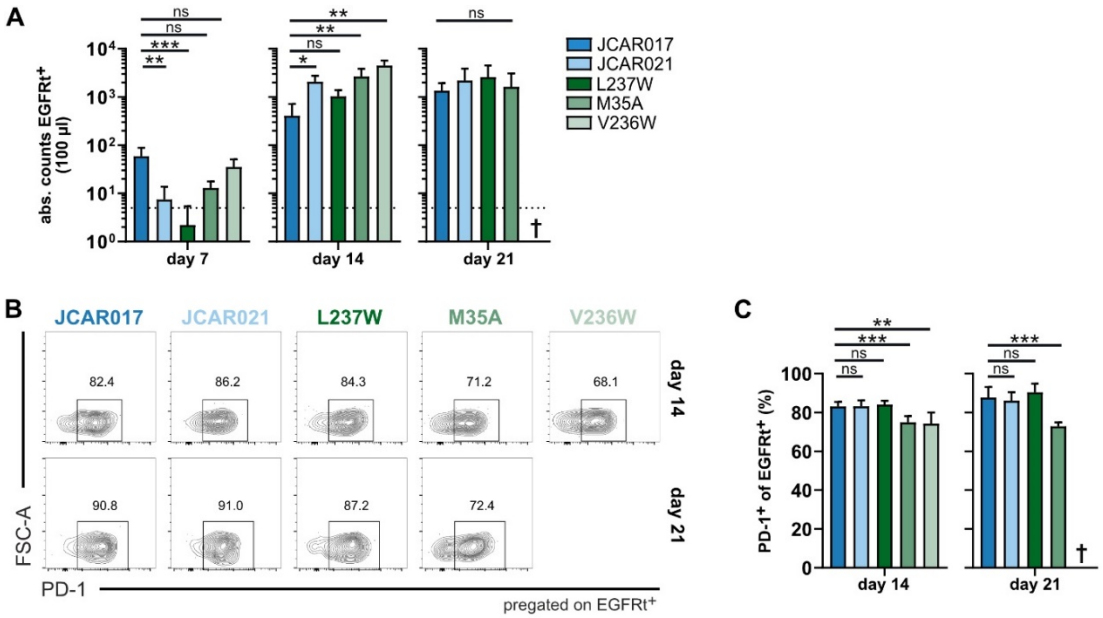

Fig. 25 Expansion and activation levels of low-affinity CAR-T cells in a suboptimal tumor model
(A) Weekly blood analysis of individual mice receiving CAR-T cells. Absolute numbers of EGFRt$^+$ CAR-T cells in 100 µl blood on day7 day 14 and day 21 after CAR-T cell transfer. Statistical testing by Kruskal-Wallis test, ns $p > 0.05$, *$p \leq 0.05$, **$p \leq 0.01$, ***$p \leq 0.001$. Data expressed as mean+SD. **(B)** Representative flow cytometry plots of circulating EGFRt$^+$ CAR-T cells expressing PD-1 on day 14 and day 21 after CAR-T cell treatment. **(C)** Frequencies of PD-1$^+$ cells of EGFRt$^+$ transduced CAR-T cells circulating in the blood on day 14 and day 21 post CAR-T cell injection. Data are expressed as mean+SD (n = 6-8). Statistical testing by one-way ANOVA, ns $p > 0.05$, **$p \leq 0.01$, ***$p \leq 0.001$ using the JCAR017 group as a reference control.

Indeed, transferred hCD45$^+$ cells of all groups successfully engrafted into the secondary lymphoid organs (bone marrow and spleen), as significantly higher absolute cell numbers were identified in mice treated with CAR-T cells than mock T cells (Fig. 26A). However, flow cytometry analysis of the bone marrow revealed significantly higher absolute numbers of EGFRt$^+$ cells in the mouse group treated with high-affinity JCAR017 CAR-T cells compared to groups treated with low-affinity CAR-T cells. Interestingly, in contrast to the stronger accumulation of low-affinity CAR-T cells in the blood on day 14, lower numbers of CAR-T cells were observed in the bone marrow (Fig. 26B-C). Additionally, no significant difference in CAR-T cell engraftment was detected in the spleen, as systemically applied Raji cells mainly accumulate in the bone marrow of NSGS mice (Fig. 26B). Overall, all CAR-T cells could engraft into the secondary lymphoid organs. However, the higher persistence of high-affinity CAR-T cells in the bone marrow is potentially linked to enhanced tumor-specific stimulation and expansion and could also explain the better anti-tumor activity compared to low-affinity CAR-T cells.

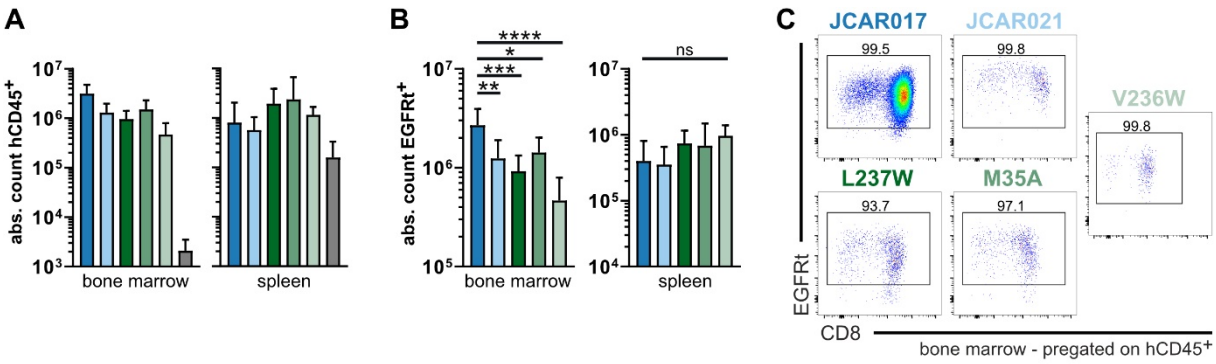

Fig. 26 Engraftment of CAR-T cells into lymphoid organs
(A) Weekly blood analysis of individual mice receiving CAR-T cells. Absolute numbers of transferred human CD45$^+$ cells in bone marrow and spleen at the endpoint of the respective mouse. Data are expressed as mean+SD (n = 6-8). **(B)** Absolute numbers of transferred EGFRt$^+$ CAR-T cells in bone marrow and spleen at the endpoint of the respective mouse. Data are expressed as mean+SD (n = 6-8). Statistical testing by one-way ANOVA for bone marrow samples and Kruskal-Wallis test for spleen samples, ns $p > 0.05$, *$p \leq 0.05$, **$p \leq 0.01$, ***$p \leq 0.001$, ****$p \leq 0.0001$ using the JCAR017 group as a reference control. **(C)** Representative flow cytometry plots illustrating the frequency of EGFRt$^+$ cells among transferred hCD45$^+$ cells in the bone marrow at the endpoint of the experiment.

A more detailed analysis of EGFRt$^+$ CAR-T cells in blood, bone marrow, and spleen at the endpoint demonstrated a clear correlation between the activation status of CAR-T cells and their receptor affinity. While over 80 % of JCAR017, JCAR021, and L237W expressing CAR-T cells in the bone marrow co-expressed the activation markers HLA-DR and PD-1, only 40 % and 60 % of M35A and V236W CAR-T cells, respectively, were positive for these two markers (Fig. 27A-B). Similar effects were also observed in the blood, where 60 % of the JCAR017, JCAR021, and L237W CAR-T cells were double-positive, but only 30 % of CAR-T cells expressing M35A and V236W were activated. Finally, frequencies of CAR-T cells expressing the examined activation markers correlated with the affinity of the receptor in spleens of the treated mice. These findings are in line with the slightly reduced activation levels of circulating super-low-affinity M35A and V236W-expressing CAR-T cells and can partially explain the overall higher number of high-affinity JCAR017 CAR-T cells found in the bone marrow. Although slightly elevated frequencies of PD-1$^+$/HLA-DR$^-$ CAR-T cells were found in the blood and spleen of mice treated with JCAR017 CAR-T cells compared to V236W CAR-T cells, these frequencies were overall too low to represent high levels of exhaustion, and thus cell death due to overstimulation (Fig. 27C). Therefore, the lower functionality of low-affinity CAR-T cells

seems to be a combination of lower infiltration in the bone marrow together or even because of a lower activation of the adoptively transferred cells.

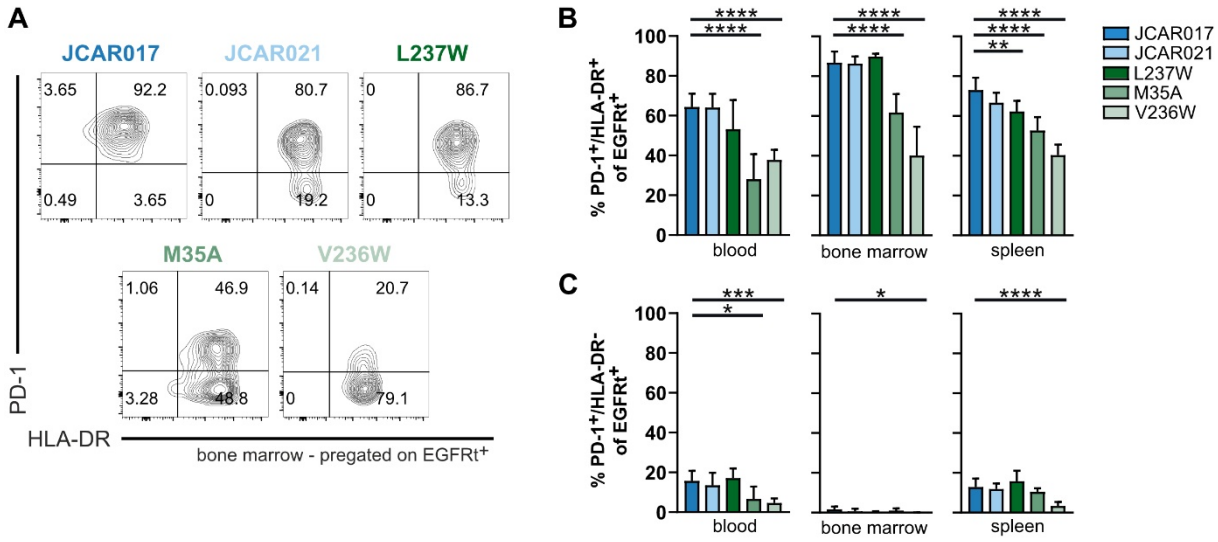

Fig. 27 Activation levels of low-affinity CAR-T cells in the secondary lymphoid organs
(A) Representative plots of co-expression of PD-1 and HLA-DR of EGFRt$^+$ transduced CAR-T cells in the bone marrow analyzed by flow cytometry. **(B)** Frequencies of PD-1$^+$/HLA-DR$^+$ cells of EGFRt$^+$ CAR-T cells in either blood, bone marrow, or spleen at the endpoint. Statistical testing by one-way ANOVA, **p ≤ 0.01, ****p ≤ 0.0001 using the JCAR017 group as a reference control. Only significant differences are depicted. **(C)** Frequencies of PD-1$^+$/HLA-DR$^-$ cells of EGFRt$^+$ CAR-T cells either in blood, bone marrow, or spleen at the endpoint of the experiment (n = 6-8). Data are expressed as mean+SD. Statistical testing by one-way ANOVA, *p ≤ 0.05, ***p ≤ 0.001, ****p ≤ 0.0001 using the JCAR017 group as a reference control.

4.5.4 Receptor downregulation and differentiation of low-affinity CAR-T cells

T cell activation is usually accompanied by downregulation of the specific receptor on the cell surface and thus represents a relatively sensitive readout for antigen-specific receptor engagement. While all transferred STII$^+$ cells were positive for the transduction marker EGFRt (Fig. 28A), different CAR expression levels of EGFRt$^+$ cells were detected in the bone marrow of the different groups (Fig. 28B-C). Frequencies of CAR-expressing cells of EGFRt$^+$ JCAR021 and L237W CAR-T cells were strongly reduced compared to EGFRt$^+$ JCAR017 CAR-T cells (Fig. 28B), potentially due to a higher tumor burden and thus higher antigen load in these mice. Also, the improved ability of serial triggering of the low-affinity CAR-T cells could explain the observed more robust internalization of the CAR. Surprisingly, the two super-low-affinity CAR-T cells M35A and V236W did not downregulate their CAR, which is in line with their diminished activation levels. In addition, none of the transferred EGFRt$^+$ CAR-T cells in the spleen

downregulated their CAR, as no or only low numbers of CD19$^+$ tumor cells accumulate at this site.

Furthermore, parallel staining of the transduction marker EGFRt and the CAR via the Strep-tag demonstrates that, although both receptors are connected via a T2A-element, they are not always equally expressed on the cell surface. While mRNA levels should stay constant, the protein expression can be different. Therefore, staining both markers or sorting the target population before the adoptive transfer is essential to precisely monitor the CAR-T cell population of interest.

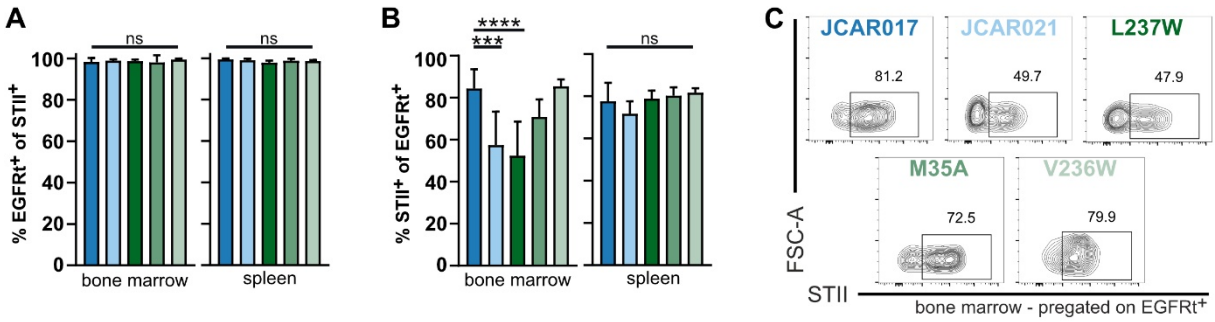

Fig. 28 Receptor downregulation of retrovirally transduced low-affinity CAR-T cells *in vivo*
(A) Frequencies of EGFRt$^+$ cells of CAR-expressing T cells in the bone marrow and spleen at the endpoint of the experiment. (n = 6-8). Data are expressed as mean+SD. Statistical testing by one-way ANOVA, ns $p > 0.05$ using the JCAR017 group as a reference control. **(B)** Frequencies of CAR-expressing (STII$^+$) cells among the EGFRt$^+$ CAR-T cells in bone marrow and spleen at the endpoint. Data are represented as mean+SD (n = 6-8). Statistical testing by one-way ANOVA, ns $p > 0.05$, ***$p \leq 0.001$, ****$p \leq 0.0001$ using the JCAR017 group as a reference control. Only significant statistics are shown. **(C)** Representative flow cytometry plots of EGFRt$^+$ CAR-T cells in the bone marrow were analyzed for CAR expression by STII staining.

Apart from the activation status and receptor downregulation, we also tested the consequences of affinity reduction on the diversification of the transferred CAR-T cells in bone marrow and spleen. The subset diversification of EGFRt$^+$ CAR-T cells was based on expression levels of the phenotypic markers CD62L and CD45RA (Fig. 29A). The main differences in the phenotypic composition of the different CAR-T cell groups were observed depending on their receptor binding strength (Fig. 29B). The main population of JCAR017 CAR-T cells in the bone marrow, with 70 % of all EGFRt$^+$ cells, were effector memory T cells (T_{em}; CD62L$^-$/CD45RA$^-$), while nearly 30 % differentiated into effector T cells (T_{eff}; CD62L$^-$/CD45RA$^+$) and 4 % of the population kept a central memory phenotype (T_{cm};

CD62L$^+$/CD45RA$^-$). In contrast, 60 % of the low-affinity CAR-T cells in the bone marrow fully differentiated into effector T cells, and only 20 % had an effector memory phenotype. Moreover, low-affinity CAR-T cells preserved a naive population (T_n; CD62L$^+$/CD45RA$^+$), underlining that they were not fully engaged and recruited into the tumor response. Interestingly, the relative frequencies of this population increased with lower receptor affinity. Even 40 % of the super-low-affinity CAR-T cells expressing V236W showed a naïve phenotype, again emphasizing the low activation of T cells expressing CARs with affinities below a certain threshold. Such enormous differences between the CAR-T cell groups were not observed in the spleen. Here, typical memory subset phenotypes made up the most prominent subset of the EGFRt$^+$ CAR-T cells, with only low levels of effector phenotype CAR-T cells among the different investigated groups. However, V236W CAR-T cells revealed the least differentiated phenotype again. Overall, the weaker differentiation and higher frequency of naïve CAR-T cells support the finding that low-affinity CAR-T cells are not or are much less engaged in the tumor response, which is in line with a lower PD-1 expression and a more potent tumor progression in these mice.

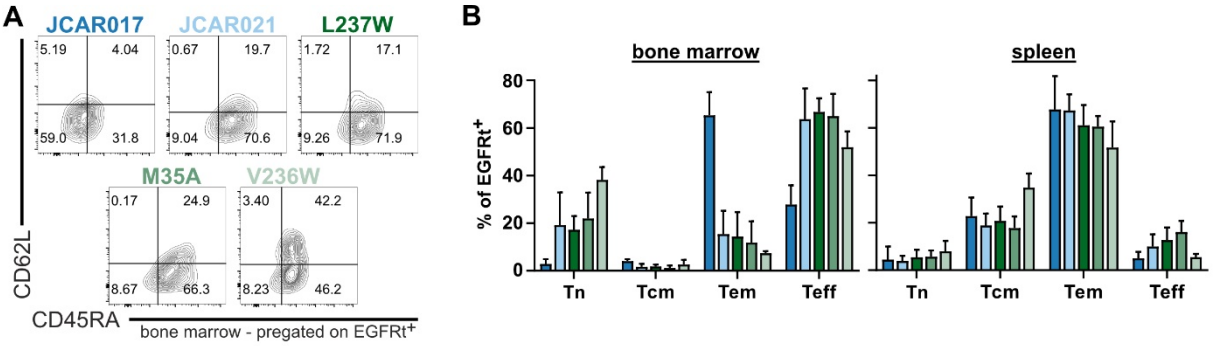

Fig. 29 Differentiation patterns of adoptively transferred CAR-T cells in secondary organs
(A) Representative flow cytometry plots illustrating the phenotypic distribution of EGFRt$^+$ CAR-T cells in the bone marrow at the endpoint analyzed by staining for CD62L and CD45RA. **(B)** Phenotypic analysis of transferred EGFRt$^+$ CAR-T cells by flow cytometry in bone marrow and spleen at the endpoint. T_n (CD62L$^+$ CD45RA$^+$), T_{CM} (CD62L$^+$ CD45RA$^-$), T_{EM} (CD62L$^-$ CD45RA$^-$), T_{EFF} (CD62L$^-$ CD45RA$^+$). Data are expressed as mean+SD.

In contrast to the unaffected *in vitro* functionality of low-affinity CAR-T cells, significant differences in the cytotoxic expansion and engraftment potential of CAR-T cells possessing different affinities were determined *in vivo*. While high and low-affinity CAR-T cells demonstrated good *in vivo* functionality, as they were able to control the tumor growth

compared to control mock T cells, we observed a clear positive correlation between higher affinities and a more prolonged survival of the treated mice. Although reasonable tumor response rates were detected for all of the tested low-affinity CAR-T cells, except the super-low-affinity ones, high-affinity CAR-T cells were beneficial in this suboptimal tumor model. In line with the *in vitro* findings, we identified the same lower limit of CAR affinity, which is necessary to preserve the cytotoxic potential of the CAR-T cells.

Furthermore, the different CAR-T cell products showed specific activation, expansion, and persistence but were still dependent on their receptor binding strength. Indeed, the strong killing capacity of CAR-T cells expressing high-affinity JCAR017 can be explained by the improved infiltration into the bone marrow, where CAR-T cells are highly activated due to the remaining tumor burden. Also, JCAR021 and L237W CAR-T cells were strongly activated, which was represented by a strong upregulation of PD-1 and HLA-DR and the internalization of their CAR. However, their engraftment rate was clearly reduced, and thus these CAR-T cells were not as efficient in controlling the tumor cells as the high-affinity ones. Finally, the low cytotoxic potential of super-low affinity CAR-T cells resulted from reduced recruitment, activation, and expansion at the relevant tumor site, as they did neither express high levels of the activation markers nor downregulated their receptor as a sign of activation and preserved a relatively high fraction of naïve T cells.

Taken together, also CAR-T cells with reduced affinity are still functional *in vivo;* however, killing efficiencies are decreased compared to high-affinity CAR-T cells, and thus sufficient functionality cannot be guaranteed in high tumor burden settings.

4.6 Analysis of CAR-related side effects in a humanized CRS mouse model

Successful CAR-T cell treatment should comprise a highly functional anti-tumor response on the one hand together with low toxicities on the other hand. The tested low-affinity CAR-T cells with binding strengths above a certain threshold still showed a certain extent of functionality *in vivo* but also lower engraftment into the bone marrow. As these results suggested a reduced initial expansion potential of low-affinity CAR-T cells, we hypothesized that the transfer of weak binders could also result in milder toxicities than CAR-T cells with high receptor affinities. So far, there are only limited possibilities to study the development of toxicities after the transfer of CAR-T cells in pre-clinical *in vivo* models. In general, the adoptive transfer of human-engineered cell products must be tested in immunocompromised mouse models to avoid transplant rejection and xenoreactivity between graft and recipient T cells. However, immunodeficient mice do not develop CAR-T cell-related side effects, as necessary bystander cells, mainly monocytes, and macrophages, are missing. In order to close this gap, a few years ago, an advanced humanized mouse model was developed to study Cytokine-Release-Syndrome (CRS) after the adoptive transfer of CAR-T cell products[95]. We established this advanced *in vivo* model at our institute and adapted it to use our available $CD19^+$ Raji tumor cell line to investigate the influence of receptor affinity on the development of CAR-T cell-related side effects. In general, tumor cells are intravenously injected into humanized NSGS mice, followed by the adoptive transfer of CAR-T cells. During the first week after CAR-T cell injection, clinical signs of CRS, e.g., weight loss and intense release of cytokines into the bloodstream, can be detected and analyzed. Additionally, the cytotoxic potential, expansion, and engraftment of the transferred CAR-T cells can be studied in this advanced humanized *in vivo* model.

4.6.1 Setup of a CRS mouse model to test low-affinity CAR-related side effects

In order to test whether the reduction of affinity has positive effects on CAR-T cell-related side effects, four-week-old female NSGS mice were sublethally irradiated with 1.5 Gy and intravenously inoculated with 0.01×10^6 $CD34^+$ human cord blood-derived hematopoietic stem

cells (hHSCs) (Fig. 30A) with a purity of 76.3 % (Fig. 30B). No adverse events due to residual hCD45$^+$ cells were observed during the weakly health monitoring (data not shown). Successful humanization was confirmed eight weeks after the transfer of the hHSCs, as all mice revealed high frequencies and absolute numbers of hCD45$^+$ cells in the blood (Fig. 30C-E). According to the Jackson Laboratory, mice are regarded to be successfully humanized when the frequencies of circulating human CD45$^+$ cells of all CD45$^+$ cells are higher than 20 %. However, we usually used mice that reached humanization levels above 50 %. Most of the hCD45$^+$ leukocytes were CD19$^+$ B cells, but mice also developed sufficiently high numbers of human CD33$^+$ macrophages and CD14$^+$ monocytes, which are necessary to study the development of CAR-T cell-related CRS (Fig. 30C-E). 0.5x10^6 CD19$^+$/GFP$^+$ Raji-ffluc tumor cells were injected intravenously into successfully humanized mice, followed by adoptive transfer of 7x10^6 EGFRt$^+$ CAR-T cells one week later (n = 8). As the number of mice was limited, we decided to compare the safety profile of the clinically relevant high-affinity JCAR017 CAR-T cells with CAR-T cells expressing the low-affinity JCAR021, which was identified as the most functional low-affinity CAR.

Additionally, untransduced mock T cells from the same donor were used as a negative control to check for allo- or xenoreactivity of the graft. The development of CAR-T cell-related CRS was monitored by daily weight and temperature measurements, whereas serum collections were used to analyze the cytokine production of the transferred cells during the first-week post CAR-T cell injection. Tumor growth was tracked by weekly non-invasive *in vivo* imaging of the mice, and CAR-T cell activation, expansion, and engraftment were evaluated during weekly blood stainings and in secondary lymphoid organs (spleen and bone marrow) latest on day 35 post CAR-T cell transfer.

CAR-T cells were generated by retroviral transduction of freshly isolated PBMCs derived from a healthy donor. To discriminate humanized CD45$^+$ cells and transferred CAR-T cells by flow cytometry, blood donors were selected according to their HLA-A2 status. While donor hHSCs were HLA-A2$^+$, CAR-T cells were produced from blood from an HLA-A2$^-$ donor. Overall, no differences were observed between the two CAR-T cell products. 80 % of both CAR-T cell

injection products were EGFRt and STII double-positive (Fig. 30F) and revealed similar expression levels of the two markers after purity sorting (Fig. 30G-H). In addition, between 30-40 % expressed PD-1$^+$ (Fig. 30I) and only 10 % CD8$^+$ T cells were detected in the CAR-T cell products (Fig. 30J) after *ex vivo* expansion.

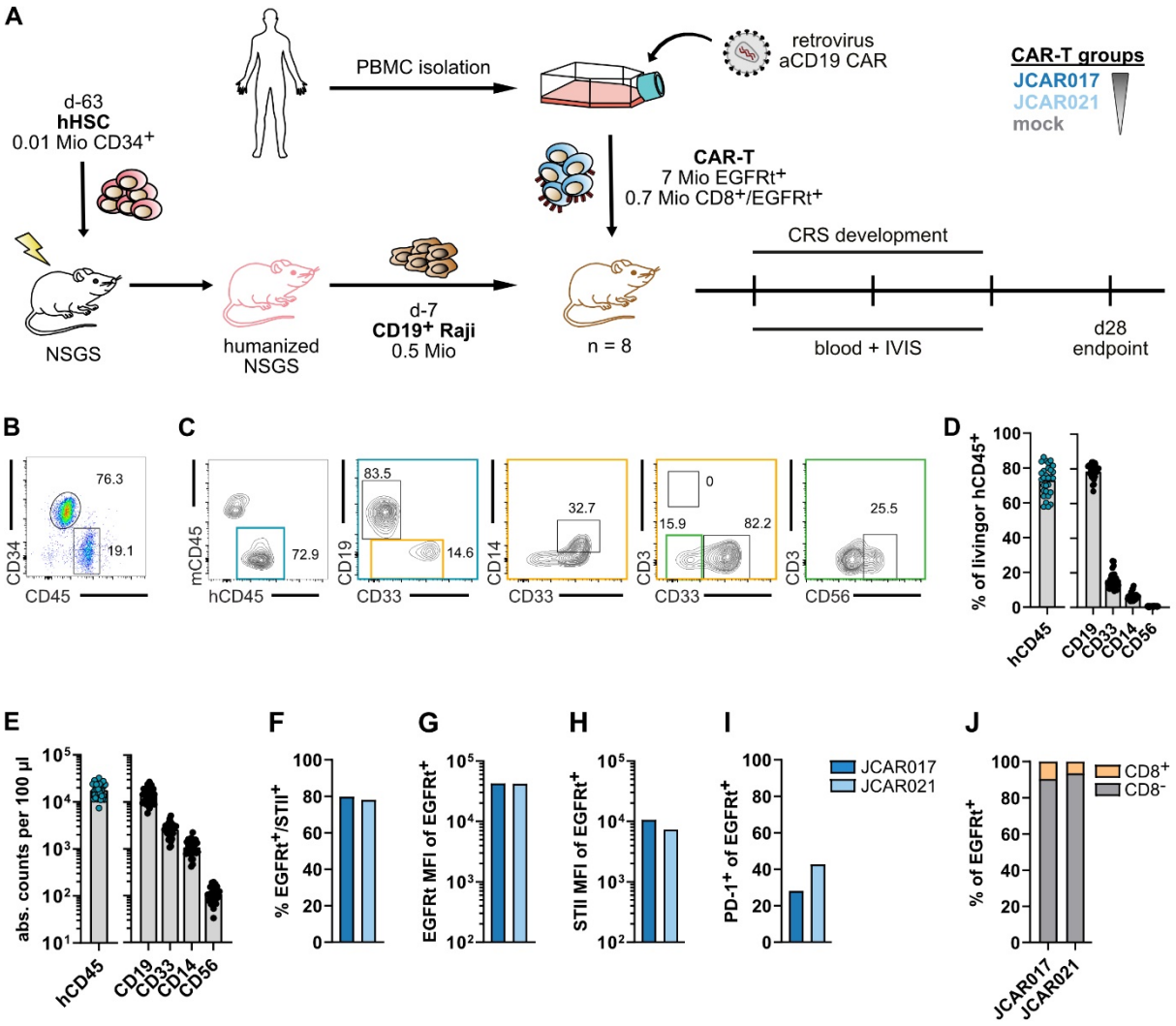

Fig. 30 Setup of a humanized CRS mouse model to study CAR-related side effects
(A) Schematic overview of the experimental setup of the humanized CRS mouse model. **(B)** Flow cytometry plot of purified hHSCs stained for CD34$^+$ and CD45$^+$ to determine the purity of the injection product. **(C)** Representative gating strategy to evaluate the humanization frequency and subpopulations of the humanized mice. **(D)** Frequencies and absolute cell numbers **(E)** of humanized cells in 100 µl of blood. **(F)** Transduction efficacies of the two CAR-T cell products are represented by frequencies of EGFRt/STII double-positive cells. **(G)** EGFRt and **(H)** STII mean fluorescent intensities (MFI) of EGFRt$^+$ CAR transduced T cells. **(I)** Frequencies of PD-1 expressing cells of the transduced injection product. **(J)** Distribution of CD8$^+$ and CD8$^-$ cells within the EGFRt$^+$ transduced CAR-T cell product.

4.6.2 Development of CRS after the adoptive transfer of low-affinity CAR-T cells

Once we set up the CRS mouse model, we followed the development of treatment-related side effects after transferring high and low-affinity CAR-T cells. As expected, all CAR-T cell-treated mice developed clinical symptoms of CRS, while no side effects were observed in mice treated with mock control T cells. However, the grade of CRS was significantly lower in mice receiving low-affinity CAR-T cells. Indeed, while the JCAR021 group showed only mild signs of CRS, mice of the high-affinity JCAR017 group developed severe symptoms. Due to a substantial weight loss and overall sickness, 25 % of the mice treated with JCAR017 CAR-T cells had to be sacrificed on day three after CAR-T cell transfer (Fig. 31A). Although weight loss was observed in all CAR-T cell treated mice, the ones belonging to the JCAR021 group lost not more than 15 % of their starting weight and already started to recover three days after CAR-T cell injection (Fig. 31B). In contrast, mice of the JCAR017 group lost over 20 % of their starting weight within three days and suffered longer until their weight increased again. In the original published CRS mouse model, elevated body temperature was identified as another clinical sign of CRS. However, in our humanized model, we noticed even a decrease in body temperature of all CAR-T cell-treated mice, which we associated with the substantial weight loss (Fig. 31C). Differences in the temperature development between the two models could be due to the different used tumor cell lines. Besides weight loss, the release of cytokines into the circulation represents another major clinical sign of CRS. Therefore, cytokine levels were measured in the serum of the mice on days 3 and 5 post CAR-T cell transfer (Fig. 31D). Elevated levels of the investigated cytokines INF-γ, TNF-α, IL-10, and IL-6, were found in both CAR-T cell groups, while no cytokine production was observed in the mock group. Notably, similar to the weight loss, JCAR021 CAR-T cells produced significantly lower amounts of cytokines than JCAR017 CAR-T cells.

Taken together, we could confirm a clear connection between the development of CAR-T cell-related toxicities and the affinity of the receptor. Consequently, a reduction of the CAR binding strength can mitigate the grade of CAR-T cell-related side effects, thus indicating that using low-affinity CAR-T cells could improve the safety of CAR-T cell therapy.

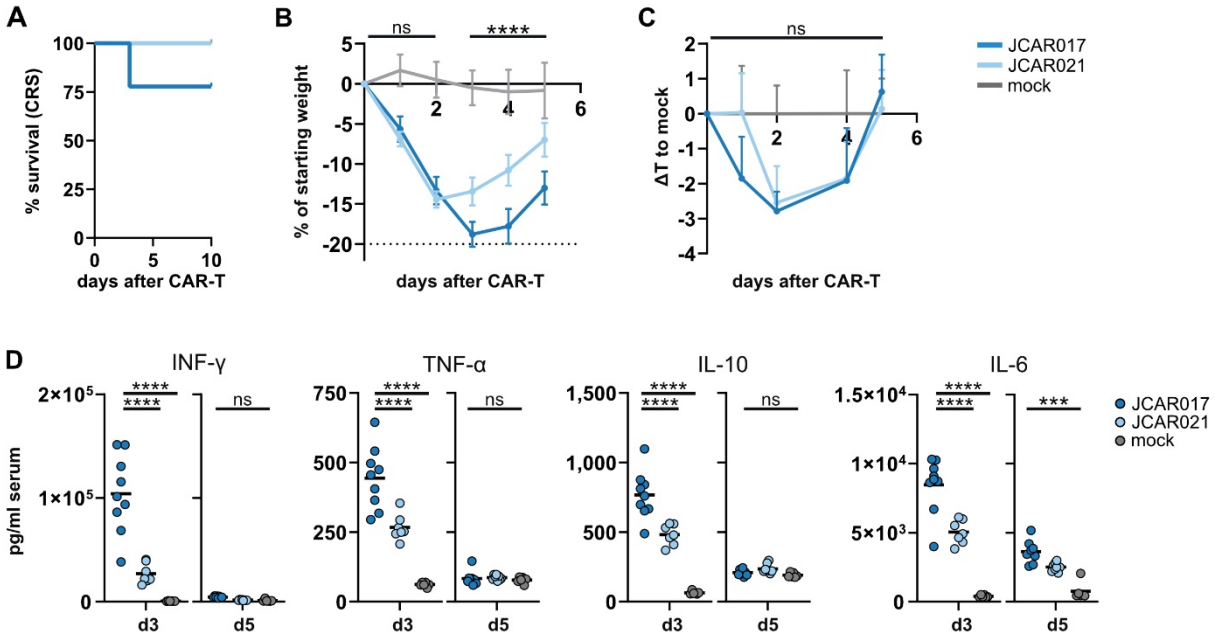

Fig. 31 CRS clinical symptoms after CAR-T cell transfer in a humanized mouse model
(A) Survival curve correlated to the development of CRS in mice during the first ten days after CAR-T cell transfer. **(B)** Kinetics of the weight development during the first five days after the administration of CAR-T cells. Weight loss was normalized to the starting weight before CAR-T cell injection. Data are presented as mean+SD (n = 6-8). Statistical testing by two-way ANOVA, ns $p > 0.05$, ****$p \leq 0.0001$ using the JCAR017 group as a reference control. **(C)** Body temperature of mice treated with CAR-T cells during the first five days after transfer. Temperatures are calculated as differences according to the average body temperature of mice treated with mock CAR-T cells. Data are represented as mean+SD. Statistical testing by two-way ANOVA, ns $p > 0.05$ using the JCAR017 group as a reference control. **(D)** Concentrations of INF-y, TNF-a, IL-10, and IL-6 in the serum on day 3 and day 5 after CAR-T cell transfer. Statistical testing by one-way ANOVA, ns $p > 0.05$, ***$p \leq 0.001$, ****$p \leq 0.0001$ using the JCAR017 group as a reference control.

4.6.3 Cytotoxicity of CAR-T cells in a humanized mouse model

Besides the development of CRS, we also looked into the cytotoxic potential of CAR-T cells in this model. However, in contrast to other non-humanized *in vivo* models, the only short-term killing can be analyzed, as alloreactive effects can occur during later time points. Nevertheless, an advantage of the humanized mouse model is that, additionally to the transferred tumor cells, humanized B cells also represent a target and thus an additional readout for the killing efficacy of anti-CD19 CAR-T cells.

As expected, both JCAR017 and JCAR021 CAR-T cells efficiently eradicated the B cells circulating in the bloodstream (Fig. 32A-C), albeit a faster B cell clearance was observed for high-affinity CAR-T cells. Indeed, B cells in mice treated with JCAR017 CAR-T cells were already depleted by day seven after CAR-T cell transfer, while B cells were still detected in the circulation of mice treated with JCAR021 CAR-T cells until day 10. Furthermore, absolute

numbers of B cells were significantly reduced in the bone marrow and spleen of CAR-T cell-treated mice compared to the mock control (Fig. 32D). However, JCAR017 CAR-T cells showed a higher functionality again, as they completely eradicated all B cells, while residual target cells were still detected in lymphoid organs of mice belonging to the JCAR021 group. It should be taken into consideration that mice of the two CAR-T cell treated groups had different endpoints; consequently, JCAR017 CAR-T cells had a longer time of activity.

Similar to the non-humanized xenograft model, extended survival of tumor-bearing mice was observed in the low-affinity JCAR021 group compared to the control group (Fig. 32E). Nevertheless, although JCAR021 CAR-T cells delayed the tumor growth shortly after their injection, they failed to inhibit tumor progression (Fig. 32F-H). On the contrary, all mice treated with JCAR017 CAR-T cells survived until the endpoint, and Raji tumor cells were completely eradicated.

Overall, this humanized CRS mouse model could confirm the findings of the suboptimal xenograft model. JCAR017 and JCAR021 CAR-T cells had an improved cytotoxic potential compared to mock T cells, but only high-affinity CAR-T cells showed efficient tumor killing. Consequently, we could demonstrate that the enormously improved safety of low-affinity CAR-T cells comes at the price of reduced functionality.

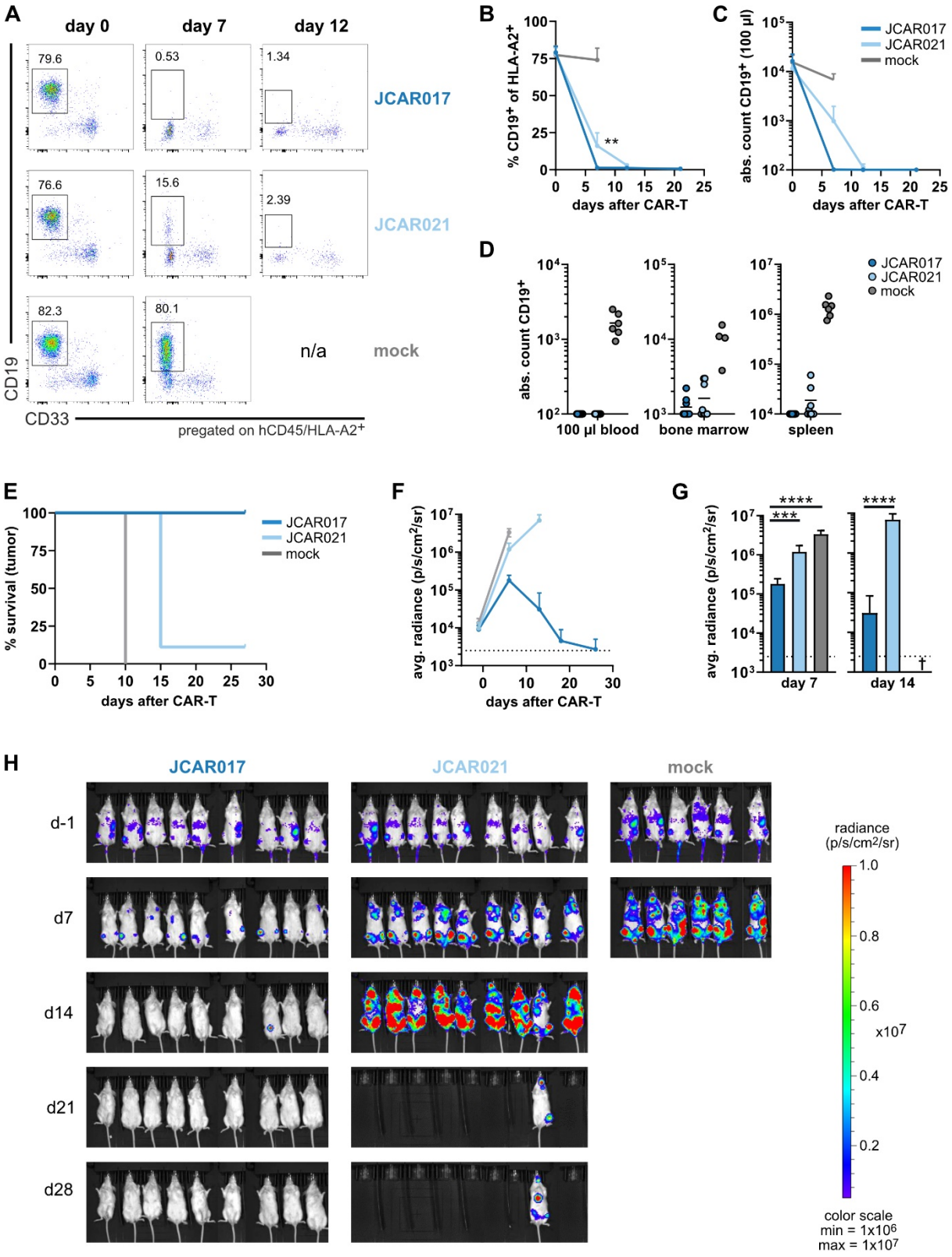

Fig. 32 Cytotoxicity of low and high-affinity CAR-T cells in a humanized mouse model
(A) Representative flow cytometry plots illustrating the killing of CD19⁺ B cells on the day of injection, seven days, and twelve days after the T cell transfer. **(B+C)** Kinetics of CD19⁺ B cells in the blood is depicted as **(B)** frequencies and **(C)** absolute counts (n = 6-9). Data represents the mean+SD. Statistical analysis by two-way ANOVA, **p ≤ 0.01 using the JCAR017 group as a reference control. **(D)** Remaining CD19⁺ B cells at the endpoint of the mice in blood, bone marrow, and spleen (n = 6-9). Data expressed as mean. **(E)** Survival curves of humanized mice treated with CAR-T cells expressing CARs with different affinities. Mice were monitored for 28 days. **(F)** The tumor burden of Raji-ffluc tumor cells was quantified and measured as the maximum photon per second per cm^2 per steradian of the whole body

of the mouse. Lines represent mean+SD of average bioluminescence signals (n = 6-9). **(G)** Average radiance of different CAR-T cell groups on day 7 and day 14 post CAR-T cell infusion. Statistical testing by one-way ANOVA (day 7) using the JCAR017 group as a reference control and Unpaired t-test (day 14), ***p ≤ 0.001, ****p ≤ 0.0001. **(H)** Representative bioluminescence images of humanized Raji-bearing mice treated with different CAR-T cell products followed weekly over one month.

4.6.4 CAR-T cell expansion and CAR downregulation in a humanized mouse model

The humanized mouse model mimics the clinical setting of systemic distribution of anti-CD19 CAR-T cell targets better than the xenograft model, as humanized mice also contain circulating human B cells, which represent an additional target for the transferred CAR-T cells. Therefore, we wanted to study how different CAR-T cells are influenced by the location of their target cells. Significantly more EGFRt$^+$ CAR-T cells were detected in the high-affinity group on day seven, which are responsible for the high amounts of released cytokines. Overall, JCAR017 CAR-T cells showed a fast expansion and contraction after a rapid elimination of B cells in the blood. On the contrary, JCAR021 CAR-T cells showed less expansion, presumably explaining why B cells were not fully eradicated within seven days. Also, no contraction was observed on day 12 after CAR-T cell transfer, as absolute numbers of low-affinity CAR-T cells stayed high in the blood.

Interestingly, also in this CRS mouse model, JCAR021 CAR-T cells strongly downregulated their receptor, as around 70 - 80 % of the EGFRt$^+$ cells showed no CAR surface expression on day seven and day 12 anymore (Fig. 33B-C), and overall CAR expression levels were significantly reduced (Fig. 33D). As this phenomenon was not observed for JCAR017 CAR-T cells, the difference between CAR-expressing T cells was even increased (Fig. 33E).

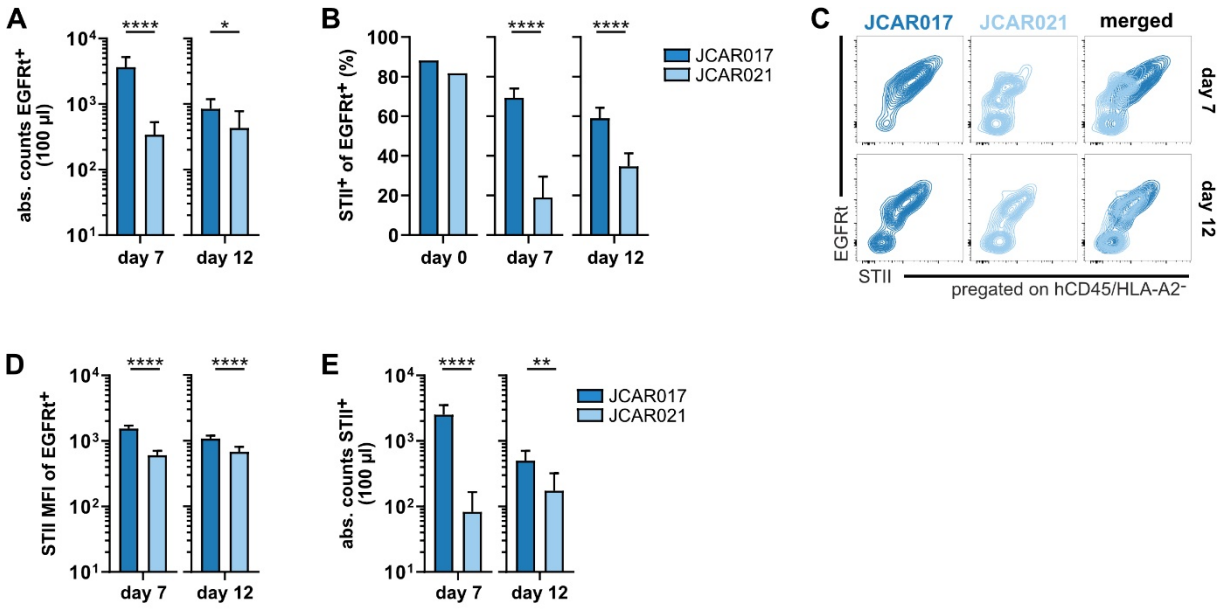

Fig. 33 CAR-T cell expansion and receptor expression levels in a CRS mouse model
(A) Weekly blood analysis of individual mice receiving CAR-T cells. Absolute numbers of EGFRt$^+$ CAR-T cells in 100 µl blood on day7 and 12 after CAR-T cell transfer. Data are represented as mean+SD. **(B)** Frequencies of CAR-expressing (STII$^+$) cells among the EGFRt$^+$ CAR-T cells of the injection product and in the blood on day seven and day twelve after CAR-T cell transfer. **(C)** Representative flow cytometry plots of transferred hCD45$^+$HLA-A2$^-$ CAR-T cells in the blood on days seven and twelve after the T cell transfer. Co-expression of the receptors was analyzed for EGFRt and STII co-staining. **(D)** STII mean fluorescent intensities (MFI) of EGFRt$^+$ CAR transduced T cells. **(E)** Absolute numbers of STII$^+$ CAR-T cells in 100 µl blood on days 7 and 12 after CAR-T cell transfer. Overall data are represented as mean+SD (n = 9). Statistical testing by Unpaired t-test, ns $p > 0.05$, *$p \leq 0.05$, **$p \leq 0.01$, ****$p \leq 0.0001$.

CAR-T cells expressing JCAR021 downregulated their receptor also in the bone marrow and spleen (Fig. 34A-B). While already significantly higher numbers of transferred EGFRt$^+$ CAR-T cells expressing JCAR017 were detected (Fig. 34C), the number of CAR$^+$ high-affinity CAR-T cells was nearly ten times higher than low-affinity CAR-T cells (Fig. 34D).

As discussed before, higher numbers of remaining B cells and tumor cells in the blood and secondary lymphoid organs of mice treated with low-affinity CAR-T cells could lead to a more extended activation of the low-affinity CAR-T cells and thus downregulation of the receptor on the examined days. However, the observed internalization of the CAR of weak binders could also represent an improved ability of low-affinity CAR-T cells to perform serial triggering similar to TCRs. Whether this effect has positive long-term effects for adoptively transferred CAR-T cells could not be determined in our model and thus needs further in-depth characterization.

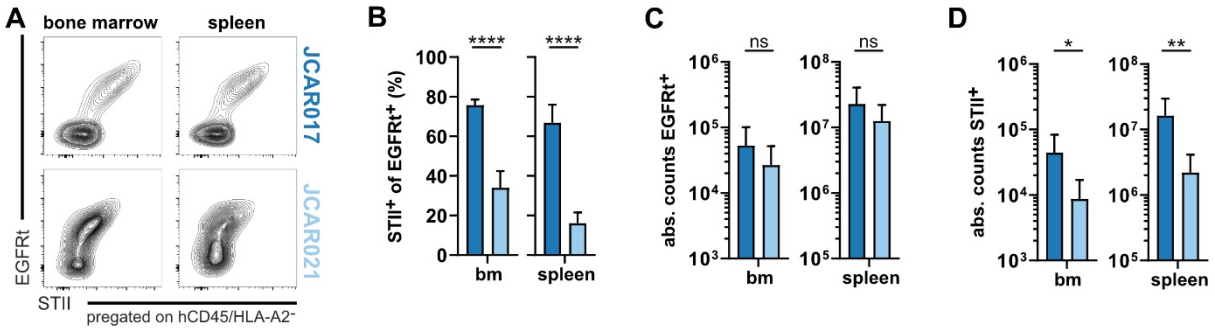

Fig. 34 CAR-T cell migration into organs and receptor downregulation in a CRS mouse model
(A) Representative flow cytometry plots of transferred hCD45$^+$HLA-A2$^-$ CAR-T cells in the bone marrow and spleen of CAR-T cell treated mice at the endpoint. Co-expression of the receptors was analyzed for EGFRt and STII co-staining (n = 9). **(B)** Frequencies of CAR-expressing (STII$^+$) cells among the EGFRt$^+$ CAR-T cells in the bone marrow (bm) and spleen on the endpoints of the mice. Data are represented as mean+SD. **(C)** Absolute numbers of EGFRt$^+$ CAR-T cells in the bone marrow (bm) and spleen on the endpoints of the mice. Data are represented as mean+SD. **(D)** Absolute counts of STII$^+$ CAR-T cells in the bone marrow (bm) and spleen on the endpoints of the mice. Data are represented as mean+SD. Statistical testing by Unpaired t-test, ns $p > 0.05$, *$p \leq 0.05$, **$p \leq 0.01$, ****$p \leq 0.0001$.

In summary, we could clearly show that the reduction of CAR affinity successfully decreases treatment-related side effects and thereby improves the safety of CAR-T cell therapy. However, milder toxicities due to the use of low-affinity CAR-T cells also come at the price of diminished CAR-T cell functionality, especially in settings with a high tumor burden. Therefore, it is essential to find optimal solutions to maintain high killing efficiencies of high-affinity CAR-T cells together with improved safety of the low-affinity counterpart.

4.7 Cell dose-dependent development of CAR-T cell-related side effects

Adoptively transferred high-affinity CAR-T cells enormously expanded directly after engagement with their target cells. During this process, they released vast amounts of cytokines which in return reinforced the development of CRS. Due to the outstanding efficiency of strong binders, we wanted to test whether low doses of high-affinity CAR-T cells would still be efficient in clearing tumor cells but would also extenuate treatment-related toxicities.

4.7.1 *In vivo* setup to test cell dose-dependency of CAR-T cell-related toxicities

Four-week-old female NSGS mice were sublethally irradiated with 1.5 Gy and humanized with $0.02x10^6$ purified $CD34^+$ hHSCs (Fig. 35A). The injected HLA-$A2^+$ stem cell product had a purity of 84.8 % (Fig. 35B) and resulted in humanization levels of around 60 % eight weeks after the injection. Mice developed high levels of B cells but also efficient numbers of macrophages and monocytes (Fig. 35C-D). Mice with humanization levels over 50 % were inoculated i.v. with $0.5x10^6$ $CD19^+$ Raji-ffluc tumor cells, and one week later, i.v. injected with either $8x10^6$ (high dose) or $4x10^6$ (low dose) CAR-T cells (n = 4-5). Again, the CAR constructs JCAR017 and JCAR021 were used to compare different doses of low and high-affinity CAR-T cells. Additionally, one group received a high dose of $16x10^6$ untransduced mock T cells as a control. Freshly isolated and activated PBMCs of a healthy HLA-$A2^-$ donor were retrovirally transduced with one of the two CAR constructs, and cells were *ex vivo* expanded for three weeks. The transduction efficacies and receptor expression of the two CAR-T cell products were similar, with frequencies of 49 % of EGFRt and STII double-positive cells (Fig. 35E) and similar MFIs of EGFRt and STII (Fig. 35F-G). Both engineered T cell products revealed similar low PD-1 expression levels (Fig. 35H) and only 8 % of $CD8^+$ T cells (Fig. 35I). Mice were followed for ten days post CAR-T cell transfer to analyze the development of CRS, CAR-T cell expansion in the blood, and tumor growth by bioluminescence measurement.

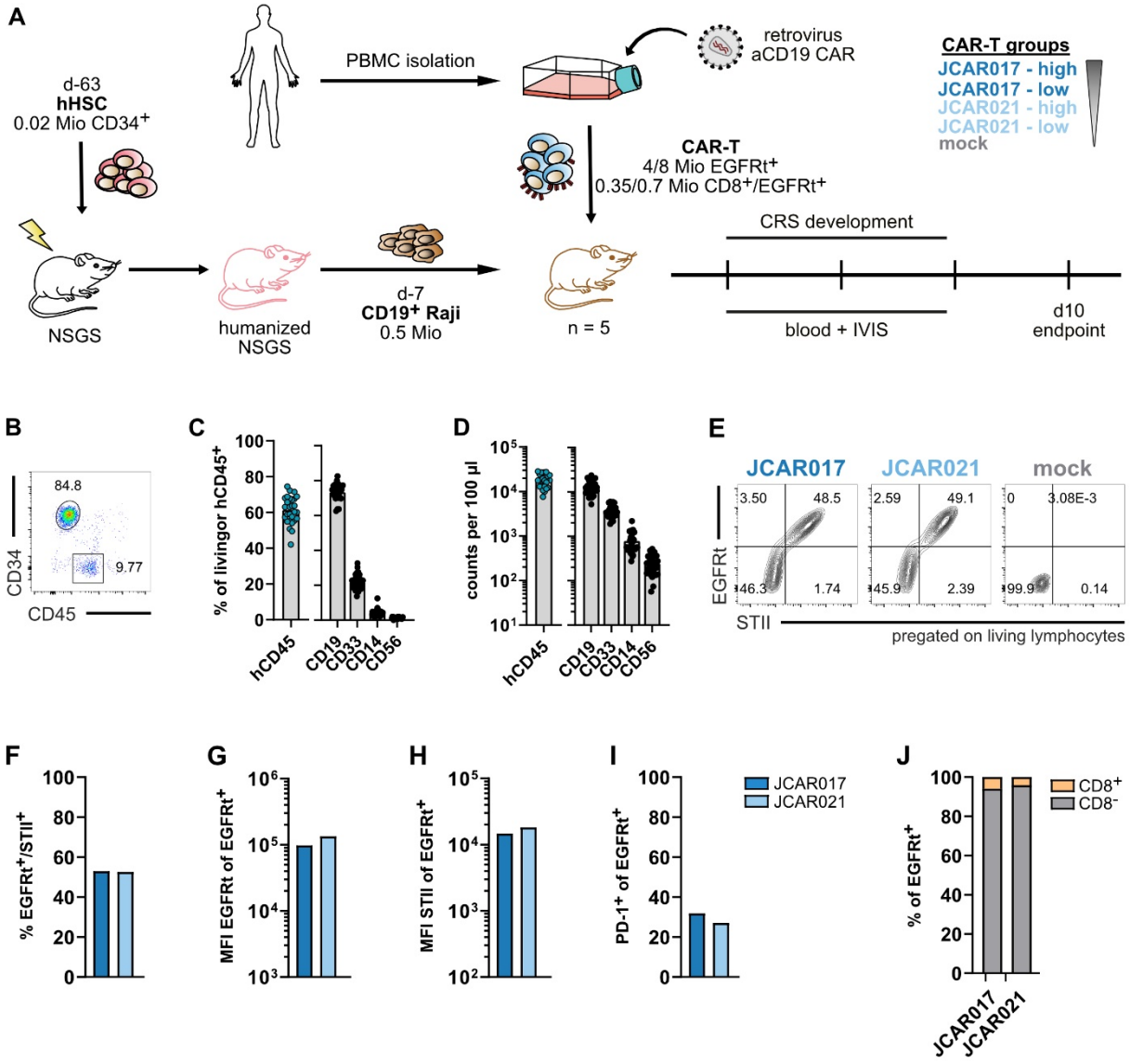

Fig. 35 Setup of a humanized CRS mouse model to study CAR-T cell dose-dependent side effects
(A) Schematic overview of the experimental setup of the humanized CRS mouse model to test different doses of high and low-affinity CAR-T cells to develop CRS. **(B)** Flow cytometry plot of purified hHSCs stained for $CD34^+$ and $CD45^+$ to determine the purity of the injection product. **(C)** Frequencies and absolute cell numbers **(D)** of humanized cells in 100 µl of blood. **(E)** Flow cytometry plots of the CAR-T cell infusion products. Transduction efficacy and CAR surface expression were determined by co-staining of EGFRt and Strep-tag (STII). **(F)** Transduction efficacies of the two CAR-T cell products are represented by frequencies of EGFRt/STII double-positive cells. **(G)** EGFRt and **(H)** STII mean fluorescent intensities (MFI) of $EGFRt^+$ CAR transduced T cells. **(I)** Frequencies of PD-1 expressing cells of the transduced injection product. **(J)** Distribution of $CD8^+$ and $CD8^-$ cells within the $EGFRt^+$ CAR-T cell product.

4.7.2 CAR-T cell dose-dependent development of CRS

Similar to the first humanized mouse experiment, all CAR-T cell-treated mice developed clinical signs of CRS. However, mice treated with high doses of JCAR017 CAR-T cells showed more severe symptoms than all other mice. While the high dose JCAR017 group lost nearly 20 % of their starting weight within three days, mice treated with high and low doses of

JCAR021 CAR-T cells lost significantly less weight and started to recover already three days post CAR-T cell transfer (Fig. 36A). As expected, the substantial weight loss of the JCAR017 high dose group was compensated by the transfer of lower doses of CAR-T cells expressing JCAR017, which resulted in comparable weight kinetics to the two JCAR021 groups. Similar results were obtained for the cytokine production after CAR-T cell transfer (Fig. 36B). Here, the highest amounts of INF-γ, IL-10, and IL-6 were produced after the injection of high doses of JCAR017 CAR-T cells, while the cytokine levels on day three and day five after CAR-T cell transfer were significantly reduced in the other groups. Again, the transfer of lower numbers of JCAR017 CAR-T cells drastically reduced the release of all three cytokines, with levels nearly comparable with the JCAR021 high dose group. Interestingly, while significantly lower levels of INF-γ and IL-10 were produced in the low dose JCAR021 group, no differences in the weight kinetics after the transfer of high and low doses of JCAR021 CAR-T cells were observed. Consequently, in addition to using CARs with lower affinity, the transfer of lower numbers of high-affinity CAR-T cells could diminish the development of CAR-T cell-related toxicities.

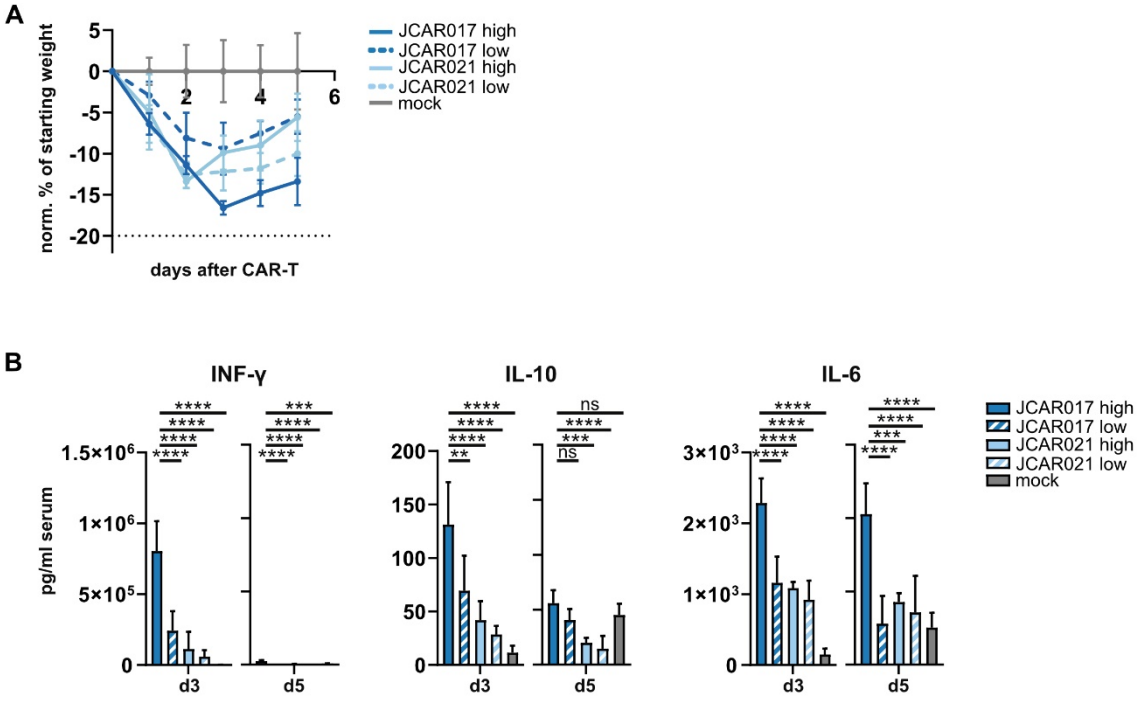

Fig. 36 Clinical symptoms of CRS after transfer of different doses of CAR-T cells
(A) Kinetics of the weight development during the first five days after the administration of CAR-T cells. Weight loss was normalized to the starting weight before CAR-T cell injection. Data are presented as mean+SD (n = 4-5). **(B)** Concentrations of INF-γ, IL-10, and IL-6 in the serum on day 3 and day 5 after CAR-T cell transfer. Statistical testing by one-way ANOVA, ns $p > 0.05$, $^{**}p \leq 0.01$, $^{***}p \leq 0.001$, $^{****}p \leq 0.0001$ using the JCAR017 high dose group as a reference control.

4.7.3 Cytotoxic potential of low doses of CAR-T cells

In addition to the development of CRS, we also monitored the influence of lower doses of transferred CAR-T cells on the cytotoxic potential. Human $CD19^+$ B cells in the blood, bone marrow, and spleens of mice treated with CAR-T cells were completely eradicated (Fig. 37A-B). While circulating B cells were not detected five days after the transfer of low and high doses of JCAR017 CAR-T cells, both JCAR021 groups needed seven days to sufficiently deplete their target. Additionally, a dose-dependent killing kinetic of circulating B cells was observed with JCAR021 expressing CAR-T cells; this effect was not detected among the JCAR017 groups. In contrast to mice that were only treated with mock T cells and thus had to be sacrificed on day eight after the transfer due to their high tumor burden, all other mice survived until the endpoint (Fig. 37C). High doses of JCAR017 CAR-T cells immediately eradicated all tumor cells, and no bioluminescent signal was measured ten days post CAR-T cell transfer. A similar efficient killing was observed in mice treated with lower doses of JCAR017 CAR-T cells despite an initial tumor growth. In contrast, JCAR021 CAR-T cells reacted slower and started to counteract tumor growth only from day seven partially.

Overall, high doses were more efficient in tumor killing than lower doses and high-affinity JCAR017 CAR-T showed faster killing kinetics than JCAR021 CAR-T cells. In summary, either JCAR017 or JCAR021 expressing CAR-T cells could clearly control the tumor growth; however, the transfer of high doses was still superior to low doses.

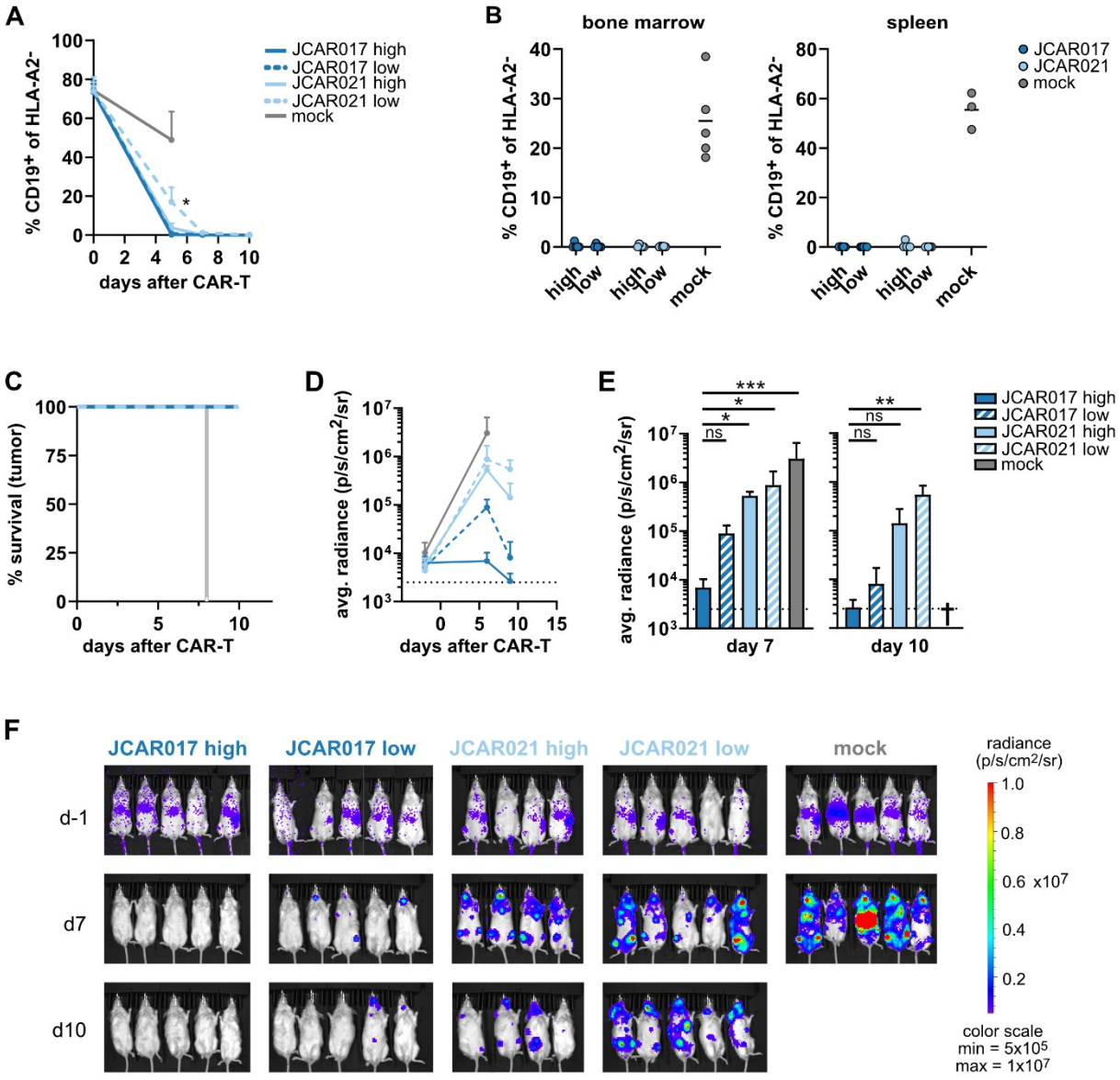

Fig. 37 Remaining cytotoxic potential of low doses of CAR-T cells in a humanized mouse model **(A)** Kinetics of HLA-A2$^-$ CD19$^+$ B cells in the blood depicted as frequencies (n = 4-5). Data represents the mean+SD. Statistical testing by mixed-effect analysis, *p ≤ 0.05. **(B)** Remaining CD19$^+$ B cells at the endpoint of the mice in bone marrow and spleen (n = 4-5). Data expressed as mean. **(C)** Survival curves of humanized mice treated with CAR-T cells expressing CARs with different affinities. Mice were monitored for ten days. **(D)** The tumor burden of Raji-ffluc tumor cells was quantified and measured as the maximum photon per second per cm^2 per steradian of the whole body of the mouse. Lines represent the mean+SD of average bioluminescence signals (n = 4-5). **(E)** Average radiance of different CAR-T cell groups on days 7 and 10 post CAR-T cell infusion. Statistical testing by Kruskal-Wallis test, ns p > 0.05, *p ≤ 0.05, **p ≤ 0.01, ***p ≤ 0.001. **(H)** Representative bioluminescence images of humanized Raji-bearing mice treated with different CAR-T cell products one day before, on day seven, and on day 10 after CAR-T cell transfer.

4.7.4 CAR-T cell expansion and receptor downregulation

Higher numbers of circulating EGFRt$^+$ CAR-T cells in the high dose groups compared to the low dose groups represented the main reason for an increased killing capability, but also for the development of unwanted, more severe side effects (Fig. 38A). In line, also the faster killing

efficacy and higher release of cytokines of high-affinity CAR-T cells can be explained by an initial increased number of EGFRt$^+$ cells in the blood. Especially during the first five to seven days, significantly higher numbers of EGFRt$^+$ CAR-T cells were detected in the JCAR017 high dose group compared to the other groups. Although a substantial expansion of the JCAR021 CAR-T cells was observed between day seven and day ten, the initial expansion rate of low doses of JCAR017 CAR-T cells was even stronger. However, on day ten, low-affinity CAR-T cell numbers enormously increased and reached similar levels as CAR-T cells of the low-dose JCAR017 group. Consequently, low-affinity CAR-T cells can strongly expand after antigen encounter but need longer to reach similar overall numbers, which would explain the delayed anti-tumor efficacy. Besides, downregulation of the CAR was only observed in the two low-affinity CAR groups (Fig. 38 B) mainly on days five and seven after T cell transfer, potentially due to the delayed response and higher remaining target B cells in the blood on these two days. Consequently, the overall difference in total numbers of CAR-expressing T cells between the JCAR017 and JCAR021 groups was even pronounced on these two days (Fig. 38C).

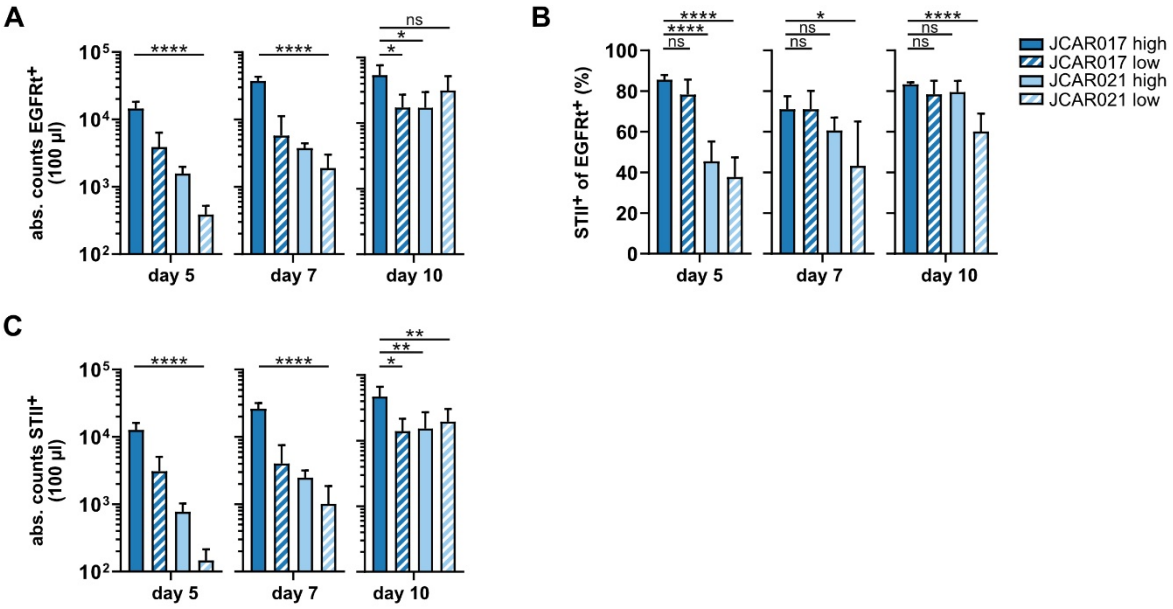

Fig. 38 CAR-T cell expansion and receptor downregulation of low CAR-T cell doses
(A) Blood analysis of individual mice receiving CAR-T cells on days five, seven, and ten after T cell transfer. Absolute numbers of EGFRt$^+$ CAR-T cells in 100 µl of blood. Data are presented as mean+SD. **(B)** Frequencies of CAR-expressing (STII$^+$) cells among the EGFRt$^+$ CAR-T cells. Data are presented as mean+SD. **(C)** Absolute numbers of STII$^+$ CAR-T cells in 100 µl of blood. Data are represented as mean+SD (n = 4-5). Statistical analysis by one-way ANOVA, ns $p > 0.05$, *$p \leq 0.05$, **$p \leq 0.01$, ****$p \leq 0.0001$ using the JCAR017 high dose group as a reference control.

This experiment could show that besides the affinity of the CAR, also the initial CAR-T cell dose plays an essential role in the development of CAR-T cell-related side effects. While low-affinity CAR-T cells have a high safety profile, also the transfer of low doses of high-affinity CAR-T cells can enormously improve the safety profile. However, as both concepts also have a reduced cytotoxic potential, it can be challenging to transfer these approaches into the clinical setting. Especially for high tumor burden settings, it would be not trivial to find the correct dose of high or low-affinity CAR-T cells that provides a good balance between safety and efficacy. It is still unclear whether low-affinity CAR-T cells could fully control high tumor burdens, while high-affinity CAR-T cells bear the risk of developing severe side effects. As decisive tumor clearance and low toxicities represent the most critical parameters for successful CAR-T cell therapy, new options that are easy to realize in the clinical setting are necessary to optimize CAR-T cell products.

4.8 Mixing of CAR affinities to generate the optimal CAR-T cell product

The insufficient killing efficacy of otherwise safe low-affinity CAR-T cell products could be improved by mixing them with low amounts of high-affinity CAR-T cells before the adoptive transfer into the patient. Thereby, the overall toxicity of the CAR-T cell product should stay low, as the separate transfer of either high doses of low-affinity CAR-T cells or low doses of high-affinity CAR-T cells resulted in the development of mild side effects in comparison to high doses of high-affinity CAR-T cells only. Additionally, the low number of high-affinity CAR-T cells would support the low-affinity CAR-T cells in depleting the tumor cells directly after the transfer until low-affinity CAR-T cells have expanded to sufficient levels.

In order to test whether the combination of low and high-affinity CAR-T cells would represent a solution to optimal balance efficacy and safety of CAR-T cell products, we tested different mixtures of CAR-T cells expressing either JCAR017 or JCAR021 in an immunocompromised xenograft mouse model (Fig. 39A). NSGS mice were intravenously inoculated with $0.5x10^6$ $CD19^+$ Raji tumor cells, followed by the intravenous injection of different CAR-T cell mixtures one week later. CAR-T cells were generated by retroviral transduction of freshly isolated PBMCs with the two CAR constructs and *ex vivo* expanded for three weeks. Directly before the injection, different ratios of JCAR017 and JCAR021 CAR-T cells were mixed. However, the number of the transferred bulk population was calculated to transfer $1.6x10^6$ $EGFRt^+CD8^+$ CAR-T cells per mouse. Bulk populations consisting of either $1.6x10^6$ $EGFRt^+CD8^+$ JCAR021 or $0.8x10^6$ $EGFRt^+CD8^+$ JCAR017 CAR-T cells were used as references for the suboptimal tumor model. The survival of the mice was tracked for four weeks after the CAR-T cell transfer. In order to distinguish the two types of transferred CAR-T cells in one mouse, the JCAR017 construct for retroviral transduction was extended with an additional sequence, which codes for the fluorescent protein Ametrine. The transgene was separated upstream of the EGFRt by an in-frame T2A ribosomal skipping sequence to enable the co-expression of the fluorescent protein together with the CAR and EGFRt. Transduction efficacies of JCAR017 and JCAR021 CAR-T cells were 71.5 % and 54.5 %, respectively (Fig. 39B+C).

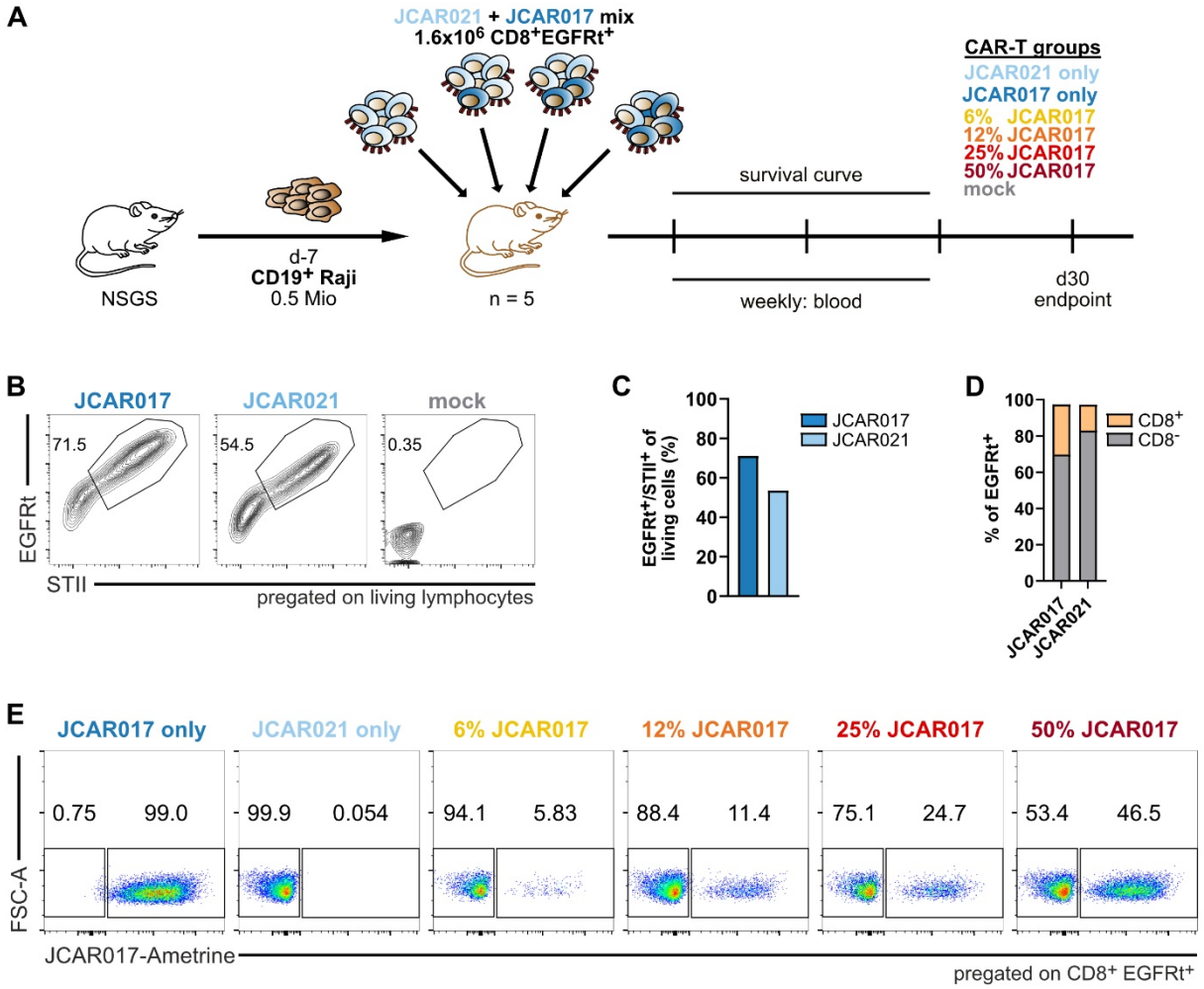

Fig. 39 Experimental setup and CAR-T cell infusion product of the CAR-T cell mixing approach
(A) Schematic overview of the experimental setup of the *in vivo* functional testing of mixed affinity CAR-T cell products in a sub-optimal Raji xenograft tumor model. CAR-T cells with low and high affinities were generated by retroviral transduction of human PBMCs. $0.5x10^6$ $CD19^+$ Raji tumor cells were i.v. injected into immunocompromised NSGS mice (n = 4-5 mice). After one week, a bulk population of $1.6x10^6$ $CD8^+EGFRt^+$ CAR-T cells was adoptively transferred into tumor-bearing mice. Before the transfer, different frequencies of high-affinity JCAR017 and low-affinity JCAR021 CAR-T cells were mixed. Survival of mice was followed for 30 days, and CAR-T cell expansion and persistence were analyzed during weekly blood stainings and in spleen and bone marrow at the endpoint of the experiment. **(B)** Representative flow cytometry plots of low and high-affinity CAR-T cell infusion products before the mixing. Transduction efficacy and CAR surface expression were determined by co-staining of EGFRt and Strep-tag (STII). **(C)** Transduction efficacies of the two original CAR-T cell products are represented by frequencies of EGFRt/STII double-positive cells before the mixing. **(D)** Distribution of $CD8^+$ and $CD8^-$ cells within the unmixed $EGFRt^+$ CAR-T cell products. **(E)** Flow cytometry plots of the different injected CAR-T cell mixtures. Frequencies of JCAR017-Ametrine are calculated from the $CD8^+EGFRt^+$ population.

Similar to the previous *in vivo* experiments, CAR-T cells expressing JCAR021 improved the survival of tumor-bearing mice significantly compared to the transfer of mock T cells (Fig. 40). However, as expected, due to the chosen suboptimal xenograft tumor model, some mice had to be sacrificed before the endpoint due to their high tumor burden. Remarkably, the addition of small numbers of JCAR017 CAR-T cells improved the survival of the treated mice. The

spike-in of 6% of JCAR017 CAR-T cells already sufficed to save nearly all mice, and none of the mice in groups with higher JCAR017 frequencies had to be sacrificed. Here, it is essential to notice that the numbers of transferred JCAR017 CAR-T cells alone would not have been able to eradicate the tumor cells. Unfortunately, due to technical problems with the imaging system, no meaningful *in vivo* imaging data of the tumor development could be produced during the experiment. Therefore, the kinetics of tumor clearance and the efficacy of the CAR-T cell products could not be assessed. Nevertheless, the experiment demonstrates the significant advantage of adding small numbers of high-affinity CAR-T cells into the low-affinity CAR-T cell product to improve its killing capability.

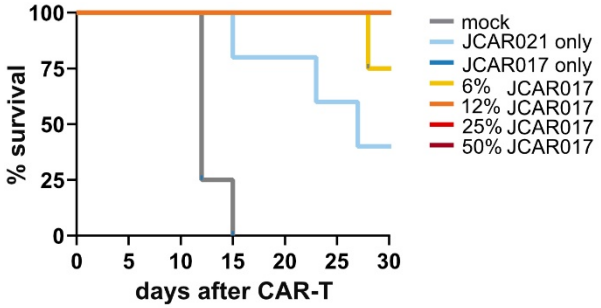

Fig. 40 Survival of tumor-bearing mice treated with mixed affinity CAR-T cell products
Survival curves of mice treated with combined CAR-T cells expressing JCAR017 or JCAR021 in different frequencies. Mice were followed for 30 days.

Overall, this mixing experiment provides proof of principle that combined CAR-T cell products with different affinities and a defined ratio might provide an optimal balance of high efficacy and probably also low toxicity for CAR-T cell therapy. Comparable to the natural immune response, not one specific receptor type can maximally optimize the complex immune response. However, the interaction of CAR-T cells with different receptor affinities is probably key to improving CAR-T cell therapy to be implementable in diverse clinical situations with high functionality and high safety.

4.9 CRISPR/Cas9 engineering of CAR-T cells

Another possibility to improve CAR-T cell functionality is the direct genetic knockout (KO) of checkpoint inhibitors like PD-1 in the T cell product. While a systemic blockade of PD-1 has become a central mechanism for immunotherapies, selective ablation of PD-1 expression on the CAR-T cell product by CRISPR/Cas9 represents an elegant way to circumvent severe toxicities due to loss of peripheral tolerance. Especially the long-term effects of PD-1 disruption on CAR-T cell functionality have not intensively been investigated but are essential for clinical usage.

In order to test the effect of PD-1 KO during constant antigen-specific triggering, we assessed the T cell functionality in a model of CAR-T cell transfer targeting mouse $CD19^+$ B cells[199]. This model represents the clinical situation in which CAR-T cells are constantly stimulated by newly generated $CD19^+$ B cells. Therefore, long-lasting B cell aplasia is a good marker for the recruitment of highly functional CAR-T cells.

PD-1 KO CAR-T cells were generated by combining the Cas9 ribonucleoprotein (RNP) gene editing protocol with viral transduction of the chimeric antigen receptor. Therefore, primary murine *in vitro* stimulated T cells were nucleofected with RNPs targeting *Pdcd1* followed by retroviral transduction of the anti-CD19 CAR. Two days after the engineering of the CAR-T cell products, 70 % of the cell population showed efficient *Pdcd1* gene disruption (Fig. 41A). Additionally, 70 % of the cells were successfully transduced with the CAR, which could be determined by co-expression of EGFRt (Fig. 41B).

The long-term functionality of PD-1-depleted CAR-T cells was tracked for over 390 days, which represented the longest *in vivo* follow-up of CAR-T cells that has been described to date. Two mouse groups were injected with CAR-T cells containing either PD-1 non-edited or ablated CAR-T cells, while two other groups received mock T cells or PD-1-depleted T cells without a CAR.

Independent of their PD-1 expression, CAR-T cells showed effective B cell killing throughout the observation period. In contrast, no significant effect on B cells was observed in the two control groups. However, two mice of the CAR group had a transient B cell recovery, which

was resolved over time. In the CAR group with the PD-1 KO, one mouse had a slight B cell reappearance at the last analyzed time point (Fig. 41C+D).

Overall, this experiment could show that the genetic depletion of the immune checkpoint inhibitor PD-1 does not significantly impair effective B cell aplasia until day 390 after CAR-T cell transfer.

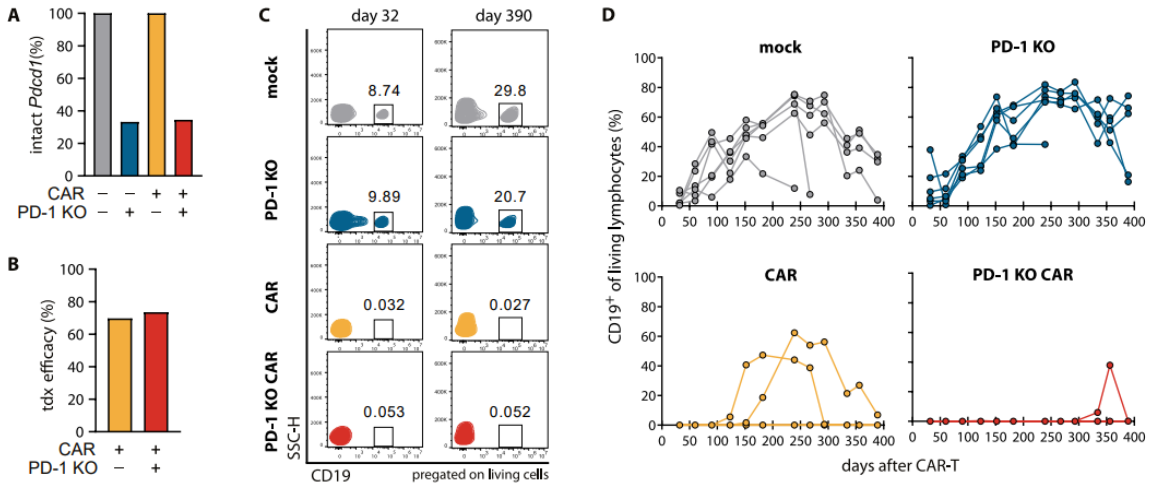

Fig. 41 Long-term functionality of PD-1 KO CAR-T cells over 390 d[199]
(A) Splenocytes were edited for PD-1 KO and anti-CD19 CAR expression and transferred into C57BL/6 mice (n=6). NGS analysis of *Pdcd1* disruption of all four infusion products [mock (gray), PD-1 KO (blue), CAR (yellow), PD-1 KO CAR (red)]. **(B)** Transduction efficacies measured by flow cytometry as a percentage of co-expressed EGFRt$^+$ of living lymphocytes **(C)** Representative flow cytometry plots of B cell frequencies in the peripheral blood after CAR-T cell injection. **(D)** Monthly blood analysis of B cells, depicted as CD19$^+$ cells of living lymphocytes. Figure adapted from Dötsch et al., PNAS, 2023.

5 Discussion

Immunotherapy with genetically engineered anti-CD19 CAR-T cells has revolutionized the treatment of patients with hematological B cell malignancies. Due to its clinical success for the treatment of otherwise therapy-refractory patients, CD19-targeting CAR-T cell therapy reached a major milestone in 2017 for being the first genetically engineered cell product to receive FDA approval, followed by EMA approval just one year later. Until today four anti-CD19 and two BCMA-targeting CAR-T cell products have been approved and marketed for the treatment of patients with certain relapsed or refractory high-grade hematological diseases, clearly demonstrating the high potential of this new form of therapy. However, despite impressive overall response and initial remission rates, CAR-T cell therapies are still in their infancy and need further improvement. The effectiveness of CAR-T cell transfer is diminished over time by a high number of relapses due to antigen loss of the tumor cells or by the intrinsic failure of long-term persistence of CAR-T cells[200]. Consequently, the initial response rate of 80-90 % drops to a five-year survival rate of only 40 %[74]. In addition, also the costs of CAR-T cell manufacturing are still enormously high and limit large-scale applicability. Therefore, so far, CAR-T cell therapy has only been approved as a second-line treatment for patients who are not responding to conventional cancer therapy. Furthermore, patients receiving CAR-T cells still face a high prevalence of severe and often even life-threatening toxicities. In up to one-third of the patients, the transfer of CAR-T cells still leads to CRS and ICANS[90], which are associated with the induction of a potent immune effector response independent of the CAR-T cell target. Although different treatment options like the administration of immunoglobulins and anti-IL-6 antibodies, as well as safety strategies to remove the transferred T cells in case of severe adverse events, have been proposed[98], they only mitigate the consequences but do not resolve the reasons for the development of side effects, and also bear the risk to prematurely terminate the therapy. Therefore, there is a major need to improve CAR-T cell therapy further. A potentially important parameter might be the ‘CAR affinity’ for its cognate target, for which perhaps an optimal balance between long-term functionality and safety can be identified. In order to optimize artificial CAR-T cells, it is worth having a closer look at natural

T cell responses, as they have evolved to effectively protect against viruses and other pathogens without inducing substantial toxicities. A major difference between currently clinically used CAR-T cells and natural T cell responses is the affinity of the antigen-targeting receptor, which is much lower for TCRs than for artificial CARs. Thus, we asked with this thesis work whether an optimal affinity window of CARs exists and whether the reduction of CAR affinity could improve the balance between sufficient functionality and higher safety of the corresponding CAR-T cell product. Furthermore, T cell immunity evolved to recruit polyclonal TCR repertoires with a broad range of affinities. Therefore, we hypothesized that mimicking a natural immune response by simultaneously transferring high and low-affinity CAR-T cells would be beneficial for CAR-T cell therapy and could lay the foundation for a whole new generation of therapeutic CAR-T cell products.

5.1 Evaluation of CAR affinities

A TCR determines the identity of the corresponding T cell and thus can be described as its fingerprint. The affinity of a given TCR for cognate epitope/MHC complexes represents the best measure for the functionality of the T cell, as substantial evidence indicates a correlation between TCR affinity and functionality. This correlation also holds true for synthetic CARs. Although CAR affinity directly influences the functionality of engineered T cells, the actual effect of high and low affinity, especially in the range of TCR binding strengths, on CAR-T cell functionality has not been studied in detail yet. In order to evaluate the role of CAR binding strengths, we firstly analyzed four available and clinically relevant CAR clones with described high and low affinities, except for JCAR021. Secondly, we designed a broad library with over 40 new anti-CD19 CAR constructs derived from JCAR021 and predicted to show lower affinities, aiming to further lower CAR affinities down to the TCR range. As a first step, we needed to establish a robust and time-efficient tool to precisely determine CAR antigen-binding strengths and classify known and newly generated CARs according to their affinity.

To date, SPR spectroscopy still represents the gold standard for the affinity measurement of protein-protein interactions. Therefore, we applied it to measure the binding kinetics of three

anti-CD19 CAR clones (JCAR017, JCAR021, CAT). Besides confirming existing data (JCAR017 and CAT being of high and low affinity, respectively), we found that their different binding strengths were mainly due to differences in their dissociation rates. Unlike TCRs, no co-receptors are involved in the antigen-binding of CARs, and thus the SPR read-out might be even more reliable for these artificial receptors. However, SPR represents a rather time-, cost- and labour-intensive method and thus is not suitable for screening and measuring many receptors as needed for our approach.

Accordingly, we established an alternative method to analyze the affinity of CARs based on our in-house developed flow cytometry-based TCR-ligand k_{off}-rate assay (Fig. 6). This approach has the advantage of monitoring monomeric ligand dissociation under natural conditions[164,165] and thus also considers receptor conformations on the cell surface and potential co-receptor help. Although only k_{off}-rates, but not k_{on}-rates, and thus K_D-values of the receptor antigen-binding, can be determined with this method, it still represents a good prediction of the overall binding strength of CARs. On one side, it has been shown that the T cell functionality mainly correlates with the dissociation constant of the TCR:pMHC binding. On the other side, we identified the off-rates of the three tested CAR clones as the responsible characteristic for the observed differences in their binding strength. Therefore, we decided to use the off-rates of the CARs as the parameter for screening our large library.

After several technical optimization steps, we adapted the flow-cytometry-based k_{off}-rate assay to use it as a reproducible and efficient tool to determine the binding kinetics of CARs. Interestingly, using either recombinantly expressed scFvs, or soluble monomeric CD19-ecd did not influence the analyzed half-lives of CAR:CD19 interactions, as we obtained comparable absolute measurements (Fig. 10E). These results nicely validate our assay and indicate that CARs are indeed not dependent on any co-receptor help like it is typical for TCRs; thus, shuttling between receptor and ligand as surface-expressed of soluble protein did not influence the outcome of the k_{off}-rate assay.

Importantly, permanently dimerized agents to determine CAR binding kinetics should be avoided. Although the produced Fc-fusion of CD19 represented an elegant way to stabilize this hard-to-produce protein, the determined CAR half-lives were enormously prolonged due to dimeric instead of monomeric interactions of CARs and the CD19 ligand. Consequently, the dissociation was not representing a one-to-one receptor binding kinetic, and the interaction half-lives were too long to be precisely determined with our method. Notably, the new version of stabilized CD19 monomers will help in the future to further increase the throughput of our assay as only a single CD19 monomer product rather than individual scFvs would need to be recombinantly expressed[195].

Comparisons of the relative k_{off}-rate values analyzed by SPR or our in-house approach validated the newly established method as a valuable tool for measuring relative CAR binding strengths (Fig. 8D). However, absolute numbers of dissociation values are difficult to compare, as they are influenced by different experimental temperatures and the quality of the recombinant protein or cell surface expression. Slight differences in relative correlations between low and high-affinity CARs were due to the long binding half-live of JCAR017, which was above the upper sensitivity limit of the k_{off}-rate assay for the analyzed time. The exact determination of k_{off}-rates for strong binders would need further optimization, e.g., longer acquisition times. Nevertheless, as the main application of the newly set-up k_{off}-rate assay was to screen low-affinity CAR kinetics, this limitation did not influence our desired resolution.

Neither the SPR measurement nor the flow-cytometry-based k_{off}-rate assay with recombinant scFv proteins fully recapitulate the binding of membrane-bound CARs and CD19 on the individual cells, as it does not take into account the physiological antigen density, cell adhesion molecules, and conformational changes during the binding. The recently marketed z-Movi® Cell Avidity Analyzer by LUMICKS represents a newly developed method to measure CAR-T cell avidities between two living cells, which might be a technology providing additional quantitative information on binding strength that helps to predict CAR-T cell function.

5.2 Generation of an anti-CD19 CAR affinity library

Different CD19-specific CAR scFvs have been tested in several clinical trials. While most of them were based on CARs possessing very high affinities towards their target, the group of Persis Amrolia recently performed a clinical study of adoptively transferred CAR-T cells expressing a low-affinity CAR called CAT in pediatric patients with ALL[183]. They reported high anti-tumor efficacies without the induction of severe CRS compared to published studies using high-affinity FMC63 CAR-T cells, but further investigations are needed to truly link the results to differences in CAR-T cell affinity. CAT CAR-T cells target the same epitope as the CAR-T cell product Tisagenlecleucel. However, the CAT CAR is under the control of a different promoter, potentially leading to higher CAR expression contributing to the observed differences. In addition, CAT CAR-T cells were manufactured differently; indeed, the used protocols generated T cell products with a mostly naïve and central memory phenotype, which could affect expansion, persistence, and efficacy independent from CAR affinity. In addition, patients treated with low-affinity CAR-T cells in this particular trial were characterized by low leukemic burdens, which *per se* associate with a decreased likelihood of developing adverse events[93]. Admittedly, it can be challenging to perform parallel clinical studies; however, a direct comparison of high and low-affinity CAR-T cells, at least in preclinical models, is necessary to demonstrate more directly and conclusively if and how differences in CAR affinity affect *in vivo* performance, especially concerning efficacy and safety.

Next to these first clinical results, other groups have started studying the quality of low-affinity CAR-T cells *in vitro* and *in vivo*. In order to investigate the impact of CAR affinity on the outcome of the treatment of solid tumors, He and colleagues have tested, for example, two human glypican-3 (hGPC3)-specific CAR clones with 17-fold affinity differences in a xenograft model[201]. They found that T cells engineered with the low-affinity CAR were less prone to apoptosis upon target recognition and more resistant to exhaustion with more durable effector functions. However, the two tested CAR clones target different epitopes, which could significantly influence underlying reasons for observed differences beyond CAR affinity.

Additionally, affinity differences between the two CARs were only determined for the CAR-derived antibodies and not the respective scFvs.

Furthermore, CD123-specific CAR mutants targeting AML blasts and leukemic stem cells with 10- and 100-fold lower affinities than the wildtype CAR were designed by single residue substitutions based on a computational structural biology tool. Two CAR mutants with different association rates but similar predicted antigen-binding epitopes were compared with the original CD123-specific CAR. However, a defined lytic and activation antigen threshold in vitro was mainly affected by lower CAR surface expression, independent of the affinity[202]. These results align with our *in vitro* findings, where CAR-T cell functionality above a certain threshold was mainly influenced by the CAR surface expression and not significantly affected by the receptor binding strength. Another study characterized four melanoma tumor-associated antigen Tyr-HLA-A2-specific CARs with affinities of the scFvs in the range of 4 to 400 nM[203]. A collection of B cell hybridomas, which target the Tyr HLA-A2 TAA, was generated to design CARs with varying affinities based on the derived antibodies. In this study, a window of antigen density and a window of CAR affinities that yield maximal responses were detected. However, the exact binding epitopes of the generated CARs had not been determined, making it challenging to fully connect the observed results with differences in CAR affinity.

In order to circumvent the described technical limitations, we started with four different clinically relevant CAR clones with clinical relevance, and we carefully analyzed their binding kinetics and antigen-binding epitopes. Analyses of standardized SPR measurements revealed distinct kinetic profiles of the JCAR017, JCAR021, and CAT scFvs (Fig. 1C-D). The next-generation humanized JCAR021 was identified as a low-affinity CAR with 37-fold lower binding strength than the clinically used high-affinity JCAR017 and an even slightly weaker binding strength than the low-affinity CAT scFv (Fig. 1D). Similar k_{on}-rates among the three constructs demonstrated that the affinity differences are mainly based on differences in the dissociation rate, which in the case of JCAR021 and CAT is only a matter of seconds. Furthermore, we identified an identical CD19 binding epitope of JCAR017, JCAR021, and CAT by SPR-based epitope mapping (Fig. 1E), suggesting that differences in synapse widths are unlikely to

contribute to potential differences in the CAR-T cell response. Taken together, the same binding epitope but different overall K_Ds of the three tested CARs gave us the unique opportunity to specifically study the impact of receptor affinity on CAR-T cell functionality.

Although few studies have started addressing the influence of CAR affinity on the mediated T cell functionality, none of the investigated binding domains possessed affinities in the TCR range. In order to generate such super-low affinity CARs down in the range of typical for TCRs, we mutated the humanized JCAR021 scFv, as it revealed the lowest binding half-live in the SPR analysis (Fig. 1D). Although alanine scanning represents a commonly used engineering tool to define essential residues in the binding site of proteins and change their binding strengths[204], we did not succeed in the generation of low-affinity CAR mutants by exchanging single aromatic amino acids in the framework region of the scFv with alanine. All mutated CAR constructs were either not stably expressed on the T cell surface (Fig. 11B) or showed binding kinetics similar to JCAR021, as determined by our in-house flow cytometry-based k_{off}-rate assay (Fig. 12 A).

Nevertheless, this first trial highlighted the importance of determining CAR surface expression of engineered T cells by direct antibody staining. We could demonstrate that the expression of a transduction marker, even connected via a T2A-element in the CAR DNA sequence, does not always guarantee a proper surface expression of the CAR (Fig. 11B). The introduction of point mutations can lead to misfolding and degradation of the transgenic receptor without influencing the expression of the transduction marker, which consequently impairs an equal co-expression of the two proteins. Still, once the proper expression of the CAR of interest is validated, the use of transduction markers facilitates the monitoring of transgenic T cells, as receptor downregulation may occur after T cell activation[205,206], especially after integrating the receptor into the endogenous locus by CRISPR/Cas9 engineering[42]. Reasons for the unequal surface expression of receptors connected via T2A elements have not been determined yet, but further analysis of mRNA and protein levels via qPCR or western blot will help understand the underlying mechanisms.

In contrast to the alanine scanning approach, we succeeded in generating 32 mutants of JCAR021 with different binding strengths by using an *in silico* algorithm[191] to predict and select single amino acid exchanges in the extracellular binding domain (Fig. 14A). Nearly all selected scFv mutants of the educated guess maintained their specificity towards CD19, and most preserved sufficient surface expression. Moreover, we obtained a decreasing range of affinities down to the range of TCRs.

Overall, we could exploit four different CAR clones with high and medium affinities that only differ in their k_{off}-rates and still target the same CD19-epitope. Additionally, we successfully engineered a broad CAR affinity library with CAR mutants showing efficient cell surface expression and affinities even in the range of TCRs (Fig. 14D). Therefore, we had the necessary tool to investigate the impact of weak CAR binders on the mediated CAR-T cell function and safety in a controlled manner.

5.3 Correlation of CAR affinity and functionality

Binding kinetics of receptor-ligand interactions mainly influence the functional potency of the respective T cell. While higher TCR affinities result in stronger cellular responses[169], enhanced TCR affinities above the physiological threshold have been demonstrated to lead to a plateau or even decrease in the T cell functionality[169,207]. Additionally, while half-lives above the optimal interaction time decrease the efficacy of TCR serial engagement[208], too short half-lives prevent sufficient T cell activation[169]. These observations indicate the existence of a window of optimal half-lives for TCR-ligand interactions; whether such an ‘optimal window’ also exists for CARs has not been investigated far.

5.3.1 *In vitro* functionality of low-affinity CAR-T cells

Similar on-rates and binding epitopes of the tested CAR variants gave us the unique opportunity to specifically study the impact of receptor affinity on CAR-T cell functionality. We started with testing the sensitivity of the corresponding CAR-T cells via intracellular cytokine staining and the anti-tumor cytotoxicity *in vitro*. Although the affinities of CAT and JCAR021

were already 20 – 40 times lower than the affinity of JCAR017, no significant differences in the *in vitro* functionality of the corresponding CAR-T cells were noticed (Fig. 2-3). Not only the killing efficacies and kinetics but also the specific cytokine production after antigen stimulation were almost identical among the different CAR-T cell products.

Regarding the generated JCAR021-derived mutants, firstly, we observed that the efficient CAR surface expression is a primary determining factor for successful CAR-T cell functionality. Indeed, impaired CAR surface expression (orange and red expression groups) limited or completely abrogated T cell functionality. By comparing engineered T cells with successful CAR expression (green group), mutant CAR-T cells with affinities in the high nanomolar and micromolar range showed a similar capacity to produce cytokines in response to antigen-presenting tumor cells, except for “super-low-affinity” CARs (variants V236W and V236F) ranging in the affinity landscape of natural TCRs (Fig. 19). Only T cells equipped with CARs showing the fastest measured half-lives within our affinity library revealed a reduction in T cell activation in terms of frequency of cytokine-releasing cells. In line with these results, we also observed comparable killing capacity or kinetics for most CAR mutants but a diminished *in vitro* cytotoxicity of CAR-T cells expressing super-low affinity receptors (Fig. 20-21).

Overall, no significant functional differences of high, middle, and low-affinity CAR-T cells expressing CARs with half-lives above the determined threshold ($t_{1/2}$ measured by flow-cytometry-based k_{off}-rate assay= at 43s; 22°C) were observed. CAR-T cells expressing CARs with affinities below this lower limit showed a slightly impaired *in vitro* functionality. However, these first findings are insufficient to draw conclusive statements on a lower overall potency of the corresponding CAR-T cells. Therefore, further *in vivo* analyses were necessary to address whether the *in vitro* results can predict *in vivo* efficacy and functionality. As the subsequent *in vivo* studies revealed significant differences in CAR-T cells expressing either JCAR017 or JCAR021, we had to learn that the array of *in vitro* assays used in this study to determine CAR-T cell functionality and safety (which are commonly used methods) has no predictive value for *in vivo* functionality.

5.3.2 *In vivo* killing capacity of low-affinity CAR-T cells

In order to evaluate the influence of CAR affinity on CAR-T cell functionality *in vivo*, we tested five CARs spanning the entire affinity library in an immunocompromised xenograft model. Additionally, we monitored the cytotoxic potential of JCAR021 and JCAR017 expressing CAR-T cells in a humanized tumor model. In both models, surprisingly, the low-affinity JCAR021 CAR-T cells only partially controlled tumor growth, whereas potent anti-tumor activity was observed for the high-affinity JCAR017 CAR-T cells, as expected. A further decrease in affinity, represented by the JCAR021 mutants, resulted in even lower functionality. Here, the tumor growth was only partially delayed. Overall, the reduction of tumor burden and the consequent survival of the treated mice positively correlated with an increased CAR affinity. These affinity-dependent differences were not observed *in vitro,* potentially due to the low sensitivity of these assays. However, we identified the same lower limit of CAR affinity to guarantee sufficient CAR-T cell activation and tumor-killing *in vitro* and *in vivo*, as super-low-affinity CAR-T cells could not control Raji tumor growth at all (Fig. 23). Notably, this bottom limit differs highly from the optimal affinity range of TCRs, potentially due to the artificial signaling cascade of CARs.

In line with our data, it has been shown for ROR-1 specific CAR-T cells that higher CAR affinities are associated with increased T cell functions and *in vivo* efficacy[147], even if the different used scFvs of this study exhibited different epitope specificities. Also, engineered T cells expressing high-affinity MART-1 and NY-ESO-1 TCRs within the physiological range improved overall response rates in the clinical setting[166]. Importantly, we identified a lower affinity threshold for detectable CAR-T cell *in vivo* efficacy; thereby, the threshold seems to be substantially higher than the described threshold for TCR functionality.

A limitation of our setting is that our engineered anti-CD19 CAR affinity library was designed to investigate CAR-T cells with affinities in the TCR range with binding strengths $>10^{-6}$ M. Only one high-affinity CAR in the nanomolar range (JCAR017) was used as a control. Therefore, no conclusions can be drawn about the potential upper limit of the affinity window of CAR-T cells targeting CD19. For ERB2-specific scFvs in the affinity range of 10^{-7} to 10^{-11} M, a threshold of 10^{-8} M has been identified above which CAR-T cell functionality does not improve

anymore[209]. CAR-T cells targeting CD20 with extra high affinities showed less proliferation than affinity-reduced CAR-T cells[210]. Consequently, also for CARs, similar to TCRs, an optimal affinity window seems to exist but within an overall higher affinity range, potentially due to the artificial structure of the CAR. In order to close the missing gap, anti-CD19 CARs with affinities between 10^{-6} and 10^{-9} M and above 10^{-9} M must be designed and tested.

5.3.3 Dynamics of CAR-T cell activation

There are multiple phases of CAR-T cell kinetics. Patient-derived data suggest that anti-CD19 CAR-T cells rapidly proliferate upon antigen recognition[211], which is followed by a contraction phase and persistence after tissue infiltration. Each phase reflects an essential part of CAR-T cell efficacy. While a rapid and high expansion of CAR-T cells is necessary for tumor clearance and thus is regarded as a positive sign for a clinical response[212], durable responses usually require long-term CAR-T cell persistence of a small pool of memory CAR-T cells[213].

Faster expansion of high-affinity JCAR017 CAR-T cells was detected in both *in vivo* models applied in our studies. While CAR-T cells expressing low-affinity receptors also proliferated *in vivo*, their expansion seemed to be somewhat delayed. Compared to their low-affinity counterparts, the more substantial initial expansion of high-affinity CAR-T cells got along with a faster and stronger tumor clearance and B cell depletion, which correlates with an improved clinical benefit.

While a trend of contraction was observed for JCAR017 CAR-T cells in the blood of humanized mice, the adoptively transferred cells persisted well in the non-humanized model, perhaps also supported by remaining tumor cells in this model (Fig. 25). Higher levels of transferred CAR-T cells were detected in the blood of humanized mice compared to non-humanized mice, most likely due to the presence and constitutively new generation of $CD19^+$ B cells as additional CAR-T cell targets (Fig. 33A).

In great contrast to cell numbers detected in the circulation and spleen, a higher accumulation of JCAR017 CAR-T cells was observed in the bone marrow, representing the central location of tumor cells in the used experimental tumor model. In line with these data, significantly

reduced numbers of “super-low-affinity” CAR-T cells accumulated at the tumor site. Consequently, increased numbers of tissue-infiltrating CAR-T cells at the tumor site correlate with a higher CAR affinity and thus represent another potential reason for the improved killing efficacy of high-affinity CAR-T cells.

Besides lower expansion and infiltration, low-affinity CAR-T cells also showed lower activation levels, as determined by PD-1 and HLA-DR expression (Fig. 27). While prolonged antigen exposure and high expression of activation markers such as PD-1 are critical features of exhaustion[32], functional T cell responses after acute stimulation have also been shown to express these receptors transiently[214]. As all adoptively transferred CAR-T cells co-expressed high levels of HLA-DR, PD-1 expression indicated activation rather than exhaustion in our experiments. In line with lower activation levels, we also observed lower frequencies of differentiated effector cells in the bone marrow of low-affinity CAR-T cells compared to the JCAR017-engineered T cells. Intriguingly, the extent of differentiation strictly correlated with CAR affinity, as a substantial fraction of transferred cells preserved a non-differentiated naïve phenotype in CAR-T cells expressing “super-low-affinity” CARs (Fig. 29).

Altogether, the stronger expansion, activation, and differentiation potential of high-affinity CAR-T cells indicate that high-affinity CAR-T cells are more engaged in the tumor response, consequently leading to improved anti-tumor cytotoxicity.

5.3.4 Regulation of CAR surface expression

Another feature we observed for low-affinity CAR-T cells is a more extensive downregulation of the receptor upon specific antigen encounter *in vivo* (Fig. 28). While all retrovirally transduced CAR-T cells revealed similar CAR expression before their adoptive transfer, low-affinity CAR-T cells such as JCAR021 downregulated CAR surface expression during the peak of expansion and highest antigen load. TCR internalization is a characteristic of serial triggering and productive receptor engagement upon activation[170]. In contrast to fast TCR interaction times within seconds, high-affinity CAR binding usually takes minutes to hours, limiting serial triggering. We observed antigen-induced CAR internalization only for low-affinity

CAR-T cells. For high-affinity JCAR017 CARs, no significant downregulation in different tumor settings was detected. Also, for “super-low-affinity” CAR-T cells, no down-regulation of surface expression was noticed, potentially due to too short interaction times to trigger sufficient activation and receptor internalization. Indeed it has been shown previously that excessively long half-lives impair serial engagement of TCRs, but also that a sufficiently long half-live is necessary to enable receptor-based signaling[208].

Low-affinity CARs might have additional advantages that could not be investigated with our *in vivo* models. It has been reported that CAR-T cells and affinity-enhanced TCRs require at least 100-fold higher antigen densities than naturally occurring TCRs to become activated productively[172,215]. As prolonged half-live interactions cannot support efficient serial triggering, they could prevent sufficient T cell activation in case of low antigen density. Therefore, impaired serial triggering of high-affinity CAR-T cells might become problematic in the case of a low antigen density of the targeted tumor cells due to the lower CAR-T cell sensitivity. Tumor cells can escape the CAR-T cells by downregulating the CAR-targeted antigen. This potential advantage of low-affinity CAR-T cells was apparently not relevant in the used xenograft Raji tumor model, as these tumor cells express very high levels of CD19, leading to simultaneous binding of CARs and thus diminishes the need for serial triggering. In order to better understand whether low-affinity CAR-T cells have an advantage in low-antigen settings, tumor cell lines expressing different CD19 densities on their cell surface should be tested in future experiments.

CAR downregulation could also prevent activation-induced cell death, which has been associated with sustained CAR signaling. Especially high-affinity CAR-T cells are more prone to exhaustion due to the strong signaling via their receptors. Consequently, longer persistence of weak CAR or TCR binders has already been demonstrated by their lower susceptibility to become exhausted or senescent after antigen encounter[183,216].

Therefore, serial triggering might be an advantage for not only improved anti-tumor activity but also an advantage for sustainable T cell fitness. The suboptimal *in vivo* xenograft models used for our studies rely on a fast initial tumor clearance, and only short-term responses are reliably

analyzable in this experimental setting. Therefore, the potential beneficial effect of reducing ongoing signaling in the presence of large tumor burdens by low-affinity CAR-T cells could not be investigated in this model. Such potential beneficial effects must be analyzed in long-term *in vivo* models, e.g., syngeneic models. Similarly, the overall long-term functionality of CAR-T cells could be better investigated in syngeneic *in vivo* experiments. In the humanized mouse model, low-affinity JCAR021 CAR-T cells started with a delayed killing of the tumor cells; however, due to the short observation period, we could not analyze whether full tumor clearance could be achieved.

5.4 Safety profile of low and high-affinity CAR-T cells

Although high-affinity CAR-T cells exhibit the strongest short-term killing efficacy, this does not necessarily mean that they represent the best engineered T cell product for clinical applications. For optimal clinical functionality, CAR-T cells must also provide an optimal balance between therapeutic efficacy and safety.

We investigated the role of CAR-T cell-related side effects in an elegant pre-clinical CRS mouse model, which was established by the team of Monica Casucci and Attilio Bondanza[95]. Briefly, NSGS mice are humanized with humane hematopoietic stem cells to create an environment similar to the human immune system, as especially monocytes and macrophages are necessary for the development of CAR-T cell-related side effects. Due to the use of highly aggressive Raji tumor cells and the potential development of xenoreactivity in humanized mice, the CRS mouse model can only be used to determine short-term effects. However, as CRS-mediated clinical side effects also usually develop shortly after the adoptive transfer of the CAR-T cells, the results from the humanized model are still likely to reflect a setting close to the clinical situation. An alternative model proposed by Sadelain and collegues[94], in which high doses of CAR-T cells are transferred into immunocompromised mice, does not provide syngeneic interactions of CAR-T cells with other components of the (innate) immune system and thus only partially enables the investigation of CAR-T cell-related toxicities.

As expected, we could demonstrate that low-affinity CAR-T cells significantly reduce CAR-T cell-induced toxicities, determined by weight loss and cytokine release (Fig. 31). Also, a first clinical study using low-affinity CAT CAR-T cells showed milder mediated side effects compared to clinical studies using high-affinity CAR-T cells[183]. As discussed before, the good safety profile of CAT CAR-T cells observed in this clinical trial could have also been mediated by the low tumor burden of treated patients. In our experiments, we could not recapitulate a more substantial expansion and killing efficacy with low-affinity CAR-T cells in an affinity range similar to CAT CAR-T cells. In order to further investigate these differences, CAR-T cells expressing either CAT or JCAR021 should be directly compared in the same *in vivo* model. However, also other groups have generated preclinical data indicating that low-affinity CAR-T cells provide better safety but have reduced functionality[84]. Whether "super-low-affinity" CAR-T cells can further reduce side effects has not been addressed in our study. The low anti-tumor functionality of these CAR-T cells would make them also weak candidates for clinical use.

As an alternative to the adoptive transfer of weaker CAR binders, we demonstrated that the adoptive transfer of lower doses of high-affinity CAR-T cells could also mitigate the development of severe side effects (Fig. 36) as absolute levels of secreted cytokines were diminished. An optimally low dose can be identified via titration, where functionality and tumor control of high affinity CAR-T cells is still fully preserved, although overall response kinetics are somehow delayed (Fig. 37). Dose-escalation clinical studies have shown that anti-tumor responses can be achieved with lower CAR-T cell doses than the dosages used for the currently FDA/EMA-approved products and that reduced levels of transferred CAR-T cells can diminish the risk of severe toxicities[107]. Interestingly, also mathematical models have been developed to predict the minimum amount of transferred CAR-T cells to provide effective tumor killing[212]. However, further clinical trials are necessary to test the validity of these predictions in real-life settings. In addition, since tumor burden and antigen loads can vary dramatically between individual patients, it will be extremely difficult - if not impossible – to determine optimal dosages of high-affinity CAR-T cells prior to therapy. Overall, our studies demonstrate that CAR-T cells expressing low-affinity receptors are safer than similar doses of high-affinity

CAR-T cells but are disadvantageous in settings of aggressive tumors due to their lower functionality. While low-affinity CAR-T cells avoid rapid activation and proliferation and thereby reduce the risk of severe CRS, high-affinity CAR-T cells are more potent in eradicating tumor cells but bear a high risk for significant toxicities. Therefore, both high and low-affinity CARs are characterized by features that are unfavorable for clinical applications.

5.5 Balanced efficacy and safety profile of mixed affinity CAR-T cell products

Similar to our *in vivo* screening of the CAR affinity library, a recent study by a different group demonstrated that the transfer of low-affinity Her2-specific CAR-T cells is characterized by high safety but only modest anti-tumor activity in sarcoma patients[84]. In addition, finding the best balance between safety and efficacy by transferring individualized numbers of high-affinity CAR-T cells depending on the tumor burden represents neither a clinically feasible nor practicable approach. These findings highlight the need for improved approaches to generate long-term efficient and highly safe CAR-T cell products.

The natural immune system consists of a heterogeneous repertoire of TCRs with different affinities for the same antigen, and polyclonal populations with variable TCR affinities are initially recruited into protective immune T cell response as demonstrated, for example, for the immune control of many different virus infections. While high avidity TCRs dominate primary and recall response over time, low avidity TCRs seem essential for ensuring long-term immunity in specific situations like chronic stimulation, where high-affinity TCRs have been shown to be more susceptible to exhaustion[185,216].

Based on these fundamental aspects of T cell immunity, we postulated that mimicking polyclonality by providing high and low affinity components within the same CAR-T cell product could be an attractive strategy to improve adoptive cell therapy by assuring high safety as well as preserving high efficacy. Indeed, we could demonstrate that the simultaneous transfer of high numbers of low-affinity CAR-T cells supplemented with low numbers of high-affinity CAR-T cells guarantees reliable survival of the treated mice (Fig. 40). Notably, while low-affinity CAR-T cells alone could not rescue all mice, the addition of small amounts of high-affinity CAR-

T cells, which are inefficient for controlling the tumor when applied alone, significantly improved the *in vivo* functionality of the transferred CAR-T cell product. Transferring CAR-T cell populations, of which only 10 % express a high-affinity CAR, already improved the survival of the treated mice. As neither high numbers of low-affinity CAR-T cells nor low numbers of high-affinity CAR-T cells alone were sufficient to control tumor load, the simultaneous transfer of high and low-affinity CAR-T cells seems to provide the perfect balance of safety and clinical efficacy independent of tumor burden. Whether the simultaneous transfer of CAR-T cells with different affinities results in high protective and long-term persistent CAR-T cells to avoid tumor relapses still needs to be further investigated.

An alternative approach to the single treatment with a mixture of high and low-affinity CAR T cells could be the sequential administration of CARs with different affinities[217]. Here, the initial tumor load may be reduced by first transferring high numbers of low-affinity CAR-T cells, followed by a second application of high-affinity CAR-T cells to ensure efficient clearance and maintenance of the tumor depletion. Our data demonstrate that larger tumor masses can already be reduced – although not completely cleared - by the treatment with high numbers of low-affinity CAR-T cells without significant risk for CRS. Later application of high-affinity CAR-T cells would be expected to hit only a smaller tumor burden, which has already been shown clinically to lead only to mild side effects. However, it will be difficult to determine the right amount and time point for the second high-affinity CAR-T cells application, which might vary between individuals. In addition, it is unclear whether patients need to be pre-conditioned with lymphopenia-inducing drugs before the second CAR-T cell transfer, which is currently standard for CAR-T cell therapies. Since preconditioning will also affect the *in vivo* functionality of the previously applied low-affinity CAR T-cells, this strategy is probably too complex to be realized. In addition, the manufacturing of two separate CAR T cell products might further raise the costs for this already quite expensive therapy. Therefore, the simultaneous application approach, as described for the first time in this thesis work, might represent the best compromise to optimize future CAR-T cell therapy.

5.6 Limitations of this Ph.D. thesis

Although the Cytokine-Release-Syndrome represents one of the most severe acute side effects that can be life-threatening for patients, other CAR-T cell-related toxicities are still influencing patients' lives. While this work mainly focused on the development of acute adverse events, the influence of CAR affinity on other clinically relevant side effects should be addressed. While no appropriate *in vivo* mouse model is available to investigate the occurrence of Neurotoxicity, highly relevant CAR-T cell-associated long-term side effects like cytopenia could be studied in a syngeneic mouse model. Although the murine immune system is still intact in immunocompetent mice, no sign of CRS or Neurotoxicity was reported in these mice, making this model irrelevant for studying acute CAR-T cell-related effects. However, long-term side effects like hematologic malignancies could be investigated more efficiently in immunocompetent than immunocompromised *in vivo* models.

In one of our recent publications[199], we showed that murine anti-CD19 CAR-T cells maintain long-term functionality even 390 days after their adoptive transfer. Combining this long-term *in vivo* CAR-T cell model, which also requires pre-conditioning, one of the risk factors for cytopenia, and different affinity CAR-T cell products would allow a better understanding and investigation of late occurring side effects. Besides, missing data about the long-term functionality of low-affinity CAR-T cells could be generated, and the possible advantage of different CAR-T cells after tumor relapse by re-transfer of tumor cells could be mimicked. The Raji model used throughout this work represents the most commonly used *in vivo* model for testing anti-CD19 CAR-T cells. However, as the tumor cell line is highly aggressive, only complete tumor eradication within some days could be followed. Therefore, long-term effects like CAR-T cell exhaustion during a prolonged killing time comparable with chronic stimulation could not be investigated in immunocompromised models.

Another CD19-expressing tumor cell line would be Nalm-6 tumor cells. Although they are not as aggressive as Raji tumors, they would only expand the tracking window for one to two more weeks, and mice often tend to relapse after CAR-T cell transfer in this mouse model.

Overall, the syngeneic mouse model represents a solution to study many more features of low-affinity CAR-T cells; however, importantly, the homology of the human and murine CD19 antigen is only 66 % (UniProt). Consequently, anti-CD19 CAR-T cells cannot bind to murine CD19; which means that the whole CAR affinity library would have to be newly generated and designed with CARs having affinities in the same range as the engineered human anti-CD19 CARs presented in this Ph.D. thesis but which bind to the murine homolog.

Another exciting research aspect would be the influence of low- and high-affinity CAR-T cells also against solid tumors. So far, CAR-T cells have not been efficient in tumor clearance due to the highly immunosuppressive tumor microenvironment. In order to better understand which impact CAR receptor affinity tuning would have on the functionality, persistence, and engraftment in these settings, CAR constructs targeting solid tumor markers like ROR1 or MUC1 should be used and tested in solid tumor models. One way to not build up a whole new library but still get a first impression of the role of the influence of affinity would be to change the injection route of tumor cells from intravenous injection to subcutaneous injection, thereby mimicking a solid tumor mass. By including a second CAR-T cell target, we could show that the approach and results of low-affinity CAR-T cells would not be restricted to CD19 as a target antigen.

One aspect that would complete the investigation of an even broader affinity range represents the engineering of CARs with affinities with even higher affinities than the clinically used JCAR017 and between JCAR021 and JCAR017. As other groups had already reported the effect of super-high affinity CAR-T cells in the picomolar range and also down to high nanomolar ranges, we were more interested in CAR affinities comparable to TCR-like binding strengths.

6 Conclusion

With this thesis work, we investigated the impact of CAR binding affinity on the functional efficacy and toxicity potential of the corresponding CAR-T cells.

Based on an *in silico* screening approach, we engineered a broad library of high-quality CAR-T cells with high to low binding strengths to CD19, which gave us the unique opportunity to specifically study the impact of receptor affinity on CAR-T cell functionality. The developed flow-cytometry-based k_{off}-rate assay represents a new tool to fast and reliably determine the affinity of low-affinity CARs. The established *in vitro* and *in vivo* screening platform subsequently enabled us to test how CAR affinity affects the functionality and safety of adoptive cell therapy (Fig.42).

With these tools, we could demonstrate a direct correlation between CAR-T cell functionality and efficacy, as well as an inverse correlation of toxicity (CRS) with increasing CAR affinity. Moreover, we identified a lower limit of CAR affinity necessary to provide functionality, which was still significantly higher than the affinity range of TCRs, further corroborating the lower sensitivity of CARs compared to natural TCRs. As functionality and safety are essential for an optimal CAR-T cell product, these data emphasize the enormous challenge of identifying a single CAR-T cell affinity that provides the highest levels of efficacy and safety for a large group of patients. The optimal affinity of a single CAR-T cell product depends on many variables, e.g., tumor burden, antigen load, and specific target. As a potential solution to this problem, our data suggest that the simultaneous transfer of low- and high-affinity CAR-T cells might provide an optimal product for CAR-T cell therapy. Indeed, while initial antigen load might be reduced through relative domination of safe low-affinity receptors, low numbers of transferred high-affinity receptors would selectively expand and ensure robust long-term tumor control without the development of severe side effects. Still, further work is needed to investigate the effect of constant stimulation, low antigen expression, and long-term functionality of therapies with mixed CAR-T cell products. Nevertheless, we believe that this newly developed approach might be of general relevance for adoptive T cell therapies and provides a relatively simple strategy to improve next-generation CAR-T cell products.

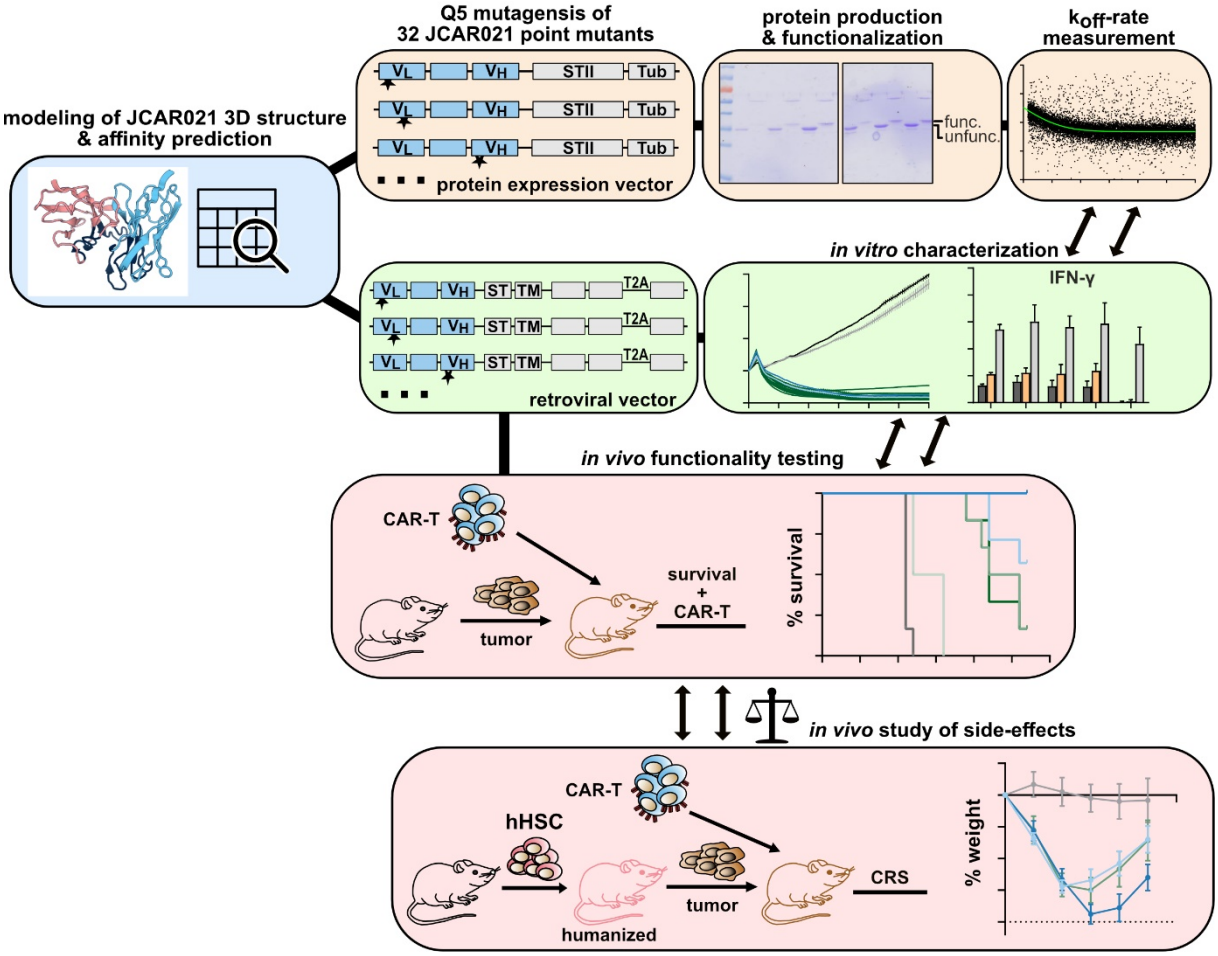

Fig. 42 CAR affinity screening platform
Illustration of a CAR screening approach to study the influence of CAR affinity on functionality and safety of the associated CAR-T cell. A CAR library containing 32 JCAR021 CAR mutants with predicted lower affinity is tested for their binding strength towards CD19. *In vitro* and *in vivo* functionality are studied and correlated with the measured affinities of the CAR-T cells. Advanced humanized mouse models are used to investigate the role of affinity in the safety of CAR-T cell products.

7 Author contributions

Sarah Dötsch is the first author of the publication titled "*Long-term persistence and functionality of adoptively transferred antigen-specific T cells with genetically ablated PD-1 expression",* published in PNAS on February 28th, 2023[199].

The first authorship is shared with Mortimer Svec.

While both first authors performed experiments and analyses presented in this study, Sarah Dötsch mainly drove the conceptualization and non-published establishment work. Besides, she was involved in all published and unpublished experiments. Sarah Dötsch was the main person responsible for performing, evaluating, and analyzing all published and non-published experiments. In contrast to the shared author and additionally to the practical work, Sarah Dötsch designed the research study, wrote the manuscript, and designed all figures of the main text and appendix. In addition to that, she wrote the animal approval and all associated amendments to this document.

Most of the data of this Ph.D. thesis are still unpublished; however, the manuscript is already in preparation.

List of abbreviations

ACT	Adoptive T cell therapy
Amp	Ampicillin
B-ALL	B-cell acute lymphoblastic leukemia
BLI	Bioluminescence imaging
BBB	Blood-brain barrier
CAR	Chimeric antigen receptor
CDR	Complementarity-determining region
CFU	Colony forming unit
CRS	Cytokine Release Syndrome
CTL	Cytotoxic lymphocyte
DBCO	Dibenzocyclooctin
ddH2O	Double distilled water
DLBCL	Diffuse large B cell lymphoma
DNA	Deoxyribonucleic acid
ECD	Extracellular domain
E. coli	Escherichia coli
EGFRt	Truncated version of the human epidermal growth factor receptor
EMA	European Medicines Agency
E:T ratio	Effector to target ratio
FACS	Fluorescence-activated cell sorting
FCS	Fetal calf serum
ffluc	Firefly luciferase
FDA	US Food & Drug Administration
GFP	Green fluorescent protein
GvHD	Graft-versus-host disease
hHSC	Human hematopoietic stem cell
HSCT	Hematopoietic stem cell transplantation
IFN-γ	Interferon gamma
IL	Interleukin
i.p.	Intraperitoneal
i.v.	Intravenous
IVIS®	In-vivo imaging system
ka	Association rate/On rate

KD	Dissociation equilibrium constant (also: kon)
kd	Dissociation rate/Off rate (also: koff)
LB	Lysogeny broth
mAb	Monoclonal antibody
MFI	Median fluorescence intensity
MHC	Major Histocompatibility Complex
MOI	Multiplicity of infection
NSG-SGM3	NOD-scid IL2Rgammanull with 3 human transgenes (SCF, GM-CSF, IL-3)
OD600	Optical density
PBMC	Peripheral blood mononuclear cells
PCR	Polymerase chain reaction
PD-1	Programmed cell death protein 1
pMHC	Peptide major histocompatibility complex
RNA	Ribonucleic acid
RT	Room Temperature
scFv	Single chain variable fragment
SPR	Surface plasmon resonance
SA	Streptavidin
ST	StrepTactin
STII	Strep-tagII
t1/2	Half-life
TAA	Tumor associated antigen
TCR	T cell receptor
tdTomato	Tandem dimer Tomato
TIL	Tumor-infiltrating lymphocyte
TNF-a	Tumor necrosis factor alpha
TTL	Tubulin tyrosine ligase
UCB	Umbilical cord blood

References

1. Thomas ED, Lochte HL, Lu WC, Ferrebee JW. Intravenous Infusion of Bone Marrow in Patients Receiving Radiation and Chemotherapy. *N Engl J Med*. 1957;257(11):491-496. doi:10.1056/nejm195709122571102
2. Kolb HJ, Mittermuller J, Clemm C, et al. Donor leukocyte transfusions for treatment of recurrent chronic myelogenous leukemia in marrow transplant patients. *Blood*. 1990;76(12):2462-2465. doi:10.1182/blood.v76.12.2462.2462
3. Riddell SR, Watanabe KS, Goodrich JM, Li CR, Agha ME, Greenberg PD. Restoration of viral immunity in immunodeficient humans by the adoptive transfer of T cell clones. *Science (80-)*. 1992;257(5067):238-241. doi:10.1126/science.1352912
4. Rooney CM, Ng CYC, Loftin S, et al. Use of gene-modified virus-specific T lymphocytes to control Epstein-Barr-virus-related lymphoproliferation. *Lancet*. 1995;345(8941):9-13. doi:10.1016/S0140-6736(95)91150-2
5. Rosenberg SA, Packard BS, Aebersold PM, et al. Use of Tumor-Infiltrating Lymphocytes and Interleukin-2 in the Immunotherapy of Patients with Metastatic Melanoma. *N Engl J Med*. 1988;319(25):1676-1680. doi:10.1056/nejm198812223192527
6. Rosenberg SA, Yang JC, Sherry RM, et al. Durable complete responses in heavily pretreated patients with metastatic melanoma using T-cell transfer immunotherapy. *Clin Cancer Res*. 2011;17(13):4550-4557. doi:10.1158/1078-0432.CCR-11-0116
7. Porter DL, Levine BL, Kalos M, Bagg A, June CH. Chimeric Antigen Receptor–Modified T Cells in Chronic Lymphoid Leukemia. *N Engl J Med*. 2011;365(8):725-733. doi:10.1056/nejmoa1103849
8. Kochenderfer JN, Wilson WH, Janik JE, et al. Eradication of B-lineage cells and regression of lymphoma in a patient treated with autologous T cells genetically engineered to recognize CD19. *Blood*. 2010;116(20):4099-4102. doi:10.1182/blood-2010-04-281931
9. Brentjens RJ, Davila ML, Riviere I, et al. CD19-targeted T cells rapidly induce molecular remissions in adults with chemotherapy-refractory acute lymphoblastic leukemia. *Sci Transl Med*. 2013;5(177). doi:10.1126/scitranslmed.3005930
10. Grupp SA, Kalos M, Barrett D, et al. Chimeric Antigen Receptor–Modified T Cells for Acute Lymphoid Leukemia. *N Engl J Med*. 2013;368(16):1509-1518. doi:10.1056/nejmoa1215134
11. Maude SL, Laetsch TW, Buechner J, et al. Tisagenlecleucel in Children and Young Adults with B-Cell Lymphoblastic Leukemia. *N Engl J Med*. 2018;378(5):439-448. doi:10.1056/nejmoa1709866
12. Neelapu SS, Locke FL, Bartlett NL, et al. Axicabtagene Ciloleucel CAR T-Cell Therapy in Refractory Large B-Cell Lymphoma. *N Engl J Med*. 2017;377(26):2531-2544. doi:10.1056/nejmoa1707447
13. Gale RP, Horowitz MM, Ash RC, et al. Identical-twin bone marrow transplants for leukemia. *Ann Intern Med*. 1994;120(8):646-652. doi:10.7326/0003-4819-120-8-199404150-00004
14. Kolb HJ, Schattenberg A, Goldman JM, et al. Graft-versus-leukemia effect of donor lymphocyte transfusions in marrow grafted patients. *Blood*. 1995;86(5):2041-2050. doi:10.1182/blood.v86.5.2041.bloodjournal8652041
15. Collins RH, Shpilberg O, Drobyski WR, et al. Donor leukocyte infusions in 140 patients with relapsed malignancy after allogeneic bone marrow transplantation. *J Clin Oncol*.

1997;15(2):433-444. doi:10.1200/JCO.1997.15.2.433

16. Seemayer TA, Gartner JG, Lapp WS. The graft-versus-host reaction. *Hum Pathol*. 1983;14(1):3-5. doi:10.1016/S0046-8177(83)80040-9

17. Goldman JM, Gale RP, Horowitz MM, et al. Bone marrow transplantation for chronic myelogenous leukemia in chronic phase. Increased risk for relapse associated with T-cell depletion. *Ann Intern Med*. 1988;108(6):806-814. doi:10.7326/0003-4819-108-6-806

18. Marr KA. Delayed opportunistic infections in hematopoietic stem cell transplantation patients: a surmountable challenge. *Hematology Am Soc Hematol Educ Program*. 2012;2012:265-270. doi:10.1182/asheducation.v2012.1.265.3800160

19. Ho M. Epidemiology of cytomegalovirus infections. *Rev Infect Dis*. 1990;12:S701-S710. doi:10.1093/clinids/12.Supplement_7.S701

20. Walter EA, Greenberg PD, Gilbert MJ, et al. Reconstitution of Cellular Immunity against Cytomegalovirus in Recipients of Allogeneic Bone Marrow by Transfer of T-Cell Clones from the Donor. *N Engl J Med*. 1995;333(16):1038-1044. doi:10.1056/nejm199510193331603

21. Heslop HE, Ng CYC, Li C, et al. Long-term restoration of immunity against Epstein-Barr virus infection by adoptive transfer of gene-modified virus-specific T lymphocytes. *Nat Med*. 1996;2(5):551-555. doi:10.1038/nm0596-551

22. Virchow R. Aetiologie der neoplastischen Geschwülste. In: *Die Krankhaften Geschwülste*. Springer, Berlin, Heidelberg; 1978:57-71. doi:10.1007/978-3-642-66491-5_4

23. Zhang L, Conejo-Garcia JR, Katsaros D, et al. Intratumoral T Cells, Recurrence, and Survival in Epithelial Ovarian Cancer. *N Engl J Med*. 2003;348(3):203-213. doi:10.1056/nejmoa020177

24. Galon J, Costes A, Sanchez-Cabo F, et al. Type, density, and location of immune cells within human colorectal tumors predict clinical outcome. *Science (80-)*. 2006;313(5795):1960-1964. doi:10.1126/science.1129139

25. Rosenberg SA, Spiess P, Lafreniere R. A new approach to the adoptive immunotherapy of cancer with tumor-infiltrating lymphocytes. *Science (80-)*. 1986;233(4770):1318-1321. doi:10.1126/science.3489291

26. Besser MJ, Shapira-Frommer R, Treves AJ, et al. Clinical responses in a phase II study using adoptive transfer of short-term cultured tumor infiltration lymphocytes in metastatic melanoma patients. *Clin Cancer Res*. 2010;16(9):2646-2655. doi:10.1158/1078-0432.CCR-10-0041

27. Goff SL, Smith FO, Klapper JA, et al. Tumor infiltrating lymphocyte therapy for metastatic melanoma: Analysis of tumors resected for TIL. *J Immunother*. 2010;33(8):840-847. doi:10.1097/CJI.0b013e3181f05b91

28. Uttenthal BJ, Chua I, Morris EC, Stauss HJ. Challenges in T cell receptor gene therapy. *J Gene Med*. 2012;14(6):386-399. doi:10.1002/jgm.2637

29. Dudley ME, Wunderlich JR, Shelton TE, Even J, Rosenberg SA. Generation of Tumor-Infiltrating Lymphocyte Cultures for Use in Adoptive Transfer Therapy for Melanoma Patients. *J Immunother*. 2003;26(4):332-342. doi:10.1097/00002371-200307000-00005

30. Scheper W, Kelderman S, Fanchi LF, et al. Low and variable tumor reactivity of the intratumoral TCR repertoire in human cancers. *Nat Med*. 2019;25(1):89-94. doi:10.1038/s41591-018-0266-5

31. Thommen DS, Schumacher TN. T Cell Dysfunction in Cancer. *Cancer Cell*.

2018;33(4):547-562. doi:10.1016/j.ccell.2018.03.012

32. Wherry EJ. T cell exhaustion. *Nat Immunol*. 2011;12(6):492-499. doi:10.1038/ni.2035

33. Cooper LJN, Kalos M, Lewinsohn DA, Riddell SR, Greenberg PD. Transfer of Specificity for Human Immunodeficiency Virus Type 1 into Primary Human T Lymphocytes by Introduction of T-Cell Receptor Genes. *J Virol*. 2000;74(17):8207-8212. doi:10.1128/jvi.74.17.8207-8212.2000

34. Sadelain M, Brentjens R, Rivière I. The basic principles of chimeric antigen receptor design. *Cancer Discov*. 2013;3(4):388-398. doi:10.1158/2159-8290.CD-12-0548

35. Stancovski I, Schindler DG, Waks T, Yarden Y, Sela M, Eshhar Z. Targeting of T lymphocytes to Neu/HER2-expressing cells using chimeric single chain Fv receptors. *J Immunol*. 1993;151(11):6577-6582. Accessed April 20, 2022. http://www.ncbi.nlm.nih.gov/pubmed/7902379

36. Schmitt TM, Ragnarsson GB, Greenberg PD. T cell receptor gene therapy for cancer. *Hum Gene Ther*. 2009;20(11):1240-1248. doi:10.1089/hum.2009.146

37. Eshhar Z, Waks T, Gross G, Schindler DG. Specific activation and targeting of cytotoxic lymphocytes through chimeric single chains consisting of antibody-binding domains and the γ or ζ subunits of the immunoglobulin and T-cell receptors. *Proc Natl Acad Sci U S A*. 1993;90(2):720-724. doi:10.1073/pnas.90.2.720

38. Marincola FM, Jaffee EM, Hickljn DJ, Ferrone S. Escape of human solid tumors from t-cell recognition: molecular mechanisms and functional significance. *Adv Immunol*. 2000;74(74):181-273. doi:10.1016/s0065-2776(08)60911-6

39. Engels B, Cam H, Schüler T, et al. Retroviral vectors for high-level transgene expression in T lymphocytes. *Hum Gene Ther*. 2003;14(12):1155-1168. doi:10.1089/104303403322167993

40. Jinek M, Chylinski K, Fonfara I, Hauer M, Doudna JA, Charpentier E. A programmable dual-RNA-guided DNA endonuclease in adaptive bacterial immunity. *Science (80-)*. 2012;337(6096):816-821. doi:10.1126/science.1225829

41. Roth TL, Puig-Saus C, Yu R, et al. Reprogramming human T cell function and specificity with non-viral genome targeting. *Nature*. 2018;559(7714):405-409. doi:10.1038/s41586-018-0326-5

42. Eyquem J, Mansilla-Soto J, Giavridis T, et al. Targeting a CAR to the TRAC locus with CRISPR/Cas9 enhances tumour rejection. *Nature*. 2017;543(7643):113-117. doi:10.1038/nature21405

43. Legut M, Dolton G, Mian AA, Ottmann OG, Sewell AK. CRISPR-mediated TCR replacement generates superior anticancer transgenic t cells. *Blood*. 2018;131(3):311-322. doi:10.1182/blood-2017-05-787598

44. Schober K, Müller TR, Gökmen F, et al. Orthotopic replacement of T-cell receptor α- and β-chains with preservation of near-physiological T-cell function. *Nat Biomed Eng*. 2019;3(12):974-984. doi:10.1038/s41551-019-0409-0

45. Stadtmauer EA, Fraietta JA, Davis MM, et al. CRISPR-engineered T cells in patients with refractory cancer. *Science (80-)*. 2020;367(6481). doi:10.1126/science.aba7365

46. Morgan RA, Dudley ME, Wunderlich JR, et al. Cancer regression in patients after transfer of genetically engineered lymphocytes. *Science (80-)*. 2006;314(5796):126-129. doi:10.1126/science.1129003

47. Johnson LA, Morgan RA, Dudley ME, et al. Gene therapy with human and mouse T-cell receptors mediates cancer regression and targets normal tissues expressing cognate antigen. *Blood*. 2009;114(3):535-546. doi:10.1182/blood-2009-03-211714

48. Chodon T, Comin-Anduix B, Chmielowski B, et al. Adoptive transfer of MART-1 T-cell

receptor transgenic lymphocytes and dendritic cell vaccination in patients with metastatic melanoma. *Clin Cancer Res*. 2014;20(9):2457-2465. doi:10.1158/1078-0432.CCR-13-3017

49. Schuster SJ, Svoboda J, Chong EA, et al. Chimeric Antigen Receptor T Cells in Refractory B-Cell Lymphomas. *N Engl J Med*. 2017;377(26):2545-2554. doi:10.1056/nejmoa1708566

50. Robbins PF, Morgan RA, Feldman SA, et al. Tumor regression in patients with metastatic synovial cell sarcoma and melanoma using genetically engineered lymphocytes reactive with NY-ESO-1. *J Clin Oncol*. 2011;29(7):917-924. doi:10.1200/JCO.2010.32.2537

51. Cameron BJ, Gerry AB, Dukes J, et al. Identification of a titin-derived HLA-A1-presented peptide as a cross-reactive target for engineered MAGE A3-directed T cells. *Sci Transl Med*. 2013;5(197). doi:10.1126/scitranslmed.3006034

52. Linette GP, Stadtmauer EA, Maus M V., et al. Cardiovascular toxicity and titin cross-reactivity of affinity-enhanced T cells in myeloma and melanoma. *Blood*. 2013;122(6):863-871. doi:10.1182/blood-2013-03-490565

53. Parkhurst MR, Yang JC, Langan RC, et al. T cells targeting carcinoembryonic antigen can mediate regression of metastatic colorectal cancer but induce severe transient colitis. *Mol Ther*. 2011;19(3):620-626. doi:10.1038/mt.2010.272

54. Chapuis AG, Ragnarsson GB, Nguyen HN, et al. Transferred WT1-reactive CD8+ T cells can mediate antileukemic activity and persist in post-transplant patients. *Sci Transl Med*. 2013;5(174). doi:10.1126/scitranslmed.3004916

55. Cohen CJ, Zheng Z, Bray R, et al. Recognition of Fresh Human Tumor by Human Peripheral Blood Lymphocytes Transduced with a Bicistronic Retroviral Vector Encoding a Murine Anti-p53 TCR. *J Immunol*. 2005;175(9):5799-5808. doi:10.4049/jimmunol.175.9.5799

56. June CH, Sadelain M. Chimeric Antigen Receptor Therapy. *N Engl J Med*. 2018;379(1):64-73. doi:10.1056/NEJMRA1706169

57. Park JR, DiGiusto DL, Slovak M, et al. Adoptive transfer of chimeric antigen receptor re-directed cytolytic T lymphocyte clones in patients with neuroblastoma. *Mol Ther*. 2007;15(4):825-833. doi:10.1038/sj.mt.6300104

58. Kershaw MH, Westwood JA, Parker LL, et al. A phase I study on adoptive immunotherapy using gene-modified T cells for ovarian cancer. *Clin Cancer Res*. 2006;12(20 PART 1):6106-6115. doi:10.1158/1078-0432.CCR-06-1183

59. Kowolik CM, Topp MS, Gonzalez S, et al. CD28 costimulation provided through a CD19-specific chimeric antigen receptor enhances in vivo persistence and antitumor efficacy of adoptively transferred T cells. *Cancer Res*. 2006;66(22):10995-11004. doi:10.1158/0008-5472.CAN-06-0160

60. Imai C, Mihara K, Andreansky M, et al. Chimeric receptors with 4-1BB signaling capacity provoke potent cytotoxicity against acute lymphoblastic leukemia. *Leukemia*. 2004;18(4):676-684. doi:10.1038/sj.leu.2403302

61. Kalos M, Levine BL, Porter DL, et al. T cells with chimeric antigen receptors have potent antitumor effects and can establish memory in patients with advanced leukemia. *Sci Transl Med*. 2011;3(95). doi:10.1126/scitranslmed.3002842

62. Sommermeyer D, Hudecek M, Kosasih PL, et al. Chimeric antigen receptor-modified T cells derived from defined CD8+ and CD4+ subsets confer superior antitumor reactivity in vivo. *Leukemia*. 2016;30(2):492-500. doi:10.1038/leu.2015.247

63. Turtle CJ, Hanafi LA, Berger C, et al. CD19 CAR-T cells of defined CD4+:CD8+ composition in adult B cell ALL patients. *J Clin Invest*. 2016;126(6):2123-2138.

doi:10.1172/JCI85309

64. Schuster SJ, Tam CS, Borchmann P, et al. Long-term clinical outcomes of tisagenlecleucel in patients with relapsed or refractory aggressive B-cell lymphomas (JULIET): a multicentre, open-label, single-arm, phase 2 study. *Lancet Oncol*. 2021;22(10):1403-1415. doi:10.1016/S1470-2045(21)00375-2

65. Shah BD, Ghobadi A, Oluwole OO, et al. KTE-X19 for relapsed or refractory adult B-cell acute lymphoblastic leukaemia: phase 2 results of the single-arm, open-label, multicentre ZUMA-3 study. *Lancet*. 2021;398(10299):491-502. doi:10.1016/S0140-6736(21)01222-8

66. Schuster SJ, Bishop MR, Tam CS, et al. Tisagenlecleucel in Adult Relapsed or Refractory Diffuse Large B-Cell Lymphoma. *N Engl J Med*. 2019;380(1):45-56. doi:10.1056/nejmoa1804980

67. Abramson JS, Palomba ML, Gordon LI, et al. Lisocabtagene maraleucel for patients with relapsed or refractory large B-cell lymphomas (TRANSCEND NHL 001): a multicentre seamless design study. *Lancet*. 2020;396(10254):839-852. doi:10.1016/S0140-6736(20)31366-0

68. Locke FL, Ghobadi A, Jacobson CA, et al. Long-term safety and activity of axicabtagene ciloleucel in refractory large B-cell lymphoma (ZUMA-1): a single-arm, multicentre, phase 1–2 trial. *Lancet Oncol*. 2019;20(1):31-42. doi:10.1016/S1470-2045(18)30864-7

69. Jain P, Nastoupil L, Westin J, et al. Outcomes and management of patients with mantle cell lymphoma after progression on brexucabtagene autoleucel therapy. *Br J Haematol*. 2021;192(2):e38-e42. doi:10.1111/bjh.17197

70. Wang M, Munoz J, Goy A, et al. KTE-X19 CAR T-Cell Therapy in Relapsed or Refractory Mantle-Cell Lymphoma. *N Engl J Med*. 2020;382(14):1331-1342. doi:10.1056/nejmoa1914347

71. Munshi NC, Anderson LD, Shah N, et al. Idecabtagene Vicleucel in Relapsed and Refractory Multiple Myeloma. *N Engl J Med*. 2021;384(8):705-716. doi:10.1056/nejmoa2024850

72. Berdeja JG, Madduri D, Usmani SZ, et al. Ciltacabtagene autoleucel, a B-cell maturation antigen-directed chimeric antigen receptor T-cell therapy in patients with relapsed or refractory multiple myeloma (CARTITUDE-1): a phase 1b/2 open-label study. *Lancet*. 2021;398(10297):314-324. doi:10.1016/S0140-6736(21)00933-8

73. Melenhorst JJ, Chen GM, Wang M, et al. Decade-long leukaemia remissions with persistence of CD4+ CAR T cells. *Nature*. 2022;602(7897):503-509. doi:10.1038/s41586-021-04390-6

74. Chong EA, Ruella M, Schuster SJ. Five-Year Outcomes for Refractory B-Cell Lymphomas with CAR T-Cell Therapy. *N Engl J Med*. 2021;384(7):673-674. doi:10.1056/nejmc2030164

75. Jagannath S, Lin Y, Goldschmidt H, et al. KarMMa-RW: comparison of idecabtagene vicleucel with real-world outcomes in relapsed and refractory multiple myeloma. *Blood Cancer J*. 2021;11(6). doi:10.1038/s41408-021-00507-2

76. Vitanza NA, Johnson AJ, Wilson AL, et al. Locoregional infusion of HER2-specific CAR T cells in children and young adults with recurrent or refractory CNS tumors: an interim analysis. *Nat Med*. 2021;27(9):1544-1552. doi:10.1038/s41591-021-01404-8

77. O'Rourke DM, Nasrallah MP, Desai A, et al. A single dose of peripherally infused EGFRvIII-directed CAR T cells mediates antigen loss and induces adaptive resistance in patients with recurrent glioblastoma. *Sci Transl Med*. 2017;9(399). doi:10.1126/scitranslmed.aaa0984

78. Hudecek M, Schmitt TM, Baskar S, et al. The B-cell tumor-associated antigen ROR1 can be targeted with T cells modified to express a ROR1-specific chimeric antigen receptor. *Blood*. 2010;116(22):4532-4541. doi:10.1182/blood-2010-05-283309

79. Chekmasova AA, Rao TD, Nikhamin Y, et al. Successful eradication of established peritoneal ovarian tumors in SCID-Beige mice following adoptive transfer of T cells genetically targeted to the MUC16 antigen. *Clin Cancer Res*. 2010;16(14):3594-3606. doi:10.1158/1078-0432.CCR-10-0192

80. Zhang T, Barber A, Sentman CL. Generation of antitumor responses by genetic modification of primary human T cells with a chimeric NKG2D receptor. *Cancer Res*. 2006;66(11):5927-5933. doi:10.1158/0008-5472.CAN-06-0130

81. Marofi F, Motavalli R, Safonov VA, et al. CAR T cells in solid tumors: challenges and opportunities. *Stem Cell Res Ther*. 2021;12(1):1-16. doi:10.1186/s13287-020-02128-1

82. Haas AR, Tanyi JL, O'Hara MH, et al. Phase I Study of Lentiviral-Transduced Chimeric Antigen Receptor-Modified T Cells Recognizing Mesothelin in Advanced Solid Cancers. *Mol Ther*. 2019;27(11):1919-1929. doi:10.1016/j.ymthe.2019.07.015

83. Beatty GL, Haas AR, Maus M V., et al. Mesothelin-specific chimeric antigen receptor mRNA-engineered T cells induce anti-tumor activity in solid malignancies. *Cancer Immunol Res*. 2014;2(2):112-120. doi:10.1158/2326-6066.CIR-13-0170

84. Ahmed N, Brawley VS, Hegde M, et al. Human epidermal growth factor receptor 2 (HER2) - Specific chimeric antigen receptor - Modified T cells for the immunotherapy of HER2-positive sarcoma. *J Clin Oncol*. 2015;33(15):1688-1696. doi:10.1200/JCO.2014.58.0225

85. Morgan RA, Yang JC, Kitano M, Dudley ME, Laurencot CM, Rosenberg SA. Case report of a serious adverse event following the administration of t cells transduced with a chimeric antigen receptor recognizing ERBB2. *Mol Ther*. 2010;18(4):843-851. doi:10.1038/mt.2010.24

86. Johnson CB, Win SY. Combination therapy with PD-1/PD-L1 blockade: An overview of ongoing clinical trials. *Oncoimmunology*. 2018;7(4). doi:10.1080/2162402X.2017.1408744

87. Dotti G, Gottschalk S, Savoldo B, Brenner MK. Design and development of therapies using chimeric antigen receptor-expressing T cells. *Immunol Rev*. 2014;257(1):107-126. doi:10.1111/imr.12131

88. Han X, Wang Y, Wei J, Han W. Multi-antigen-targeted chimeric antigen receptor T cells for cancer therapy. *J Hematol Oncol*. 2019;12(1):1-10. doi:10.1186/s13045-019-0813-7

89. Mansilla-Soto J, Eyquem J, Haubner S, et al. HLA-independent T cell receptors for targeting tumors with low antigen density. *Nat Med*. 2022;28(2):345-352. doi:10.1038/s41591-021-01621-1

90. Morris EC, Neelapu SS, Giavridis T, Sadelain M. Cytokine release syndrome and associated neurotoxicity in cancer immunotherapy. *Nat Rev Immunol*. 2022;22(2):85-96. doi:10.1038/s41577-021-00547-6

91. Schmidts A, Wehrli M, Maus M V. Toward Better Understanding and Management of CAR-T Cell-Associated Toxicity. *Annu Rev Med*. 2021;72:365-382. doi:10.1146/annurev-med-061119-015600

92. Brudno JN, Kochenderfer JN. Toxicities of chimeric antigen receptor T cells: Recognition and management. *Blood*. 2016;127(26):3321-3330. doi:10.1182/blood-2016-04-703751

93. Hay KA, Hanafi LA, Li D, et al. Kinetics and biomarkers of severe cytokine release syndrome after CD19 chimeric antigen receptor–modified T-cell therapy. *Blood*.

2017;130(21):2295-2306. doi:10.1182/blood-2017-06-793141

94. Giavridis T, Van Der Stegen SJC, Eyquem J, Hamieh M, Piersigilli A, Sadelain M. CAR T cell-induced cytokine release syndrome is mediated by macrophages and abated by IL-1 blockade letter. *Nat Med*. 2018;24(6):731-738. doi:10.1038/s41591-018-0041-7

95. Norelli M, Camisa B, Barbiera G, et al. Monocyte-derived IL-1 and IL-6 are differentially required for cytokine-release syndrome and neurotoxicity due to CAR T cells. *Nat Med*. 2018;24(6):739-748. doi:10.1038/s41591-018-0036-4

96. Neelapu SS, Tummala S, Kebriaei P, et al. Chimeric antigen receptor T-cell therapy-assessment and management of toxicities. *Nat Rev Clin Oncol*. 2018;15(1):47-62. doi:10.1038/nrclinonc.2017.148

97. Le RQ, Li L, Yuan W, et al. FDA Approval Summary: Tocilizumab for Treatment of Chimeric Antigen Receptor T Cell-Induced Severe or Life-Threatening Cytokine Release Syndrome. *Oncologist*. 2018;23(8):943-947. doi:10.1634/theoncologist.2018-0028

98. Perales MA, Kebriaei P, Kean LS, Sadelain M. Reprint of: Building a Safer and Faster CAR: Seatbelts, Airbags, and CRISPR. *Biol Blood Marrow Transplant*. 2018;24(3):S15-S19. doi:10.1016/j.bbmt.2017.12.789

99. Fitzgerald JC, Weiss SL, Maude SL, et al. Cytokine release syndrome after chimeric antigen receptor T cell therapy for acute lymphoblastic leukemia. *Crit Care Med*. 2017;45(2):e124-e125. doi:10.1097/CCM.0000000000002053

100. Strati P, Ahmed S, Kebriaei P, et al. Clinical efficacy of anakinra to mitigate CAR T-cell therapy associated toxicity in large B-cell lymphoma. *Blood Adv*. 2020;4(13):3123-3127. doi:10.1182/bloodadvances.2020002328

101. Davila ML, Riviere I, Wang X, et al. Efficacy and toxicity management of 19-28z CAR T cell therapy in B cell acute lymphoblastic leukemia. *Sci Transl Med*. 2014;6(224). doi:10.1126/scitranslmed.3008226

102. Lee DW, Kochenderfer JN, Stetler-Stevenson M, et al. T cells expressing CD19 chimeric antigen receptors for acute lymphoblastic leukaemia in children and young adults: A phase 1 dose-escalation trial. *Lancet*. 2015;385(9967):517-528. doi:10.1016/S0140-6736(14)61403-3

103. Maude SL, Frey N, Shaw PA, et al. Chimeric Antigen Receptor T Cells for Sustained Remissions in Leukemia. *N Engl J Med*. 2014;371(16):1507-1517. doi:10.1056/nejmoa1407222

104. Teachey DT, Lacey SF, Shaw PA, et al. Identification of predictive biomarkers for cytokine release syndrome after chimeric antigen receptor T-cell therapy for acute lymphoblastic leukemia. *Cancer Discov*. 2016;6(6):664-679. doi:10.1158/2159-8290.CD-16-0040

105. Meng J, Wu XQ, Sun Z, et al. Corrigendum: Efficacy and Safety of CAR-T Cell Products Axicabtagene Ciloleucel, Tisagenlecleucel, and Lisocabtagene Maraleucel for the Treatment of Hematologic Malignancies: A Systematic Review and Meta-Analysis (Frontiers in Oncology, (2021), 11, (69860. *Front Oncol*. 2021;11:2699. doi:10.3389/fonc.2021.768128

106. Santomasso BD, Park JH, Salloum D, et al. Clinical and biological correlates of neurotoxicity associated with car t-cell therapy in patients with B-cell acute lymphoblastic leukemia. *Cancer Discov*. 2018;8(8):958-971. doi:10.1158/2159-8290.CD-17-1319

107. Gust J, Hay KA, Hanafi LA, et al. Endothelial activation and blood–brain barrier disruption in neurotoxicity after adoptive immunotherapy with CD19 CAR-T cells.

Cancer Discov. 2017;7(12):1404-1419. doi:10.1158/2159-8290.CD-17-0698

108. Galea J, Ogungbenro K, Hulme S, et al. Intravenous anakinra can achieve experimentally effective concentrations in the central nervous system within a therapeutic time window: Results of a dose-ranging study. *J Cereb Blood Flow Metab*. 2011;31(2):439-447. doi:10.1038/jcbfm.2010.103

109. Logue JM, Zucchetti E, Bachmeier CA, et al. Immune reconstitution and associated infections following axicabtagene ciloleucel in relapsed or refractory large B-cell lymphoma. *Haematologica*. 2021;106(4):978-986. doi:10.3324/haematol.2019.238634

110. Fried S, Avigdor A, Bielorai B, et al. Early and late hematologic toxicity following CD19 CAR-T cells. *Bone Marrow Transplant*. 2019;54(10):1643-1650. doi:10.1038/S41409-019-0487-3

111. Nahas GR, Komanduri K V., Pereira D, et al. Incidence and risk factors associated with a syndrome of persistent cytopenias after CAR-T cell therapy (PCTT). *Leuk Lymphoma*. 2020;61(4):940-943. doi:10.1080/10428194.2019.1697814

112. Rejeski K, Perez A, Sesques P, et al. CAR-HEMATOTOX: a model for CAR T-cell–related hematologic toxicity in relapsed/refractory large B-cell lymphoma. *Blood*. 2021;138(24):2499. doi:10.1182/BLOOD.2020010543

113. Hayden PJ, Roddie C, Bader P, et al. Management of adults and children receiving CAR T-cell therapy: 2021 best practice recommendations of the European Society for Blood and Marrow Transplantation (EBMT) and the Joint Accreditation Committee of ISCT and EBMT (JACIE) and the European Haematology Association (EHA). *Ann Oncol Off J Eur Soc Med Oncol*. 2022;33(3):259-275. doi:10.1016/J.ANNONC.2021.12.003

114. Chiappella A, Guidetti A, Dodero A, et al. Real-Life CAR-T Cell Treatment in Large B-Cell Lymphomas Indicates That Axi-Cel and Tisa-Cel Have Similar Outcomes, but Long-Term Cytopenia Is an Emerging Problem. *Blood*. 2021;138(Supplement 1):3867. doi:10.1182/BLOOD-2021-154037

115. Meir J, Abid MA, Abid MB. State of the CAR-T: Risk of Infections with Chimeric Antigen Receptor T-Cell Therapy and Determinants of SARS-CoV-2 Vaccine Responses. *Transplant Cell Ther*. 2021;27(12):973. doi:10.1016/J.JTCT.2021.09.016

116. Wudhikarn K, Perales MA. Infectious complications, immune reconstitution, and infection prophylaxis after CD19 chimeric antigen receptor T-cell therapy. *Bone Marrow Transplant 2022 5710*. 2022;57(10):1477-1488. doi:10.1038/s41409-022-01756-w

117. Wang L, Hong R, Zhou L, et al. New-Onset Severe Cytopenia After CAR-T Cell Therapy: Analysis of 76 Patients With Relapsed or Refractory Acute Lymphoblastic Leukemia. *Front Oncol*. 2021;11. doi:10.3389/FONC.2021.702644/FULL

118. Sharma N, Reagan PM, Liesveld JL. Cytopenia after CAR-T Cell Therapy-A Brief Review of a Complex Problem. *Cancers (Basel)*. 2022;14(6). doi:10.3390/CANCERS14061501

119. Jacobson C, Chavez JC, Sehgal AR, et al. Primary Analysis of Zuma-5: A Phase 2 Study of Axicabtagene Ciloleucel (Axi-Cel) in Patients with Relapsed/Refractory (R/R) Indolent Non-Hodgkin Lymphoma (iNHL). *Blood*. 2020;136(Supplement 1):40-41. doi:10.1182/BLOOD-2020-136834

120. Frey N V., Gill S, Hexner EO, et al. Long-Term Outcomes From a Randomized Dose Optimization Study of Chimeric Antigen Receptor Modified T Cells in Relapsed Chronic Lymphocytic Leukemia. *J Clin Oncol*. 2020;38(25):2862-2871. doi:10.1200/JCO.19.03237

121. Jain T, Knezevic A, Pennisi M, et al. Hematopoietic recovery in patients receiving

chimeric antigen receptor T-cell therapy for hematologic malignancies. *Blood Adv*. 2020;4(15):3776. doi:10.1182/BLOODADVANCES.2020002509

122. Wudhikarn K, Palomba ML, Pennisi M, et al. Infection during the first year in patients treated with CD19 CAR T cells for diffuse large B cell lymphoma. *Blood Cancer J*. 2020;10(8). doi:10.1038/S41408-020-00346-7

123. Cordeiro A, Bezerra ED, Hirayama A V., et al. Late Events after Treatment with CD19-Targeted Chimeric Antigen Receptor Modified T Cells. *Biol Blood Marrow Transplant*. 2020;26(1):26-33. doi:10.1016/J.BBMT.2019.08.003

124. Savoldo B, Ramos CA, Liu E, et al. CD28 costimulation improves expansion and persistence of chimeric antigen receptor-modified T cells in lymphoma patients. *J Clin Invest*. 2011;121(5):1822-1826. doi:10.1172/JCI46110

125. Ghobadi A, Fiala MA, Ramsingh G, et al. Fresh or Cryopreserved CD34+-Selected MobilizedPeripheral Blood Stem and Progenitor Cells for the Treatment of Poor GraftFunction following Allogeneic Hematopoietic Cell Transplantation. *Biol Blood Marrow Transplant*. 2017;23(7):1072. doi:10.1016/J.BBMT.2017.03.019

126. Galli E, Allain V, Di Blasi R, et al. G-CSF does not worsen toxicities and efficacy of CAR-T cells in refractory/relapsed B-cell lymphoma. *Bone Marrow Transplant 2020 5512*. 2020;55(12):2347-2349. doi:10.1038/s41409-020-01006-x

127. Kochenderfer JN, Yu Z, Frasheri D, Restifo NP, Rosenberg SA. Adoptive transfer of syngeneic T cells transduced with a chimeric antigen receptor that recognizes murine CD19 can eradicate lymphoma and normal B cells. *Blood*. 2010;116(19):3875-3886. doi:10.1182/blood-2010-01-265041

128. Uckun FM, Ledbetter JA. Immunobiologic differences between normal and leukemic human B-cell precursors. *Proc Natl Acad Sci U S A*. 1988;85(22):8603-8607. doi:10.1073/pnas.85.22.8603

129. Kochenderfer JN, Dudley ME, Feldman SA, et al. B-cell depletion and remissions of malignancy along with cytokine-associated toxicity in a clinical trial of anti-CD19 chimeric-antigen-receptor-transduced T cells. *Blood*. 2012;119(12):2709-2720. doi:10.1182/blood-2011-10-384388

130. Parker KR, Migliorini D, Perkey E, et al. Single-Cell Analyses Identify Brain Mural Cells Expressing CD19 as Potential Off-Tumor Targets for CAR-T Immunotherapies. *Cell*. 2020;183(1):126-142.e17. doi:10.1016/j.cell.2020.08.022

131. Lamers CHJ, Sleijfer S, Vulto AG, et al. Treatment of metastatic renal cell carcinoma with autologous T-lymphocytes genetically retargeted against carbonic anhydrase IX: first clinical experience. *J Clin Oncol*. 2006;24(13). doi:10.1200/JCO.2006.05.9964

132. Maude SL, Pulsipher MA, Boyer MW, et al. Efficacy and Safety of CTL019 in the First US Phase II Multicenter Trial in Pediatric Relapsed/Refractory Acute Lymphoblastic Leukemia: Results of an Interim Analysis. *Blood*. 2016;128(22):2801-2801. doi:10.1182/blood.v128.22.2801.2801

133. Bonini C, Ferrari G, Verzeletti S, et al. HSV-TK gene transfer into donor lymphocytes for control of allogeneic graft-versus-leukemia. *Science (80-)*. 1997;276(5319):1719-1724. doi:10.1126/science.276.5319.1719

134. Bordignon C, Bonini C, Verzeletti S, et al. Transfer of the HSV-tk Gene into Donor Peripheral Blood Lymphocytes for In Vivo Modulation of Donor Anti Tumor Immunity after Allogeneic Bone Marrow Transplantation. The San Raffaele Hospital, Milan, Italy. *Hum Gene Ther*. 1995;6(6):813-819. doi:10.1089/hum.1995.6.6-813

135. Berger C, Flowers ME, Warren EH, Riddell SR. Analysis of transgene-specific immune responses that limit the in vivo persistence of adoptively transferred HSV-TK-modified donor T cells after allogeneic hematopoietic cell transplantation. *Blood*.

2006;107(6):2294-2302. doi:10.1182/blood-2005-08-3503

136. Di Stasi A, Tey S-K, Dotti G, et al. Inducible Apoptosis as a Safety Switch for Adoptive Cell Therapy. *N Engl J Med*. 2011;365(18):1673-1683. doi:10.1056/nejmoa1106152

137. Adams GP, Weiner LM. Monoclonal antibody therapy of cancer. *Nat Biotechnol*. 2005;23(9):1147-1157. doi:10.1038/nbt1137

138. Serafini M, Manganini M, Borleri G, et al. Characterization of CD20-Transduced T Lymphocytes as an Alternative Suicide Gene Therapy Approach for the Treatment of Graft-Versus-Host Disease. *Hum Gene Ther*. 2004;15(1):63-76. doi:10.1089/10430340460732463

139. Wang X, Chang WC, Wong CLW, et al. A transgene-encoded cell surface polypeptide for selection, in vivo tracking, and ablation of engineered cells. *Blood*. 2011;118(5):1255-1263. doi:10.1182/blood-2011-02-337360

140. Andrea AE, Chiron A, Bessoles S, Hacein-Bey-abina S. Engineering next-generation car-t cells for better toxicity management. *Int J Mol Sci*. 2020;21(22):1-25. doi:10.3390/ijms21228620

141. Wu CY, Roybal KT, Puchner EM, Onuffer J, Lim WA. Remote control of therapeutic T cells through a small moleculeâ€"gated chimeric receptor. *Science (80-)*. 2015;350(6258). doi:10.1126/science.aab4077

142. Mestermann K, Giavridis T, Weber J, et al. The tyrosine kinase inhibitor dasatinib acts as a pharmacologic on/off switch for CAR T cells. *Sci Transl Med*. 2019;11(499). doi:10.1126/scitranslmed.aau5907

143. Fedorov VD, Themeli M, Sadelain M. PD-1- and CTLA-4-based inhibitory chimeric antigen receptors (iCARs) divert off-target immunotherapy responses. *Sci Transl Med*. 2013;5(215). doi:10.1126/scitranslmed.3006597

144. Cho JH, Okuma A, Sofjan K, Lee S, Collins JJ, Wong WW. Engineering advanced logic and distributed computing in human CAR immune cells. *Nat Commun*. 2021;12(1). doi:10.1038/s41467-021-21078-7

145. Hombach A, Wieczarkowiecz A, Marquardt T, et al. Tumor-Specific T Cell Activation by Recombinant Immunoreceptors: CD3ζ Signaling and CD28 Costimulation Are Simultaneously Required for Efficient IL-2 Secretion and Can Be Integrated Into One Combined CD28/CD3ζ Signaling Receptor Molecule. *J Immunol*. 2001;167(11):6123-6131. doi:10.4049/jimmunol.167.11.6123

146. Milone MC, Fish JD, Carpenito C, et al. Chimeric receptors containing CD137 signal transduction domains mediate enhanced survival of T cells and increased antileukemic efficacy in vivo. *Mol Ther*. 2009;17(8):1453-1464. doi:10.1038/mt.2009.83

147. Hudecek M, Lupo-Stanghellini MT, Kosasih PL, et al. Receptor affinity and extracellular domain modifications affect tumor recognition by ROR1-specific chimeric antigen receptor T cells. *Clin Cancer Res*. 2013;19(12):3153-3164. doi:10.1158/1078-0432.CCR-13-0330

148. Guest RD, Hawkins RE, Kirillova N, et al. The role of extracellular spacer regions in the optimal design of chimeric immune receptors: Evaluation of four different scFvs and antigens. *J Immunother*. 2005;28(3):203-211. doi:10.1097/01.cji.0000161397.96582.59

149. Brentjens RJ, Latouche JB, Santos E, et al. Eradication of systemic B-cell tumors by genetically targeted human T lymphocytes co-stimulated by CD80 and interleukin-15. *Nat Med*. 2003;9(3):279-286. doi:10.1038/nm827

150. Till BG, Jensen MC, Wang J, et al. Adoptive immunotherapy for indolent non-hodgkin lymphoma and mantle cell lymphoma using genetically modified autologous CD20-

specific T cells. *Blood*. 2008;112(6):2261-2271. doi:10.1182/blood-2007-12-128843

151. Finney HM, Akbar AN, Lawson ADG. Activation of Resting Human Primary T Cells with Chimeric Receptors: Costimulation from CD28, Inducible Costimulator, CD134, and CD137 in Series with Signals from the TCRζ Chain. *J Immunol*. 2004;172(1):104-113. doi:10.4049/jimmunol.172.1.104

152. Hombach AA, Rappl G, Abken H. Arming Cytokine-induced Killer cells with chimeric antigen receptors: CD28 outperforms combined CD28-OX40 “super-stimulation.” *Mol Ther*. 2013;21(12):2268-2277. doi:10.1038/mt.2013.192

153. Long AH, Haso WM, Shern JF, et al. 4-1BB costimulation ameliorates T cell exhaustion induced by tonic signaling of chimeric antigen receptors. *Nat Med*. 2015;21(6):581-590. doi:10.1038/nm.3838

154. Daniyan AFO, Brentjens RJ. At the Bench: Chimeric antigen receptor (CAR) T cell therapy for the treatment of B cell malignancies. *J Leukoc Biol*. 2016;100(6):1255-1264. doi:10.1189/jlb.5bt1215-556rr

155. Wang J, Jensen M, Lin Y, et al. Optimizing adoptive polyclonal T cell immunotherapy of lymphomas, using a chimeric T cell receptor possessing CD28 and CD137 costimulatory domains. *Hum Gene Ther*. 2007;18(8):712-725. doi:10.1089/hum.2007.028

156. Till BG, Jensen MC, Wang J, et al. CD20-specific adoptive immunotherapy for lymphoma using a chimeric antigen receptor with both CD28 and 4-1BB domains: Pilot clinical trial results. *Blood*. 2012;119(17):3940-3950. doi:10.1182/blood-2011-10-387969

157. Dwyer CJ, Knochelmann HM, Smith AS, et al. Fueling cancer immunothery with common gamma chain cytokines. *Front Immunol*. 2019;10(FEB). doi:10.3389/fimmu.2019.00263

158. Chmielewski M, Kopecky C, Hombach AA, Abken H. IL-12 release by engineered T cells expressing chimeric antigen receptors can effectively muster an antigen-independent macrophage response on tumor cells that have shut down tumor antigen expression. *Cancer Res*. 2011;71(17):5697-5706. doi:10.1158/0008-5472.CAN-11-0103

159. Valitutti S, Coombs D, Dupré L. The space and time frames of T cell activation at the immunological synapse. *FEBS Lett*. 2010;584(24):4851-4857. doi:10.1016/j.febslet.2010.10.010

160. Stone JD, Chervin AS, Kranz DM. T-cell receptor binding affinities and kinetics: impact on T-cell activity and specificity. *Immunology*. 2009;126(2):165-176. doi:10.1111/j.1365-2567.2008.03015.x

161. Corse E, Gottschalk RA, Allison JP. Strength of TCR–Peptide/MHC Interactions and In Vivo T Cell Responses. *J Immunol*. 2011;186(9):5039-5045. doi:10.4049/jimmunol.1003650

162. Stone JD, Kranz DM. Role of T cell receptor affinity in the efficacy and specificity of adoptive T cell therapies. *Front Immunol*. 2013;4(AUG). doi:10.3389/fimmu.2013.00244

163. Nauerth M, Weißbrich B, Knall R, et al. TCR-ligand koff rate correlates with the protective capacity of antigen-specific CD8+ T cells for adoptive transfer. *Sci Transl Med*. 2013;5(192). doi:10.1126/scitranslmed.3005958

164. Nauerth M, Stemberger C, Mohr F, et al. Flow cytometry-based TCR-ligand Koff-rate assay for fast avidity screening of even very small antigen-specific T cell populations ex vivo. *Cytom Part A*. 2016;89(9):816-825. doi:10.1002/cyto.a.22933

165. Weissbrich B, Nauerth M, Busch DH. Adoptive immunotherapy: New assay for the

identification of T cells with optimal avidity. *Oncoimmunology*. 2013;2(10). doi:10.4161/onci.26199

166. Kunert A, Straetemans T, Govers C, et al. TCR-engineered T cells meet new challenges to treat solid tumors: Choice of antigen, T cell fitness, and sensitization of tumor milieu. *Front Immunol*. 2013;4(NOV). doi:10.3389/fimmu.2013.00363

167. Busch DH, Pamer EG. T cell affinity maturation by selective expansion during infection. *J Exp Med*. 1999;189(4):701-709. doi:10.1084/jem.189.4.701

168. Zehn D, Lee SY, Bevan MJ. Complete but curtailed T-cell response to very low-affinity antigen. *Nature*. 2009;458(7235):211-214. doi:10.1038/nature07657

169. Zhong S, Malecek K, Johnson LA, et al. T-cell receptor affinity and avidity defines antitumor response and autoimmunity in T-cell immunotherapy. *Proc Natl Acad Sci U S A*. 2013;110(17):6973-6978. doi:10.1073/pnas.1221609110

170. Valitutti S, Miller S, Cella M, Padovan E, Lanzavecchia A. Serial triggering of many T-cell receptors by a few peptide-MHC complexes. *Nature*. 1995;375(6527):148-151. doi:10.1038/375148a0

171. Engels B, Engelhard VH, Sidney J, et al. Relapse or eradication of cancer is predicted by peptide-major histocompatibility complex affinity. *Cancer Cell*. 2013;23(4):516-526. doi:10.1016/j.ccr.2013.03.018

172. Thomas S, Xue SA, Bangham CRM, Jakobsen BK, Morris EC, Stauss HJ. Human T cells expressing affinity-matured TCR display accelerated responses but fail to recognize low density of MHC-peptide antigen. *Blood*. 2011;118(2):319-329. doi:10.1182/blood-2010-12-326736

173. Tan MP, Gerry AB, Brewer JE, et al. T cell receptor binding affinity governs the functional profile of cancer-specific CD8+ T cells. *Clin Exp Immunol*. 2015;180(2):255-270. doi:10.1111/cei.12570

174. Holler PD, Holman PO, Shusta E V., O'Herrin S, Wittrup KD, Kranz DM. In vitro evolution of a T cell receptor with high affinity for peptide/MHC. *Proc Natl Acad Sci U S A*. 2000;97(10):5387-5392. doi:10.1073/pnas.080078297

175. Kalergis AH, Boucheron N, Doucey MA, et al. Efficient T cell activation requires an optimal dwell-time of interaction between the TCR and the pMHC complex. *Nat Immunol*. 2001;2(3):229-234. doi:10.1038/85286

176. Schmid DA, Irving MB, Posevitz V, et al. Evidence for a TCR Affinity Threshold Delimiting Maximal CD8 T Cell Function. *J Immunol*. 2010;184(9):4936-4946. doi:10.4049/jimmunol.1000173

177. Watanabe K, Kuramitsu S, Posey AD, June CH. Expanding the therapeutic window for CAR T cell therapy in solid tumors: The knowns and unknowns of CAR T cell biology. *Front Immunol*. 2018;9(OCT):2486. doi:10.3389/fimmu.2018.02486

178. Liu X, Jiang S, Fang C, et al. Affinity-tuned ErbB2 or EGFR chimeric antigen receptor T cells exhibit an increased therapeutic index against tumors in mice. *Cancer Res*. 2015;75(17):3596-3607. doi:10.1158/0008-5472.CAN-15-0159

179. ZOLA H, MACARDLE PJ, BRADFORD T, WEEDON H, YASU H, KUROSAWA Y. Preparation and characterization of a chimeric CD 19 monoclonal antibody. *Immunol Cell Biol*. 1991;69(6):411-422. doi:10.1038/icb.1991.58

180. Sabbagh L, Pulle G, Liu Y, Tsitsikov EN, Watts TH. ERK-Dependent Bim Modulation Downstream of the 4-1BB-TRAF1 Signaling Axis Is a Critical Mediator of CD8 T Cell Survival In Vivo. *J Immunol*. 2008;180(12):8093-8101. doi:10.4049/jimmunol.180.12.8093

181. Oren R, Hod-Marco M, Haus-Cohen M, et al. Functional Comparison of Engineered T

Cells Carrying a Native TCR versus TCR-like Antibody–Based Chimeric Antigen Receptors Indicates Affinity/Avidity Thresholds. *J Immunol*. 2014;193(11):5733-5743. doi:10.4049/jimmunol.1301769

182. Salter AI, Rajan A, Kennedy JJ, et al. Comparative analysis of TCR and CAR signaling informs CAR designs with superior antigen sensitivity and in vivo function. *Sci Signal*. 2021;14(697). doi:10.1126/scisignal.abe2606

183. Ghorashian S, Kramer AM, Onuoha S, et al. Enhanced CAR T cell expansion and prolonged persistence in pediatric patients with ALL treated with a low-affinity CD19 CAR. *Nat Med*. 2019;25(9):1408-1414. doi:10.1038/s41591-019-0549-5

184. Martinez RJ, Evavold BD. Lower affinity T cells are critical components and active participants of the immune response. *Front Immunol*. 2015;6(SEP):468. doi:10.3389/fimmu.2015.00468

185. Utzschneider DT, Alfei F, Roelli P, et al. High antigen levels induce an exhausted phenotype in a chronic infection without impairing T cell expansion and survival. *J Exp Med*. 2016;213(9):1819-1834. doi:10.1084/jem.20150598

186. Kim C, Williams MA. Nature and nurture: T-cell receptor-dependent and T-cell receptor-independent differentiation cues in the selection of the memory T-cell pool. *Immunology*. 2010;131(3):310-317. doi:10.1111/j.1365-2567.2010.03338.x

187. Skerra A, Schmidt TGM. Use of the Strep-tag and streptavidin for detection and purification of recombinant proteins. *Methods Enzymol*. 2000;326:271-304. doi:10.1016/s0076-6879(00)26060-6

188. Liu L, Sommermeyer D, Cabanov A, Kosasih P, Hill T, Riddell SR. Inclusion of Strep-tag II in design of antigen receptors for T-cell immunotherapy. *Nat Biotechnol*. 2016;34(4):430-434. doi:10.1038/nbt.3461

189. Paszkiewicz PJ, Fräßle SP, Srivastava S, et al. Targeted antibody-mediated depletion of murine CD19 CAR T cells permanently reverses B cell aplasia. *J Clin Invest*. 2016;126(11):4262-4272. doi:10.1172/JCI84813

190. Effenberger M, Stengl A, Schober K, et al. FLEXamers: A Double Tag for Universal Generation of Versatile Peptide-MHC Multimers. *J Immunol*. 2019;202(7):2164-2171. doi:10.4049/jimmunol.1801435

191. Dunbar J, Krawczyk K, Leem J, et al. SAbPred: a structure-based antibody prediction server. *Nucleic Acids Res*. 2016;44(W1):W474-W478. doi:10.1093/NAR/GKW361

192. Pires DEV, Ascher DB. mCSM-AB: a web server for predicting antibody–antigen affinity changes upon mutation with graph-based signatures. *Nucleic Acids Res*. 2016;44(W1):W469-W473. doi:10.1093/nar/gkw458

193. Poltorak MP, Graef P, Tschulik C, et al. Expamers: a new technology to control T cell activation. *Sci Rep*. 2020;10(1). doi:10.1038/s41598-020-74595-8

194. Knabel M, Franz TJ, Schiemann M, et al. Reversible MHC multimer staining for functional isolation of T-cell populations and effective adoptive transfer. *Nat Med*. 2002;8(6):631-637. doi:10.1038/nm0602-631

195. Laurent E, Sieber A, Salzer B, et al. Directed Evolution of Stabilized Monomeric CD19 for Monovalent CAR Interaction Studies and Monitoring of CAR-T Cell Patients. *ACS Synth Biol*. 2021;10(5):1184-1198. doi:10.1021/acssynbio.1c00010

196. Guo X zhi J, Dash P, Calverley M, Tomchuck S, Dallas MH, Thomas PG. Rapid cloning, expression, and functional characterization of paired αβ and γδ T-cell receptor chains from single-cell analysis. *Mol Ther - Methods Clin Dev*. 2016;3:15054. doi:10.1038/mtm.2015.54

197. Lobner E, Wachernig A, Gudipati V, et al. Getting CD19 Into Shape: Expression of

Natively Folded “Difficult-to- Express” CD19 for Staining and Stimulation of CAR-T Cells. *Front Bioeng Biotechnol*. 2020;8:49. doi:10.3389/fbioe.2020.00049

198. Masuda S, Mielke S, Amadei F, et al. Nonlinear Viscoelasticity of Highly Ordered, Two-Dimensional Assemblies of Metal Nanoparticles Confined at the Air/Water Interface. *Langmuir*. 2018;34(43):13025-13034. doi:10.1021/acs.langmuir.8b02713

199. Dötsch S, Svec M, Schober K, et al. Long-term persistence and functionality of adoptively transferred antigen-specific T cells with genetically ablated PD-1 expression. *Proc Natl Acad Sci U S A*. 2023;120(10). doi:10.1073/PNAS.2200626120

200. Xu X, Sun Q, Liang X, et al. Mechanisms of Relapse After CD19 CAR T-Cell Therapy for Acute Lymphoblastic Leukemia and Its Prevention and Treatment Strategies. *Front Immunol*. 2019;10. doi:10.3389/fimmu.2019.02664

201. Caraballo Galva LD, Jiang X, Hussein MS, et al. Novel low-avidity glypican-3 specific CARTs resist exhaustion and mediate durable antitumor effects against HCC. *Hepatology*. Published online 2021. doi:10.1002/hep.32279

202. Arcangeli S, Rotiroti MC, Bardelli M, et al. Balance of Anti-CD123 Chimeric Antigen Receptor Binding Affinity and Density for the Targeting of Acute Myeloid Leukemia. *Mol Ther*. 2017;25(8):1933-1945. doi:10.1016/j.ymthe.2017.04.017

203. Greenman R, Pizem Y, Haus-Cohen M, et al. Shaping functional avidity of CAR T Cells: Affinity, avidity, and antigen density that regulate response. *Mol Cancer Ther*. 2021;20(5):872-884. doi:10.1158/1535-7163.MCT-19-1109

204. Morrison KL, Weiss GA. Combinatorial alanine-scanning. *Curr Opin Chem Biol*. 2001;5(3):302-307. doi:10.1016/S1367-5931(00)00206-4

205. Liu H, Rhodes M, Wiest DL, Vignali DAA. On the dynamics of TCR:CD3 complex cell surface expression and downmodulation. *Immunity*. 2000;13(5):665-675. doi:10.1016/S1074-7613(00)00066-2

206. Li W, Qiu S, Chen J, et al. Chimeric Antigen Receptor Designed to Prevent Ubiquitination and Downregulation Showed Durable Antitumor Efficacy. *Immunity*. 2020;53(2):456-470.e6. doi:10.1016/j.immuni.2020.07.011

207. Irving M, Zoete V, Hebeisen M, et al. Interplay between T cell receptor binding kinetics and the level of cognate peptide presented by major histocompatibility complexes governs CD8+ T cell responsiveness. *J Biol Chem*. 2012;287(27):23068-23078. doi:10.1074/jbc.M112.357673

208. Valitutti S. The serial engagement model 17 years after: Fromtcr triggering to immunotherapy. *Front Immunol*. 2012;3(AUG). doi:10.3389/fimmu.2012.00272

209. Chmielewski M, Hombach A, Heuser C, Adams GP, Abken H. T Cell Activation by Antibody-Like Immunoreceptors: Increase in Affinity of the Single-Chain Fragment Domain above Threshold Does Not Increase T Cell Activation against Antigen-Positive Target Cells but Decreases Selectivity. *J Immunol*. 2004;173(12):7647-7653. doi:10.4049/jimmunol.173.12.7647

210. Watanabe K, Terakura S, Martens AC, et al. Target Antigen Density Governs the Efficacy of Anti–CD20-CD28-CD3 ζ Chimeric Antigen Receptor–Modified Effector CD8 + T Cells. *J Immunol*. 2015;194(3):911-920. doi:10.4049/jimmunol.1402346

211. Stein AM, Grupp SA, Levine JE, et al. Tisagenlecleucel Model-Based Cellular Kinetic Analysis of Chimeric Antigen Receptor–T Cells. *CPT Pharmacometrics Syst Pharmacol*. 2019;8(5):285-295. doi:10.1002/psp4.12388

212. Liu C, Ayyar VS, Zheng X, et al. Model-Based Cellular Kinetic Analysis of Chimeric Antigen Receptor-T Cells in Humans. *Clin Pharmacol Ther*. 2021;109(3):716-727. doi:10.1002/cpt.2040

213. Porter DL, Hwang WT, Frey N V., et al. Chimeric antigen receptor T cells persist and induce sustained remissions in relapsed refractory chronic lymphocytic leukemia. *Sci Transl Med*. 2015;7(303). doi:10.1126/scitranslmed.aac5415

214. Wherry EJ, Ha SJ, Kaech SM, et al. Molecular Signature of CD8+ T Cell Exhaustion during Chronic Viral Infection. *Immunity*. 2007;27(4):670-684. doi:10.1016/j.immuni.2007.09.006

215. Lehner M, Götz G, Proff J, et al. Redirecting T cells to ewing's sarcoma family of tumors by a chimeric NKG2D receptor expressed by lentiviral transduction or mRNA transfection. *PLoS One*. 2012;7(2). doi:10.1371/journal.pone.0031210

216. Caserta S, Kleczkowska J, Mondino A, Zamoyska R. Reduced Functional Avidity Promotes Central and Effector Memory CD4 T Cell Responses to Tumor-Associated Antigens. *J Immunol*. 2010;185(11):6545-6554. doi:10.4049/jimmunol.1001867

217. D'Ippolito E, Schober K, Nauerth M, Busch DH. T cell engineering for adoptive T cell therapy: safety and receptor avidity. *Cancer Immunol Immunother*. 2019;68(10):1701-1712. doi:10.1007/s00262-019-02395-9

Acknowledgments

There are many people I am eternally grateful to for their encouragement and support throughout my entire time at the MIH in Munich.

First of all, a very special thanks to my doctor's father, Prof. Dirk Busch, for his dedicated, motivating, and encouraging support throughout my time as a PhD student in this lab, which has pushed and advanced my work enormously. Besides, I am really grateful for all the exceptional opportunities to work on inspiring and challenging projects in an ambitious environment, to participate at several international congresses, and for his trust and belief in my work, but also in me as a person.

A special thank you to my mentor Prof. Stan Riddell from the FHCRC in Seattle, for his invaluable input in my PhD project and to Prof. Dietmar Zehn for his agreement to supervise this work and to participate in my thesis committee. Elvira D'Ippolito deserves my gratitude for all her guidance. I really appreciate her assistance, especially in the beginning and at the end. Thank you for your detailed advice and corrections of my thesis, manuscripts and talks.

I want to thank all collaboration partners at Juno Therapeutics – a BMS company, for providing reagents, constructs, and critical discussions, as well as all collaborators at the BOKU in Vienna, the San Raffaele Institute in Milan, the Klinikum Rechts der Isar and Ludwig-Maximilians-University in Munich for great discussions and excellent cooperation.

The five years of my PhD have been an amazing experience. Although it has been a rollercoaster ride with many ups and downs, I was surrounded by a team of great people at the MIH, and I know that this time has prepared me for everything that comes next. It was a pleasure being part of the Busch lab, and I feel privileged to have been surrounded by such enthusiastic and experienced scientists. All the help, laughs, coffees, lunch breaks, chats, and rooftop celebrations have been unforgettable.

A special thanks goes to you, Mortimer Svec, Linda Warmuth, Saskia Kolb, and Jack Barton, for being by my side not only as colleagues but also as friends over many years and in the future. Thanks for making this experience so unique, for sharing a lot of laughs and tears, and

for all your moral support during crazy times. You are the best friends I could wish for, and I will never forget our wonderful time.

I also want to give thanks to my master's students, Wenzel Manlik, Linda Warmuth, Manuel Trebo, and Beate Honold, who contributed with outstanding commitment and passion to this project and who gave me the chance to learn how to guide and lead other people. I am very grateful to our technical assistants, especially Franziska Graml, Anna Hochholzer, and Monika Hammel, for providing support on many different levels and their help with daily problems. I would also like to thank Julius Schütz, who was closely involved in the humanization experiments, and Sebastian Jarosch for helpful discussions. Thanks to the sorting facility for performing endless sorts and especially to Immanuel Andrä aka. Wichtl for fixing the flow cytometers even after working hours.

There is a whole world outside of work, and I feel very privileged to be surrounded by a fantastic group of friends who helped me not to forget about it. Thanks for always providing me with enough distraction I needed to keep "sanish" during the course of this PhD and to walk with me through all the good and bad times. I am incredibly grateful for the sublime friendship with Anna and Vroni, who had given me strength when I needed it the most and who always believed in me.

My never-ending thankfulness goes to my boyfriend Andy. I could not have wished for a more caring person in my life who always helped me to stay calm and focused. Thanks for being very patient and tolerating during all my night and weekend shifts, as well as during the writing process of my thesis. Without you, I would not have performed any of the mouse experiments, and this project would not have been finished. Thanks for the beautiful time and for just being there.

Last but definitively not least, my family has been the cornerstone of my professional and personal development, extending much further than this PhD. Infinite thanks to my parents and grandparents for their unexceptional and loving support and for always being there in any way possible. Thank you for your unconditional love and all our memories which are never taken for granted. I could not have managed all the challenges during the long way of my thesis

but also during my whole life without you. Thanks for giving me the mental strength, always believing in me, and helping me become the strong woman I am today.

Thank you!

List of Figures

List of Tables